cp 2

CONTRACTOR REPORT

SAND90—7111
Unlimited Release
UC—261

An Experimental Investigation of the Effect of Vortex Generators on the Aerodynamic Characteristics of a NACA 0021 Airfoil Undergoing Large Amplitude Pitch Oscillations

Mathew L. Rueger, Gerald M. Gregorek
Department of Aeronautical and Astronautical Engineering
The Ohio State University
Columbus, OH 43220

Prepared by Sandia National Laboratories Albuquerque, New Mexico 87185 and Livermore, California 94550 for the United States Department of Energy under Contract DE-AC04-76DP00789

Printed April 1991

Issued by Sandia National Laboratories, operated for the United States Department of Energy by Sandia Corporation.

Available to DOE and DOE contractors from
Office of Scientific and Technical Information
PO Box 62
Oak Ridge, TN 37831

Prices available from (615) 576-8401, FTS 626-8401

Available to the public from
National Technical Information Service
US Department of Commerce
5285 Port Royal Rd
Springfield, VA 22161

NTIS price codes
Printed copy: A07
Microfiche copy: A01

Distribution Category
UC-261

SAND90-7111

Unlimited Release
Printed April 1991

AN EXPERIMENTAL INVESTIGATION OF THE EFFECT OF VORTEX GENERATORS ON THE AERODYNAMIC CHARACTERISTICS OF A NACA 0021 AIRFOIL UNDERGOING LARGE AMPLITUDE PITCH OSCILLATIONS

Mathew L. Rueger
Gerald M. Gregorek

Department of Aeronautical and Astronautical Engineering
The Ohio State University
Columbus, Ohio 43220

Sandia Contract 57-1337

ABSTRACT

A NACA 0021 14-chord airfoil was subjected to large amplitude pitch oscillations in The Ohio State University AARL Low Speed Wind Tunnel at a Reynolds number (based on chord) of 1.2×10^6. The pitch waveforms consisted of a 10^0 amplitude sine function, a 20^0 amplitude inverse-tangent function, and a 30^0 inverse-tangent function, all about a zero mean angle. Frequencies of oscillation varied from 0 to 1.3 Hz. Surface pressures were measured with an electronically scanned pressure measurement system at sampling rates up to 50 Hz. Data were acquired for the clean airfoil and for the airfoil with vortex generators located at 0.1 and 0.3 chord distances aft of the leading edge. The vortex generators increase the maximum lift coefficient and the lift curve slope for both the static and dynamic tests. The magnitude and detail of the vortex generator effects were found to depend on the amplitude and frequency of the pitch oscillations.

ACKNOWLEDGMENT

The lead author wishes to express his gratitude to Sandia National Laboratories for funding the research presented here, and to his advisor Dr. G. M. Gregorek for making this work possible through his patience and guidance. He would also like to thank the faculty, staff and students of the Aeronautical and Astronautical Research Laboratory whose support was much appreciated. Special thanks go to Mr. Michael J. Hoffmann whose active interest and participation were essential to the completion of this work.

TABLE OF CONTENTS

LIST OF FIGURES

LIST OF FIGURES
(Continued)

LIST OF FIGURES
(Continued)

LIST OF FIGURES
(Continued)

LIST OF FIGURES
(Concluded)

LIST OF TABLES

LIST OF TABLES
(Concluded)

NOMENCLATURE

Symbol	Description
A_n	Fourier series coefficient
c	Airfoil chord length
C_D	Drag coefficient
C_L	Lift coefficient
$C_{L_{ref}}$	Static lift coefficient at angle of attack $\alpha = \alpha_{ref}$
F	Real part of Theodorsen's function (function of k)
g	Acceleration due to gravity
G	Gain. Imaginary part of Theodorsen's function (function of k)
i	Square root of -1
k	Reduced frequency
k_n	Reduced frequency based on ω_n
L	Tube length
p	Ambient pressure
Q	Non-dimensional parameter
r	Tube radius
R	Specific gas constant
T	Ambient temperature
t	Time
u	Local velocity
U_∞	Freestream velocity
V	Reservoir volume
α	Angle of attack
$\dot{\alpha}$	Angular velocity

NOMENCLATURE
(Concluded)

Symbol	Description
a_n	Fourier series term
$\dot{a}_n$	Fourier series term
α_{ref}	Reference angle of attack
α_{eq}	Circulatory equivalent-angle-of-attack
$\bar{\alpha}$	Non-circulatory equivalent-angle-of-attack
$\Delta\alpha_{ds}$	Increase in stall angle due to dynamic effects
α_{ss}	Static stall angle
γ	Ratio of specific heats. Empirically derived constant
λ	Tip-speed ratio
μ	Coefficient of viscosity
τ	Time lag
ξ	System damping ratio
ω	Oscillation frequency
ω_o	System natural frequency
ω_n	Fourier series term

I. INTRODUCTION

As a result of modern industrialization and technology, energy demands in our society have continued to rise at an ever-increasing rate. Declining resources and concern over the environment have prompted research in recent decades into alternatives to conventional fossil fuels. One such alternative is wind energy.

Simple wind-powered machinery has been in use for centuries, but the application of wind energy to large-scale electric power generation is a relatively recent phenomenon. As for any system, cost effectiveness is the key to success; efficiency and reliability are essential in this respect. It is for this reason that modern aerodynamic theory is being applied to wind turbine research with increasing vigor in the United States and abroad.

One particular area of active research has been vertical axis wind turbines (VAWTs), or Darrieus rotors. VAWTs have proven to be an especially challenging area of research because of rapid changes in flow direction, velocity, and loading associated with their motion.

Encouraging results from the use of vortex generators on conventional horizontal axis wind turbines prompted testing of these devices on a VAWT. The results demonstrated a marked increase in power output for certain configurations, indicating that significant gains might be achieved from a more intensive study of the effects of vortex generators on airfoils undergoing large amplitude pitch oscillations.

A. Review of Literature

Unsteady aerodynamics in general, and dynamic stall in particular, have been areas of active research for some time. A theoretical basis for unsteady inviscid flow was originally formulated by Theodorsen and outlined by Bisplinghoff [1]. This work was expanded upon by Gormont for application to helicopter rotors [2]. In addition to the radial flow and

compressibility effects, Gormont used existing experimental data to develop an empirical dynamic stall correction to the inviscid theory. More rigorous experimental and theoretical investigations of viscous interaction in unsteady aerodynamics have been attempted by McCroskey et al. [3,4], Jumper [5,6], and others.

One common element of almost all the experimental and theoretical investigations in unsteady aerodynamics done to date is their restriction to small amplitude oscillations. This is in direct contrast to the situation encountered by a Darrieus rotor blade, however. The work involving large amplitude oscillations, specifically by Walker [7], is of a qualitative nature only. Parashcivoiu [8] has used a vortex panel method to describe the flowfield of a Darrieus rotor specifically, but no viscous correction was applied. In order to successfully develop any theoretical or empirical model of airfoil performance in the Darrieus rotor environment, a comprehensive set of experimental data for airfoils undergoing large amplitude oscillations is needed.

The application of vortex generators to improve airfoil performance has developed a great deal in recent years. A good outline of vortex generator types and applications is given by Pearcey [9]. The specific use of vortex generators on wind turbine airfoils was addressed by McMasters et al. [10], and the vortex generators were found to nearly double the maximum lift in some situations. Extensive field tests of vortex generators on horizontal axis wind turbines have been done, [11, 12], and they have been found to be a viable method for increasing power output under certain conditions.

The only known paper that addresses the use of vortex generators under oscillatory conditions was by Moss and Murdin [13]. Even though the oscillation amplitudes were relatively low, tests made in the stall region demonstrated a significant increase in maximum lift. These results, coupled with the results of tests of vortex generators on vertical axis wind turbines, pointed to the need for a qualitative and quantitative

series of tests examining the effects of vortex generators on airfoils undergoing large amplitude pitch oscillations. This document is a presentation of the results of a series of such experiments.

B. Test Objectives

The testing consisted of wind tunnel runs of a wind turbine airfoil model under oscillatory conditions similar to those seen by a Darrieus rotor blade section. Specifically, the tests were designed to determine the effects of vortex generators on the lift, drag and pitching moment of a wind turbine airfoil oscillating over a range of frequencies and amplitudes. The objective of this series of tests was to discover any trends in the data that might aid in optimizing vortex generator position and size, as well as to develop a deeper understanding of the aerodynamics of airfoil performance under such conditions.

Presented here are results for a NACA 0021 airfoil at a Reynolds number (based on chord length) of approximately 1.20 million. Both steady-state and oscillatory data are presented for the clean airfoil and the airfoil with two different chordwise vortex generator locations. The airfoil was oscillated at several frequencies ranging from 0.3 Hz to 1.3 Hz. This corresponds to a range of reduced frequencies from 0.009 to 0.034, where reduced frequency is given by the following relation:

$$k = \omega c/2U_{\infty} \quad . \tag{1}$$

In addition to the frequency variation, the tests were conducted at maximum amplitudes of oscillation of plus and minus 10°, 20°, and 30°.

II. EXPERIMENTAL APPARATUS

A. Wind-Tunnel Facilities

The series of tests to be presented here was conducted in the low-speed wind-tunnel facility at The Ohio State University Aeronautical and Astronautical Research Laboratory (AARL). The low-speed wind tunnel is a continuous flow, open return tunnel constructed primarily of wood and fiberglass. The airflow is driven by a 125-hp 440-volt electric motor connected through a set of belts to a six-bladed 8-ft diameter fan located at the tunnel exit. The wind velocity is controlled by blade pitch angle. Blade pitch is set manually and independently for each blade and can be varied from 0 to 20 degrees, resulting in a test section velocity range from 10 to 220 ft/s.

The tunnel test section measures approximately 39 in. high, 55 1/2-in. wide, and 96 in. long (Figure 1). The walls of the test section are designed with a 0.7-degree divergence in the flow direction to minimize buoyancy effects resulting from the growth of the wall boundary layer. Vortex generators are located in the diffuser, 2 ft behind the test section, to help maintain attached flow in the wide-angle diffuser.

The airfoil model is mounted vertically in the tunnel by removing the ceiling of the test section. The model is anchored by a 1 1/2-in. diameter pipe imbedded in the model and passing through the floor and ceiling of the test section. A foam and Mylar seal is used to close any gap between the airfoil model and the tunnel ceiling and floor. In addition to the removable ceiling, a hinged Plexiglas window on the north wall allows observation and access to the test section.

Flow conditions (total and static pressure) are measured in the test section by a Pitot probe and two static pressure ports located near the beginning of the test section. A north-south traversing Pitot probe is mounted two chord lengths downstream of the model to allow wake total pressure deficit measurements for drag determination.

The necessity of acquiring accurate pressure data from a time-dependent oscillating system immediately suggests the need for a data acquisition system capable of sampling a number of signals quickly with little or no lag. An electronically scanned pressure measurement system manufactured by Pressure Systems, Inc. (PSI), was already available for use in the low-speed facility, and was found to be the most cost effective means of satisfying these requirements. In addition to the system's ability to measure 64 individual pressures and 32 analog inputs at a satisfactory sample rate, the pressure scanners were small enough to be mounted directly inside the airfoil model, thereby minimizing any pressure response problem.

B. Model Design and Construction

The predominant concern in the design of the airfoil models was to make them strong enough to withstand inertial and aerodynamic loads while keeping the model moment of inertia as low as possible. A combination fiberglass skin, foam interior, and wood-rib reinforced design was determined to be the best means of accomplishing this objective.

The construction of the NACA 0021 airfoil model was done by a local contractor according to design specifications (Figure 2). The model was constructed with a nominal 14-in. chord and 38 1/2-in. span. The span dimension allowed for a 1/4-in. foam rubber and Mylar seal to be added to both ends of the model. The seals allowed model oscillation without damage to tunnel walls and eliminated any gap airflow problem. The 1 1/2-in. diameter stainless steel pipe necessary for model mounting and oscillating was located at the 1/2 chord location. The model was supported at the top and bottom tunnel walls by tapered bearings in order to minimize friction.

Fifty-four pressure taps were located in the model surface at the tunnel centerline location. The pressure taps were 0.04 in. in diameter and were connected by polyurethane tubing to the pressure scanner compartment.

The pressure scanner compartment was divided into two separate sections, one on each side of the steel pipe. Each section held a separate pressure scanner module. The pressure tap lines were divided between the sections so as to minimize the lengths of tap lead-in tubing required. In order to keep the tap lines relatively short, the door to the compartment was placed 3 in. below the tap locations, allowing the lines to be no longer than 10 in. The door was designed flush with the model surface and was secured by 10 flathead screws.

The model fabrication process began with construction of a female mold made from a male counterpart constructed from profile coordinates. The female mold was made in separate upper and lower surface parts. The fiberglass skin was laid up and the ribs attached. The mounting pipe was then fastened to the four wooden ribs. After the taps were drilled and the lines laid out, the shells were bonded together and held by the molds while liquid foam was injected between the ribs. The surface was then filled, finished and painted to complete the model construction.

C. Oscillation System Design and Construction

The design of the oscillating drive system centered on the ability to maintain a consistent, clean wave form under different loading conditions and at various oscillation frequencies. Previous experience in the design of such systems pointed to a cam-driven mechanical system as having the greatest chance of success. Design, construction cost, and time were minimized, since such systems were already available for adaptation from previous experiments.

The initial drive system was powered by a 1/3-hp dc electric motor with variable speed control. The motor was connected via belts and an idler shaft to a camshaft and flywheel combination. The cam follower was mounted on a shaft pinned at one end. The follower arm was connected by a tie rod to a drive arm clamped onto the model pipe. In this way the wave function of the cam was transferred directly to the airfoil model. The cam follower maintained contact with the cam surface through the use of a coil spring. Unfortunately, at higher oscillation frequencies the spring was not stiff enough to maintain this contact, and the waveform degraded. A

higher tension spring could not be overcome by the motor. Use of this system was discontinued in favor of a higher powered face-cam system.

The face cam system was originally designed for use with the AARL transonic tunnels and was adapted for use in the low-speed testing facility (Figure 3). In the face-cam system, the cam follower rides in a track or groove in the cam face instead of on the outside edge. Thus, the follower is limited in its ability to lift off the surface. The design of this system was similar to the previous one, differing only in the type of cam used and the motor. The face-cam system was powered by a 5-hp ac motor with frequency controller. The amplitude and waveform of oscillation were controlled by cam design. Frequency was determined by the motor speed as set by the controller.

Three cams were available for use in the face-cam system: a 10° amplitude sine function cam and two inverse-tangent function cams with maximum amplitudes of 20° and 30°. These cams were chosen so airfoil performance could be evaluated under unstalled, initial stall, and deep stall conditions respectively. The waveform of the inverse-tangent function is given by the following equation:

$$\alpha = \arctan \{\sin(k\lambda U_\infty t/c)/[\lambda + \cos(k\lambda U_\infty t/c)]\} \quad . \tag{2}$$

This equation models the angle of attack of a blade section of a Darrieus rotor operating at constant rotation rate.

Minimizing pressure response problems was a major concern throughout the experimental apparatus design process. A simple analysis was made for an idealized model of the pressure tap-tube-transducer combination, consisting of a 12-in. long, 0.04-in. diameter tube connected to a reservoir with ten times the volume of the tube itself. A theoretical method for analyzing the pressure response of such a system was outlined by Delio and Schwent [14]. Frequency response of such a system is given by the following equation:

$$G_e^{i\tau} = \left[-\left(\frac{\omega}{\omega_o}\right)^2 + 2i\xi \frac{\omega}{\omega_o} + 1 \right]^{-1} . \qquad (3)$$

For the configuration outlined above, the undamped natural frequency and damping factor are given by the following relations:

$$\omega_o = \left[\pi r^2 \gamma g RT/LV \right]^{1/2} \qquad (4)$$

$$\xi = \left[4\mu/pr^3 \right] \left[VLgRT/\pi\gamma \right]^{1/2} . \qquad (5)$$

A 10-Hz sinusoidal input at typical test section conditions results in a gain of 98% with a 12° phase lag. As a conservative estimate of pressure response, this result shows the loss in pressure amplitude and change in phase to be insignificant. No attempt was made, therefore, to account for these effects in the data reduction.

III. TEST PROCEDURES

A. Data Acquisition System

The data acquisition system used in these experiments centered around the PSI pressure measuring system consisting of the following:

780B Data Acquisition and Control Unit (DACU)
780B Pressure Calibrate Unit (PCU)
80-IFC Interface Module
RAMM 30 (Remotely Addressed Millivolt Module)
2 ESP-32 Pressure Scanners

The ESP-32 Scanners each have 32 input pressure ports connected to 32 individual piezoresistive transducers. Model surface pressure measurements were made by electronically scanning the outputs of these transducers.

Calibration of the pressure scanner module transducers was done before each run to ensure minimal output drift problems. To calibrate, the PCU applied regulated pressures to all transducers simultaneously. The DACU then computed calibration coefficients for each transducer and saved those coefficients to disk for later use in data reduction.

In addition to the model tap pressures, the following data were also acquired:

Test section freestream conditions (total and static pressures)
Model angle of attack
Traversing wake probe position
Wake total pressure

For the above measurements, the desired quantity was converted to an analog voltage signal which was wired directly into the RAMM 30 module.

One scan of data could be completed by sampling, in series, each transducer in the pressure scanners and each channel in the RAMM 30 module. This allowed data to be acquired at rates up to 50 Hz.

The PSI Pressure Measurement System was controlled through an IEEE 488 Serial Interface connected to an IBM PC/XT microcomputer. The operator could vary both the data sample rate and the number of samples taken. After completing a "run," the raw data were passed from the DACU to the IBM PC and written directly to floppy disc. A schematic of the data acquisition system is shown in Figure 4.

Freestream total and static pressures were measured through the use of differential pressure transducers of 2 psid range or less. Tunnel north side static, south side static, and total pressures were measured. Excitation voltages were supplied separately for each transducer by individual carrier demodulators. All transducers were calibrated over a 0.5 psid range to a maximum of 5 volts full scale. Transducer bench calibration was done by using a water manometer and was electrically checked before each set of runs by using the shunt resistor calibration technique. The transducers were mounted as near as possible to the actual orifice so as to minimize pressure response problems in the connecting lines. As was previously stated, the output voltage of each transducer was wired into a separate channel in the RAMM 30 module. Three open ports on the pressure scanner modules were also connected to static and total pressure ports in order to provide a secondary measure of the tunnel conditions. These measurements were not used for the actual data reduction; they were used only for cross-checking.

Angle of attack was measured by a potentiometer coupled to the upper end of the stainless steel mounting pipe. In this way geometric angle of attack could be measured directly. Excitation voltage for the potentiometer was supplied by a 5-volt dc power supply. Calibration of the potentiometer was done before each series of tests through the use of fixed angle markings on the wind tunnel wall. The accuracy of this procedure was on the order of 1/4 degree which was judged sufficient for the type of comparisons to be made.

In order to determine the drag on the airfoil under steady-state conditions, a wake momentum deficit method was used. The steady flow assumption is implicit in this scheme and therefore these measurements were not taken for oscillating airfoil tests. The measurement of wake total pressure was accomplished through the use of a traversing Pitot probe attached to a gear drive system. Probe position was measured through the use of a potentiometer geared into the drive system. The wake probe extended 22.5 in. into the test section in fully retracted position and was located approximately 6 in. above the pressure tap line in order to minimize any interference.

A 0.5 psid pressure transducer was connected to the wake Pitot probe with a polyurethane tube. The transducer operation and calibration were exactly the same as for the transducers referred to earlier. The operator set the desired length of traverse and number of samples in the wake measurement, and output voltages were sampled and stored on the IBM PC for later determination of wake size and location.

B. Data Reduction

Most of the data reduction system used for this series of experiments was written specifically for this purpose. Significant portions of the program, however, were taken from previous versions of data reduction software available at AARL. The reduction process was done on a Harris H800 Superminicomputer and required the transfer of acquired data from the IBM PC to the Harris. The data reduction process was done completely by computer although certain processes (e.g., limits for wake integration) required user interaction.

The dynamic pressure was computed for each data scan from total and static pressure measurements, and was then used to nondimensionalize the data from that scan. In this way, variations in test section velocity could be taken into account.

Pressure coefficients were determined for each tap location through a standard non-dimensionalization process. Once the coefficients were

determined, numerical integration of the results yielded normal force, axial force, and moment coefficients for each data scan. The integration scheme was an airfoil pressure integration routine in standard use at the AARL. Finally, by applying the model angle of attack, the lift and pressure drag coefficients could also be determined. No averaging of measurements was done for oscillating tests; however, twenty data scans were averaged for each steady-state data point.

Wake total pressure measurements were made for varying length traverses with a density of approximately 12 samples per inch. The total pressure deficit in the wake was integrated to determine the drag coefficient using the Jones equation given by Schlichting [15];

$$C_D = 2/c \int u/U_\infty(1 - u/U_\infty)\, dy \quad . \tag{6}$$

Wind tunnel blockage and streamline curvature corrections as given by Rae and Pope [17] were applied for the static data. Due to the unsteady nature of oscillating airfoil data, standard corrections could not be applied with confidence. Consequently, no corrections were applied to the time-dependent data.

The reduced data from each wind tunnel run were output both in tabular and graphical form. Typical reduced data plots are given in Figures 5 and 6. Due to the excessive volume of data for the oscillatory tests, only cycle-averaged data are presented here. However, a comparison of unaveraged data with cycle-averaged data is displayed in Figure 7.

C. Test Procedure

A typical sequence of wind-tunnel runs began with the installation of vortex generators. The vortex generators used in this series of tests were supplied by Sandia National Laboratories. They are of the counter-rotating vane type and were punched out in thin metal strips, the dimensions of which are given in Figure 8. Only this single vortex generator configuration was tested, although tests were made with generators at two separate chord locations.

Applying the vortex generators to the model surface while still allowing them to be removed without damage to model or generators was a problem. Several methods were tried before one was found to be satisfactory. Carpet tape was laid down in a strip on the model surface, and the vortex generators were then applied on top of this strip. In addition small strips of tape were used to hold down the leading edge of each generator pair. Since the model was oscillating to large angles of attack about a zero mean angle, vortex generators were applied to both the upper and lower model surfaces.

Once the vortex generators were applied, a complete series of calibrations and static and oscillatory runs were performed. Just before the wind tunnel was started, calibration of facility transducers and potentiometers was performed. These calibrations were updated at least twice per day of testing. After initial tunnel start-up, calibration of the pressure scanning modules was performed. This scheme minimized the effect of temperature on the scanner modules. The wind tunnel then remained in operation until the series of runs for the particular configuration was completed. Typically, a series of runs consisted of a range of reduced frequencies for an oscillatory case, or a series of different angle of attack settings for a steady-state case. Raw data were stored directly on floppy disc for each run. After a series of runs was completed, the raw data were transferred to the Harris computer for reduction.

The wind tunnel data presented were acquired over a period of several weeks. Due to outside air temperature variations, the test Reynolds numbers had significant variation. Runs were repeated as necessary, and the resultant Reynolds numbers varied between 1.1 million and 1.29 million.

IV. RESULTS

A. Steady-State Data

Initial steady-state runs were made without vortex generators to provide a baseline of airfoil performance for the desired Reynolds number. The results of these runs are tabulated in Table 1, and are plotted in Figure 9. Twenty data points were taken for angles of attack ranging from -4° to 40°. Lift and pitching moment were calculated from surface pressure measurements, while drag was calculated from wake momentum deficit measurements. At the point of airfoil stall, the wake became too large and unsteady to measure accurately. Therefore, no wake data were taken for angles of attack exceeding 14°, and wake blockage corrections could not be applied beyond this point. Solid blockage and streamline curvature corrections were still applied, however. At high angles of attack the blockage became large enough to have a visible effect on measured velocity in the test section. An illustration of the drop in measured velocity vs. angle of attack is made in Figure 10. The plot shows a discernible drop in measured velocity for angles of attack exceeding 20°, indicating the difference between local velocity and measured velocity could be significant.

Representative pressure distributions for the airfoil without vortex generators are displayed in Figure 11. To maintain clarity, only one-third of the measured surface pressures are actually plotted.

Integrated airfoil-surface-pressure data for the 0.1c and 0.3c vortex generator locations are tabulated in Tables 2 and 3, and plotted in Figures 12 and 13 respectively. Data were acquired over the same range of angle of attack as for the clean case. The values of drag coefficient for the airfoil with vortex generators applied were found to depend strongly on the spanwise position of the wake probe. Apparently, the viscous cores of the vortices shed by the vortex generators were still discernible at this wake probe position. This effect was seen by McMasters et al. [10], but for a wake probe positioned much closer to the airfoil model. Figure 14 shows the variation in wake size and shape with position of the wake probe.

Several series of tests were made at different spanwise positions for both vortex generator locations in order to determine an average curve.

B. Oscillatory Data

Oscillatory data were taken for the three separate cams at frequencies ranging from 0.3 Hz to 1.3 Hz, corresponding to reduced frequencies ranging from 0.009 to 0.034. Concern over possible damage to the equipment limited the maximum reduced frequency to 0.023 for the 30° inverse-tangent cam. Figure 15 shows the angle of attack variation with time for each cam at a low reduced frequency. The signal quality is satisfactory although some "chatter" of the cam follower can be seen in the 30° inverse-tangent case. At the higher reduced frequencies the signals tend to flatten somewhat near the peaks, although signal quality remains adequate. The maximum amplitude for each cam was found to change by as much as 2° under different loading conditions. This could have a significant effect on data in the near stall or post stall region. The asymmetry of the inverse-tangent function is evident in both the 20° and 30° cams. Note the relatively slow rise in angle of attack followed by a sharp drop. Since the airfoil characteristics near stall depend on the rate of change of angle of attack, this asymmetry is important in the data analysis.

Just as in the steady-state case, a complete baseline of data for the clean airfoil was established. Integrated data for two frequencies and the three different cams are tabulated in Tables 4 through 9, and plotted in Figures 16 through 21. It should be pointed out once again that these data have been cycle averaged, so only one complete cycle is represented. Data repeatability from cycle to cycle was good, and the cycle averaging technique was found to be an accurate qualitative and quantitative means of displaying the results.

To illustrate more detail, pressure distribution time histories are shown in Figures 22 through 27. Cycle averaging was not used in these cases; a single time cycle was chosen from the data, and the pressure distributions for that cycle were displayed.

Oscillatory data for the two vortex generator locations are given in the same manner as for the clean airfoil case. Data are tabulated in Tables 10 through 21 and plotted in Figures 28 through 51, including pressure distributions.

An important point to note is that the drag measurements given in the oscillatory data are integrated-pressure values. The drag due to skin friction and any drag on the vortex generators are therefore not taken into account. As a result, care should be taken in drawing any quantitative conclusions from these drag data.

V. DISCUSSION

A. Steady-State Data

The C_L vs. angle of attack plot for the airfoil without vortex generators (Figure 52) is consistent with the trailing edge separation type of stall expected for a NACA 0021 airfoil in this Reynolds number range. In this respect the results are similar to those of McMasters [10]. In addition to the "shallow" type stall, the effects of trailing edge separation and boundary layer thickening also act to effectively reduce the airfoil camber. Thus, the lift curve slope in the linear region (about 0.091 per degree) is significantly below the 0.13 per degree value predicted by inviscid potential flow theory [16]. This effect can be seen even more clearly in the C_M vs. angle of attack plot (Figure 9) where inviscid analysis calls for a value of C_M of nearly zero over the full range of angle of attack. The wind tunnel data show a relatively large increase in pitching moment with angle of attack until airfoil stall is reached. The C_M rise is associated with the reduction in effective airfoil camber and correspondingly higher surface pressures over the model's upper surface. This effect increases with angle of attack until the flow separation associated with airfoil stall causes a drastic decrease in pitching moment about the quarter chord.

The effect of vortex generators in this situation is twofold; the higher energy boundary layer counters the effects of adverse pressure gradient and delays separation while also decreasing the boundary layer displacement thickness. The delay in separation allows for a higher than baseline maximum lift coefficient and stall angle, while the decrease in displacement thickness increases the lift curve slope. Both of these effects are readily apparent in Figure 52. The maximum lift coefficient is increased by over 50% with the application of vortex generators at the 0.1c location. In addition to the effects seen near stall, the lift curve slope in the linear region is increased to a value of approximately 0.12, which is very close to the 0.13 value predicted by inviscid flow theory. The airfoil stall with vortex generators in place is very sharp in comparison

with the clean airfoil data, an effect also observed by McMasters [10]. Examination of the pressure distributions shows that the flow is separating very near the leading edge.

The increase in lift curve slope resulting from the application of vortex generators at the 0.3c location is greater than that for the 0.1c location. However, the vortex generators at the 0.3c location do not achieve as large an increase in maximum lift coefficient or stall angle as for the 0.1c location. Some insight into this effect can be obtained by comparison of vortex generator height with boundary layer thickness. An order of magnitude estimation of the boundary layer thickness at 13° angle of attack was obtained from the Eppler airfoil design and analysis code [17]. Analysis showed that the boundary layer thickness at the 0.1c location is approximately one-quarter the height of the vortex generators, while at the 0.3c location the boundary layer thickness and vortex generator height are about the same. The effectiveness of vortex generators is related to the efficiency of the mixing taking place. As angle of attack increases, the boundary layer continues to thicken until the vortex generators, when located at the 0.3c location, lie well within the boundary layer itself. At this stage, the vortex generator effect is diminished, and the mixing of freestream air into the boundary layer does not take place. At the 0.1c location, however, the boundary layer never thickens enough to "swallow" the vortex generators; instead, the boundary layer eventually separates ahead of the vortex generator location.

Figure 53 shows a comparison of pressure distributions for the clean airfoil and the airfoil with the two vortex generator locations. The delay in separation associated with the vortex generators is clearly evident.

Figure 54 displays comparisons of drag coefficient for the clean airfoil and for the airfoil with vortex generators installed. Note the large increase in drag due to the vortex generators. It should be pointed out that, in this series of tests, vortex generators were mounted on both airfoil surfaces. Not only is the laminar flow over the lower surface lost, but the total drag resulting from the vortex generators is roughly doubled with respect to that reported from other sources which used vortex

generators mounted on only one airfoil surface. A comparison of the drag data for the two different vortex generator locations shows the drag to be lower for the 0.3c location as might be expected.

The effect of vortex generators on pitching moment as seen in Figure 55 is quite dramatic. The relatively large increase in pitching moment associated with the de-cambering effect seen in the clean case is almost completely eliminated. As a result the pitching moment about the quarter chord remains close to zero until the point of airfoil stall. In this respect the 0.1c vortex generator location is more effective, as it was for the maximum lift coefficient.

B. Oscillatory Data

A comparison of the C_L vs. angle of attack plots for the airfoil without vortex generators for the different forcing functions and reduced frequencies is made in Figure 56. Note the change in character of the curve for both an increase in amplitude and an increase in reduced frequency. In the case of the 10° sine cam the angle of attack always remains below the static stall limit; there is no significant stall hysteresis. As reduced frequency is increased, the hysteresis loop in the linear region of the lift curve widens. It should be pointed out that the hysteresis in the linear region is not associated with boundary layer phenomena, but can be predicted using unsteady inviscid flow equations.

The pressure drag results for the 10° sine cam remain near zero over the full range of angle of attack (Figure 57). This gives some support to the assumption that the tap distribution is giving an accurate representation of the pressure distribution on the airfoil surface. The effects of boundary layer thickening are evident in the pitching moment data (Figure 16) just as they were in the steady-state case.

For the case of the 20° inverse-tangent cam, stall hysteresis begins to play a significant role (Figures 18 and 19). One obvious characteristic is that the stall hysteresis loops are not symmetric for positive and negative angles of attack. This is due to the asymmetry of the cam

waveform referred to earlier. The magnitude of the maximum lift coefficient is greater for the negative angle stall due to the higher angular velocities in approaching stall. Conversely, the reattachment takes place sooner at the negative stall angles because the angular velocities are lower on the return portion of the cycle. This effect becomes more pronounced at the higher reduced frequency where the angular velocities are increased. As a result, the maximum lift coefficient, which increases only slightly over the steady-state value at the low reduced frequency, increases by 30% at a reduced frequency k=0.034. A corresponding increase in the stall angle also takes place.

The effects of airfoil stall are also evident in the pressure drag data, where the drag increase resulting from separation is plainly evident. The same is true for pitching moment, where the sharp change due to airfoil stall can be seen at both amplitude extremes.

The 30° inverse-tangent cam (Figures 20 and 21) gives results similar to the 20° amplitude cam. The difference arises from the extension of the angle of attack more deeply into the post stall region. As a result of this extension, the stall hysteresis is larger and the maximum lift coefficient is increased. Also, increases in pressure drag and magnitude of pitching moment are more evident.

The 10° sine function never reaches the stall region for the clean airfoil. Thus, the effect of vortex generators is primarily one of increasing the lift curve slope (Figure 58). Just as in the steady-state data the vortex generators located at the 0.3c location are more effective in increasing lift curve slope than the vortex generators at the 0.1c location. Also, the pitching moment is reduced to near zero for both vortex generator locations just as in the steady-state case (Figure 59).

The 20° inverse-tangent function reaches the stall region of the clean airfoil, and therefore the vortex generators affect both the lift curve slope and the airfoil stall. In the case of the 0.1c vortex generator location, the maximum lift is increased by 40% over the value for the clean airfoil at the low reduced frequency (Figure 60). Since the amplitude of

oscillation remains below the static stall limit for the 0.1c vortex generator location, the stall hysteresis evident in the clean airfoil case is all but eliminated.

In contrast, stall hysteresis is present for the 0.3c vortex generator location. The maximum lift coefficient for the airfoil with vortex generators at 0.3c is higher than that for the 0.1c vortex generator location, however. This is in direct contrast to the static data where the vortex generators improved maximum lift more at the 0.1c location. Some insight can be gained into this effect through examinations of the pressure distributions (Figure 61). The separation near the maximum angle of attack is clearly evident in the clean airfoil case. In contrast, the 0.1c vortex generator location case shows almost no separation throughout the cycle. When the vortex generators are located at 0.3c, separation occurs, but at a higher angle of attack than was observed for the static airfoil (Figure 13). The increased effectiveness of the 0.3c vortex generator location at higher angles of attack is probably due to a delay in boundary layer development associated with airfoil oscillation. This effect might prove important in an attempt to optimize vortex generator location.

Another important effect of the vortex generators located at 0.3c is the effect on airfoil lift in the post stall region (Figure 60). Note that even after airfoil stall the lift coefficient remains above the maximum value seen for the clean airfoil. It appears that the vortex generators may still have some beneficial effect even after significant flow separation has taken place. An examination of the pressure distributions shows that even though the amount of separation is comparable to the clean airfoil case, the suction peak near the leading edge of the airfoil is higher. A possible explanation is the vortex generators are reducing the size of the separated zone and thus increasing flow circulation. The ability of vortex generators to restrict the size of a separated region is mentioned briefly by Pearcey [9] in reference to reattachment of a laminar separation; but the ability of the vortex generators to reduce the effect of large-scale turbulent separation is not addressed.

The data for the airfoil with vortex generators installed exhibit the same characteristics with increased reduced frequency as the data for the clean airfoil (Figure 62). The maximum lift is increased by roughly the same amount for both the clean airfoil and the 0.1c vortex generator location. The increase in maximum lift is greater for the 0.3c vortex generator location, again probably due to an increased lag in boundary layer development.

In the 30° inverse-tangent case, the airfoil angle of attack exceeds the static stall limit of the clean airfoil by a significant margin. Figure 63 shows a comparison of the lift curves at the low reduced frequency for the clean airfoil and the airfoil with vortex generators at the two locations. In contrast to the 20° amplitude case, the airfoil with vortex generators at the 0.1c location also reaches stall. The maximum lift coefficient is maintained almost to the point of maximum amplitude, but the subsequent stall hysteresis is larger with the vortex generators at the 0.1c location than for the clean airfoil. Examination of the pressure distributions (Figure 64) shows that for the 0.1c vortex generator location, the suction peak is lost as a result of laminar separation. This effect does not take place at the low reduced frequency for either the clean airfoil or the airfoil with vortex generators at 0.3c. It is observed at the higher reduced frequency for the 0.3c vortex generator location, however. One possible explanation is the increased circulation resulting from the vortex generators creates a more adverse pressure gradient behind the minimum pressure point; the laminar separation bubble bursts resulting in complete laminar separation. This separation results in a drastic increase in pressure drag until the time of flow reattachment (Figure 65). Also, the drop in lift coefficient is larger and reattachment is subsequently delayed.

A comparison of maximum lift coefficient with reduced frequency for the 30° amplitude case is made in Figure 66. Note that the 0.3c vortex generator location improves maximum lift as a function of increased reduced frequency to such a degree that it actually gives a higher $C_{L_{max}}$ at the higher reduced frequencies than the 0.1c vortex generator location.

C. Theoretical Considerations

Large amplitude airfoil oscillation of the type seen here is an extremely difficult flowfield to model. In the unsteady environment, airfoil performance is influenced by wake vorticity as well as by strong viscous interaction in the stall region. An inviscid analysis for a flat plate undergoing small amplitude oscillations was originally formulated by Theodorsen [1]. The results of this analysis were modified by Gormont [2] for application to helicopter rotor blade environments. In addition to the modifications to the inviscid theory, an empirical dynamic stall correction was also applied based on static airfoil data. This method of analysis was applied to the experimental data obtained in this series of tests in order to determine its efficacy in predicting airfoil performance under large amplitude oscillations.

Figure 67 shows a comparison of inviscid theory with experiment for the 10° sine function. Note that the inviscid theory predicts a significantly higher lift curve slope than is actually obtained. When vortex generators are added (Figure 68), however, the experimental data match inviscid theory much more closely.

The method of empirical correction given by Gormont is outlined in the appendix. A comparison of the empirical dynamic stall correction with empirical data is made in Figures 69 through 72. The empirical result shows excellent agreement in the linear region for the low reduced frequency 20° cam case. The maximum lift coefficients and stall angle are also relatively close even though the hysteresis loops are somewhat undersized. As reduced frequency is increased, however, the empirical result differs more from the experiment, significantly underpredicting maximum lift coefficient and predicting flow reattachment at too high an angle of attack magnitude. The 30° amplitude case shows roughly the same sort of trend, but the minimum lift coefficient at negative angle of attack is not adequately predicted even at the low reduced frequencies.

An attempt was made to improve the results of the analysis through use of the experimental data from this series of experiments. Figures 73

through 76 show the results of this modified empirical analysis. The correction overpredicts the lift coefficient extrema at low reduced frequencies but shows a marked improvement at the high reduced frequency, both in the values of maximum and minimum lift coefficients and in the character of the stall hysteresis. An improvement is also seen in the correction for the 30° amplitude case, although the stall hysteresis is still not quite captured.

Gormont's analysis was designed for oscillation amplitudes much lower than those encountered here. Still, the method is remarkably successful in predicting, both qualitatively and quantitatively, the characteristics of large amplitude dynamic stall.

VI. CONCLUSIONS

The purpose of this research was to develop a better understanding of the effect of vortex generators on an airfoil under steady-state conditions and while undergoing large amplitude oscillations. A 14-in. chord NACA 0021 airfoil model was constructed so that reliable surface pressure measurements could be obtained under oscillatory conditions. The model was tested in The Ohio State University AARL Low Speed Wind Tunnel Facility at a Reynolds number of 1.2 million. Tests were conducted for the clean airfoil as well as for the airfoil with vortex generators at 0.1c- and 0.3c-chord locations. From the results of the static tests, the following observations can be made:

1. When located at the 0.1c position, vortex generators increase the maximum lift coefficient from the the 1.1 of the clean airfoil to 1.7. When the vortex generators are at the 0.3c location, maximum lift coefficient is increased to 1.5. The increase in maximum lift is associated with the ability of the vortex generators to delay or prevent trailing edge separation.

2. In addition to increasing the maximum lift coefficient, vortex generators also significantly increase the lift curve slope. While the vortex generators are more effective at increasing maximum lift when positioned at the 0.1c location, they are more effective at increasing lift curve slope when positioned at the 0.3c location.

3. When vortex generators are applied to both airfoil surfaces, a large increase in drag results. For the 0.1c vortex generator location, the averaged drag coefficient as measured by the momentum deficit at zero angle of attack increases from approximately 0.0085 to 0.0225. The drag coefficient at zero angle of attack for the 0.3c vortex generator location is 0.0195.

4. The variation in pitching moment about the quarter chord associated with boundary layer thickening and separation is significantly reduced by vortex generators. With vortex generators located at the 0.1c position, the pitching moment remains near zero up to an angle of attack of 24°, while vortex generators at the 0.3c location keep the pitching moment near zero up to 18° angle of attack.

The airfoil model was tested under oscillatory pitch conditions for three different waveforms about a zero mean angle. These waveforms consisted of a 10° amplitude sine function, a 20° amplitude inverse-tangent function, and a 30° amplitude inverse-tangent function. Tests were made at frequencies varying from 0.3 to 1.3 Hz for the same vortex generator configurations used in the static tests. From the results of these tests, the following observations can be made:

1. The maximum lift coefficient undergoes a large increase with increase in reduced frequency. For a change in reduced frequency from 0.009 to 0.034, the $C_{L_{max}}$ increases from 1.13 to 1.41 for the 20° amplitude oscillations. Similar results were seen for the 30° amplitude oscillations, although the maximum lift was higher over the whole range of reduced frequencies. Airfoil stall is caused by trailing edge separation, just as it is in the static case.

2. The ability of vortex generators to increase the lift curve slope in the static case holds for the oscillating airfoil as well. The vortex generators are more effective in this respect when located at the 0.3c location as opposed to the 0.1c location.

3. The increase in maximum lift coefficient associated with the use of vortex generators, when compared with the clean airfoil case, remains roughly constant with increasing reduced frequency for the 0.1c vortex generator location, but increases with reduced frequency for the 0.3c location in the range of frequencies examined.

The maximum lift coefficient for the 0.3c vortex generator location eventually exceeds that for the 0.1c vortex generator location as reduced frequency is increased for each oscillation amplitude. The lag in boundary layer development seems to allow the vortex generators to remain more effective to higher angles of attack when located at the 0.3c position than was the case under static conditions.

4. The vortex generators located at the 0.3c position seem to reduce the effect of separation on airfoil performance. Even though separation occurs, the lift coefficient remains higher than for the clean airfoil case with comparable separation.

5. For the 30° amplitude oscillations, the vortex generators located at the 0.1c position greatly reduce trailing edge separation but seem to induce a leading edge separation near the maximum angle of attack. This separation causes a large increase in pressure drag and delays flow reattachment on the return portion of the waveform. This phenomenon occurs for the 0.3c vortex generator location also, but only at the high reduced frequency.

It is unfortunate that total drag measurements could not be made under oscillating conditions. A large increase in total drag upon application of vortex generators is plainly evident in the static data, and there is no reason to expect this effect would be reduced for an airfoil oscillating in pitch. This would be an important factor in any aerodynamic application.

The need for further work in this area cannot be over-emphasized. Particular areas in which further research might prove fruitful are

1. Investigation of Reynolds number effects
2. Vortex generator configuration sensitivity
3. Drag measurements under oscillatory conditions.

In addition to the above, flow visualization techniques such as smoke or liquid crystals should prove useful in developing a more detailed understanding of the aerodynamics of the airfoil flowfield.

Theoretical analysis is also an area that may yield useful information, especially in the computational area. The empirical method for predicting airfoil performance developed by Gormont [2] for helicopter rotor analysis shows promise in predicting airfoil performance for large amplitude oscillations as well. More experimental data are needed in order to develop a generalized method for a variety of oscillatory conditions.

REFERENCES

1. R. L. Bisplinghoff, H. Ashley, and R. L. Halfman, Aeroelasticity, Cambridge Mass: Addison - Wesley Publishing, 1955.

2. R. E. Gormont, "A Mathematical Model of Unsteady Aerodynamics and Radial Flow for Application to Helicopter Rotors," USAAMRDL Technical Report 72-67, May 1973.

3. W. J. McCroskey and J. J. Philippe, "Unsteady Viscous Flow on Oscillating Airfoils," Journal of Aircraft, Vol. 13, No. 1, January 1975.

4. W. J. McCroskey and S. L. Pucci, "Viscous-Inviscid Interaction on Oscillating Airfoils in Subsonic Flow," Journal of Aircraft, Vol. 20, No. 2, February 1982.

5. E. J. Jumper and J. E. Hitchkock, "Investigation of Dynamic Stall Using a Modified Momentum-Integral Method," Presented at A.I.A.A., 25th Aerospace Sciences Meeting - Reno, NV, January 1987.

6. D. C. Daley and E. J. Jumper, "Experimental Investigation of Dynamic Stall for a Pitching Airfoil," Journal of Aircraft, Vol. 21, No. 10, October 1984.

7. J. M. Walker, H. E. Helin, and J. H. Strickland," An Experimental Investigation of an Airfoil Undergoing Large-Amplitude Pitching Motions," AIAA Journal, Vol. 23, No. 8, August 1985.

8. I. Paraschivoiu and J. M. Parrouffe, "Unsteady Potential Flow for Oscillating Airfoils," Canadian Aeronautics and Space Journal, Vol. 31, No. 2, June 1985.

9. H. H. Pearcey, "Shock-Induced Separation and Its Prevention by Design and Boundary Layer Control," in Boundary Layer and Flow Control, Its Principal and Applications, Vol. 2, edited by G. V. Lachman, Pergamon Press, Oxford, England, 1961.

10. J. H. McMasters and M. L. Henderson, "Recent Applications of Vortex Generators to Wind Turbine Airfoils in Subsonic Flow," Journal of Aircraft, Vol. 20, No. 2, February 1982.

11. G. W. Gyatt, "Development and Testing of Vortex Generators for Small Horizontal Axis Wind Turbines," NASA CR-179514, July 1986.

12. T. W. Nyland, "Surface Pressure Measurements on the Blade of An Operating Mod-2 Wind Turbine With and Without Vortex Generators," prepared for the US Department of Energy, NASA TM89903, August 1987.

REFERENCES
(Concluded)

13. G. F. Moss and P. M. Murdin, "Two Dimensional Low Speed Tunnel Tests on the NACA 0012 Section Including Measurements Made During Pitch Oscillations at the Stall," Ministry of Aviation Supply, Aeronautical Research Council C.P. No. 1145, London: Her Majesty's Stationary Office, 1971.

14. G. J. Delio, G. V. Schwent, and R. S. Cesaro, "Transient Behavior of Lumped-Constant Systems for Sensing Gas Pressures," NACA TN-1988, December 1949.

15. H. Schlichting, Boundary Layer Theory, New York, McGraw-Hill Inc., 1979.

16. J. D. Anderson, Fundamentals of Aerodynamics, New York, McGraw-Hill Inc., 1984.

17. R. Eppler and D. M. Somers, "A Computer Program for the Design and Analysis of Low-Speed Airfoils," NASA TM-80210, 1980.

18. D. W. Gross and F. D. Harris, "Prediction of Inflight Stalled Airloads from Oscillating Airfoil Data," Presented at the 25th Annual National Forum of the American Helicopter Society, Washington, D.C., May 1969.

APPENDIX

AN EMPIRICAL STALL HYSTERESIS CORRECTION TO INVISCID UNSTEADY AERODYNAMIC THEORY

The stall hysteresis correction method outlined by Gormont [2] is based on the assumption that dynamic stall effects can be expressed as a linear function of the parameter:

$$Q = \sqrt{c|\dot{\alpha}|/4U_\infty} \tag{7}$$

This method was originally developed by Gross and Harris [18]. Specifically this correction consists of the following equation.

$$\Delta\alpha_{ds} = \gamma\dot{\alpha}Q/|\dot{\alpha}| \tag{8}$$

where γ = an empirically determined constant.

A reference angle of attack is then defined as:

$$\alpha_{ref} = \alpha - \Delta\alpha_{ds} \tag{9}$$

In this way lift coefficient is given by:

$$C_L = \left(C_{L_{ref}}/\alpha_{ref}\right) \left(\alpha_{eq} + \bar{\alpha}\right) \tag{10}$$

where $C_{L_{ref}}$ is a value of C_L for an angle of attack equal to that obtained from static data. $\bar{\alpha}$ and α_{eq} are calculated from inviscid theory according to the following relations.

$$\alpha_{eq} = \sum_{n=1}^{\infty} \left[Fc\dot{\alpha}_n/4U_\infty + F\alpha_n + G\dot{\alpha}_n/\omega_n - Gk_n\alpha_n/2\right] \tag{11}$$

$$\bar{\alpha} = c\dot{\alpha}/4U_\infty \tag{12}$$

$$\omega_n = n\omega \tag{13}$$

$$\alpha_n = A_n \sin(\omega_n t) \tag{14}$$

$$k_n = \omega_n c/2U_\infty \tag{15}$$

This relationship holds for an arbitrary waveform given by the half range Fourier series:

$$\alpha = \sum_{n=1}^{\infty} A_n \sin(\omega_n t) \tag{16}$$

Note that the sign of $\Delta\alpha_{ds}$ is the same as that for $\dot{\alpha}$. Thus, for an increasing angle of attack, α_{ref} is less than α, and for decreasing α, α_{ref} is greater. In this way both the dynamic stall and delay in flow reattachment are accounted for. In the linear region of the static lift coefficient versus angle of attack curve, the value of C_L is unchanged. Only when α exceeds α_{ss} is the lift coefficient modified.

Gormont used test data for four different airfoils (V23010-1.58, NACA 0012 MOD, V13006-.7, NACA 0006) to develop a method for determining the value of γ. The resulting formula, based on airfoil thickness to chord ratio and Mach number, gives a value of 1.012 for the present case.

An attempt was made to improve the accuracy of the results by determining a new value of γ from the wind tunnel results. A plot of $C_{L_{max}}$ versus α was made and a value of 2.04 for γ was found to fit the available data more closely. The value 2.04 was used for data comparison purposes under the "Modified Gormont Model" label.

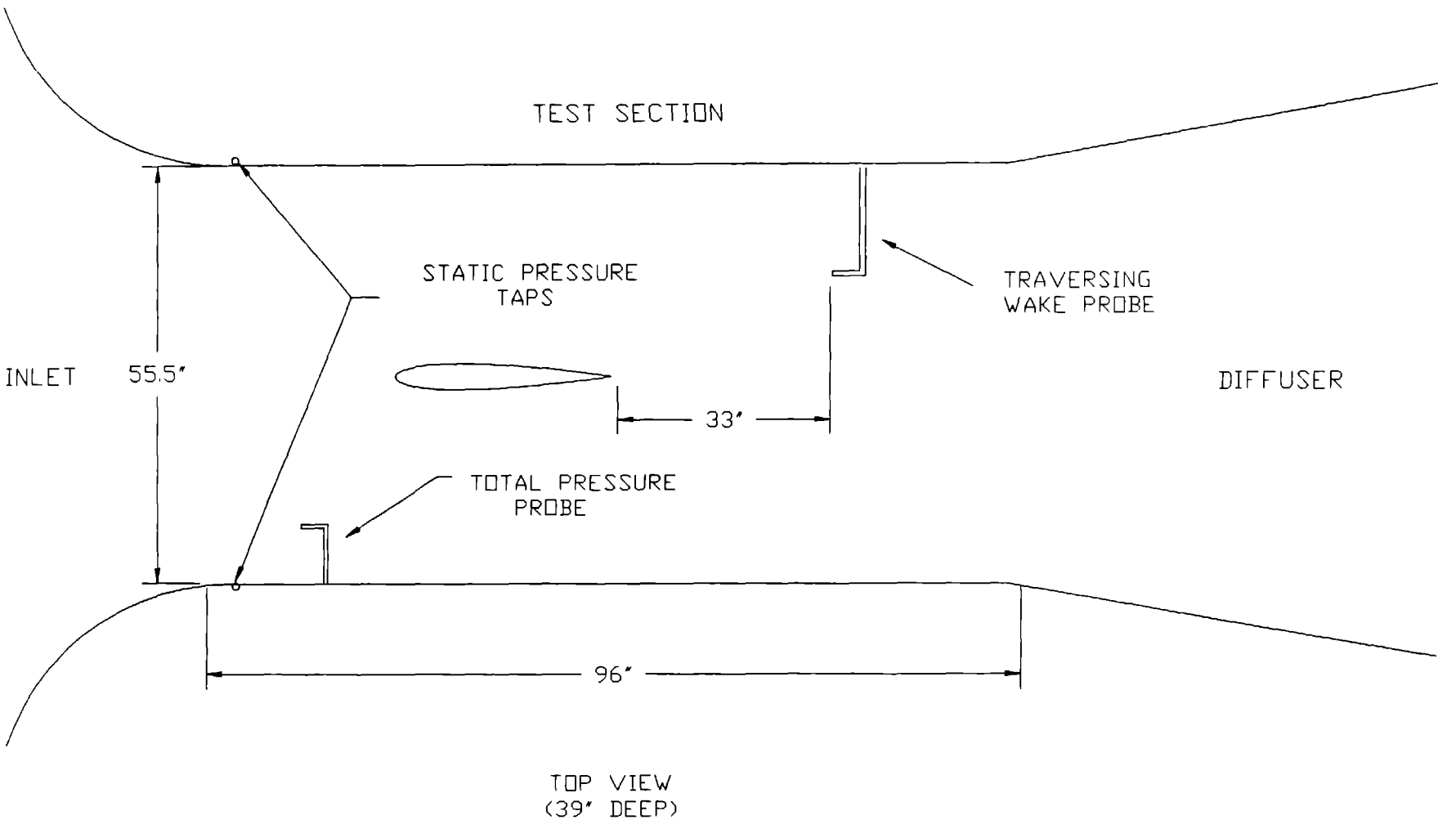

FIGURE 1. LOW SPEED WIND TUNNEL TEST-SECTION DESIGN

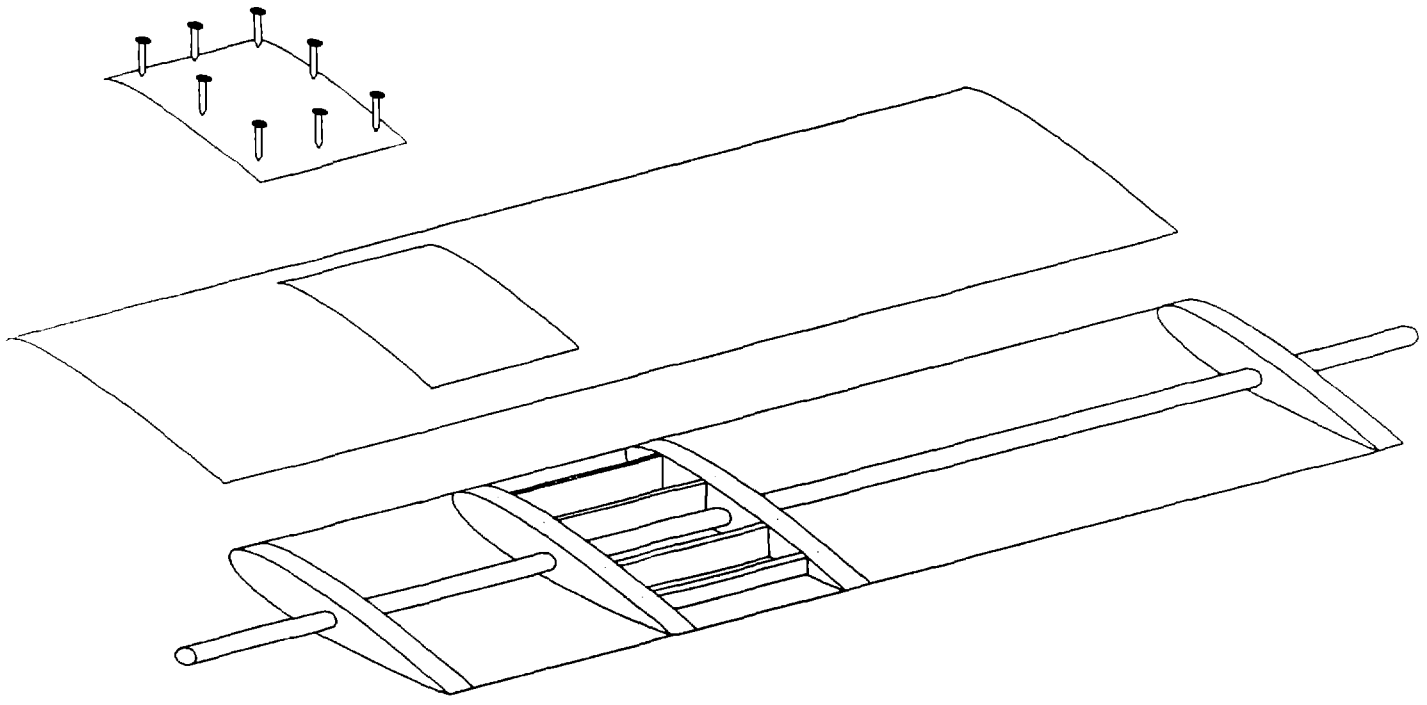

FIGURE 2. AIRFOIL MODEL DESIGN

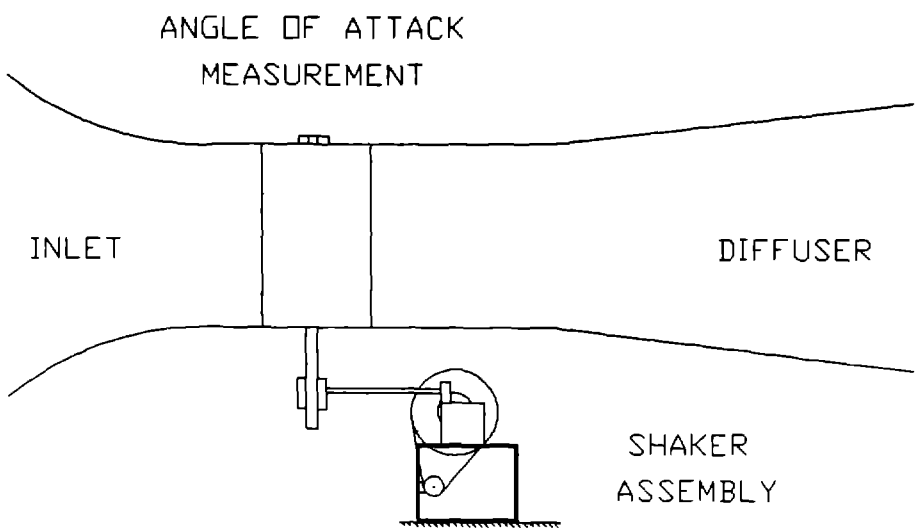

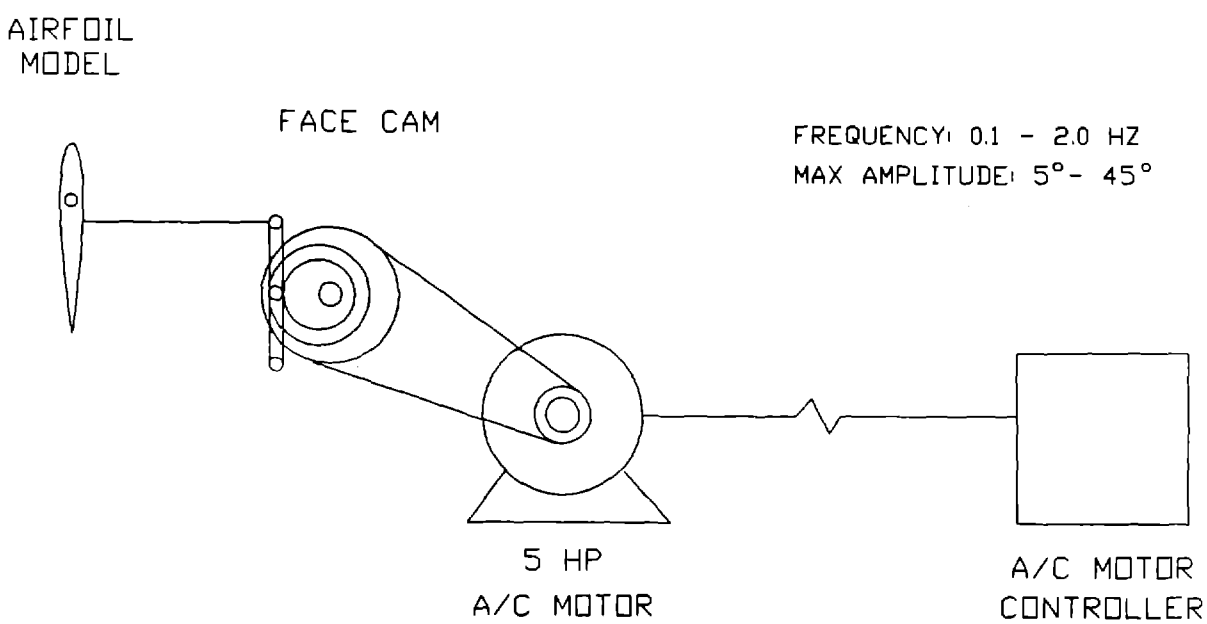

FIGURE 3. OSCILLATORY SYSTEM DESIGN

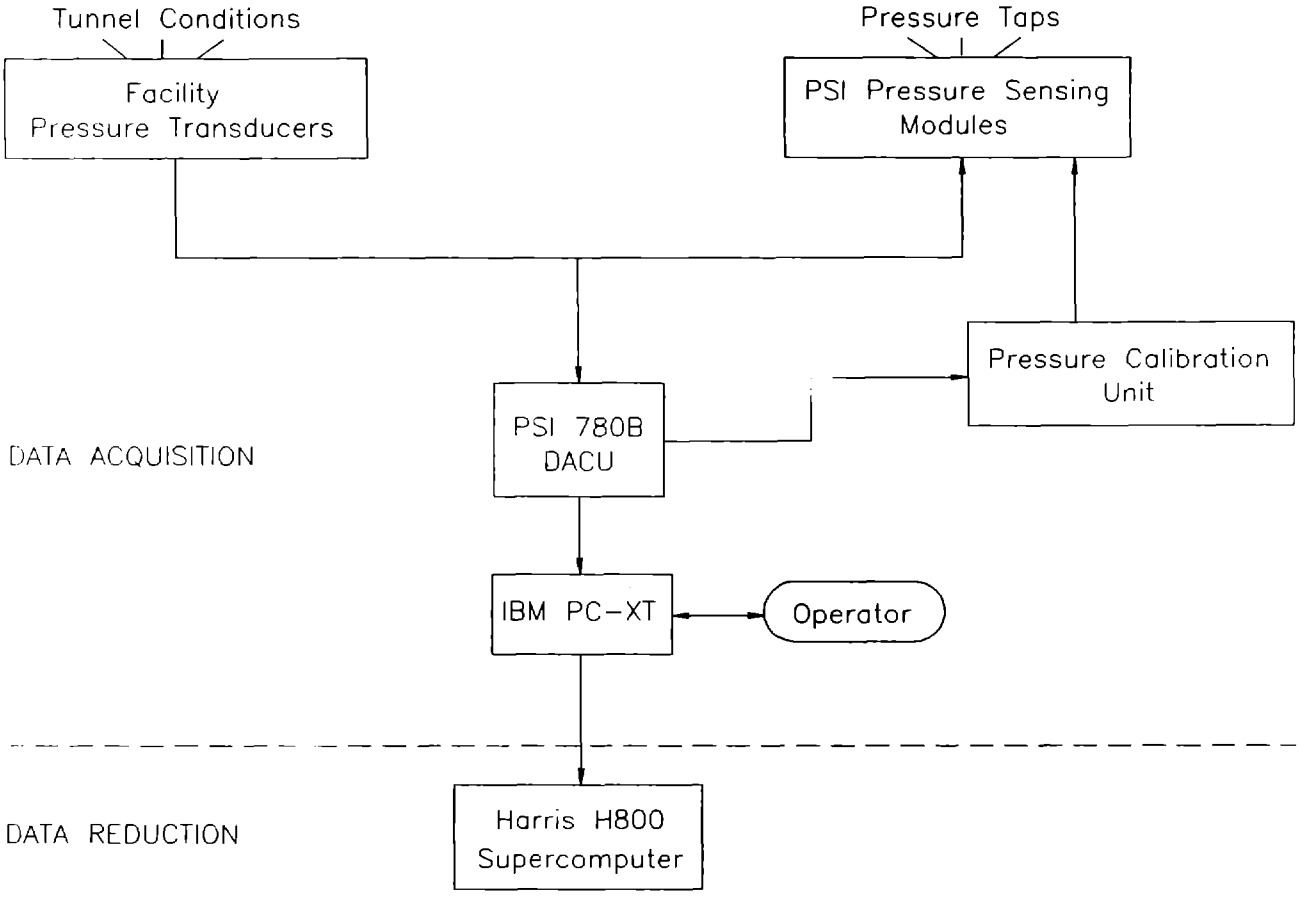

FIGURE 4. DATA ACQUISITION AND REDUCTION SYSTEM

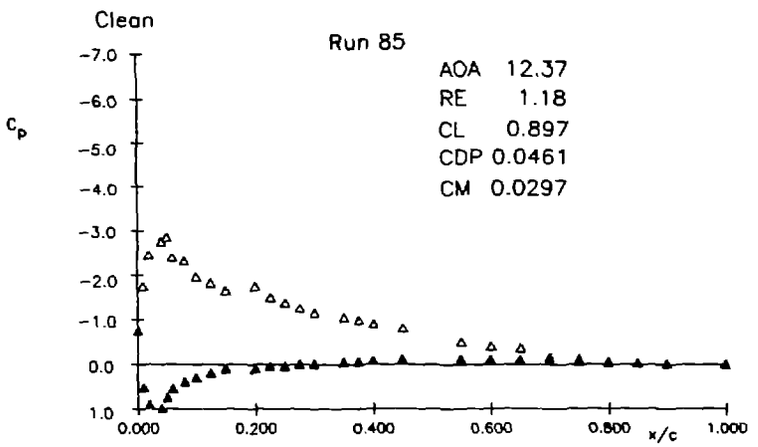

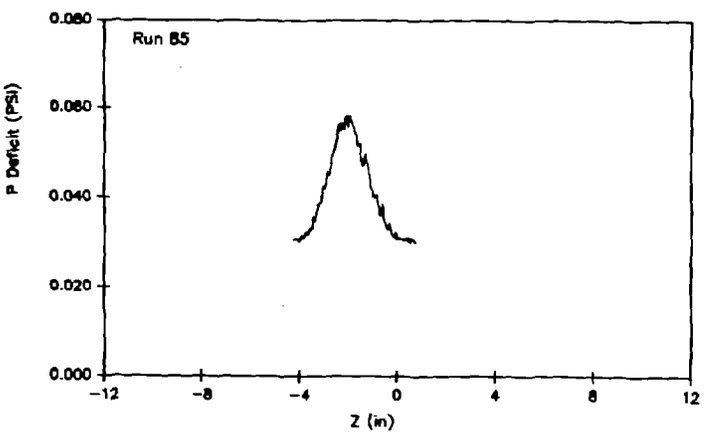

Figure 5. Typical Steady-State Output

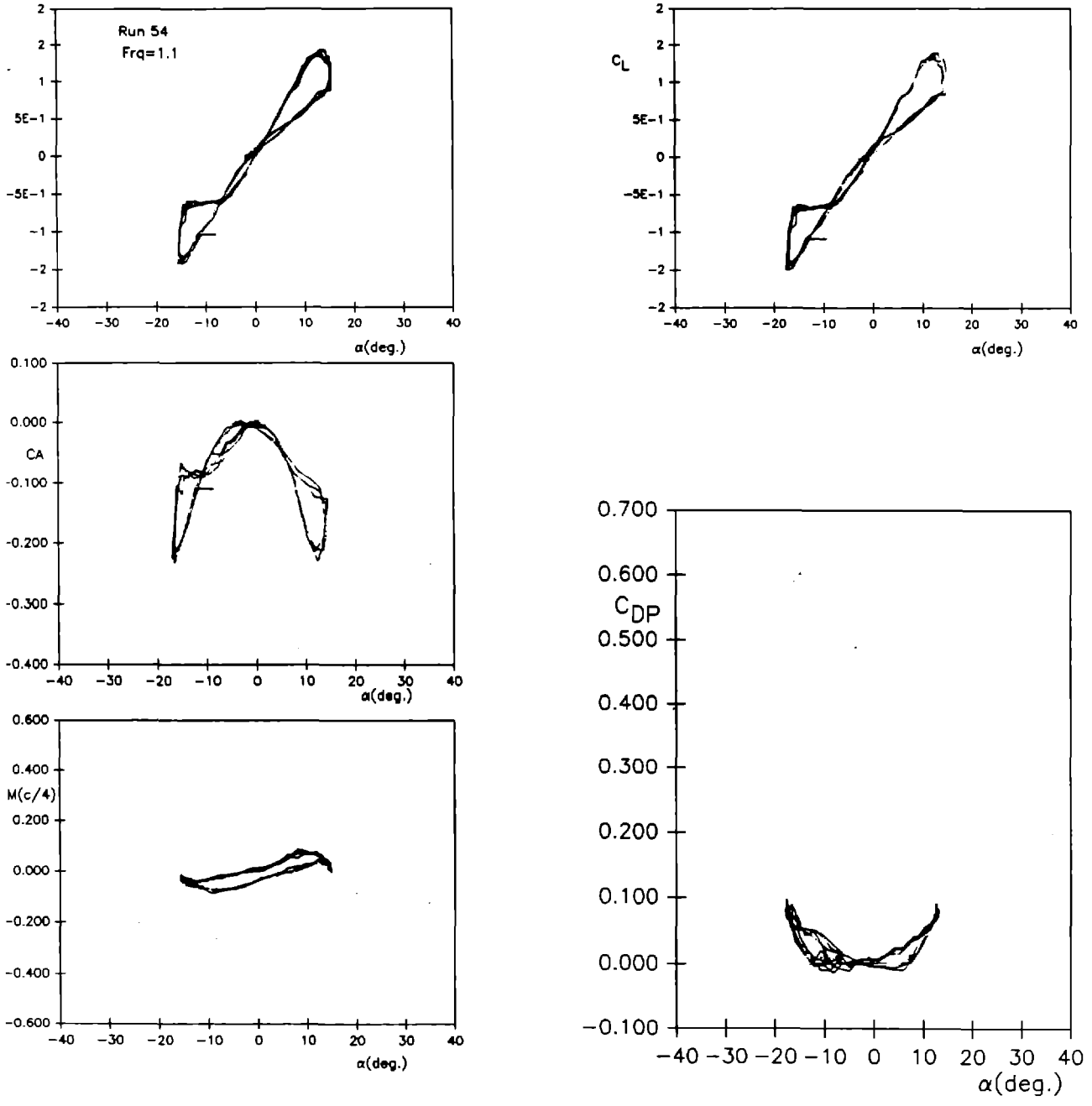

Figure 6. Typical Oscillatory Output

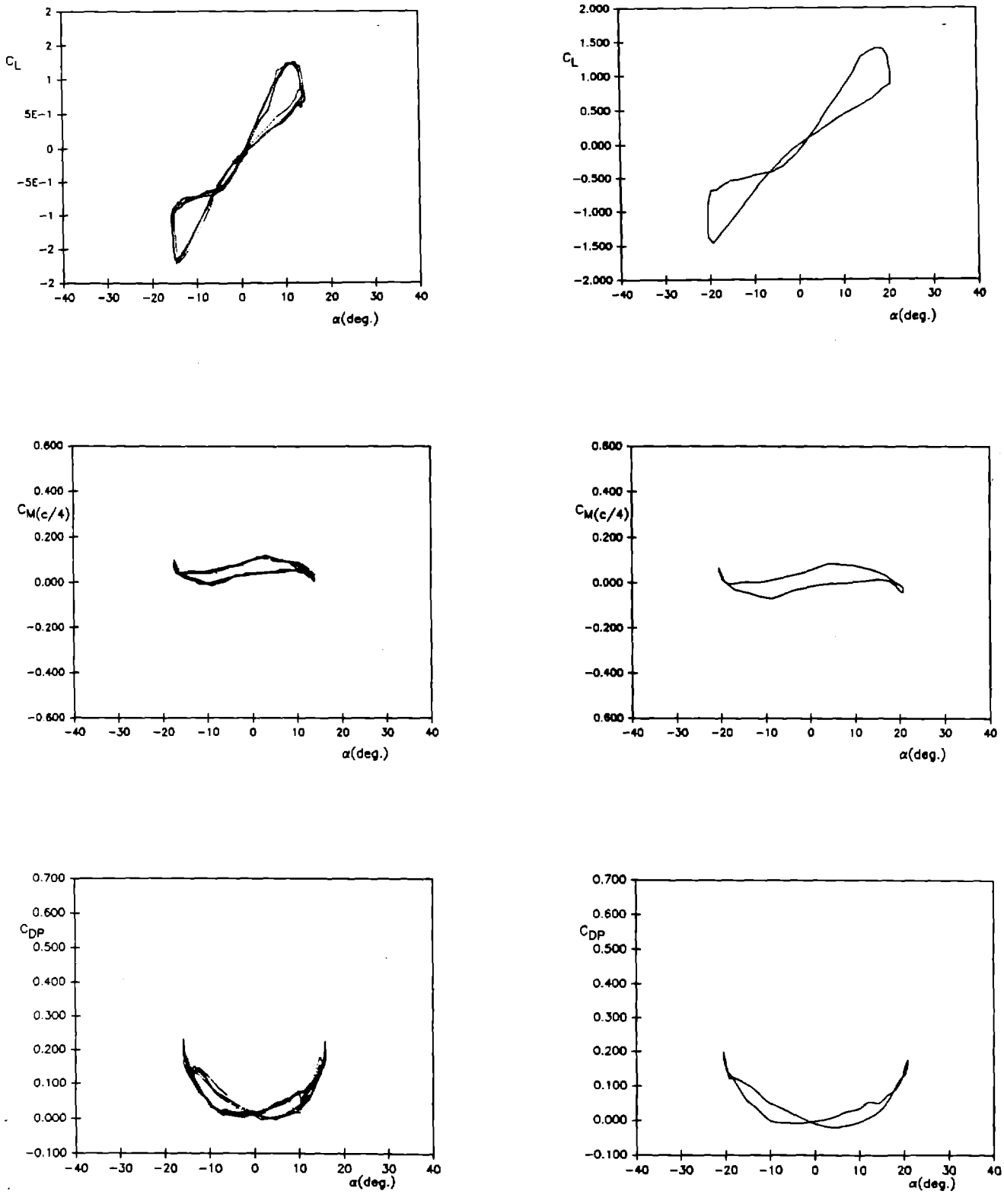

Figure 7. Comparison of Cycle Averaged Data

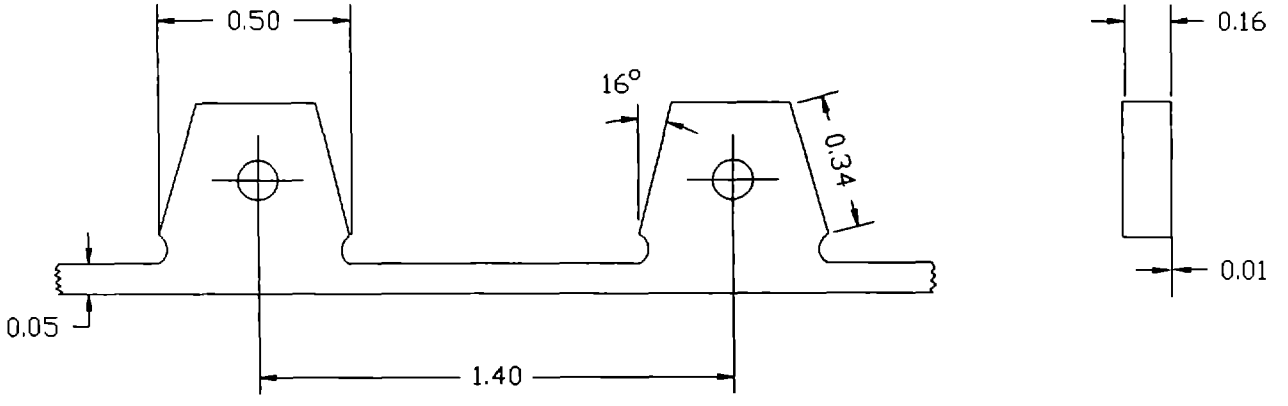

* all dimensions in inches

FIGURE 8. VORTEX GENERATOR CONFIGURATION

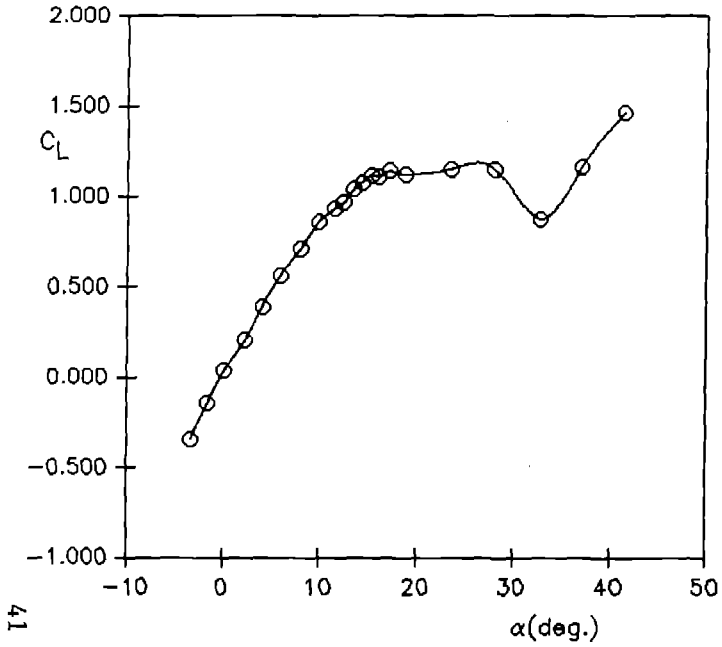

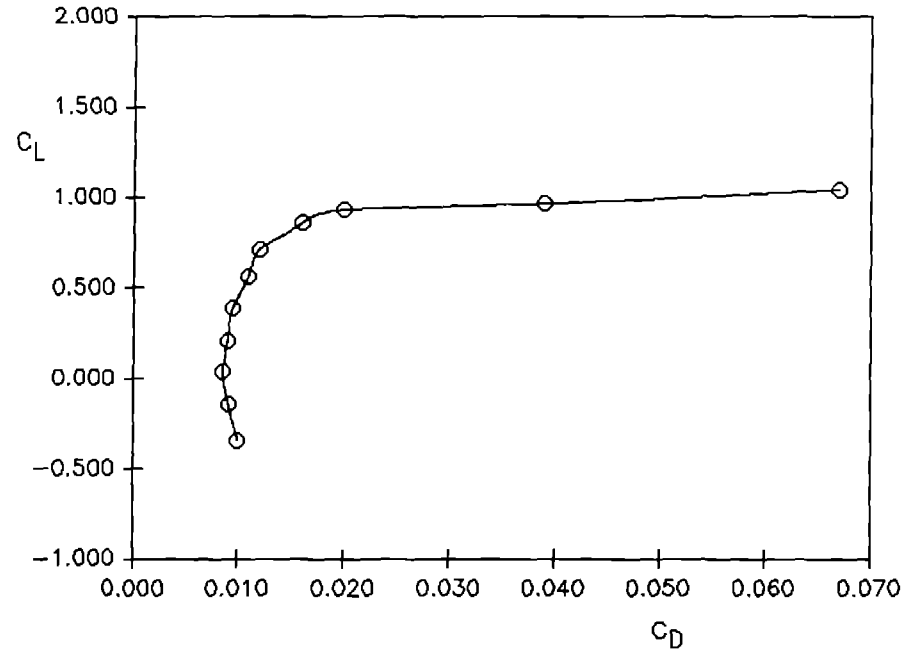

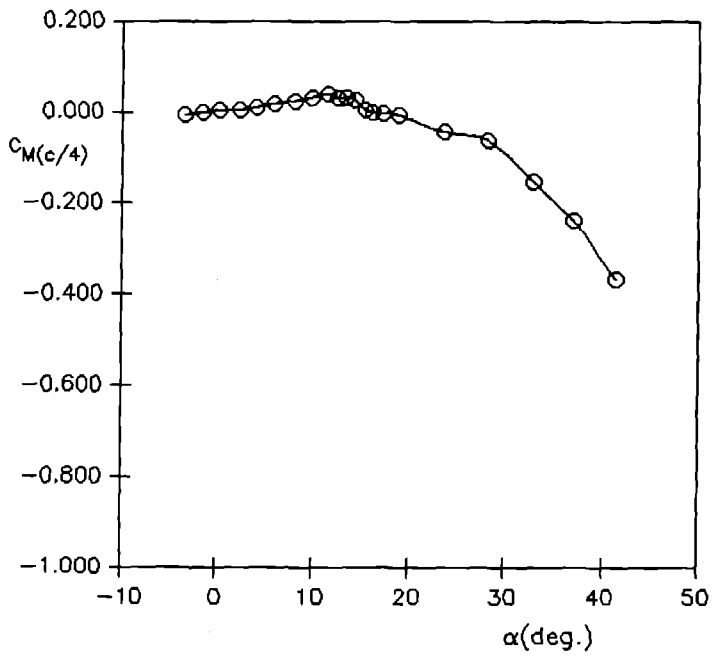

Figure 9. Integrated Static Data for NACA 0021 with No Vortex Generators

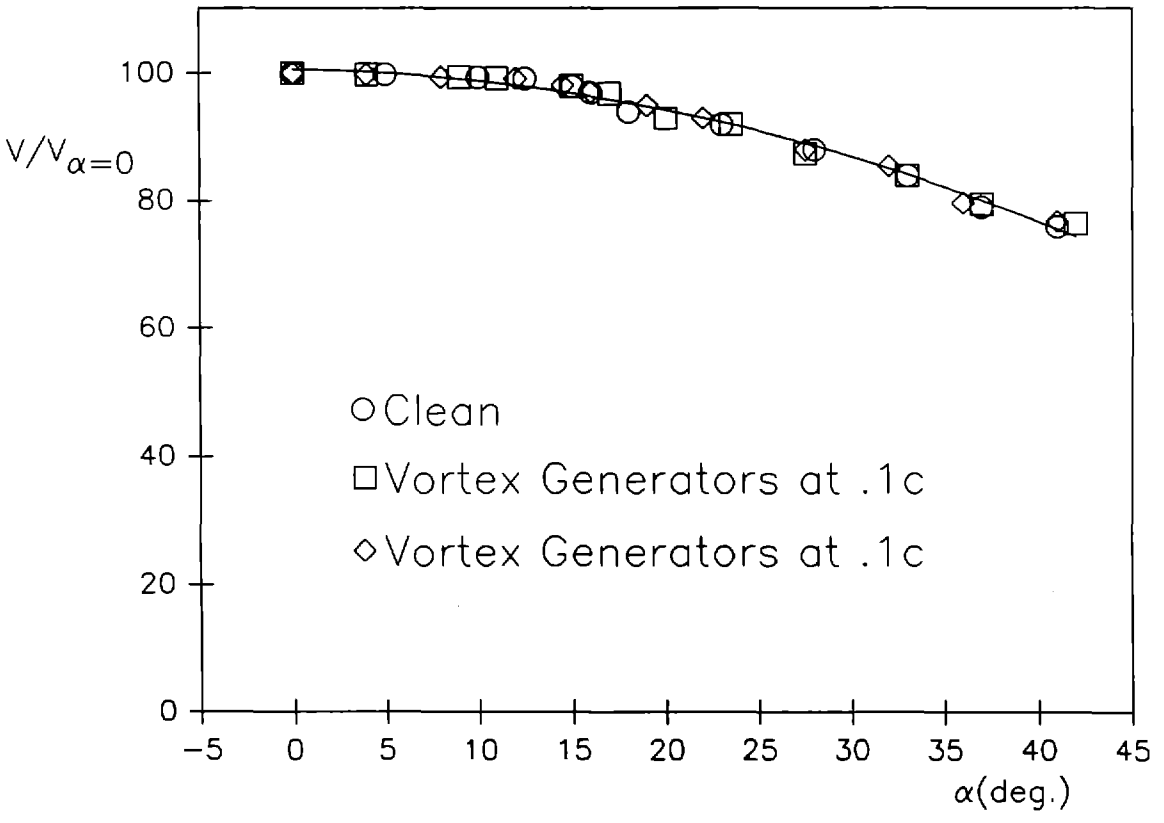

Figure 10. Percentage Loss in Measured Test–Section Velocity versus Model Angle of Attack

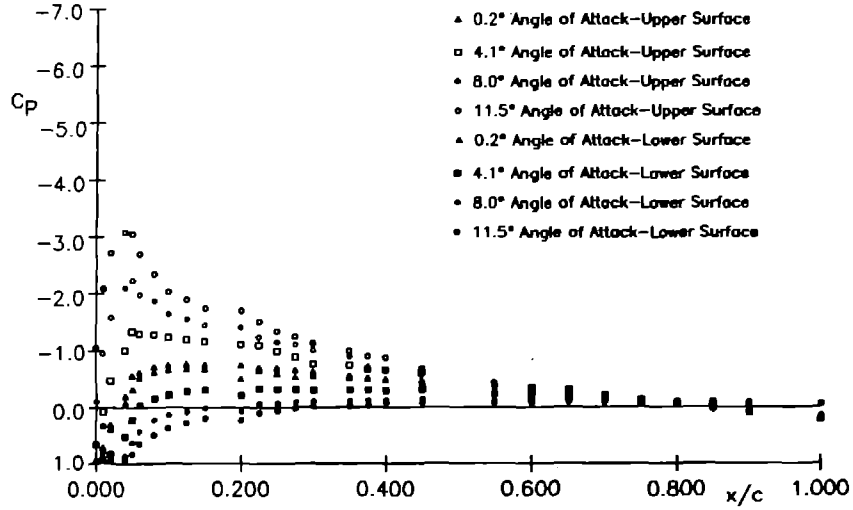

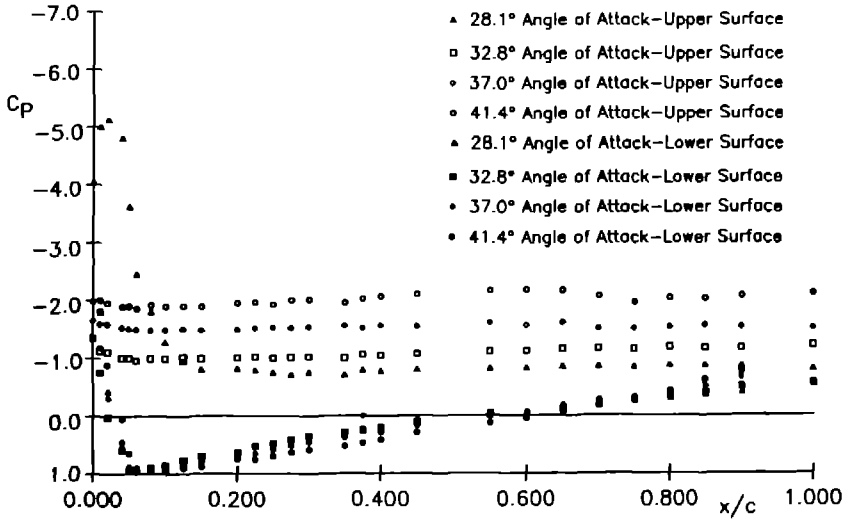

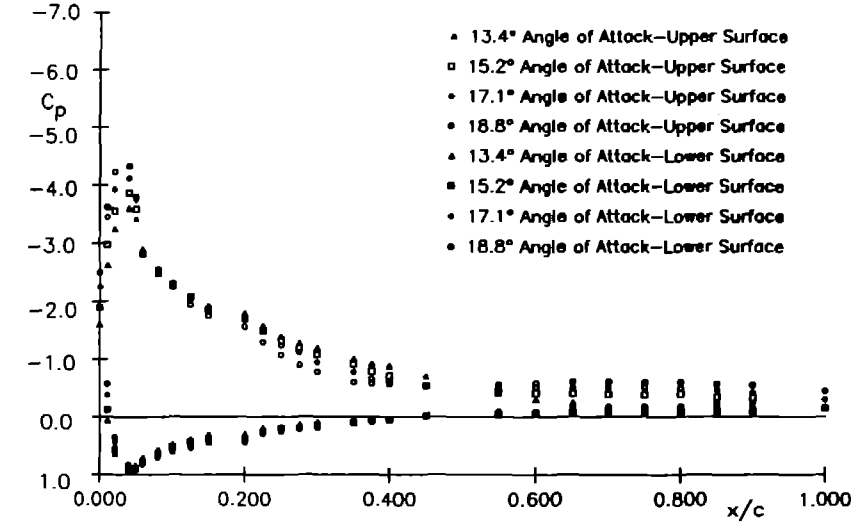

Figure 11. Steady State Pressure Distributions for NACA 0021 with No Vortex Generators

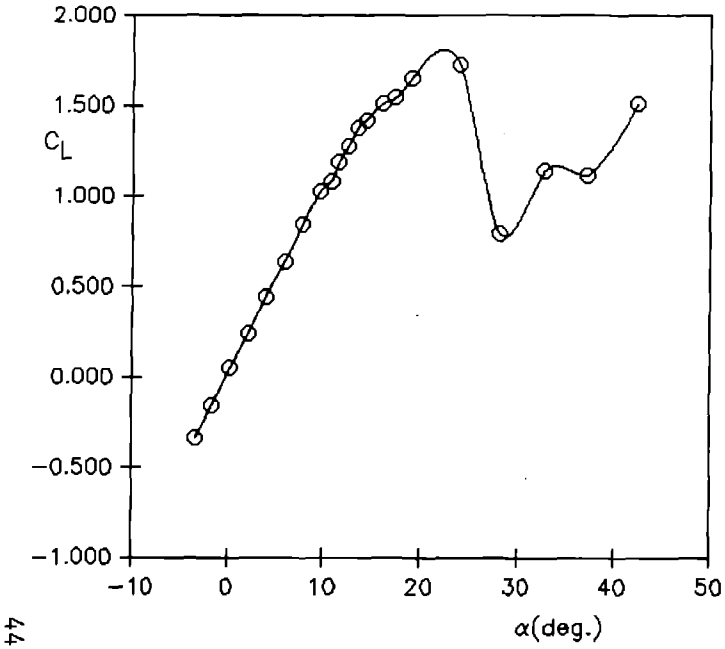

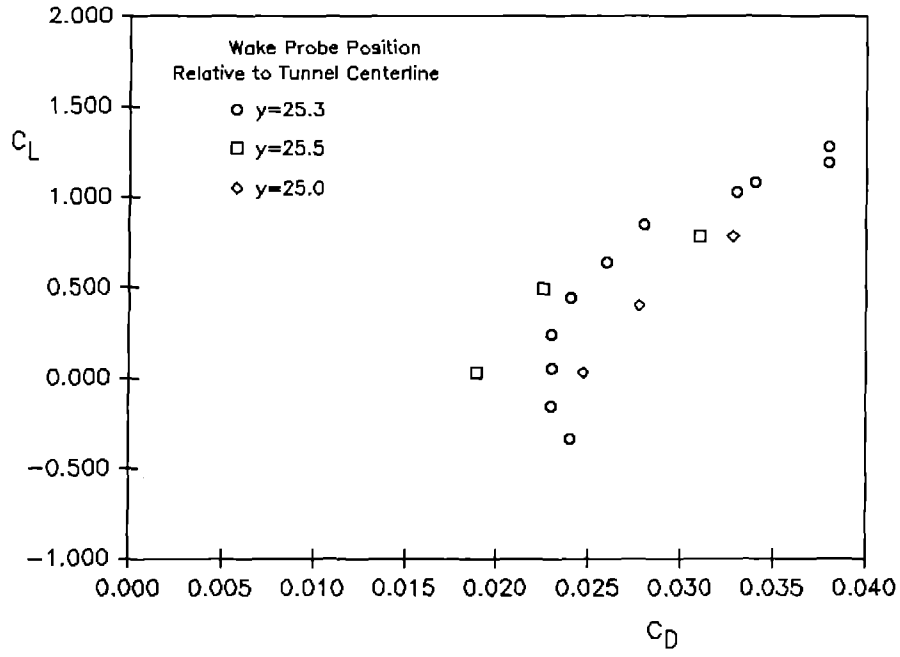

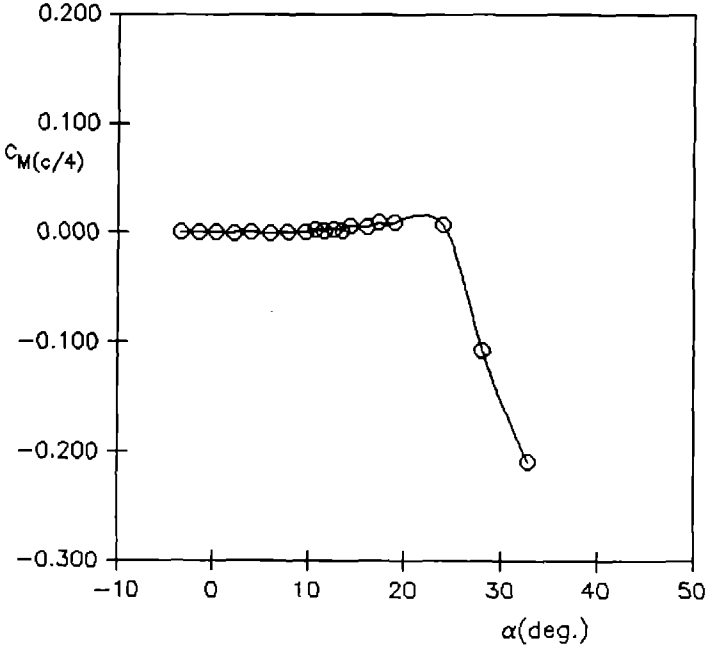

Figure 12. Integrated Static Data for NACA 0021 with Vortex Generators at the .1c Chord Positior

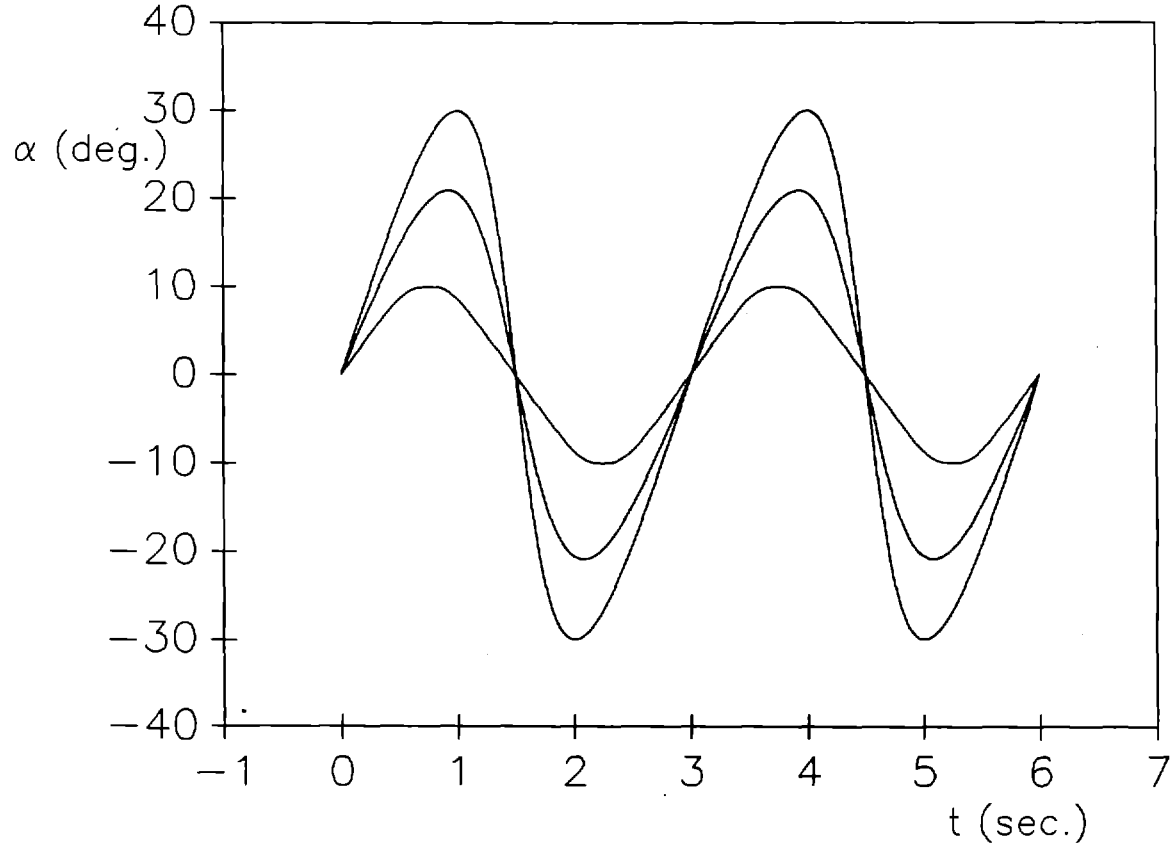

Figure 15. Angle of Attack vs. Time for 10° Sine, 20° Inverse Tangent , and 30° Inverse Tangent Cams

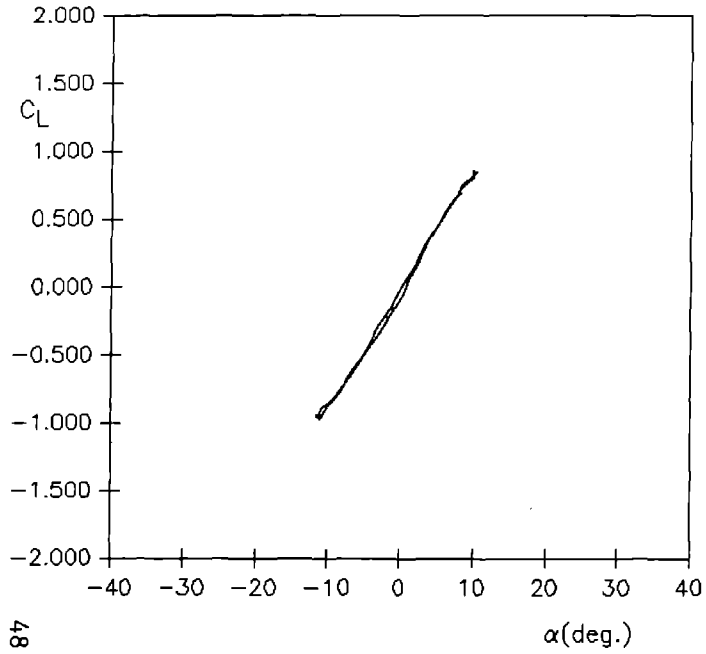

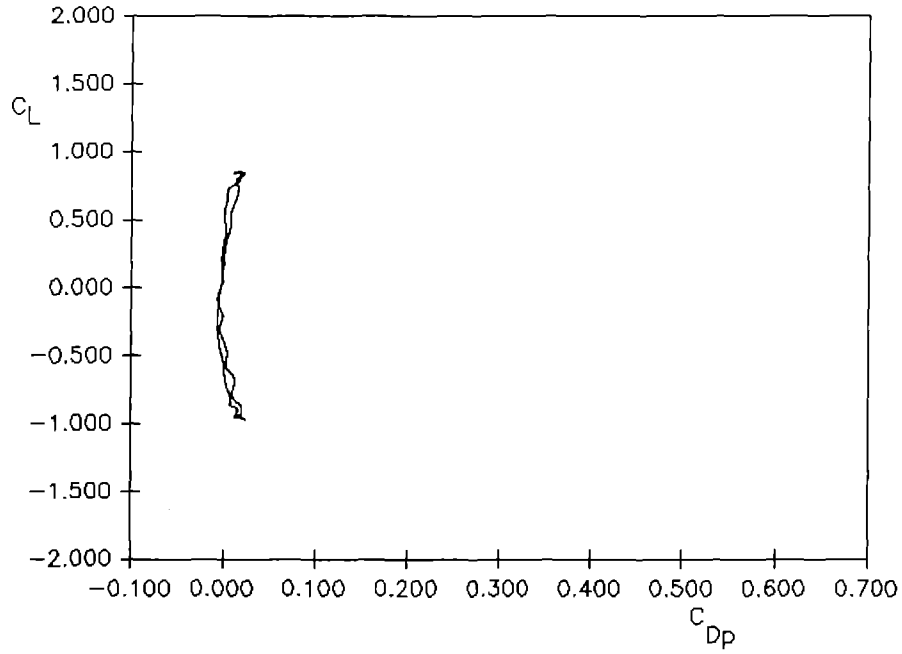

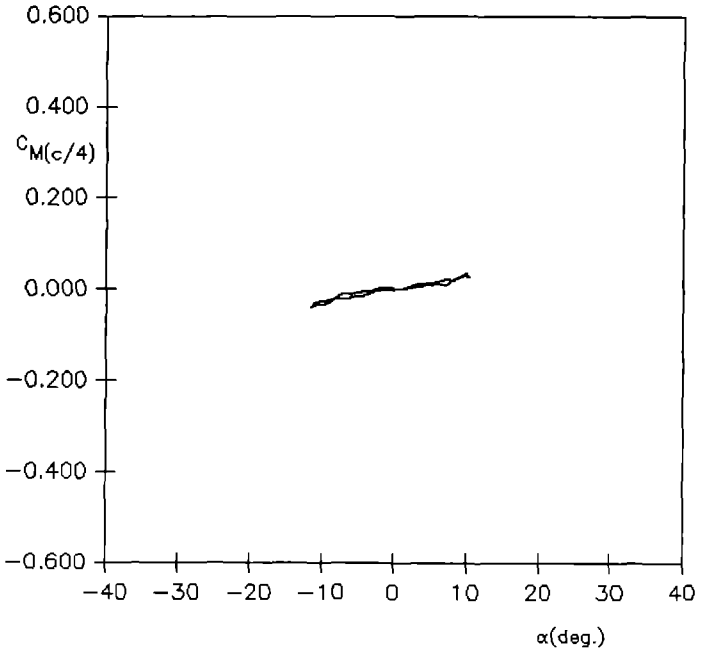

Reduced Frequency = .009

Figure 16. Integrated Oscillatory Pressure Data for NACA 0021 with No Vortex Generators 10° Sine Function

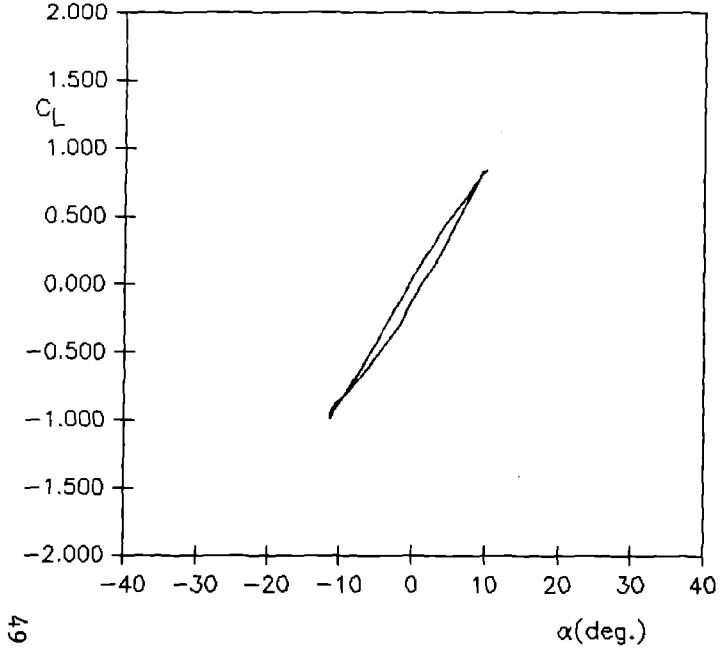

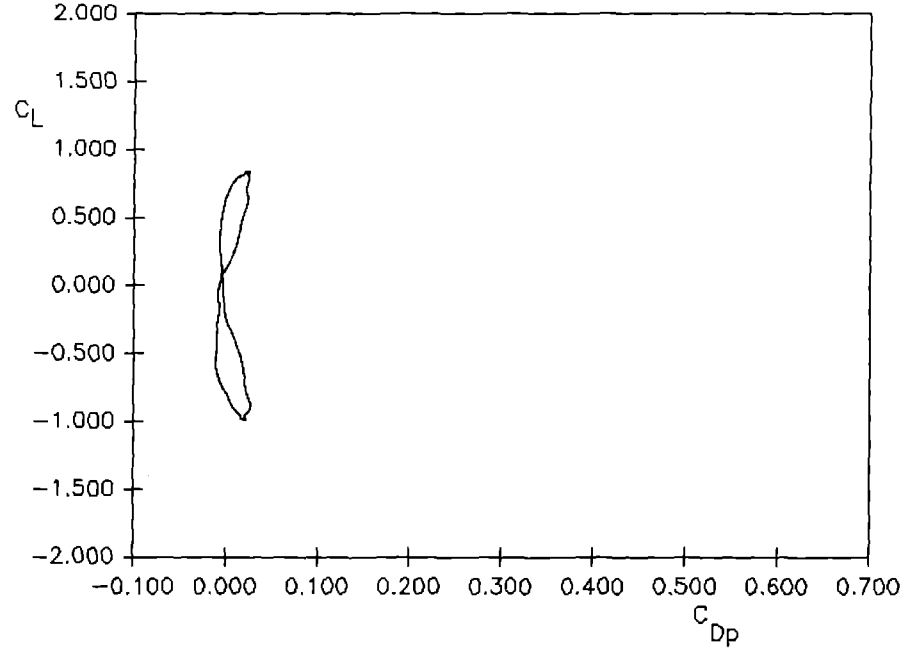

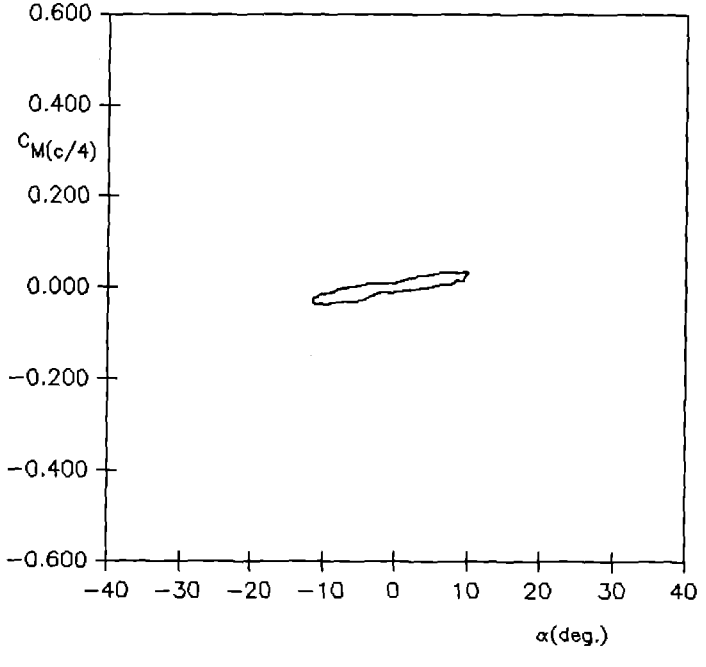

Reduced Frequency = .034

Figure 17. Integrated Oscillatory Pressure Data for NACA 0021 with No Vortex Generators 10° Sine Function

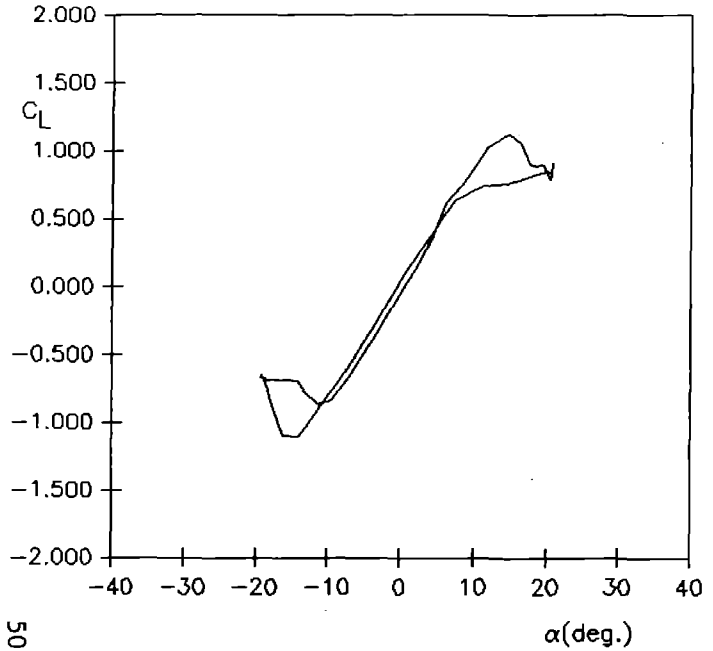

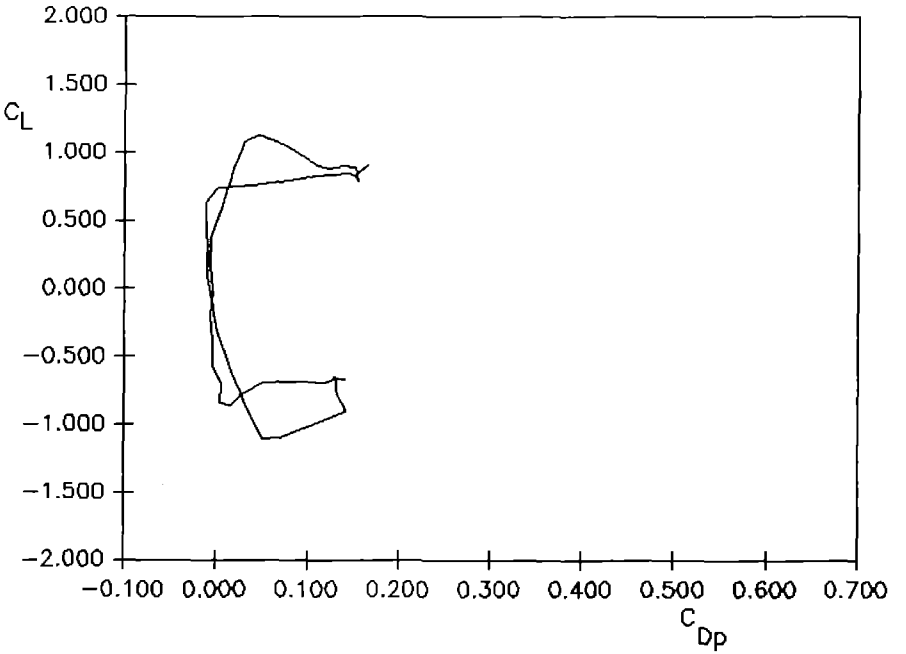

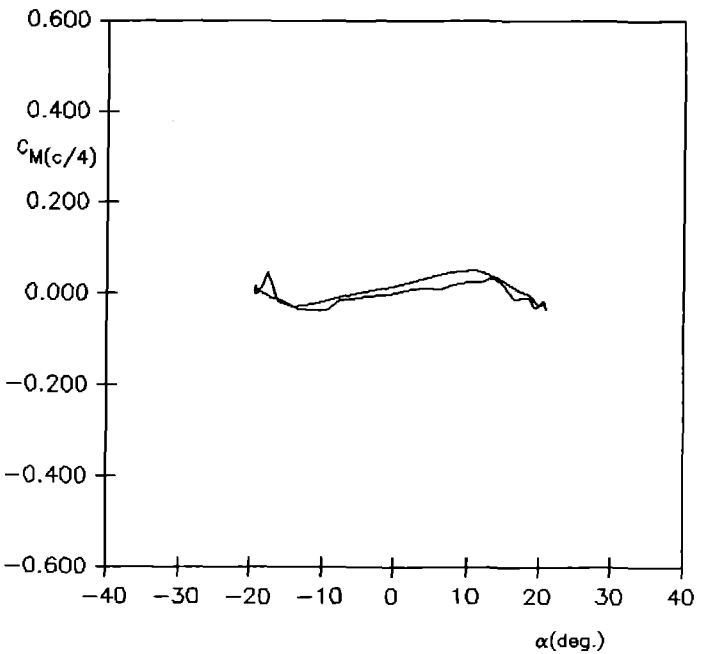

Reduced Frequency = .009

Figure 18. Integrated Oscillatory Pressure Data for NACA 0021 with No Vortex Generators 20° Inverse–Tangent Function

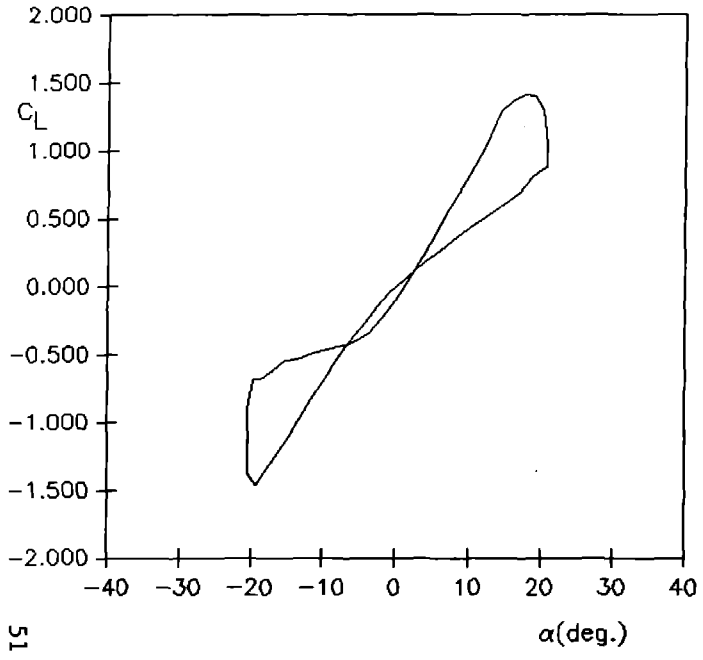

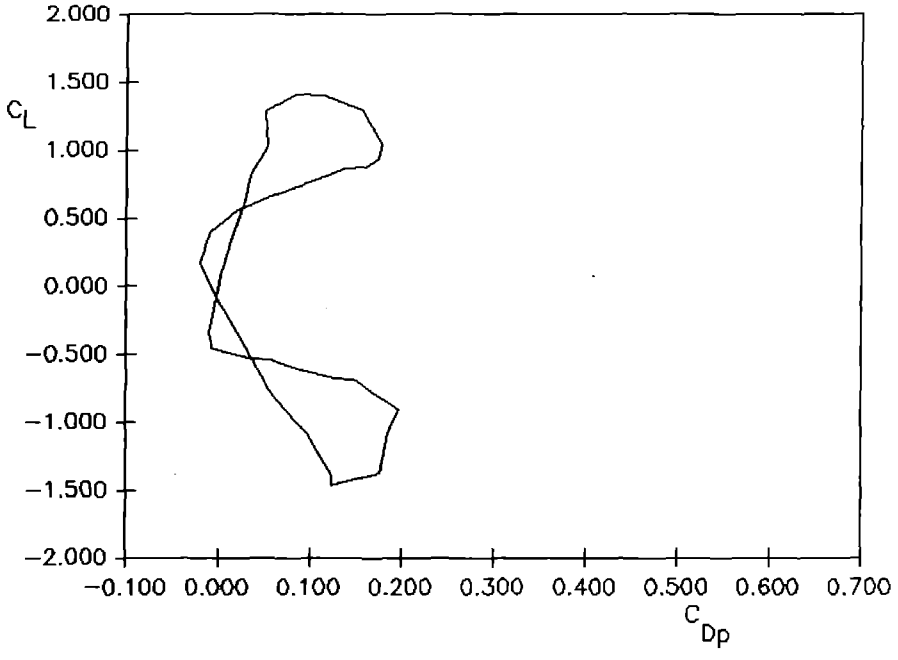

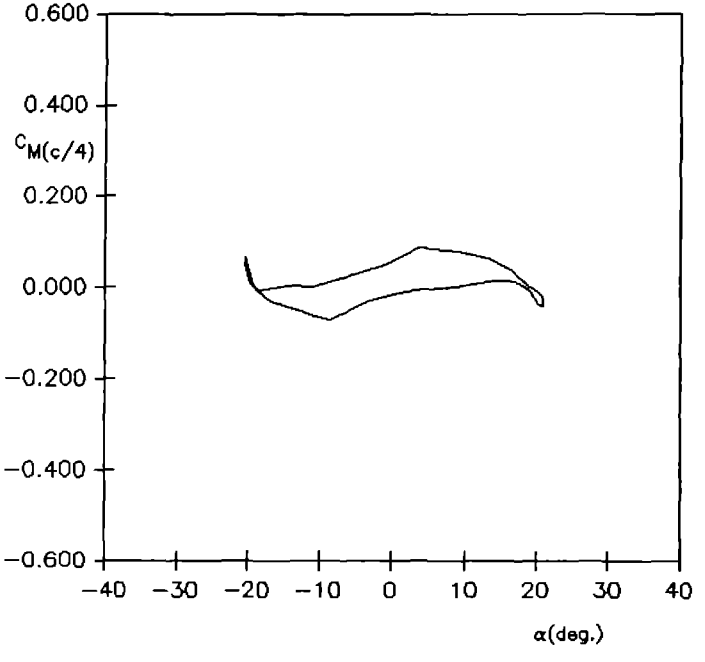

Reduced Frequency = .034

Figure 19. Integrated Oscillatory Pressure Data for NACA 0021 with No Vortex Generators 20° Inverse–Tangent Function

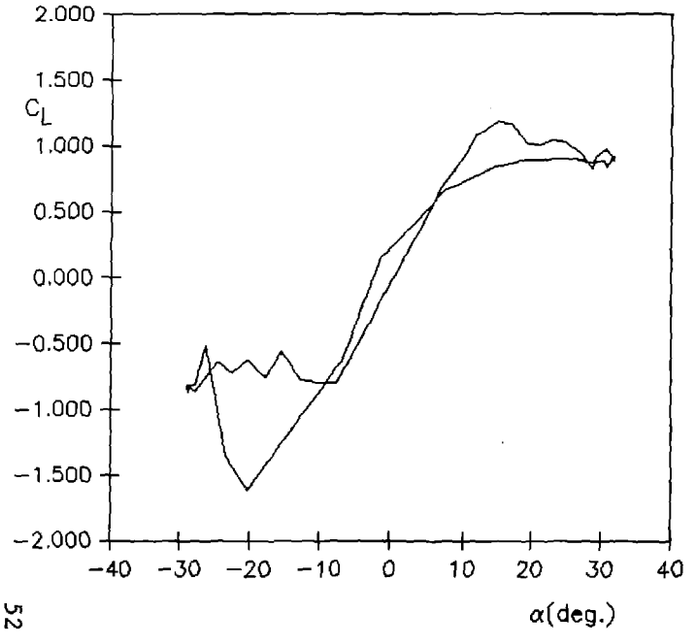

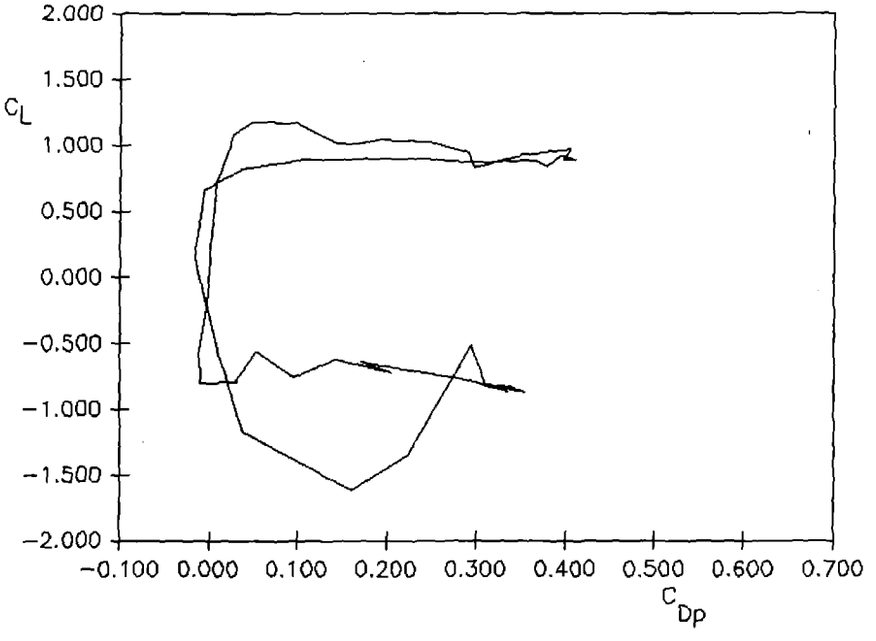

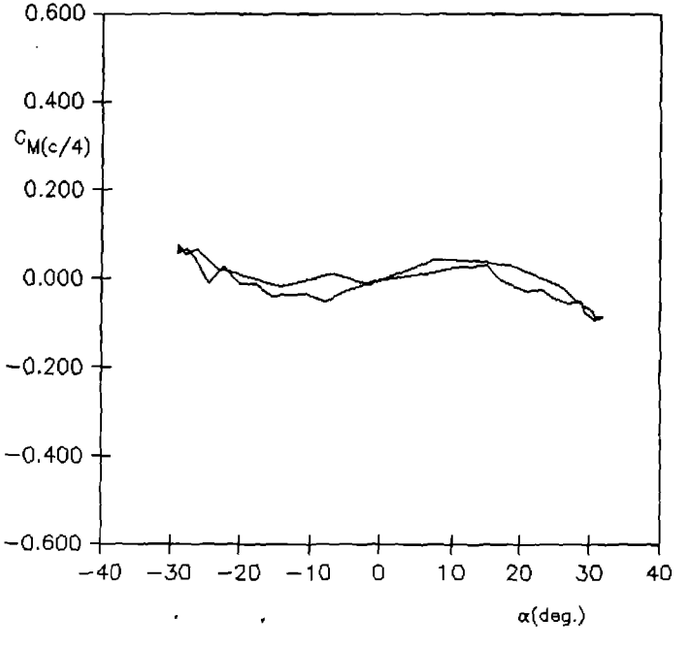

Reduced Frequency = .009

Figure 20. Integrated Oscillatory Pressure Data for NACA 0021 with No Vortex Generators 30° Inverse–Tangent Function

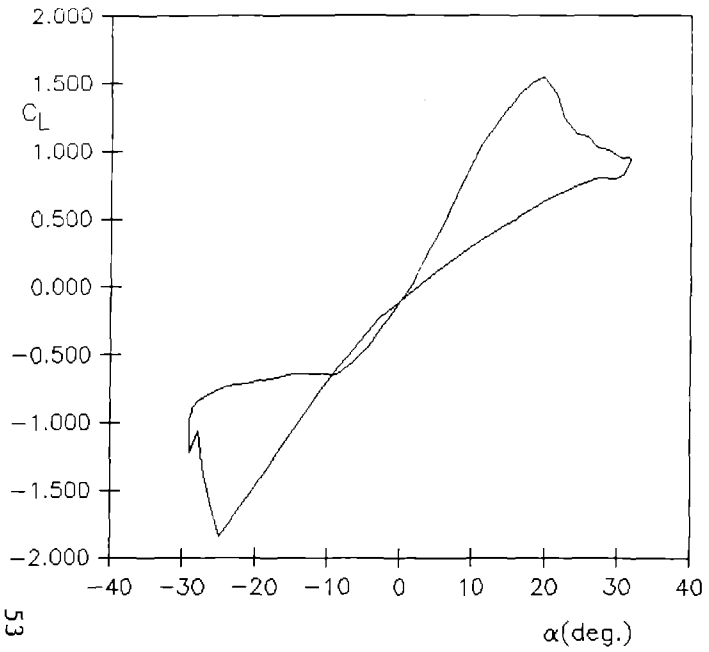

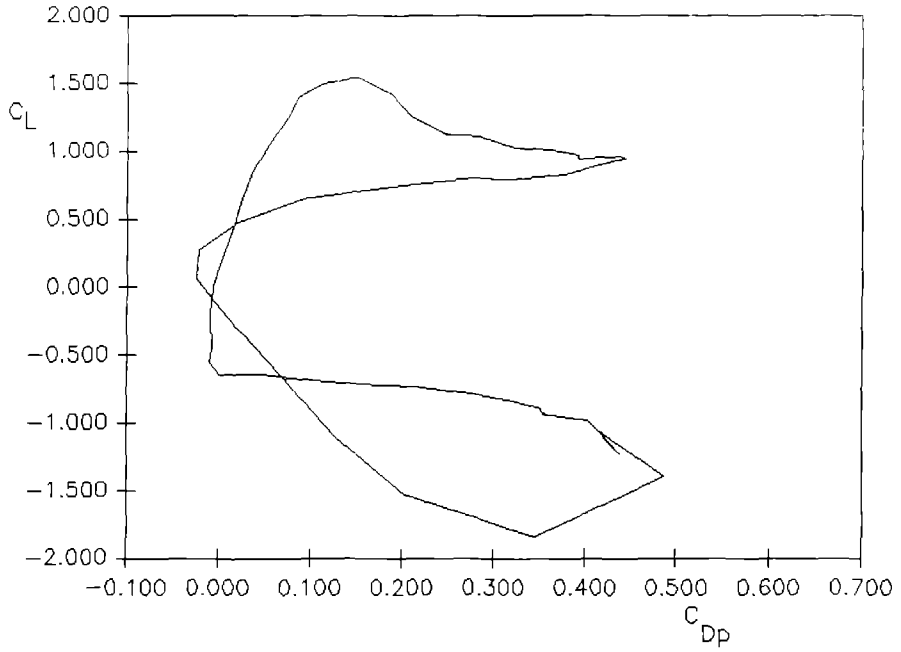

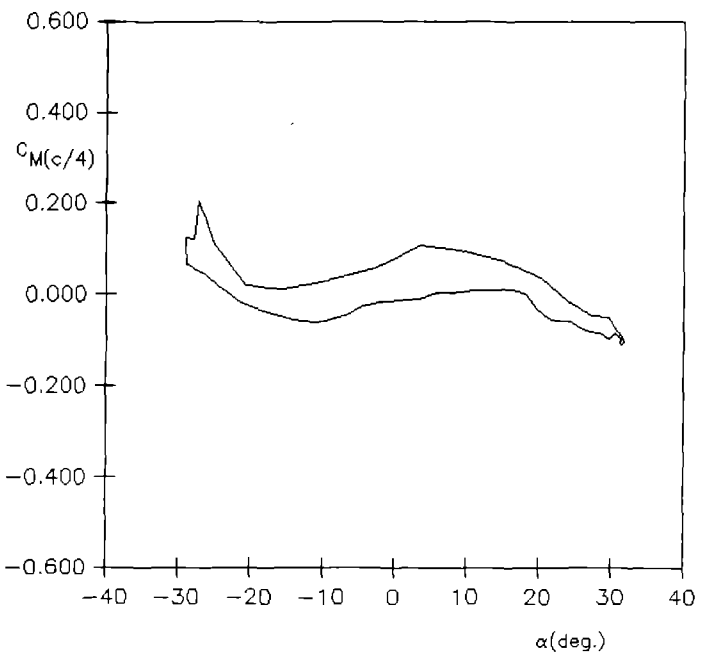

Reduced Frequency = .023

Figure 21. Integrated Oscillatory Pressure Data for NACA 0021 with No Vortex Generators 30° Inverse–Tangent Function

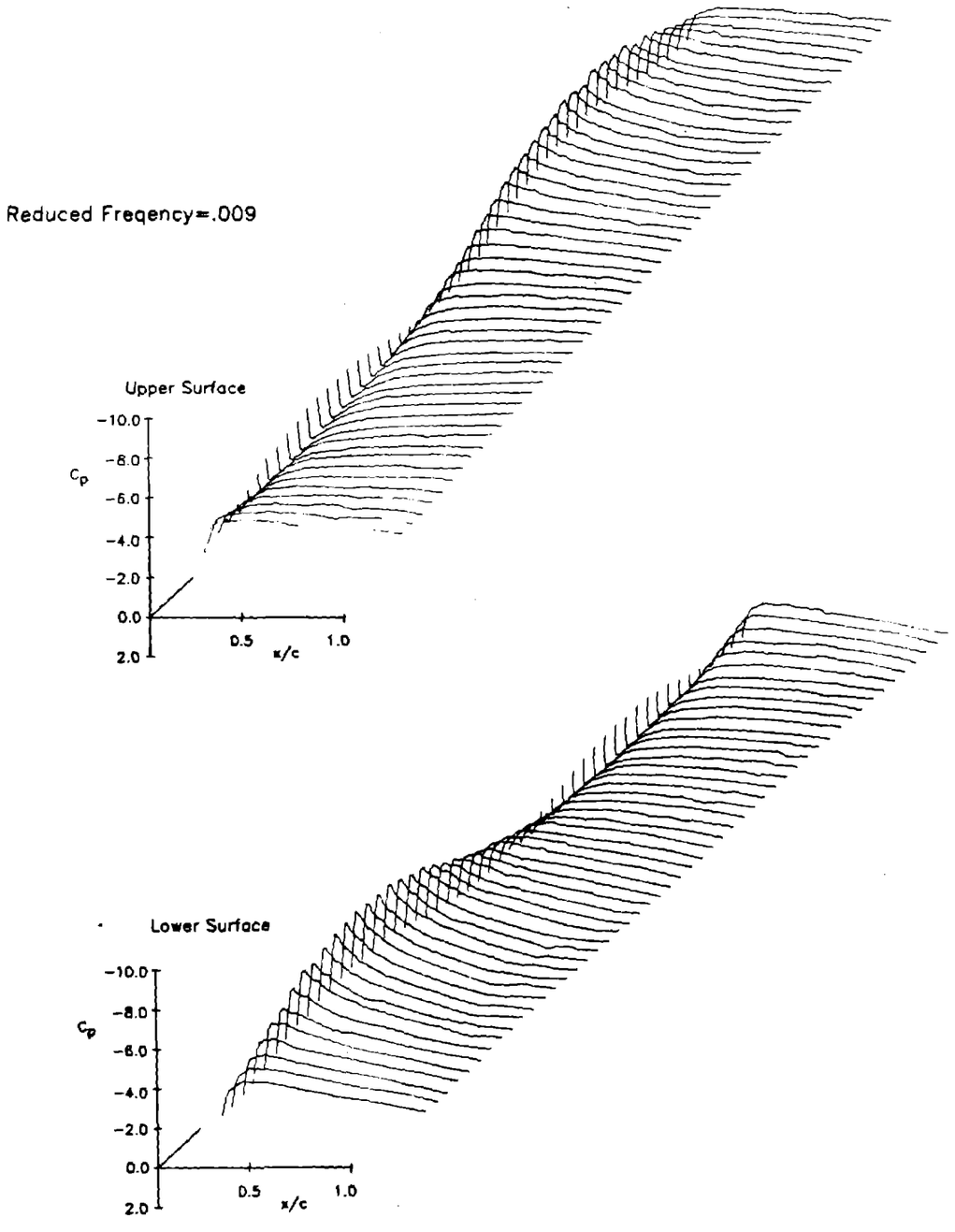

Figure 22. Oscillatory Pressure Distributions for NACA 0021 with No Vortex Generators—10° Sine Function

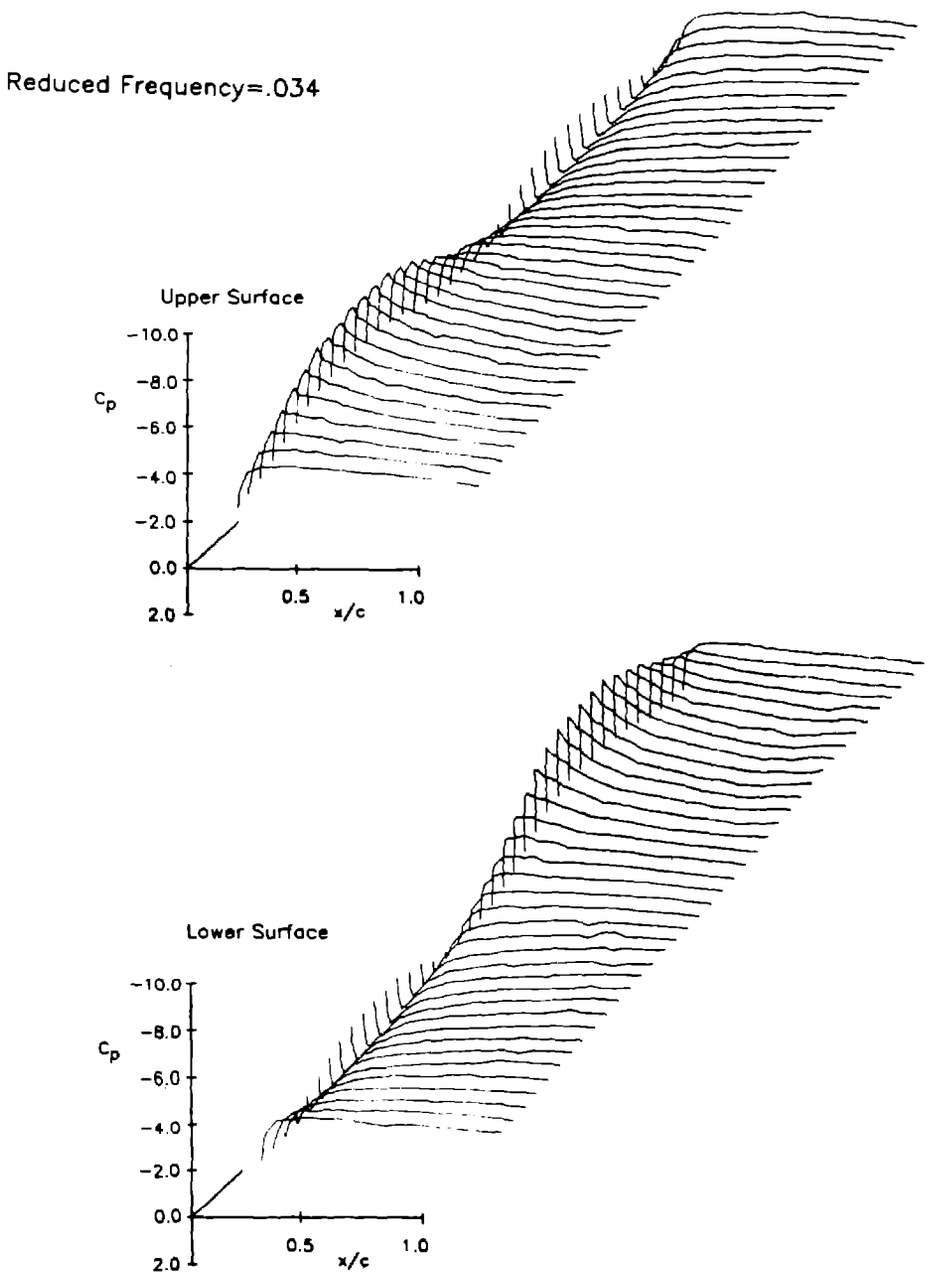

Figure 23. Oscillatory Pressure Distributions for NACA 0021 with No Vortex Generators—10° Sine Function

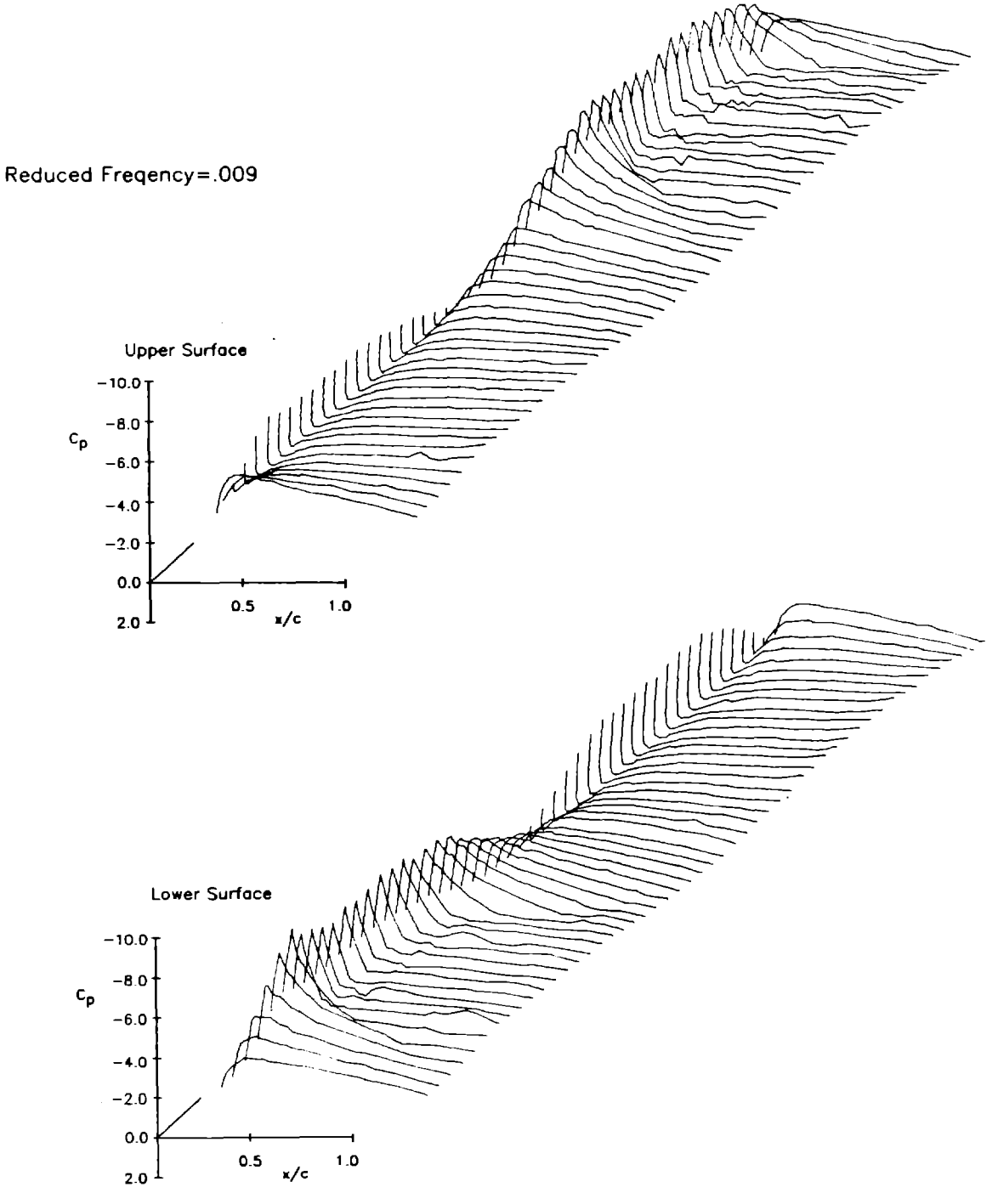

Figure 24. Oscillatory Pressure Distributions for NACA 0021 with No Vortex Generators—20° Inverse Tangent Function

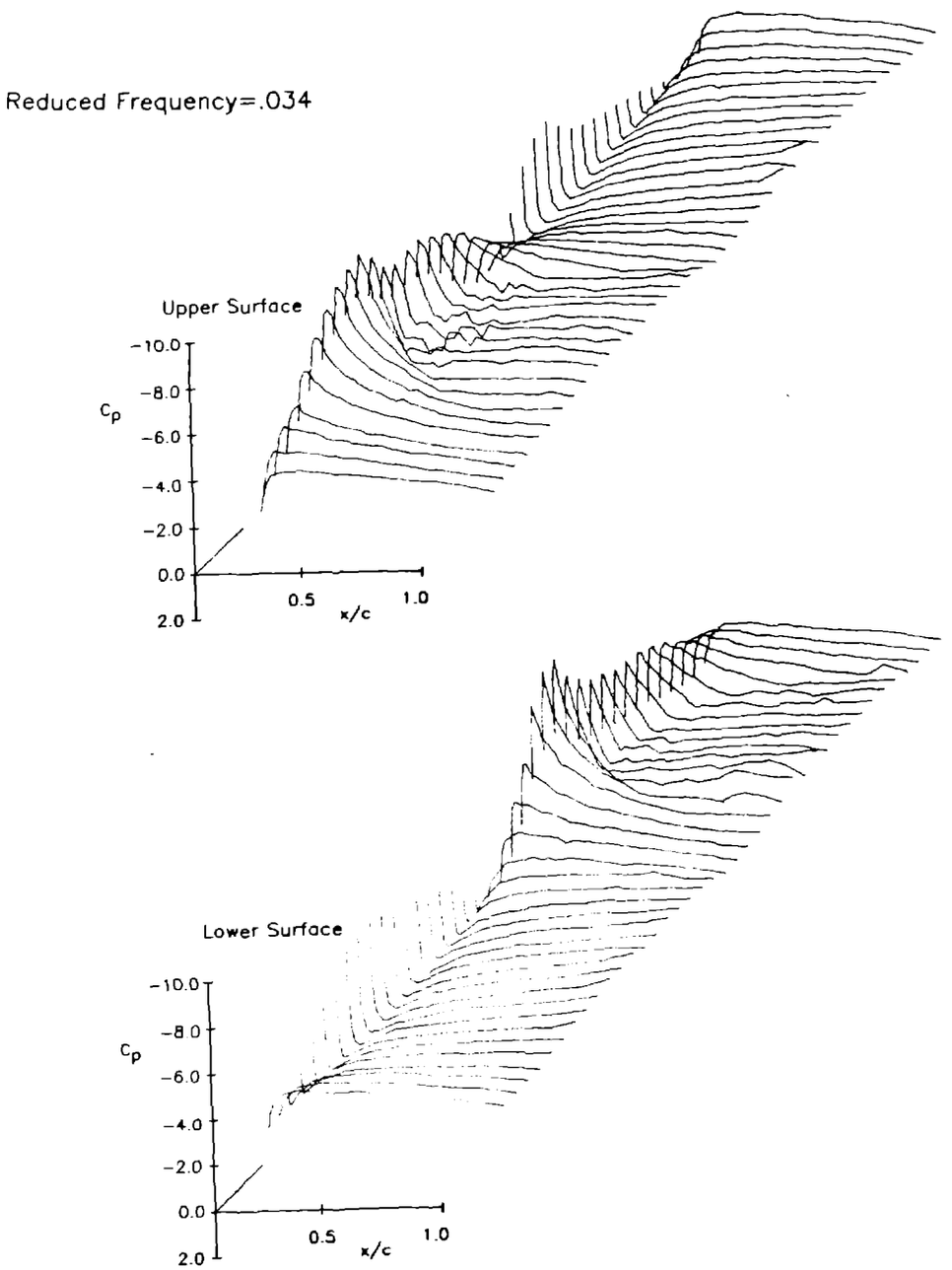

Figure 25. Oscillatory Pressure Distributions for NACA 0021 with No Vortex Generators—20° Inverse Tangent Function

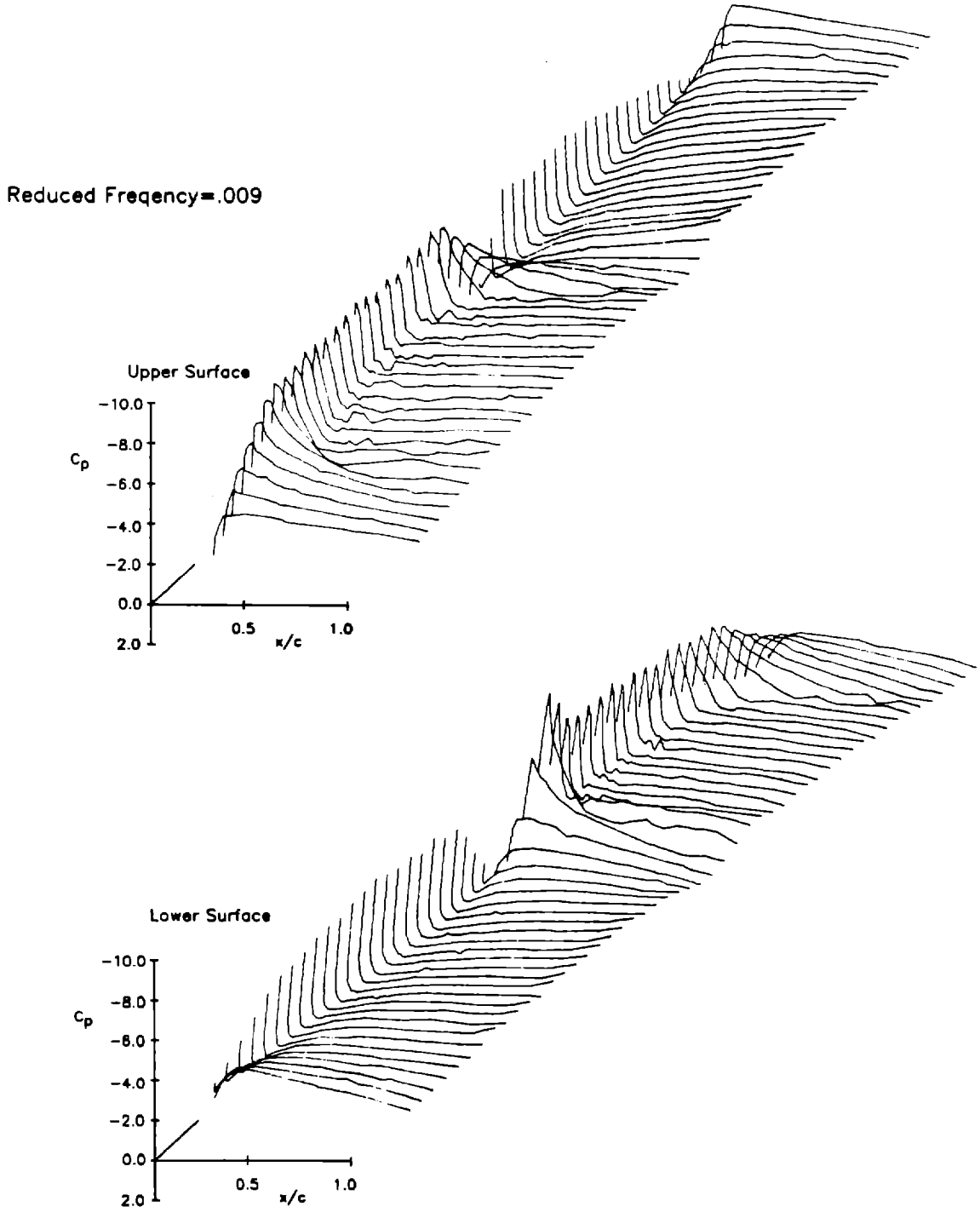

Figure 26. Oscillatory Pressure Distributions for NACA 0021 with No Vortex Generators–30° Inverse Tangent Function

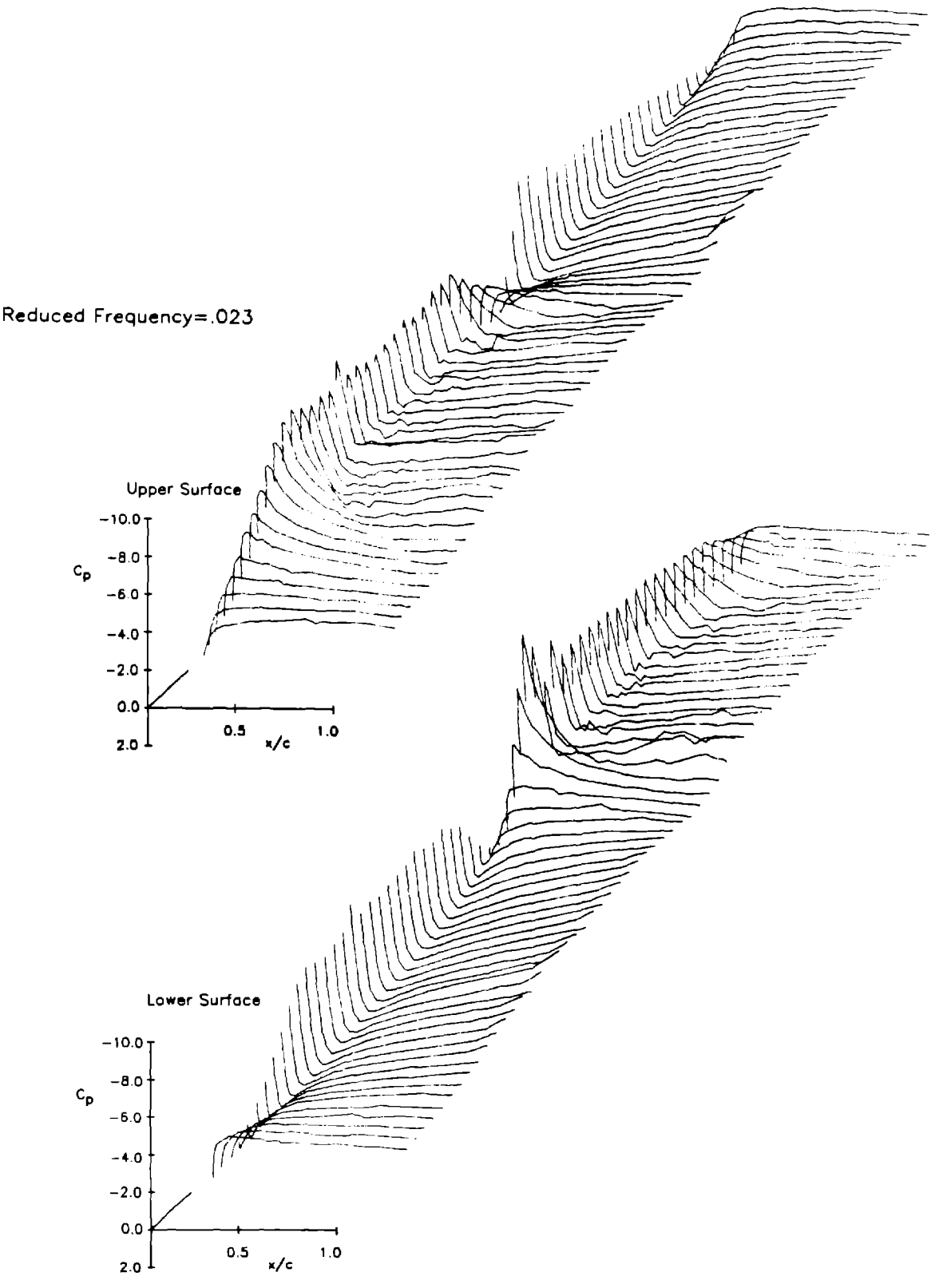

Figure 27. Oscillatory Pressure Distributions for NACA 0021 with No Vortex Generators—30° Inverse Tangent Function

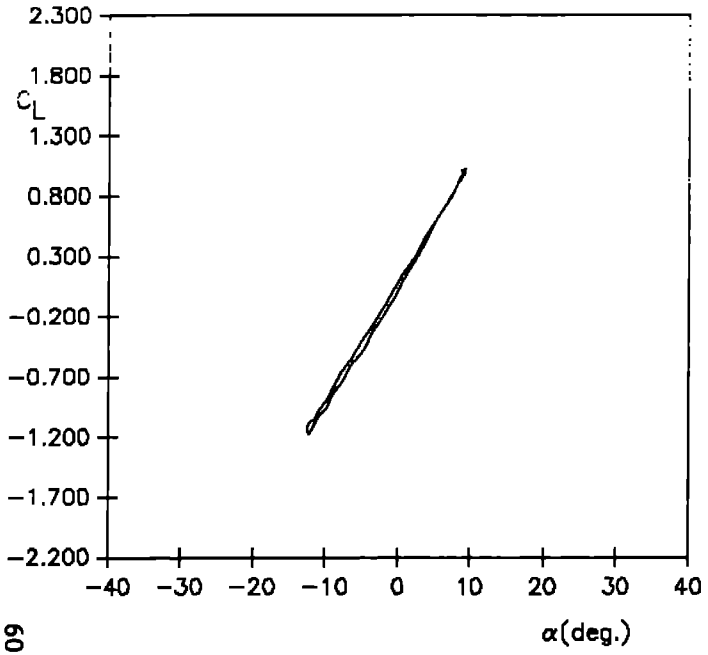

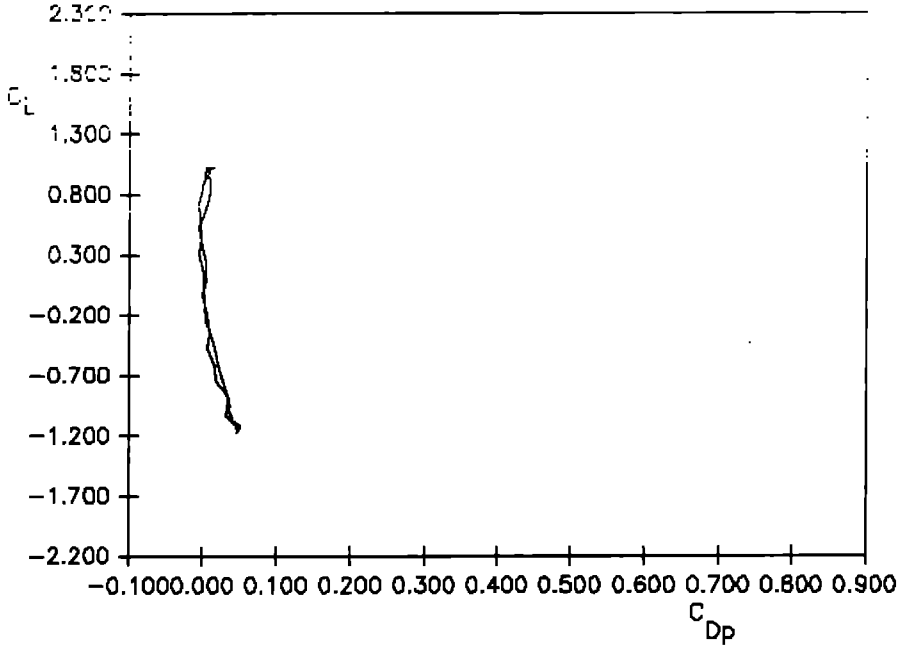

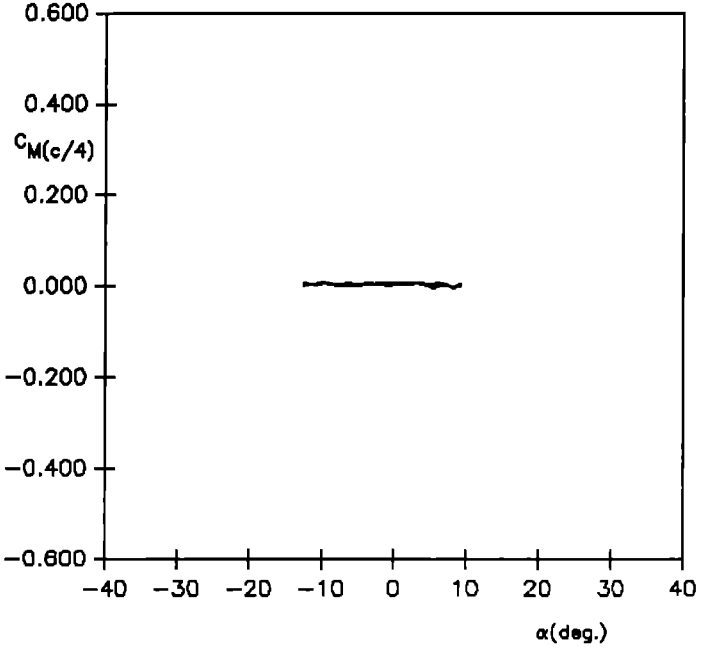

Reduced Frequency = .009

Figure 28. Integrated Oscillatory Pressure Data for NACA 0021 with Vortex Generators at .1c Chord Location−10° Sine Function

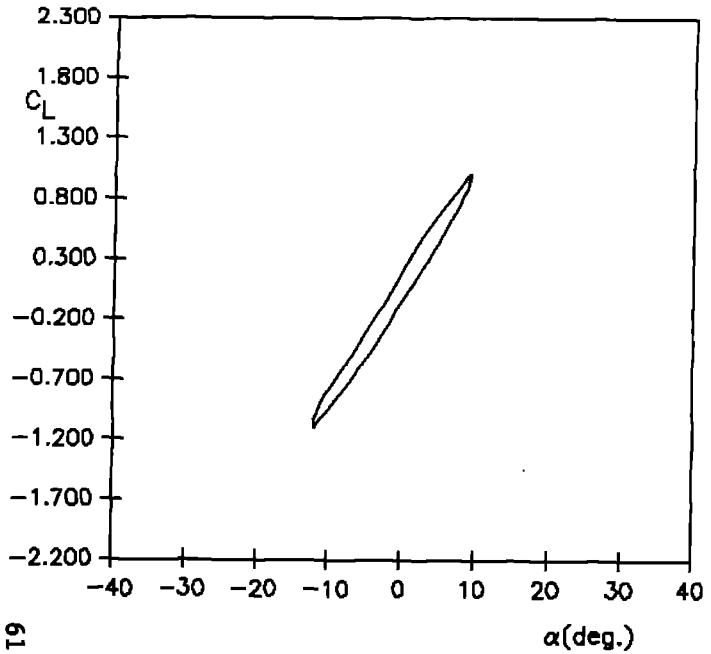

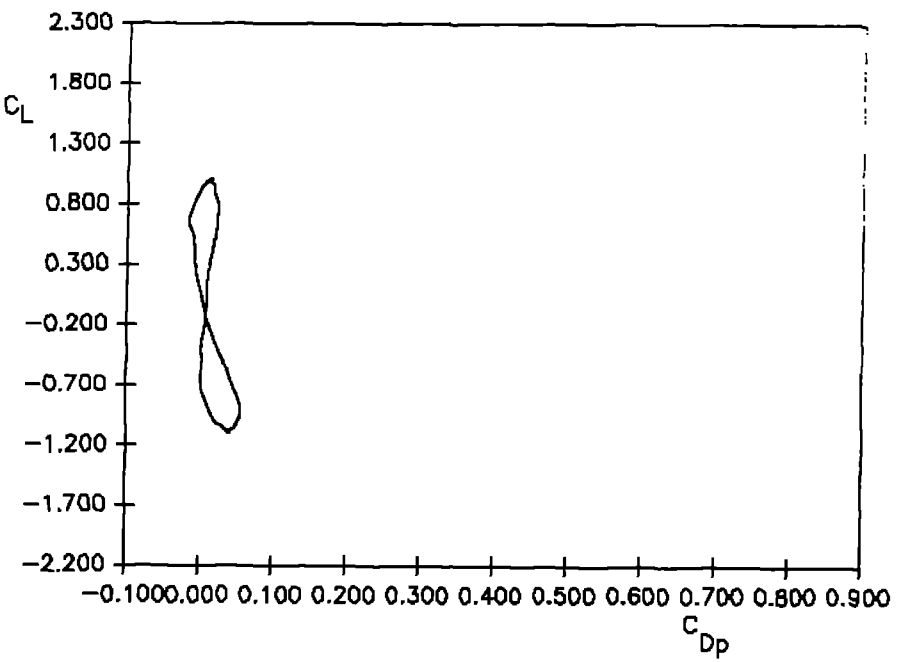

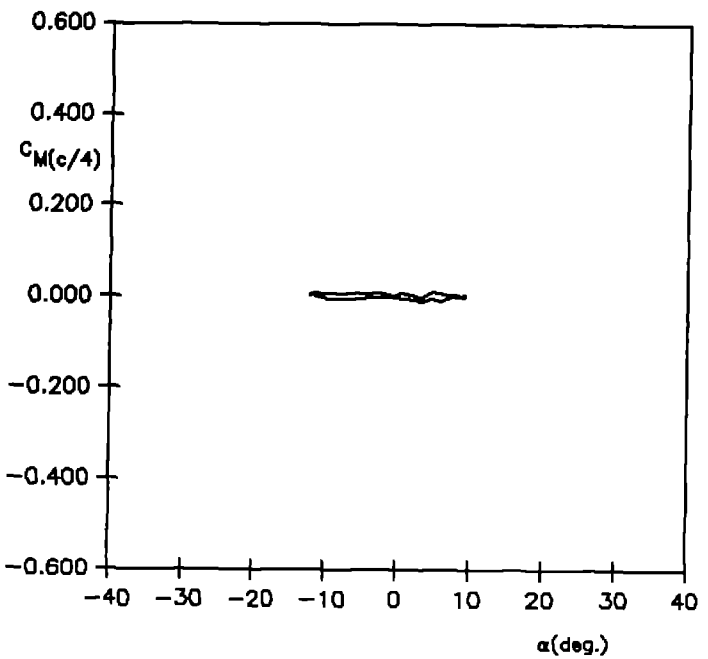

Reduced Frequency = .034

Figure 29. Integrated Oscillatory Pressure Data for NACA 0021 with Vortex Generators at .1c Chord Location—10° Sine Function

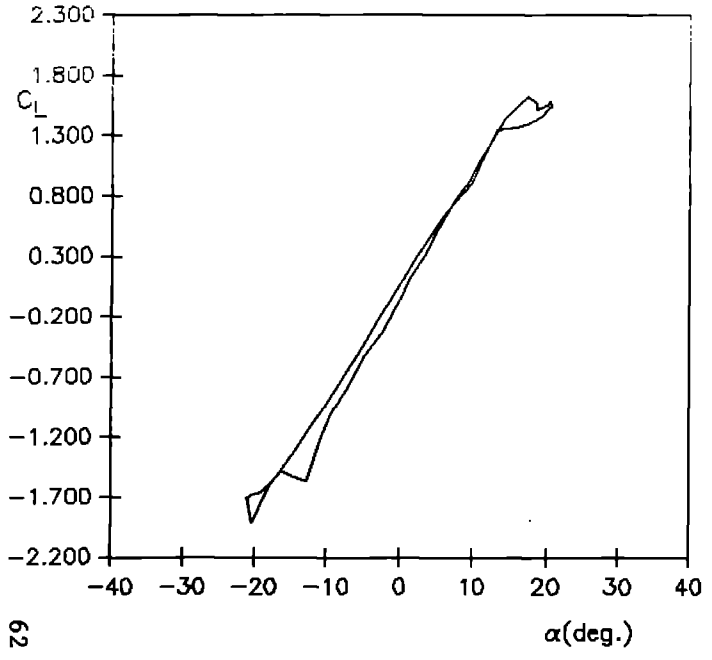

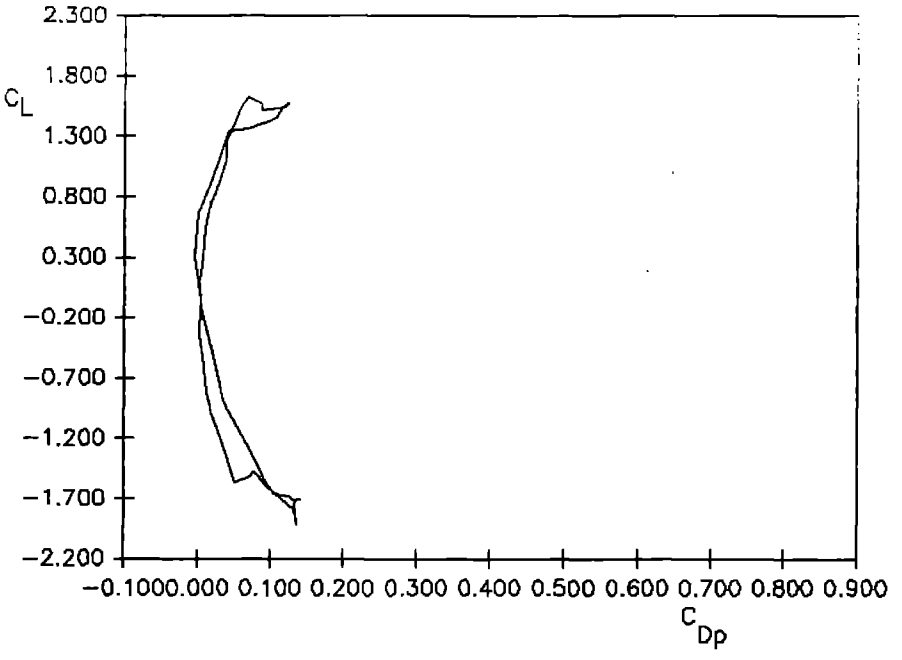

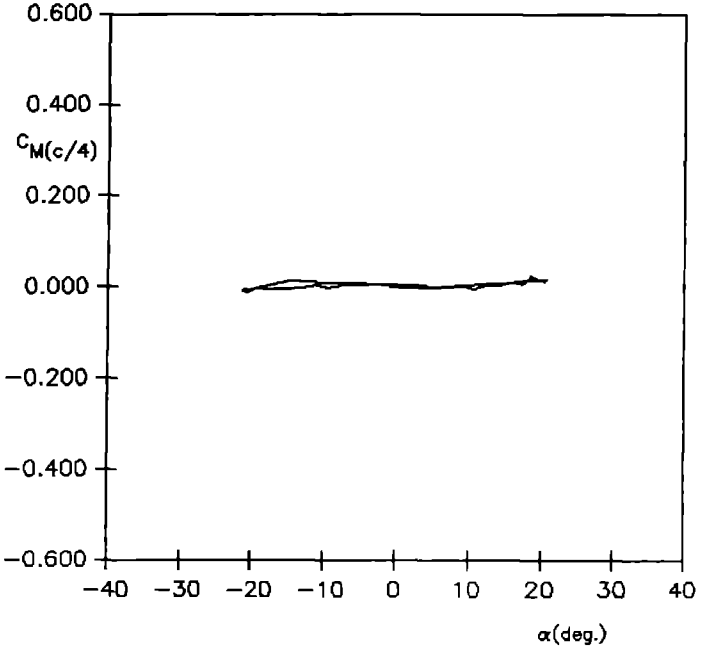

Reduced Frequency = .009

Figure 30. Integrated Oscillatory Pressure Data for NACA 0021 with Vortex Generators at .1c Chord Location−20° Inverse−Tangent Function

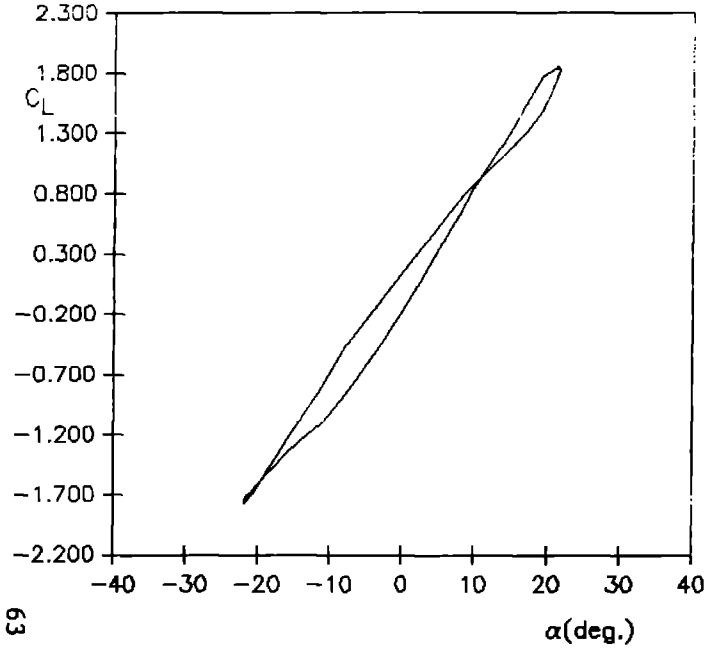

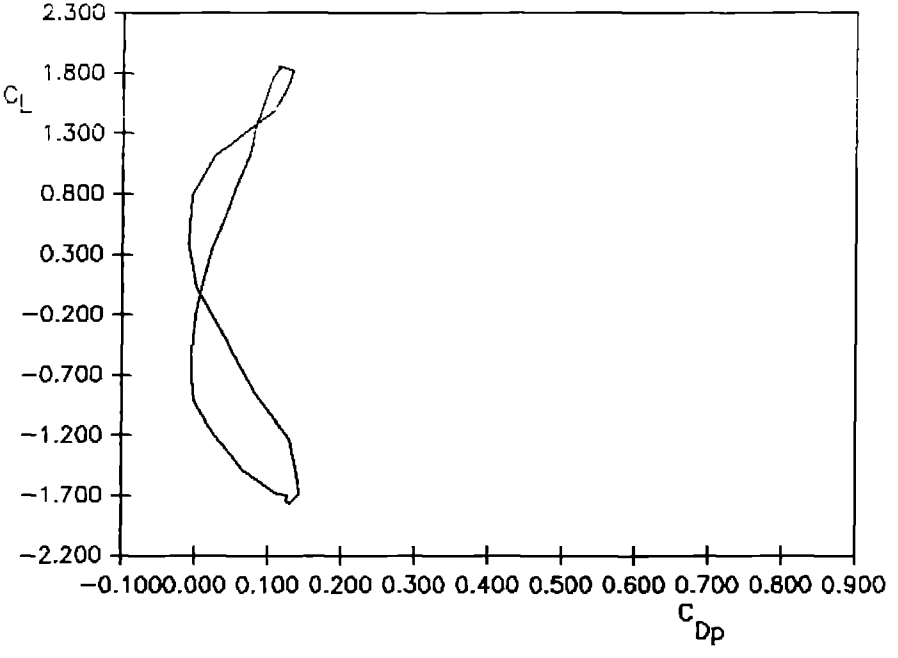

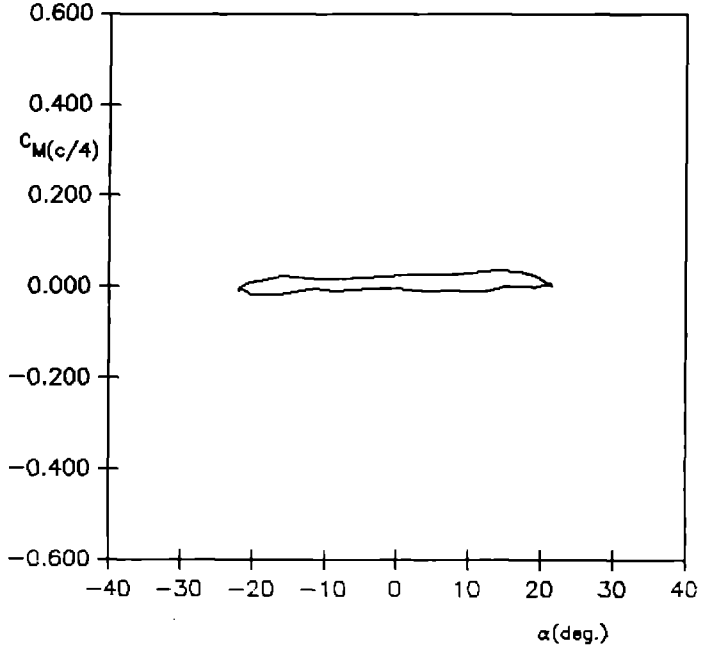

Reduced Frequency = .034

Figure 31. Integrated Oscillatory Pressure Data for NACA 0021 with Vortex Generators at .1c Chord Location−20° Inverse−Tangent Function

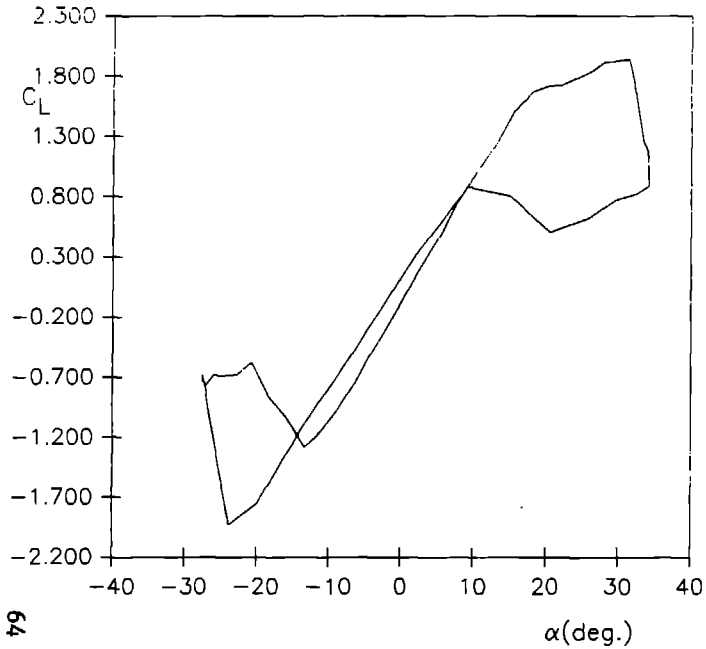

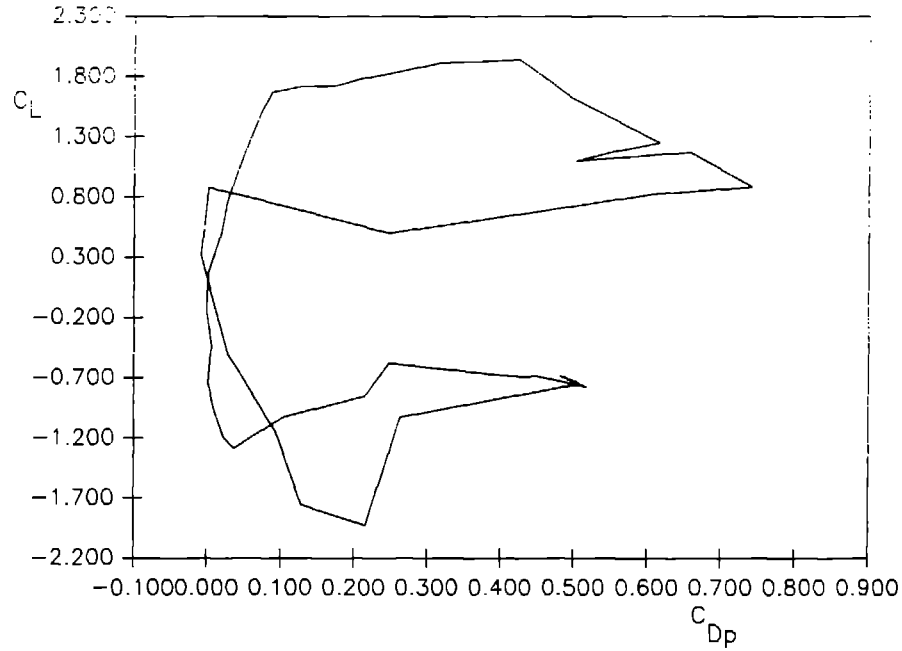

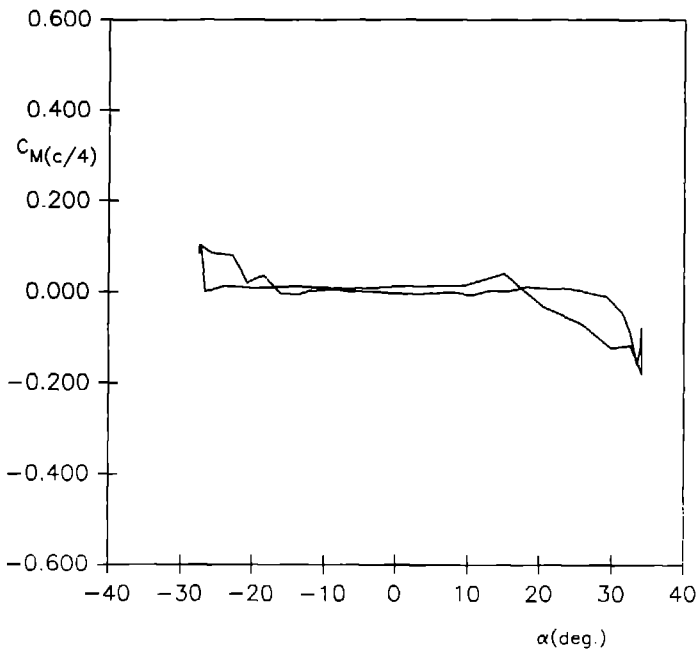

Reduced Frequency = .009

Figure 32. Integrated Oscillatory Pressure Data for NACA 0021 with Vortex Generators at .1c Chord Location–30° Inverse–Tangent Function

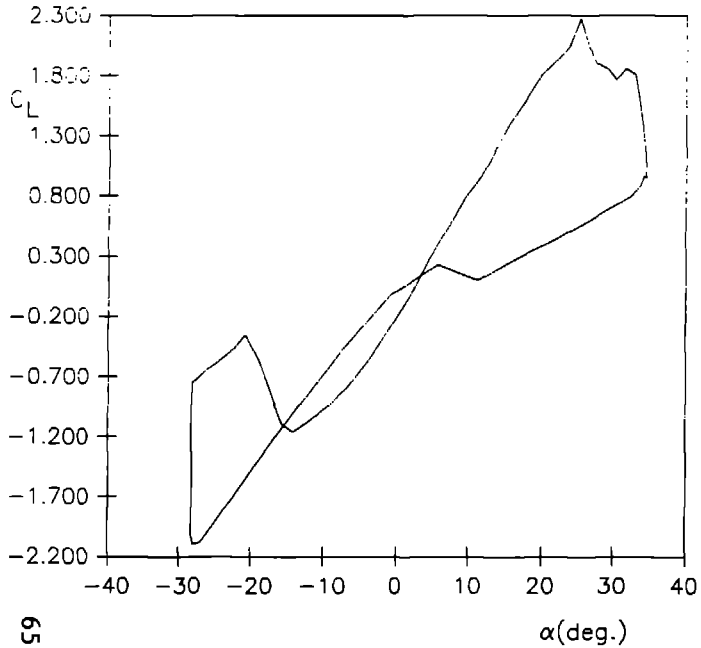

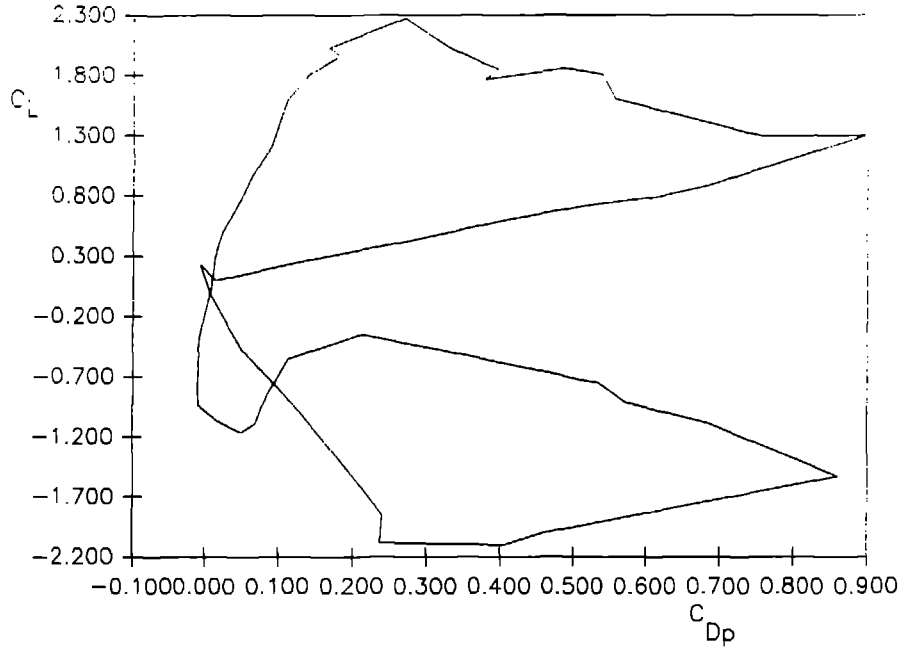

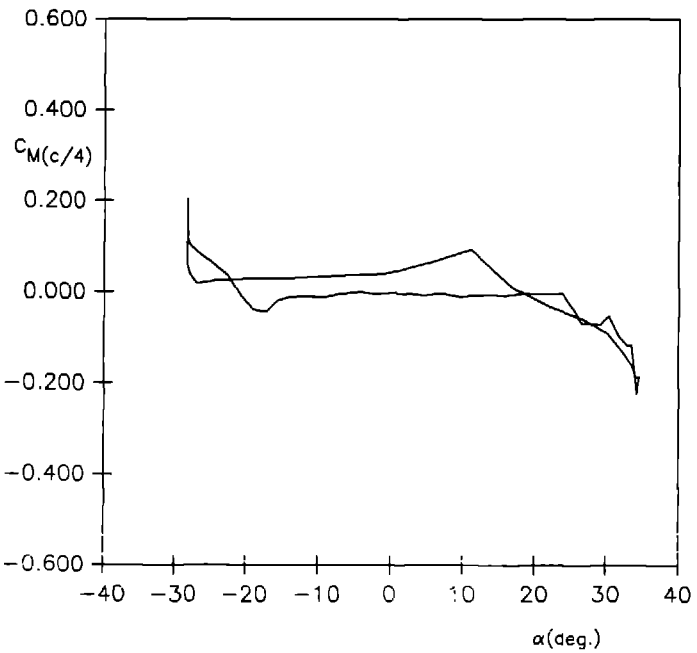

Reduced Frequency = .023

Figure 33. Integrated Oscillatory Pressure Data for NACA 0021 with Vortex Generators at .1c Chord Location−30° Inverse−Tangent Function

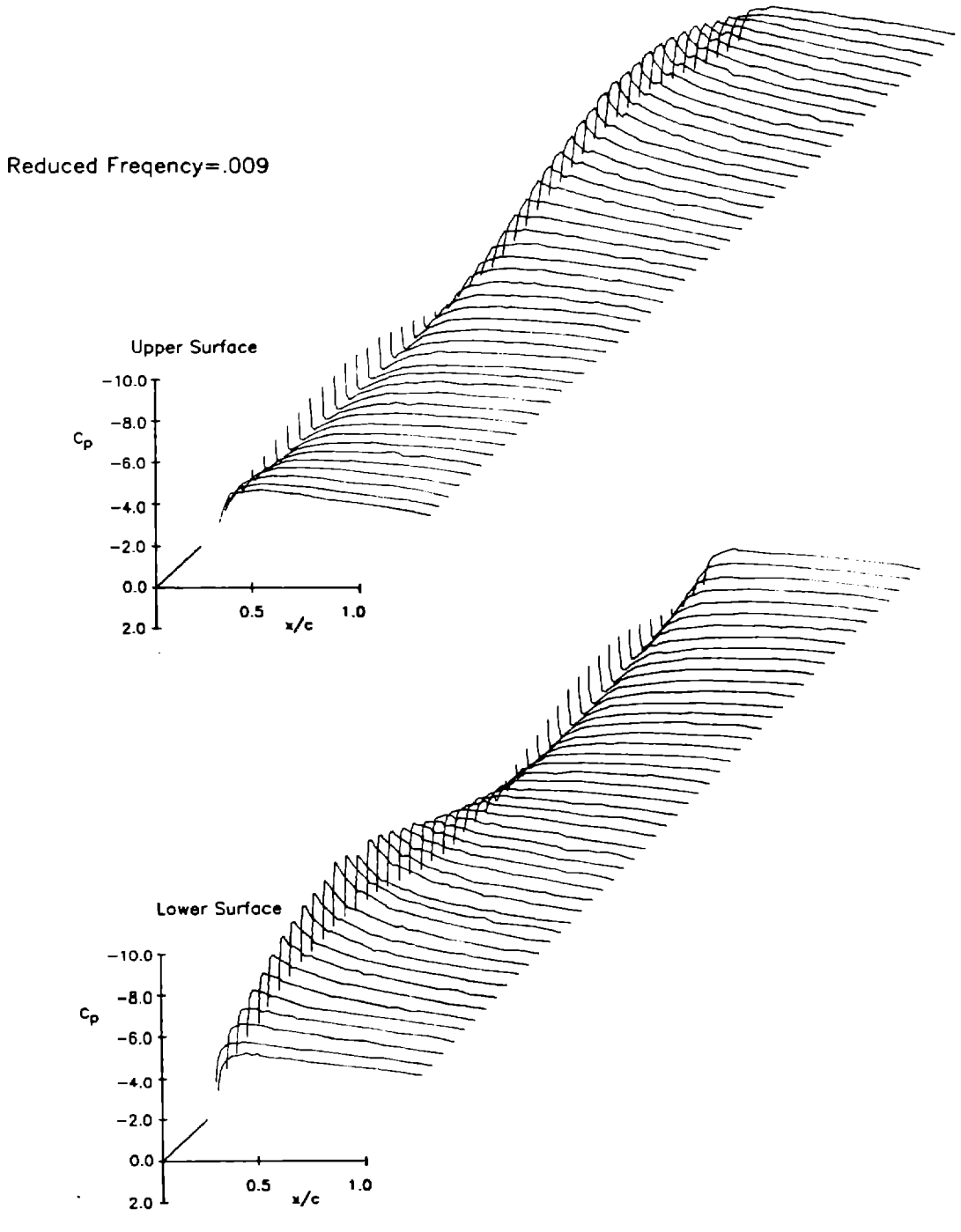

Figure 34. Oscillatory Pressure Distributions for NACA 0021 with Vortex Generators at .1c Chord Location–10° Sine Function

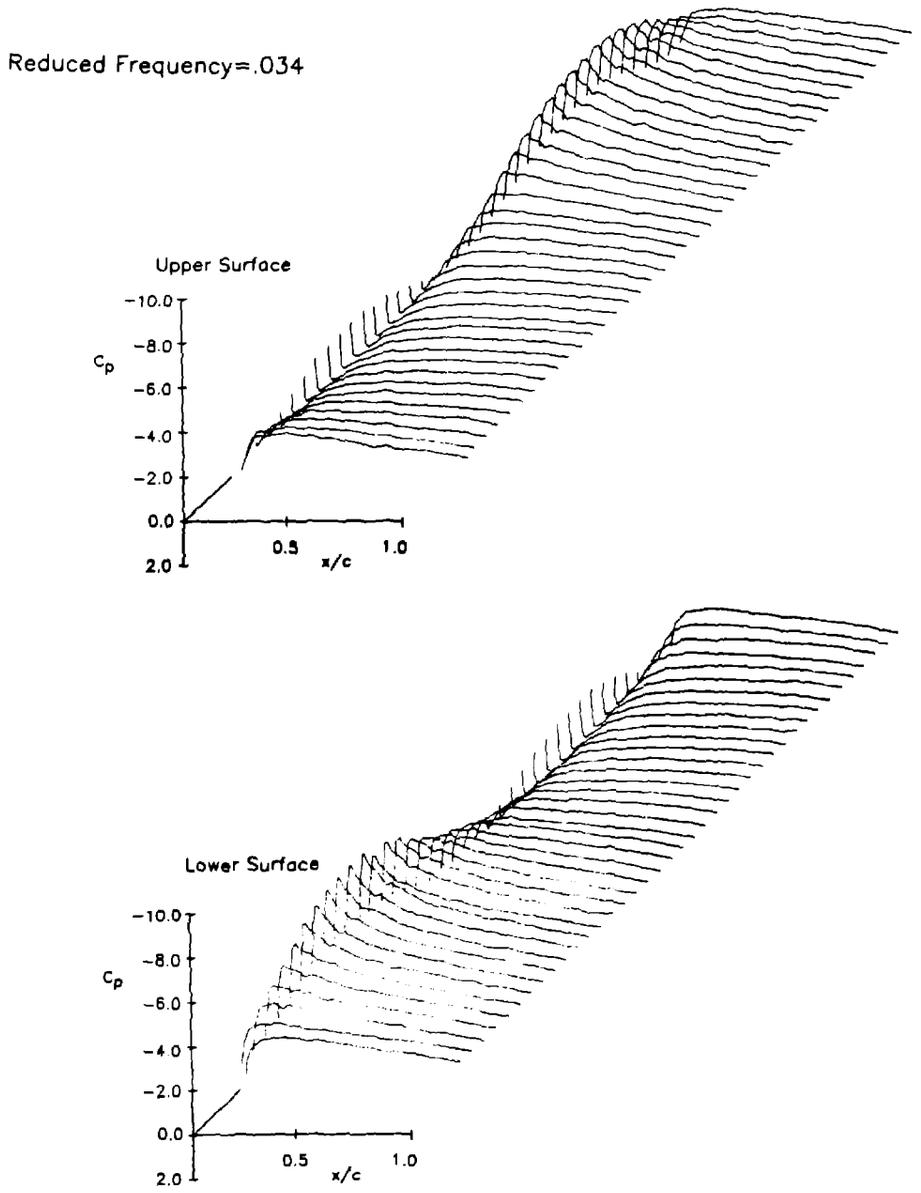

Figure 35. Oscillatory Pressure Distributions for NACA 0021 with Vortex Generators at .1c Chord Location−10° Sine Function

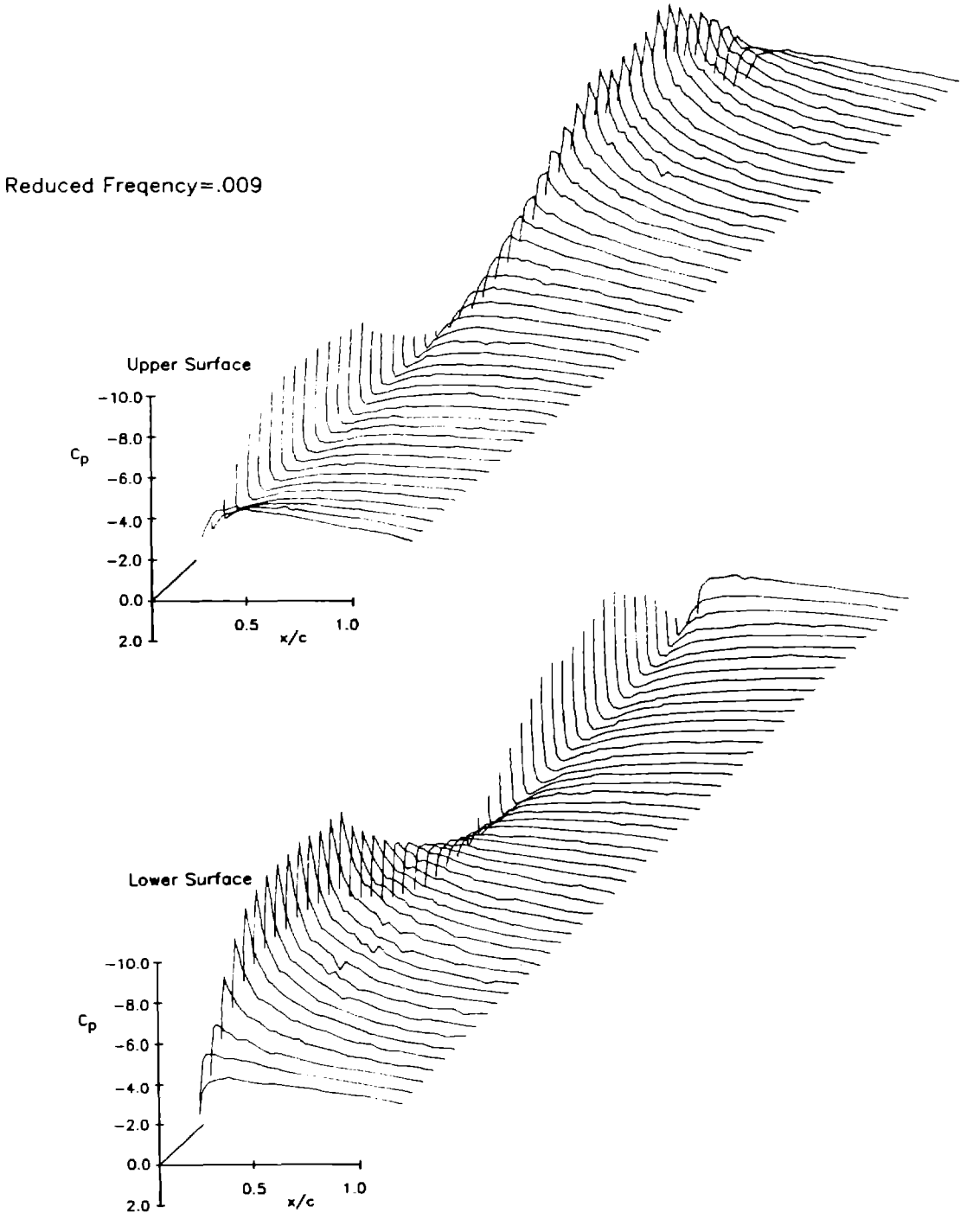

Figure 36. Oscillatory Pressure Distributions for NACA 0021 with Vortex Generators at .1c Chord Location–20° Inverse Tangent Function

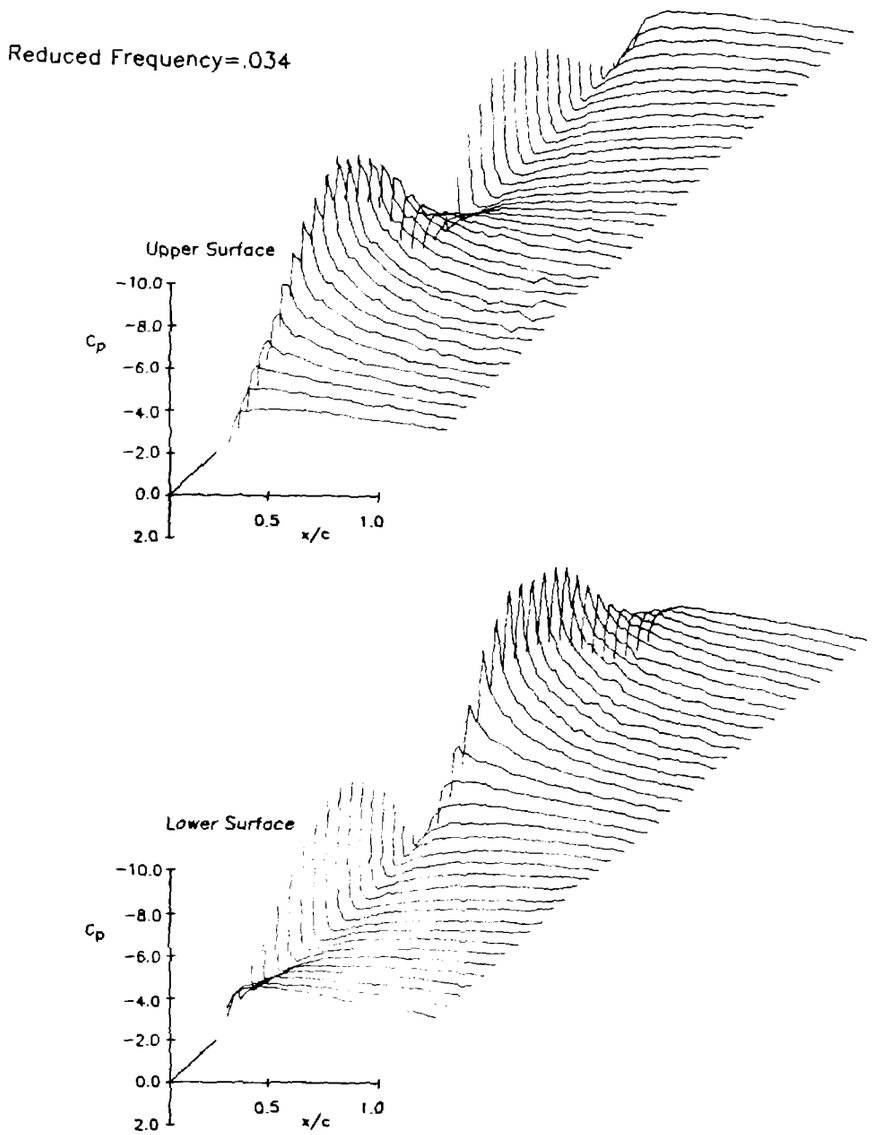

Figure 37. Oscillatory Pressure Distributions for NACA 0021 with Vortex Generators at .1c Chord Location–20° Inverse Tangent Function

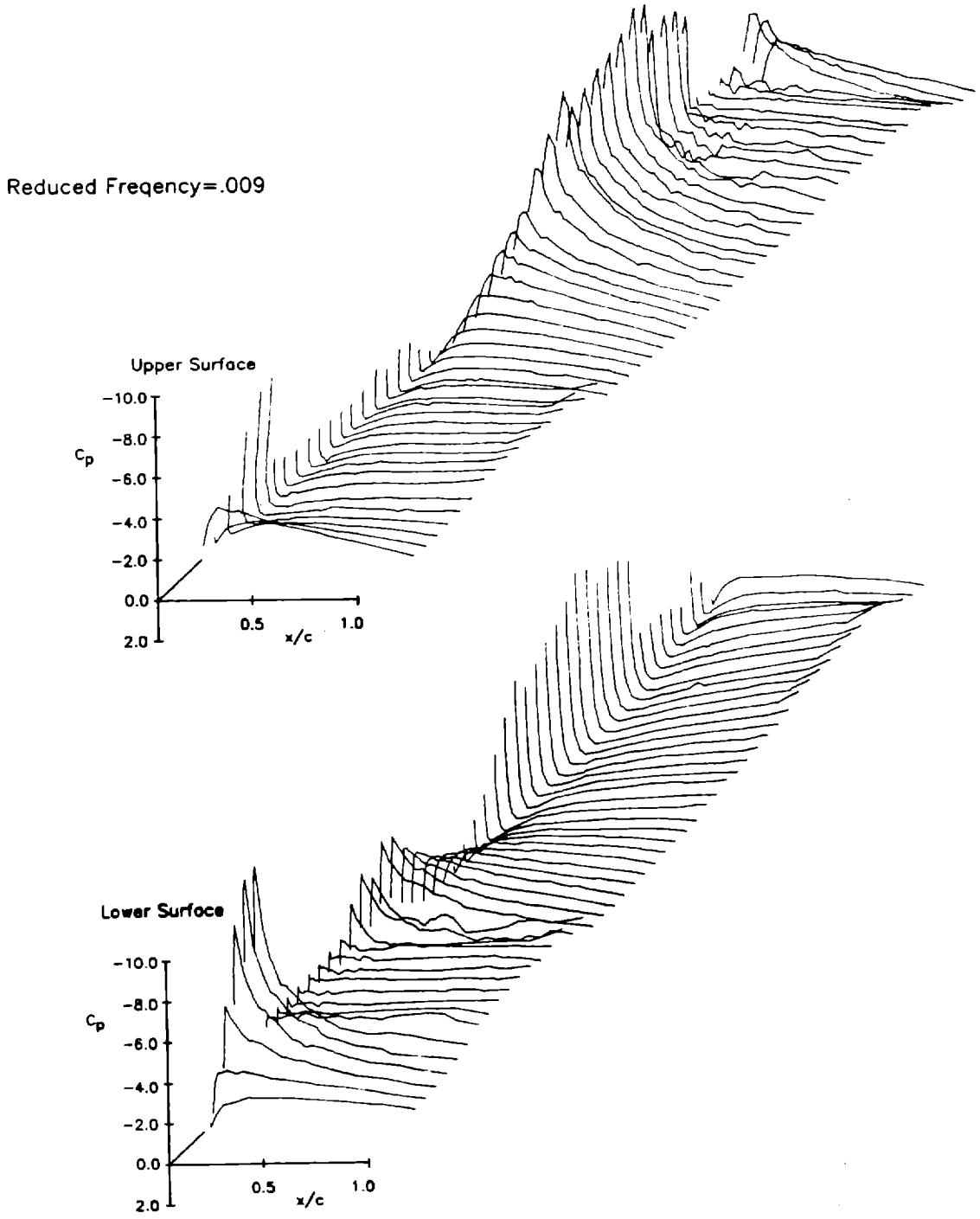

Figure 38. Oscillatory Pressure Distributions for NACA 0021 with Vortex Generators at .1c Chord Location—30° Inverse Tangent Function

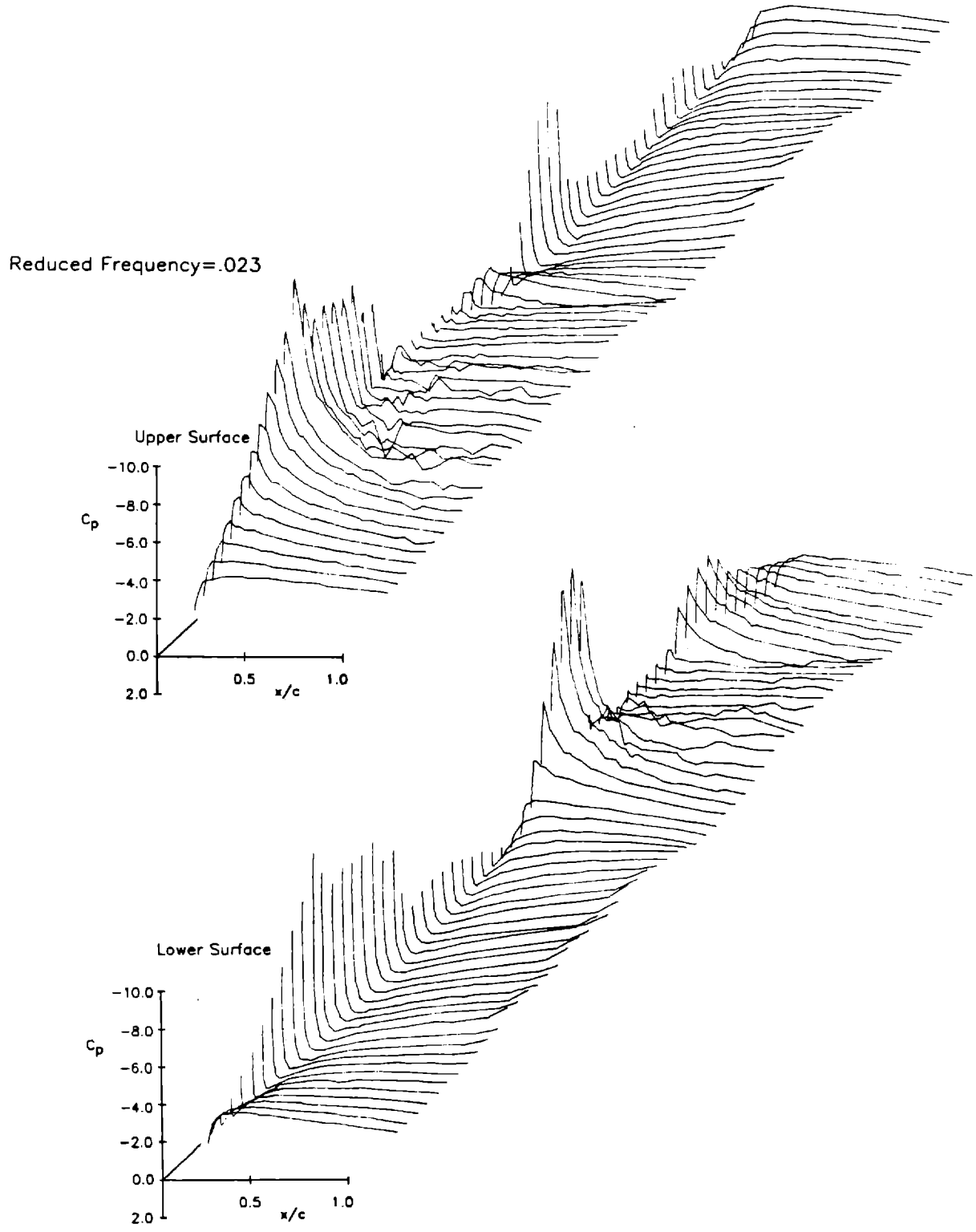

Figure 39. Oscillatory Pressure Distributions for NACA 0021 with Vortex Generators at .1c Chord Location–30° Inverse Tangent Function

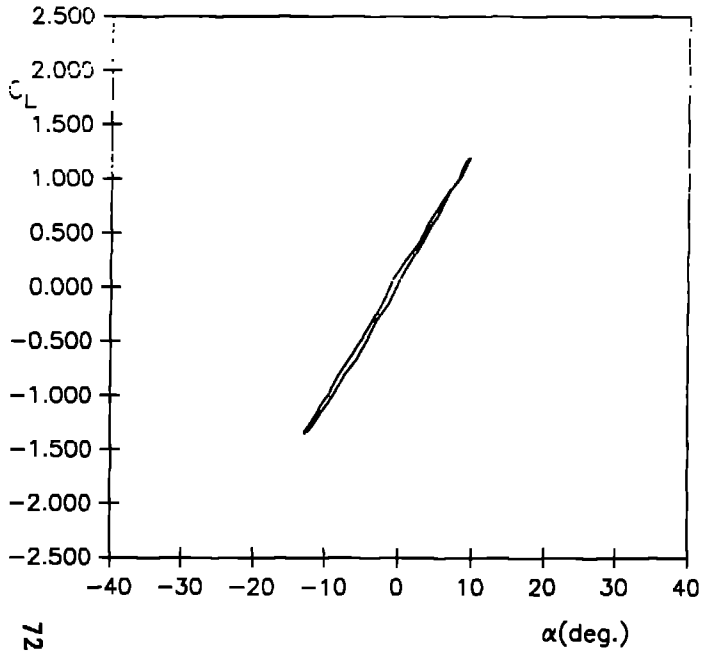

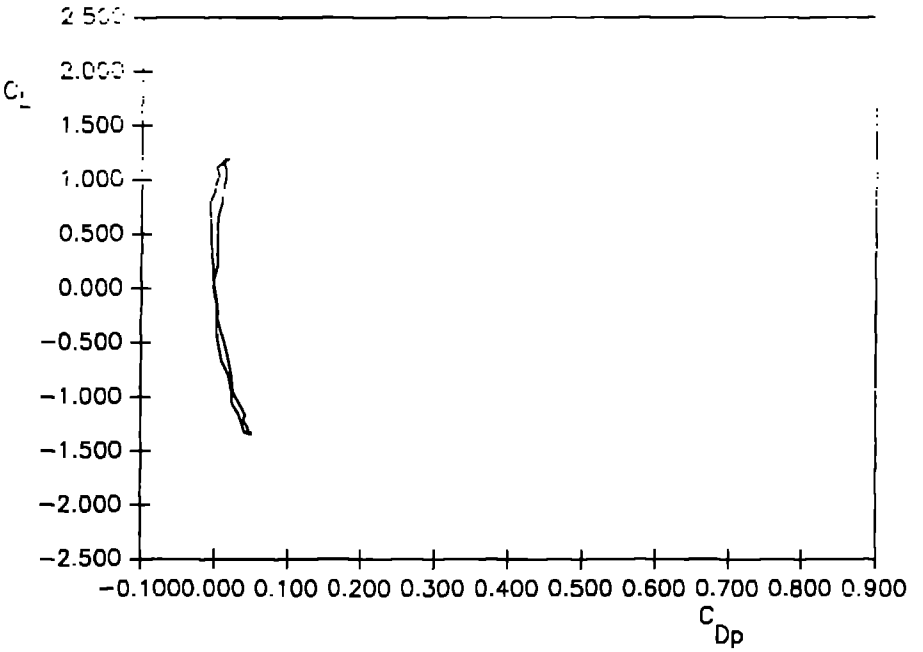

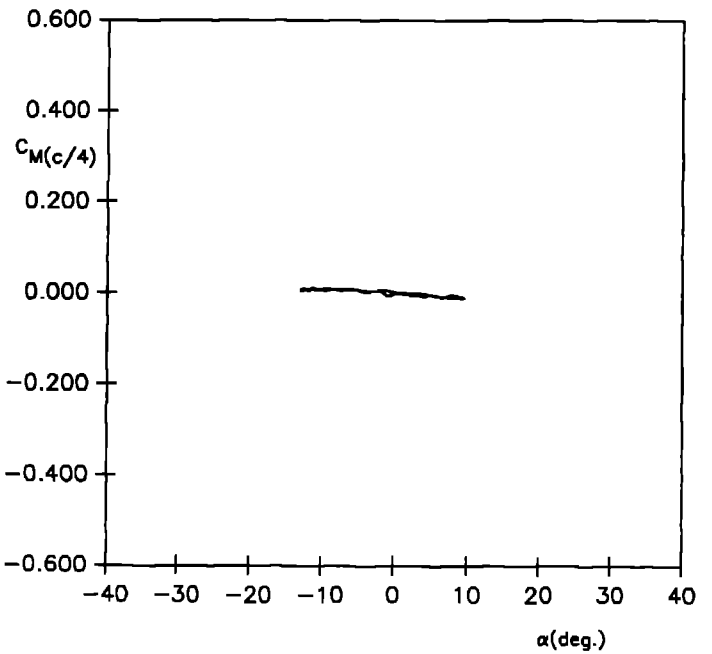

Reduced Frequency = .009

Figure 40. Integrated Oscillatory Pressure Data for NACA 0021 with Vortex Generators at .3c Chord Location−10° Sine Function

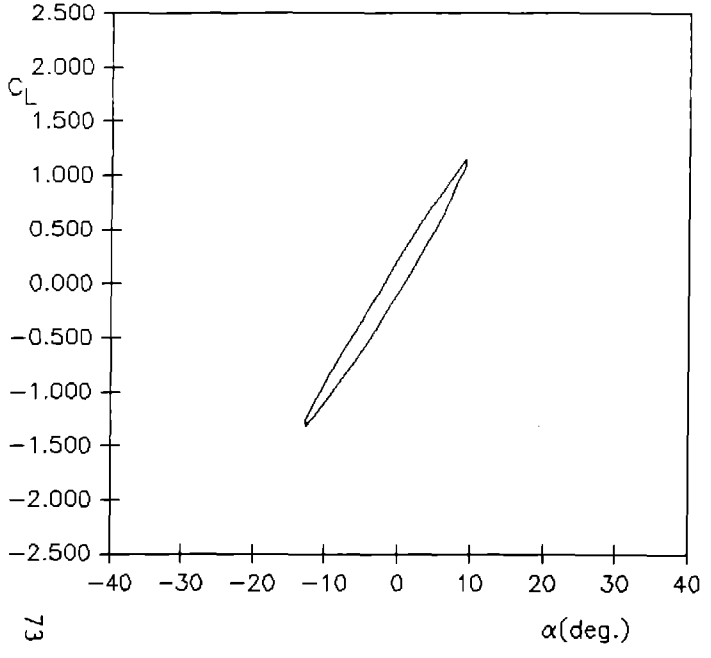

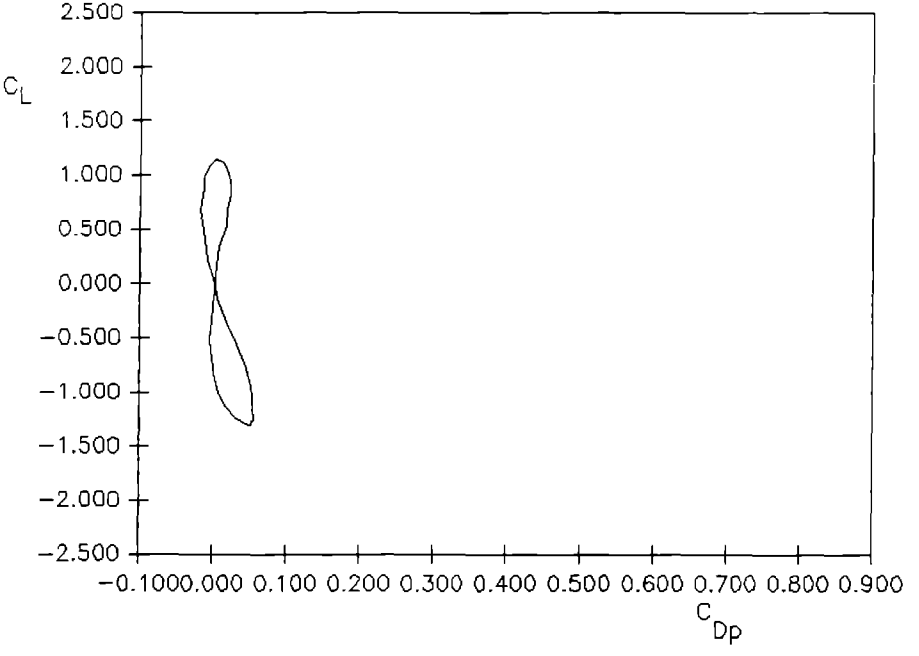

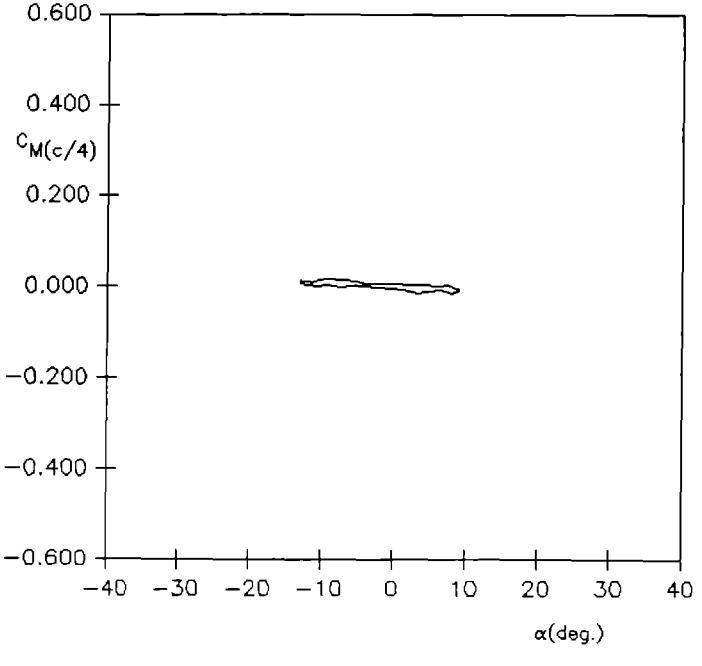

Reduced Frequency = .034

Figure 41. Integrated Oscillatory Pressure Data for NACA 0021 with Vortex Generators at .3c Chord Location—10° Sine Function

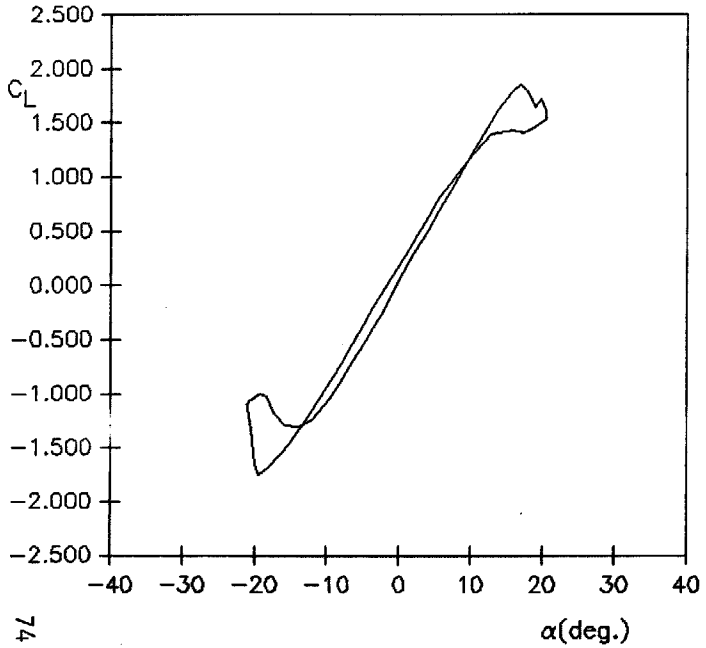

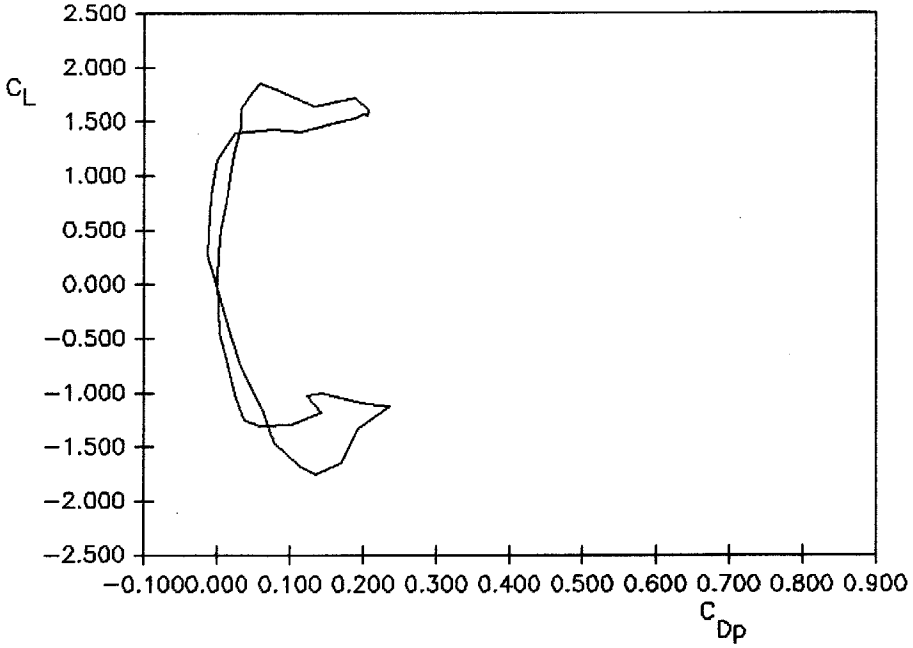

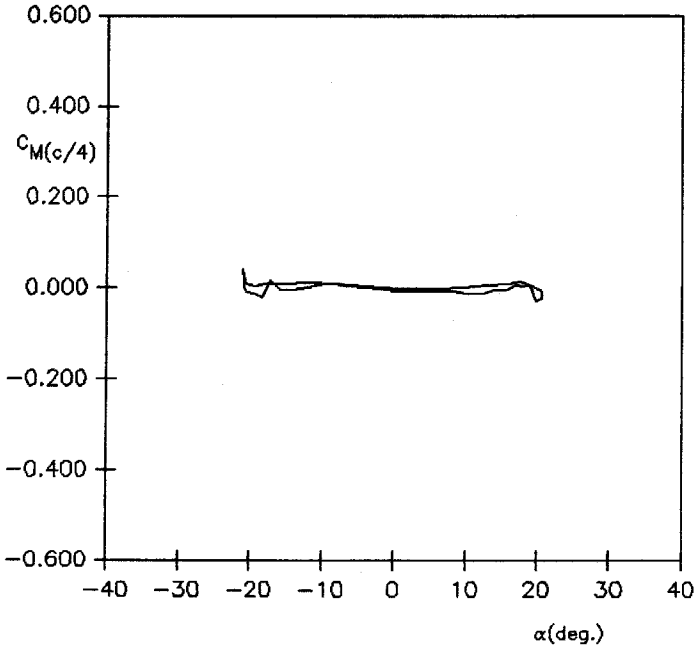

Reduced Frequency = .009

Figure 42. Integrated Oscillatory Pressure Data for NACA 0021 with Vortex Generators at .3c Chord Location−20° Inverse Tangent Function

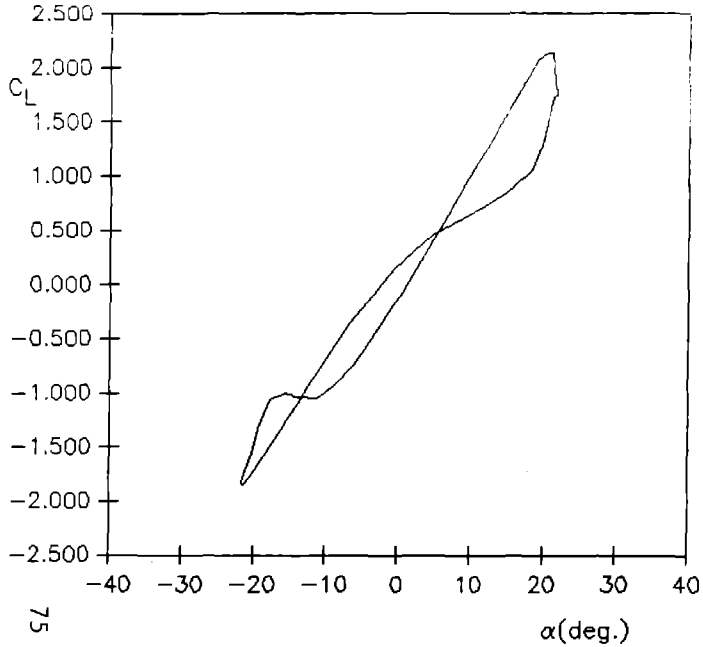

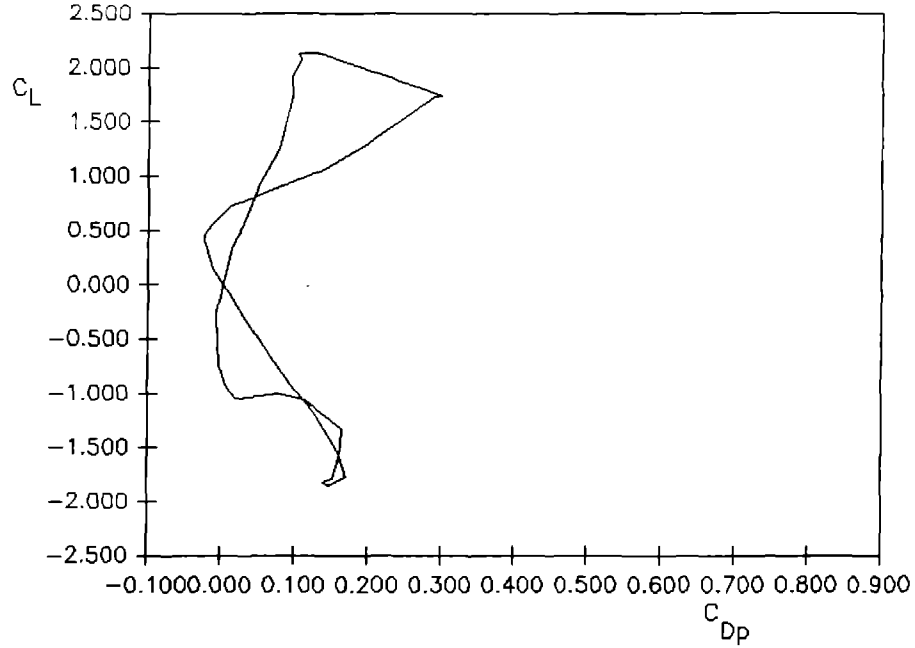

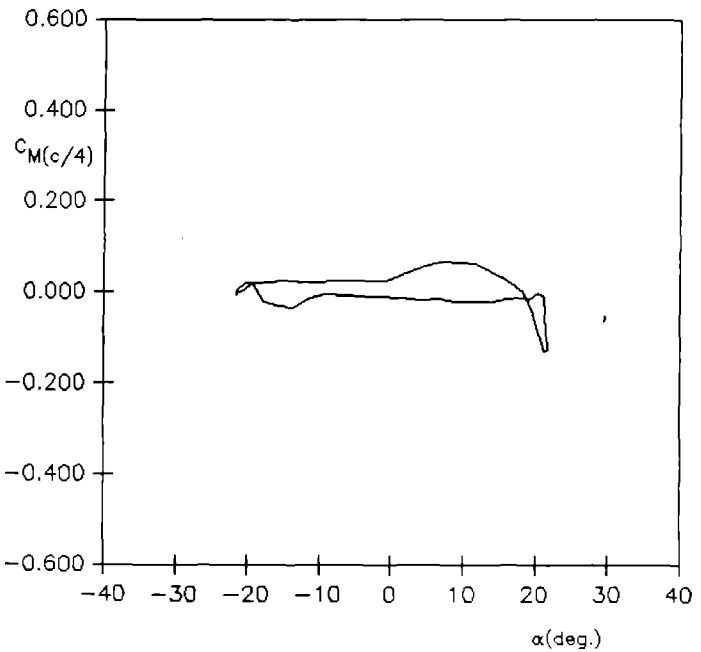

Reduced Frequency = .034

Figure 43. Integrated Oscillatory Pressure Data for NACA 0021 with Vortex Generators at .3c Chord Location−20° Inverse Tangent Function

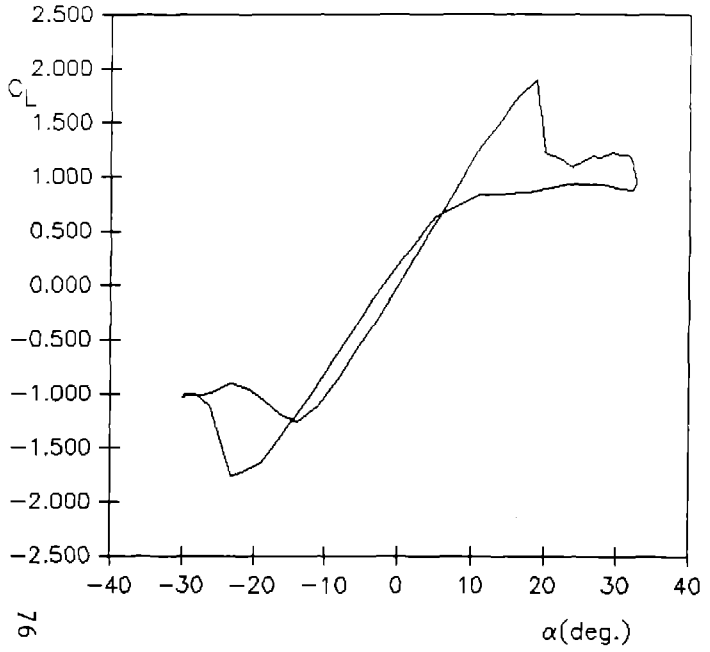

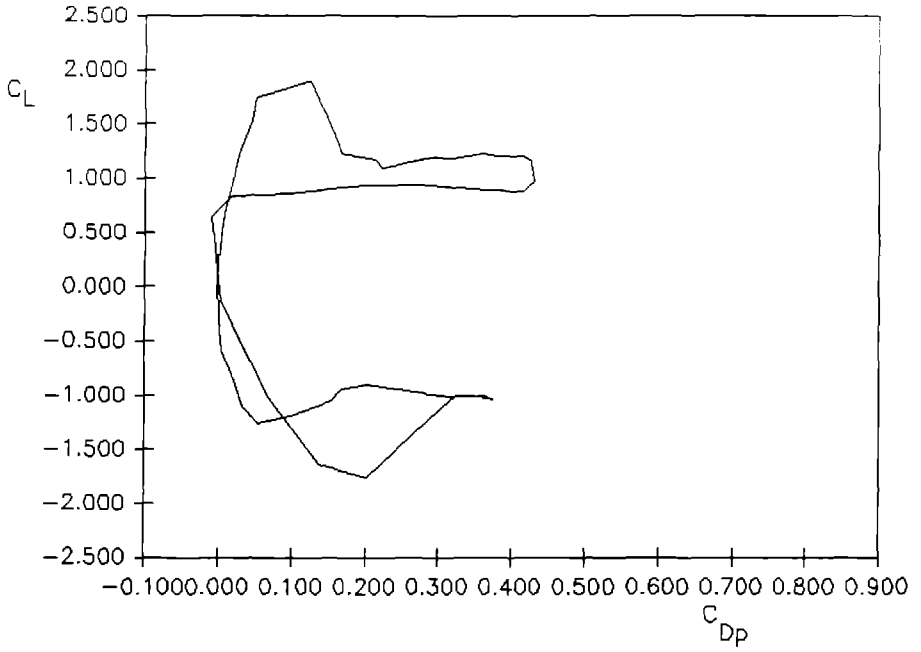

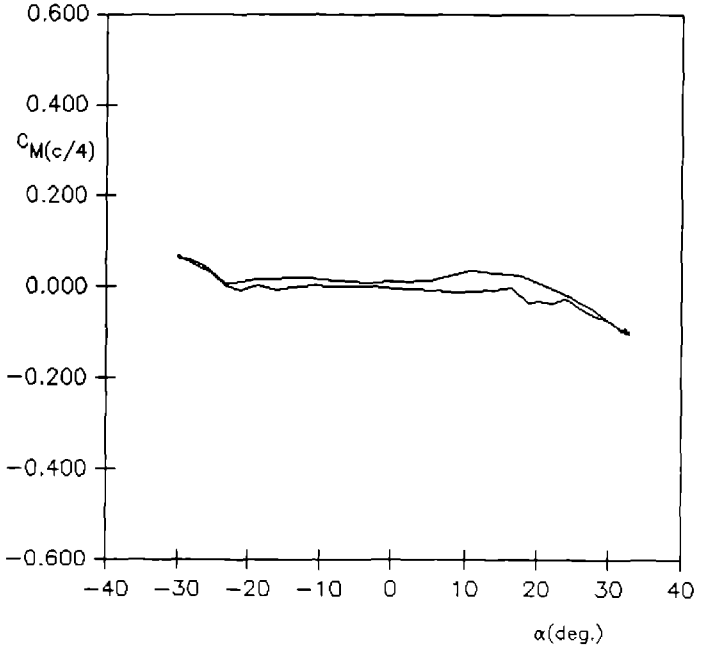

Reduced Frequency = .009

Figure 44. Integrated Oscillatory Pressure Data for NACA 0021 with Vortex Generators at .3c Chord Location−30° Inverse Tangent Function

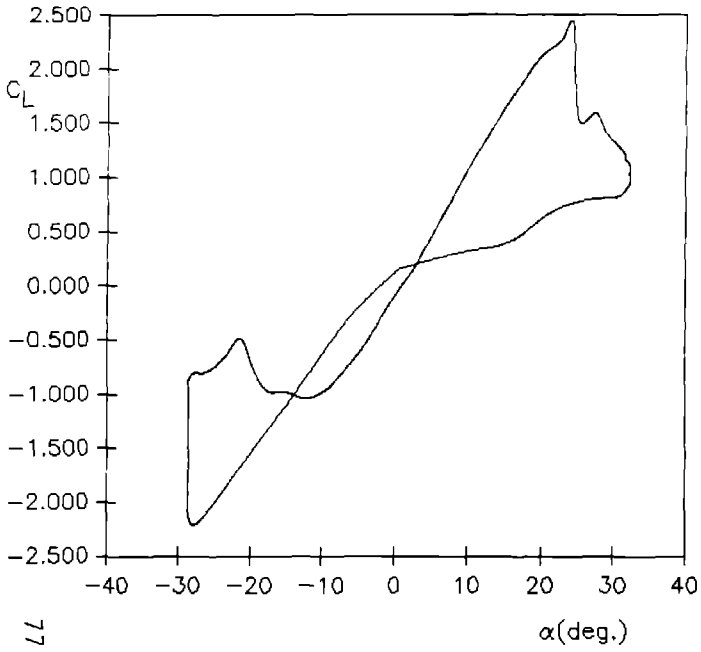

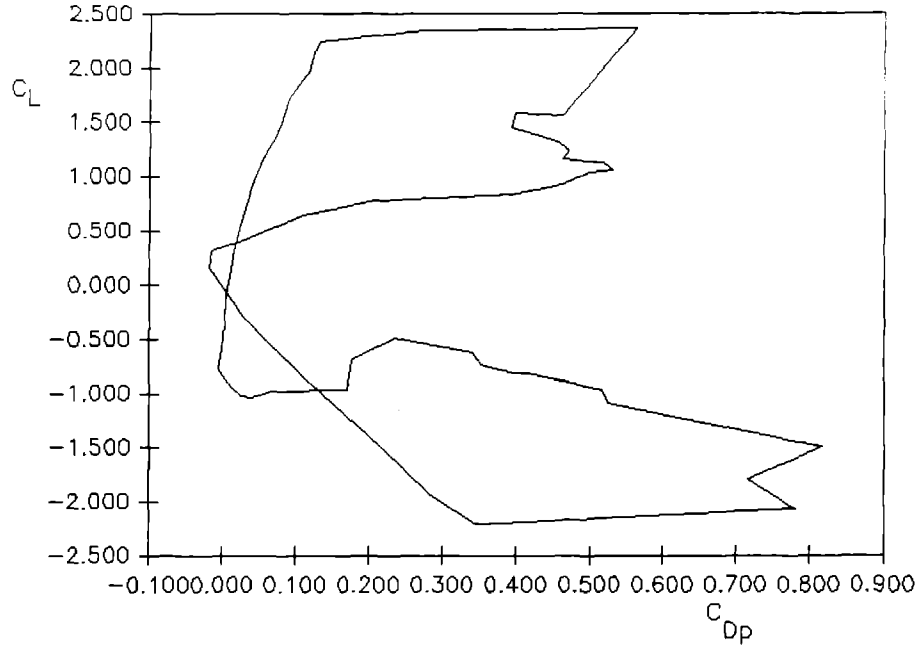

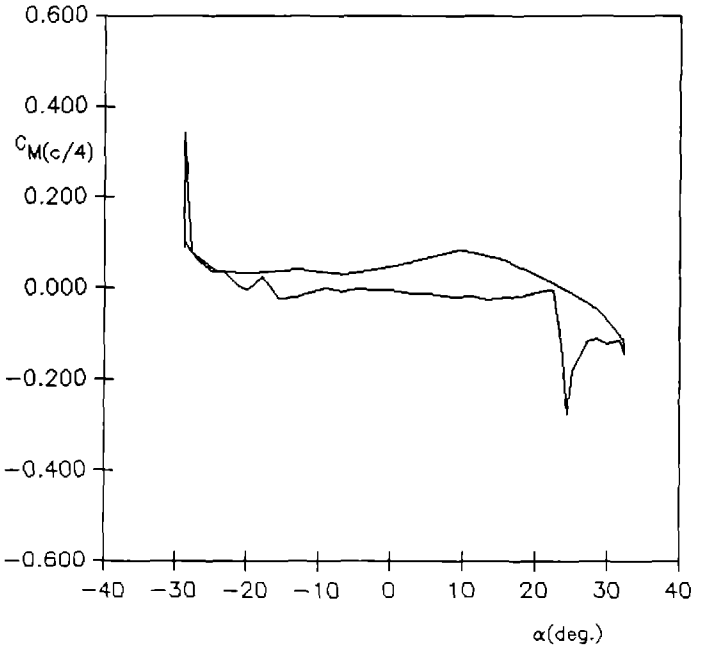

Reduced Frequency = .023

Figure 45. Integrated Oscillatory Pressure Data for NACA 0021 with Vortex Generators at .3c Chord Location−30° Inverse Tangent Function

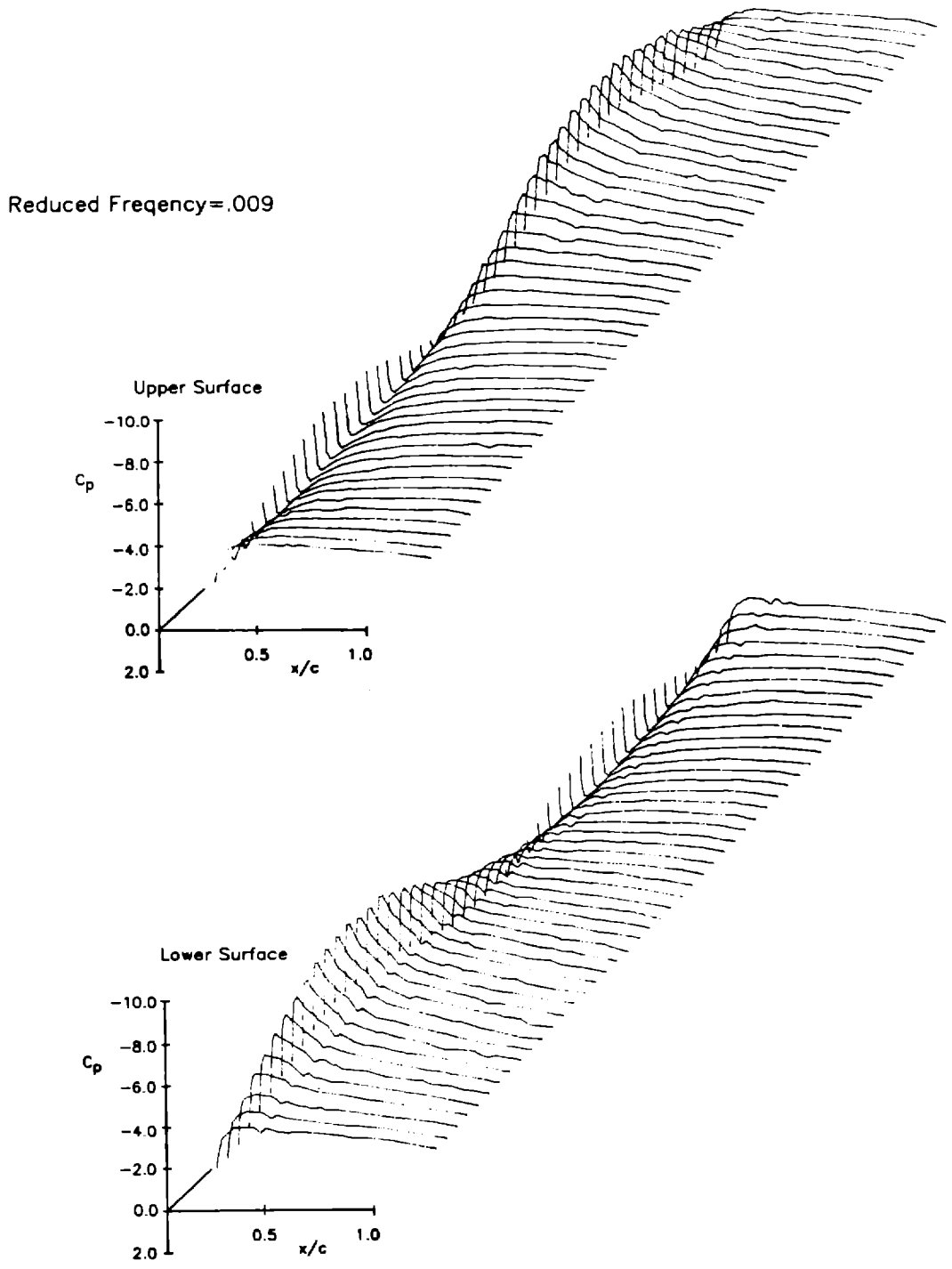

Figure 46. Oscillatory Pressure Distributions for NACA 0021 with Vortex Generators at .3c Chord Location–10° Sine Function

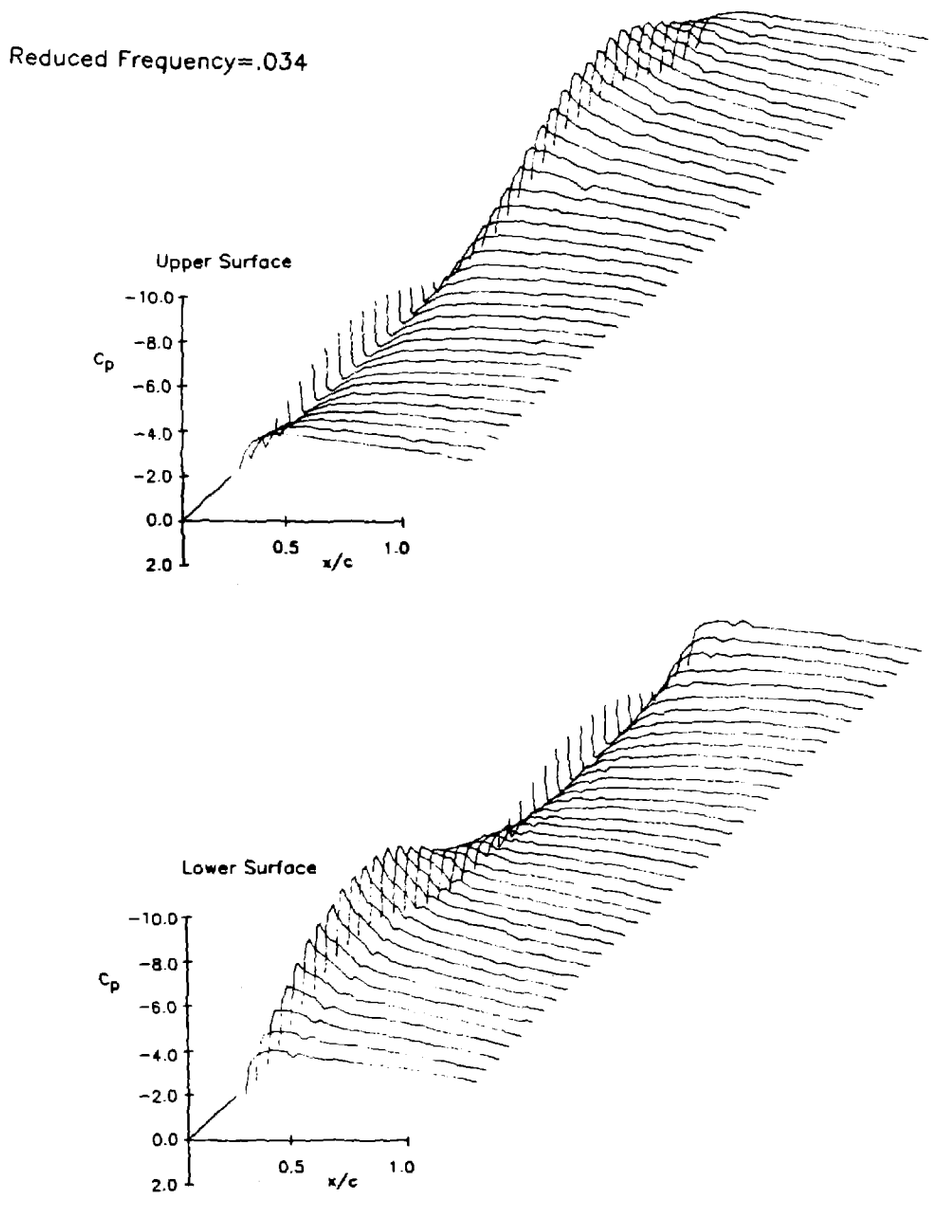

Figure 47. Oscillatory Pressure Distributions for NACA 0021 with Vortex Generators at .3c Chord Location–10° Sine Function

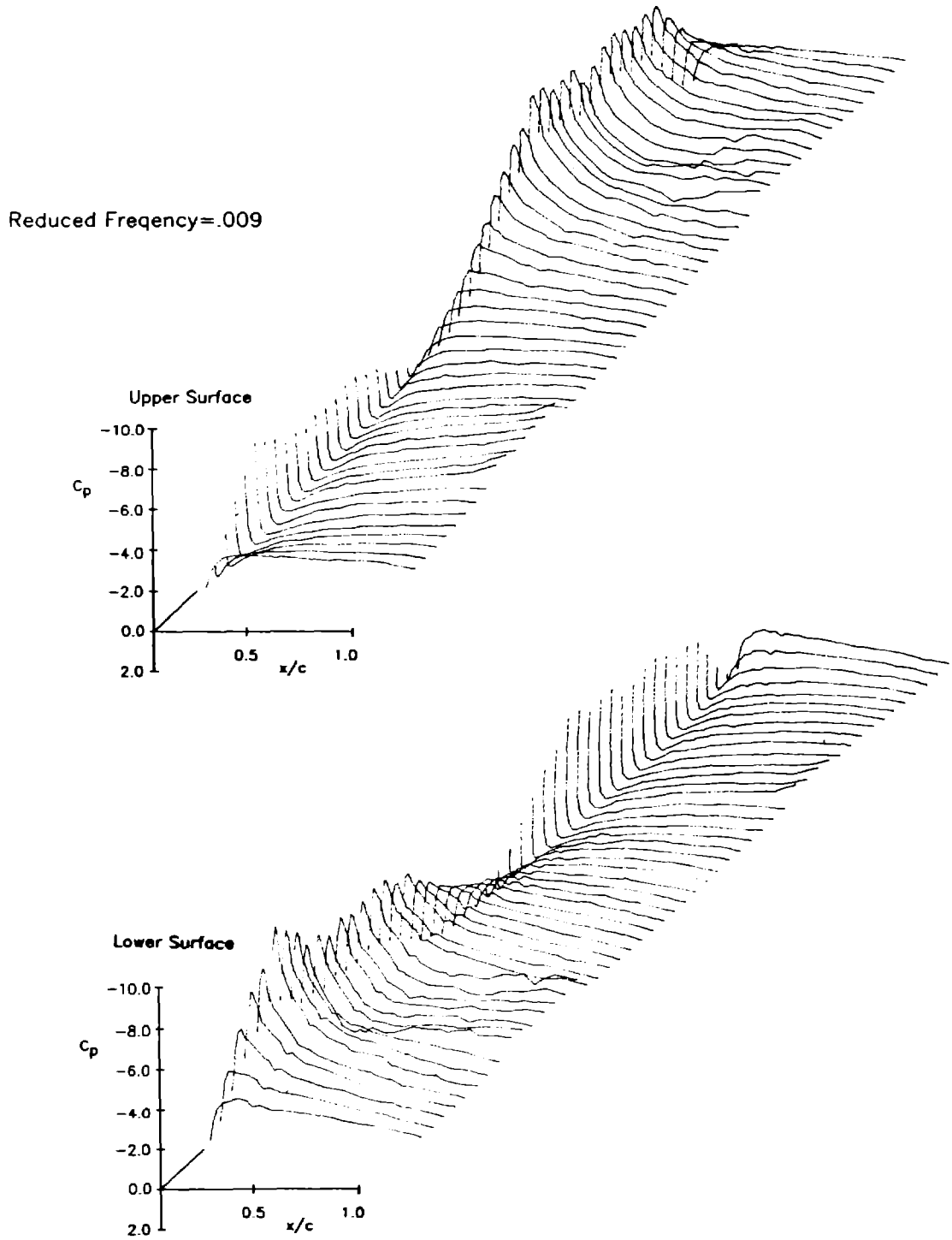

Figure 48. Oscillatory Pressure Distributions for NACA 0021 with Vortex Generators at .3c Chord Location–20° Inverse Tangent Function

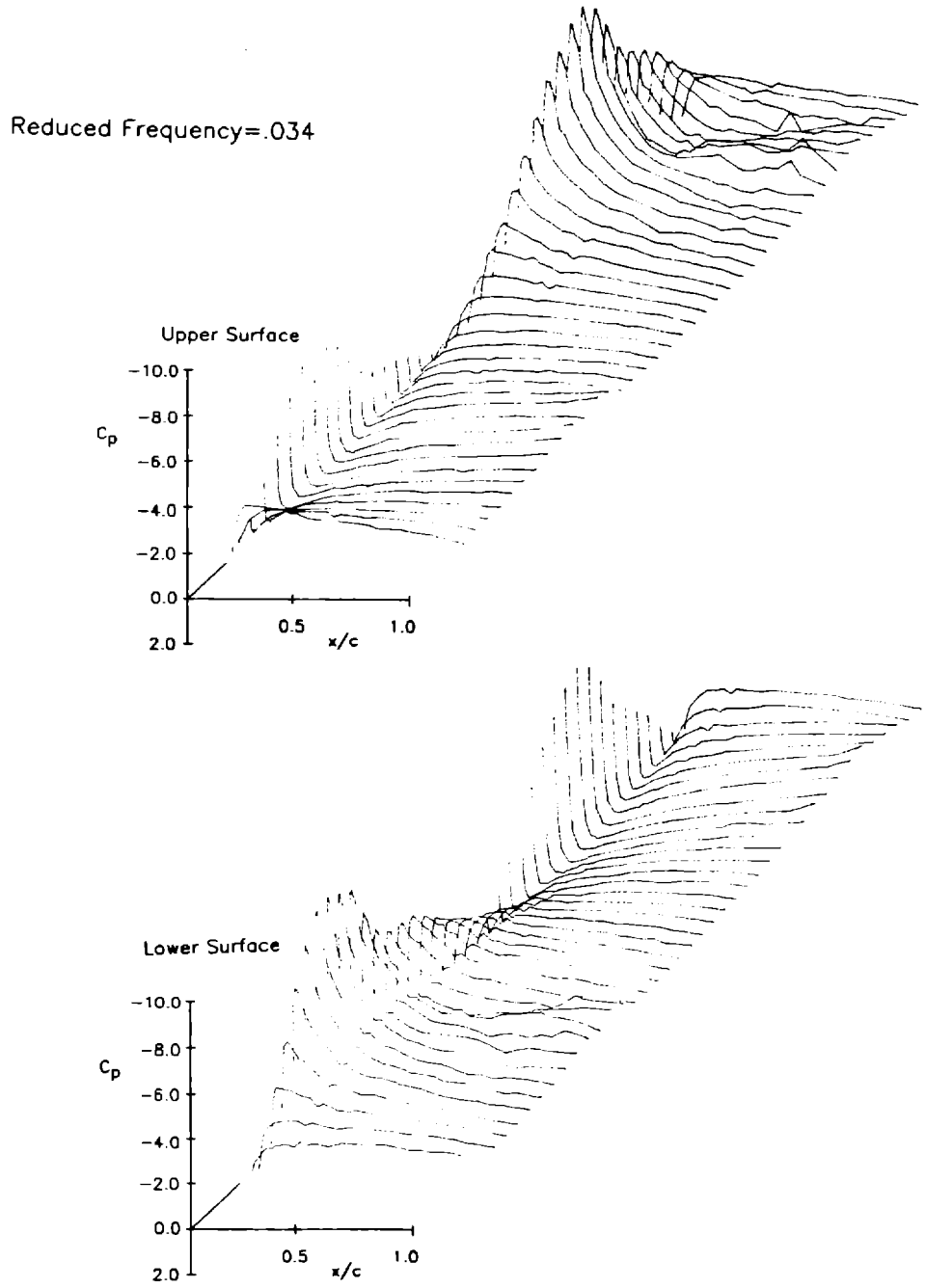

Figure 49. Oscillatory Pressure Distributions for NACA 0021 with Vortex Generators at .3c Chord Location–20° Inverse Tangent Function

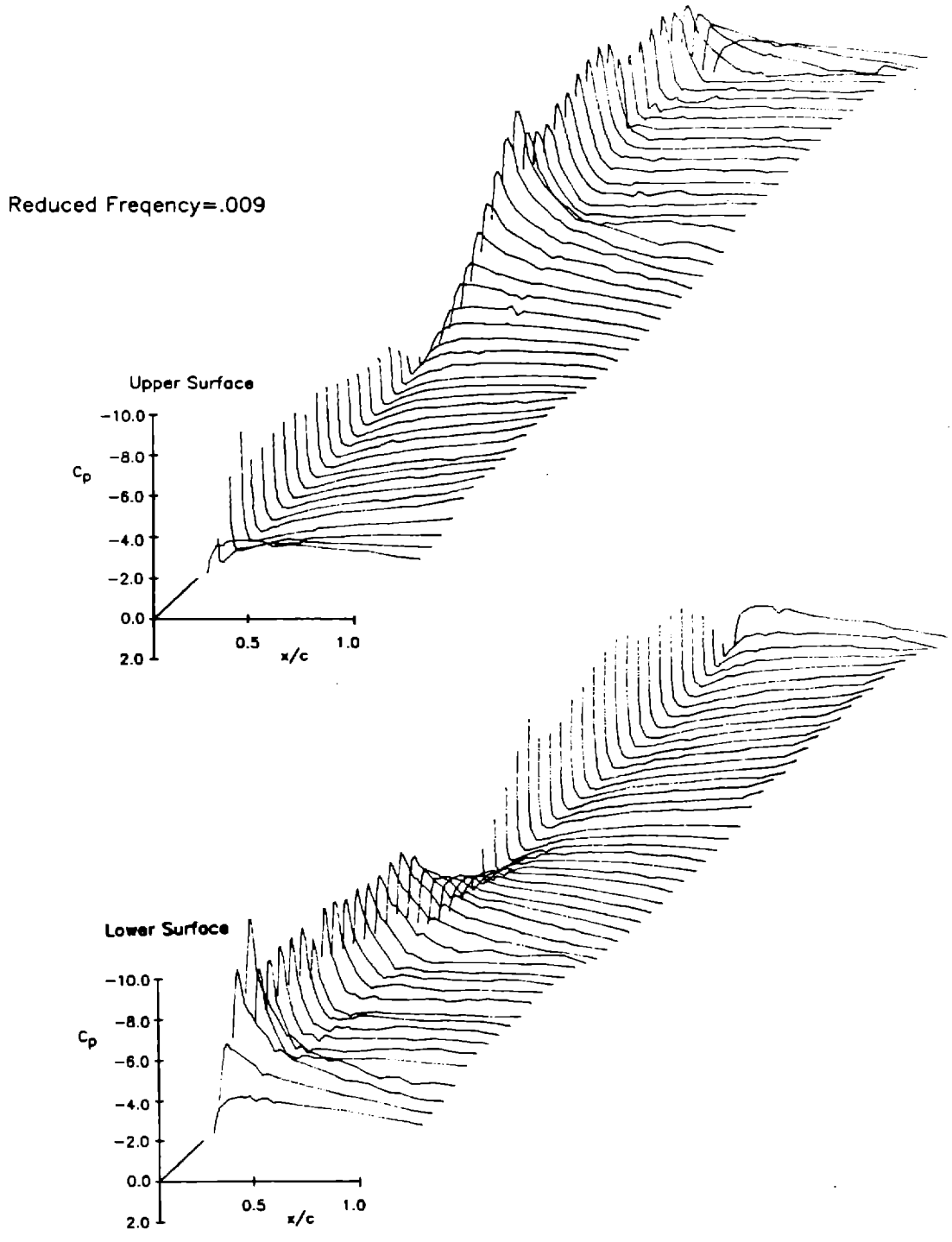

Figure 50. Oscillatory Pressure Distributions for NACA 0021 with Vortex Generators at .3c Chord Location–30° Inverse Tangent Function

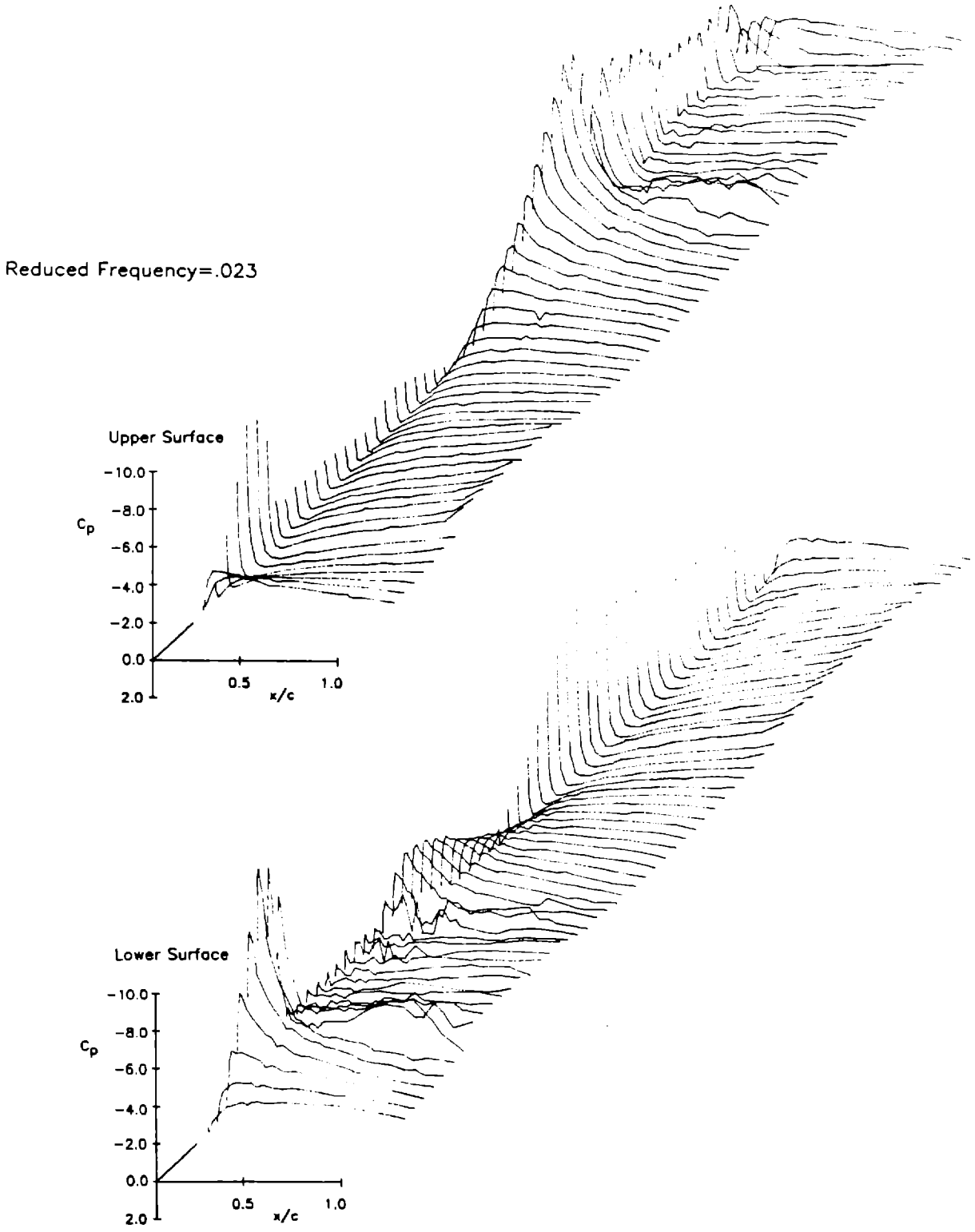

Figure 51. Oscillatory Pressure Distributions for NACA 0021 with Vortex Generators at .3c Chord Location–30° Inverse Tangent Function

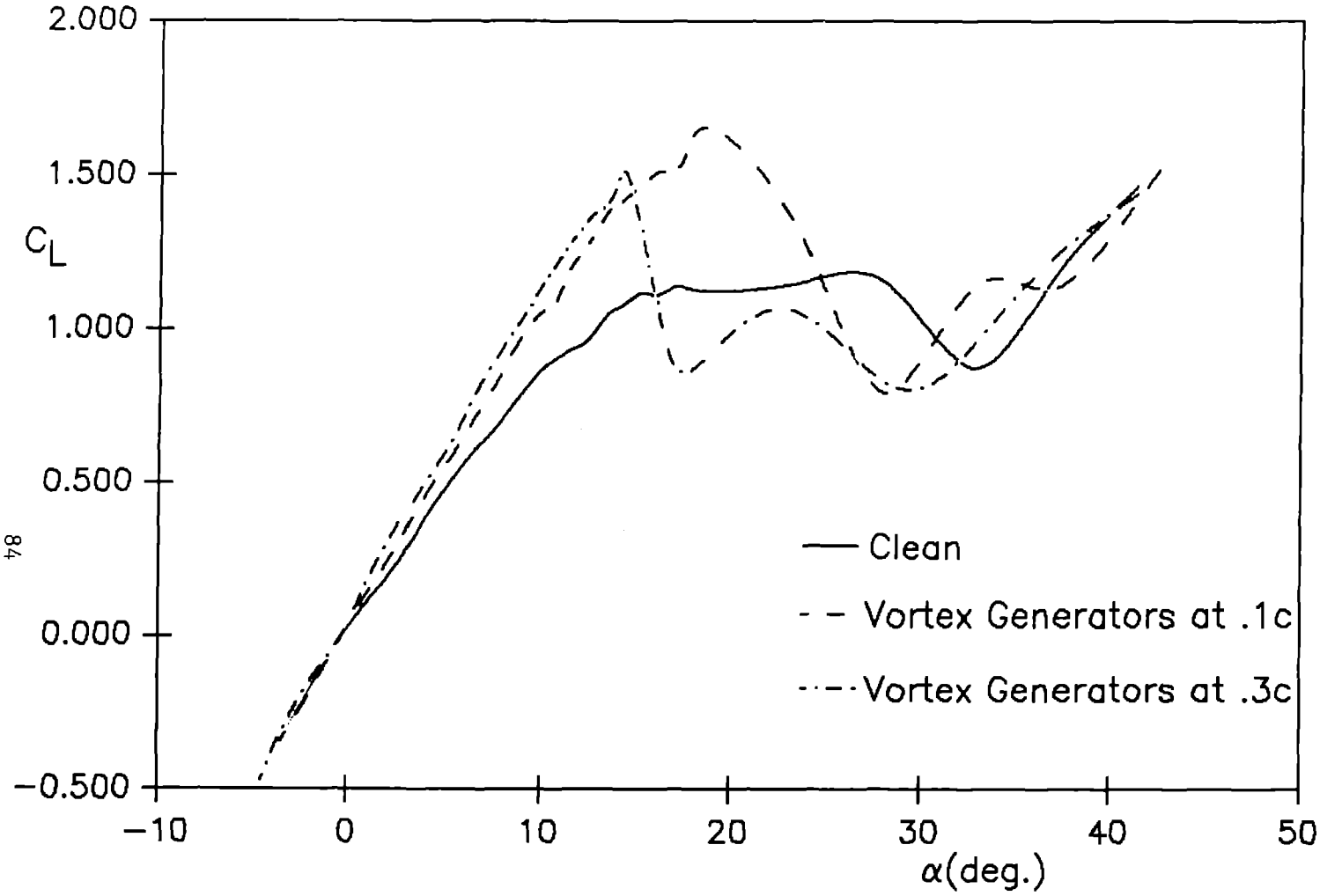

Figure 52. Lift Coefficient versus Angle of Attack for NACA 0021—Steady State

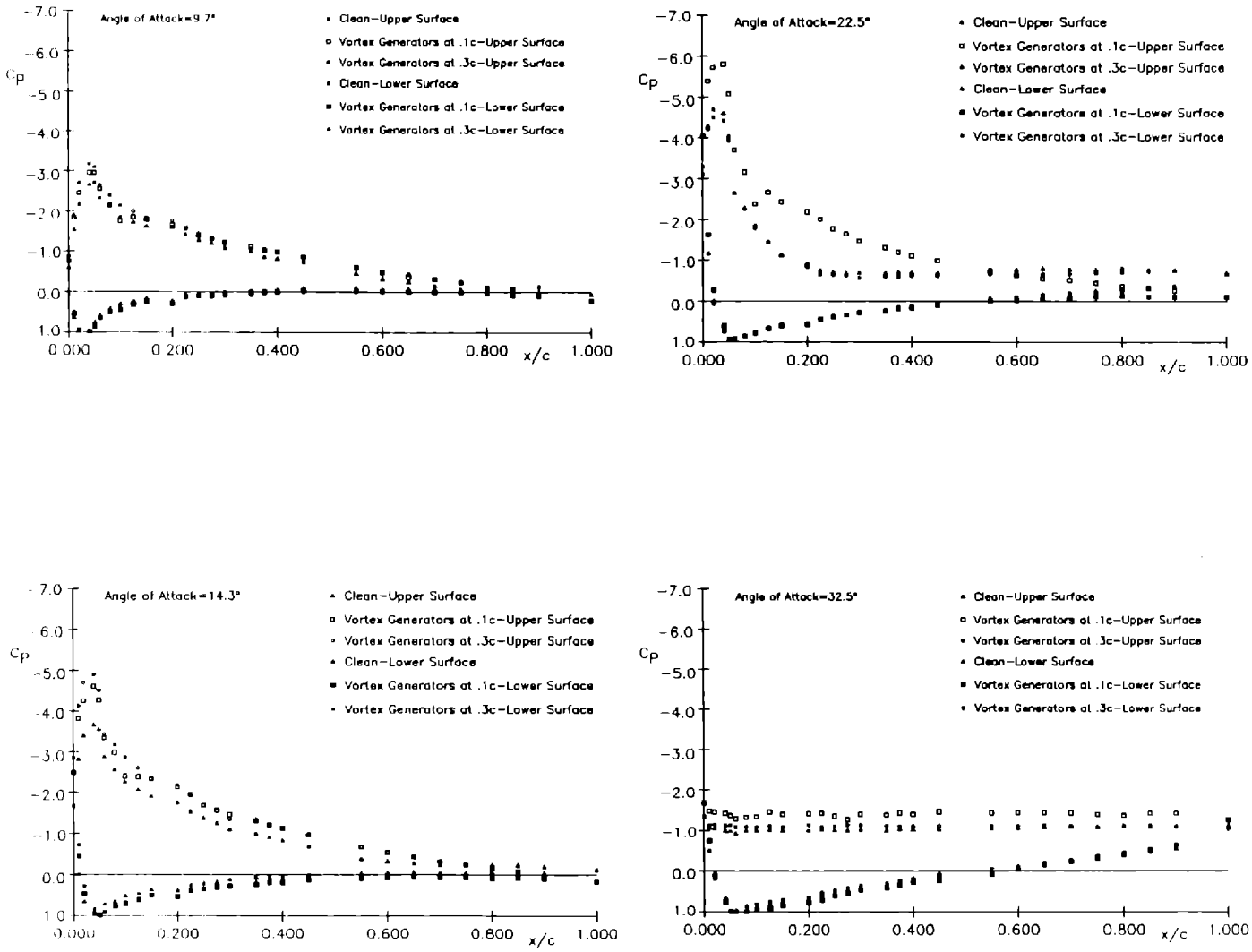

Figure 53. Pressure Distributions for NACA 0021–Steady State

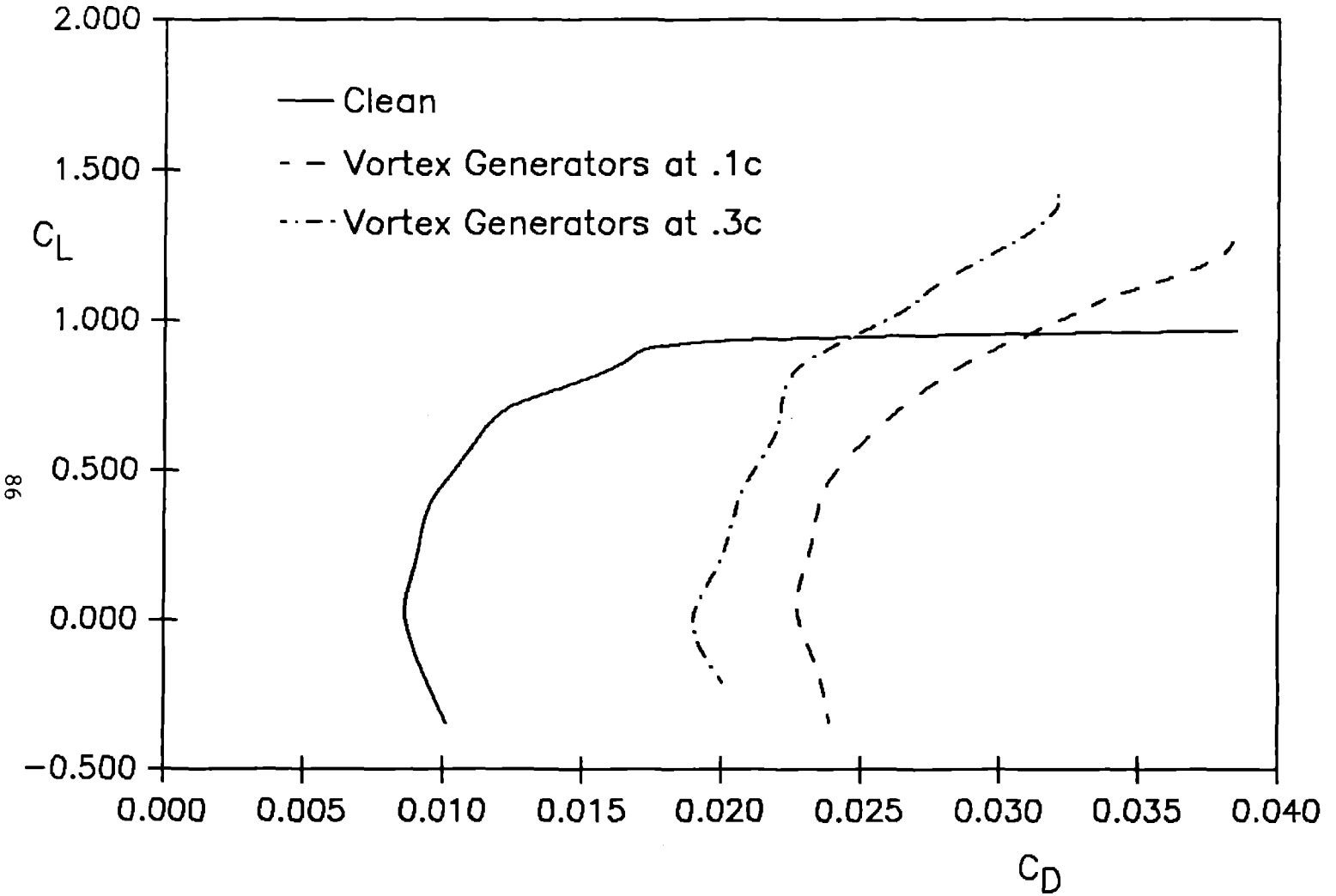

Figure 54. Lift Coefficient versus Drag Coefficient for NACA 0021−Steady State

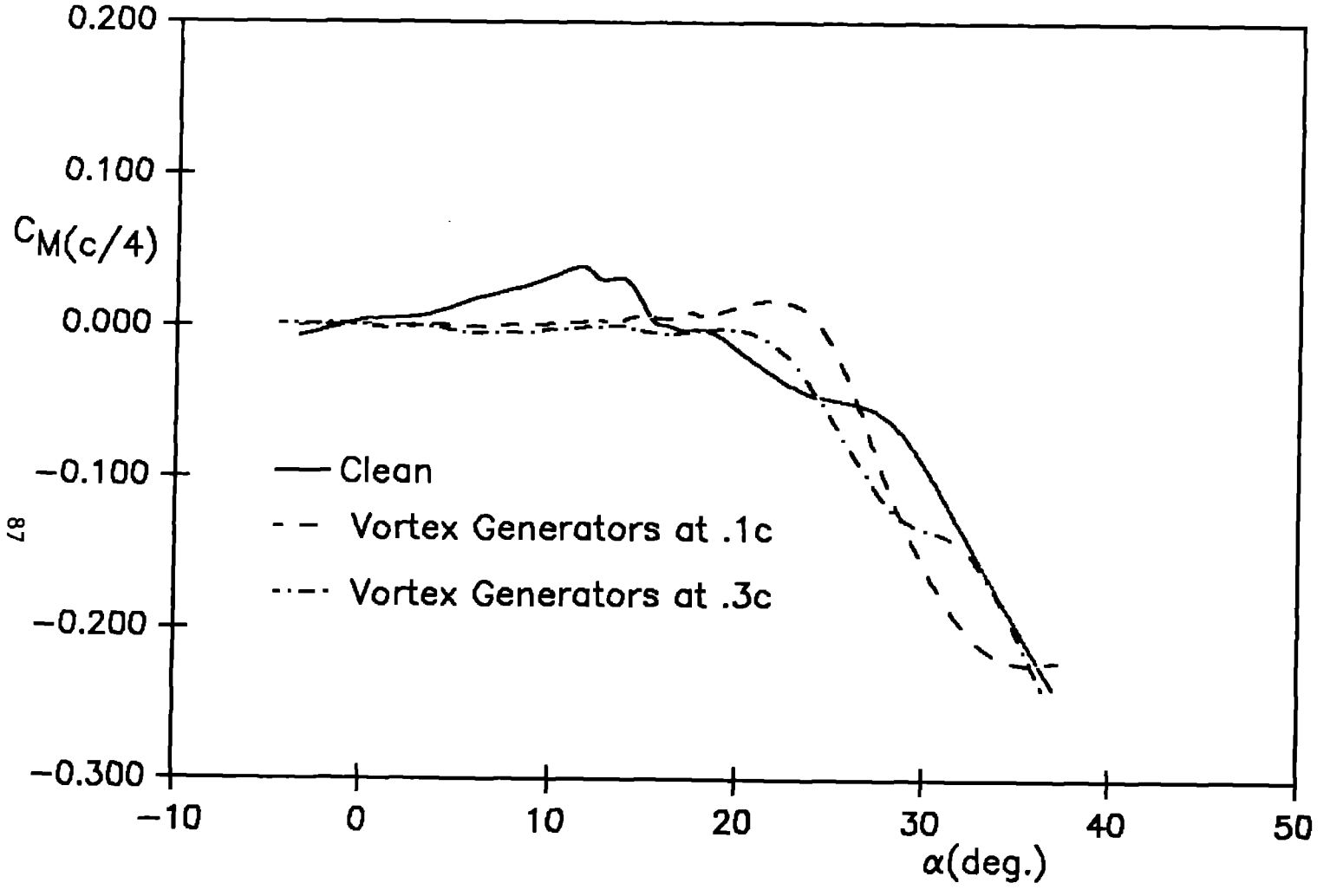

Figure 55. Coefficient of Pitching Moment about the Quarter Chord versus Angle of Attack for NACA 0021 – Steady State

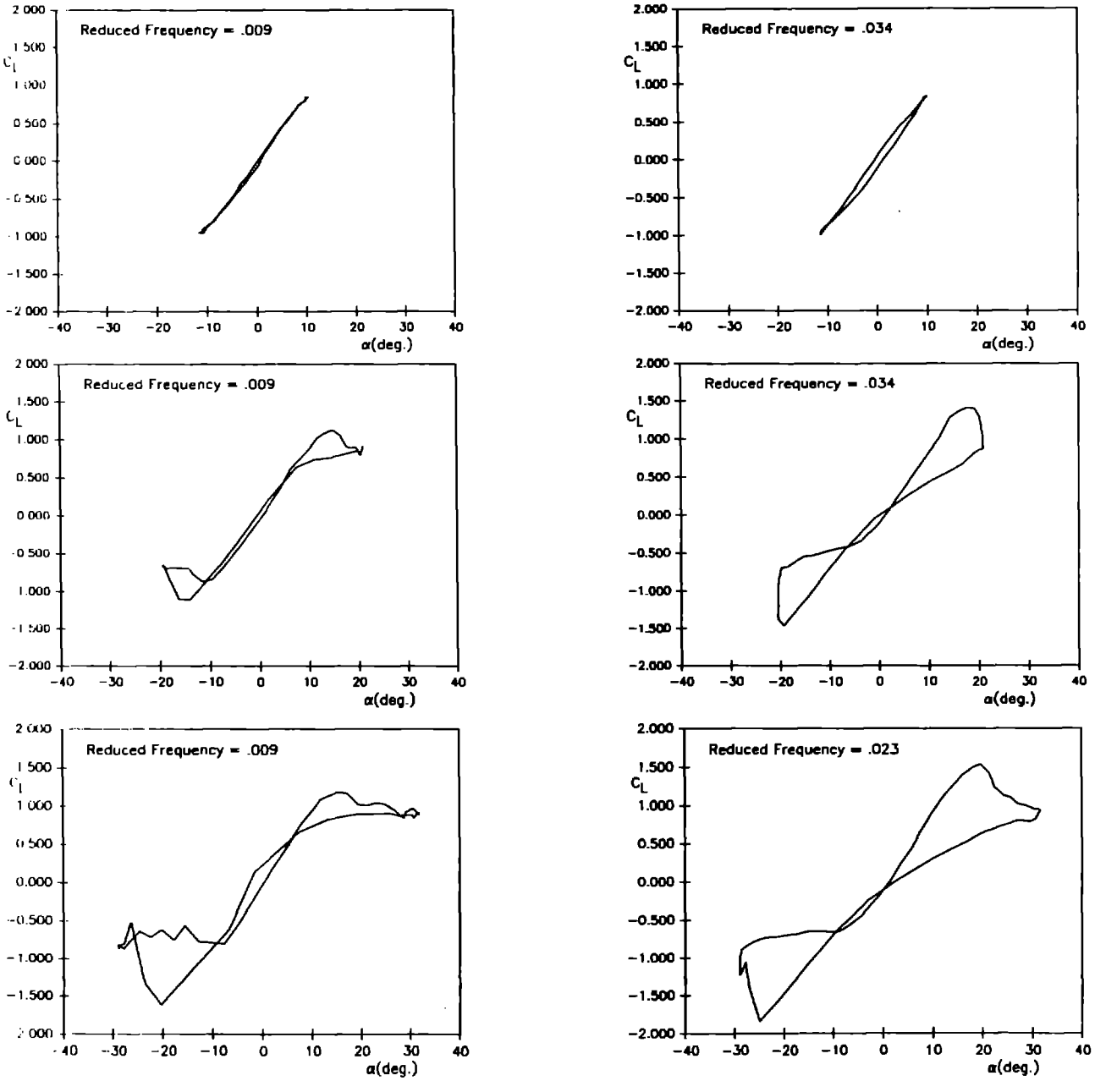

Figure 56. Lift Coefficient versus Angle of Attack for NACA 0021 with No Vortex Generators—Oscillatory

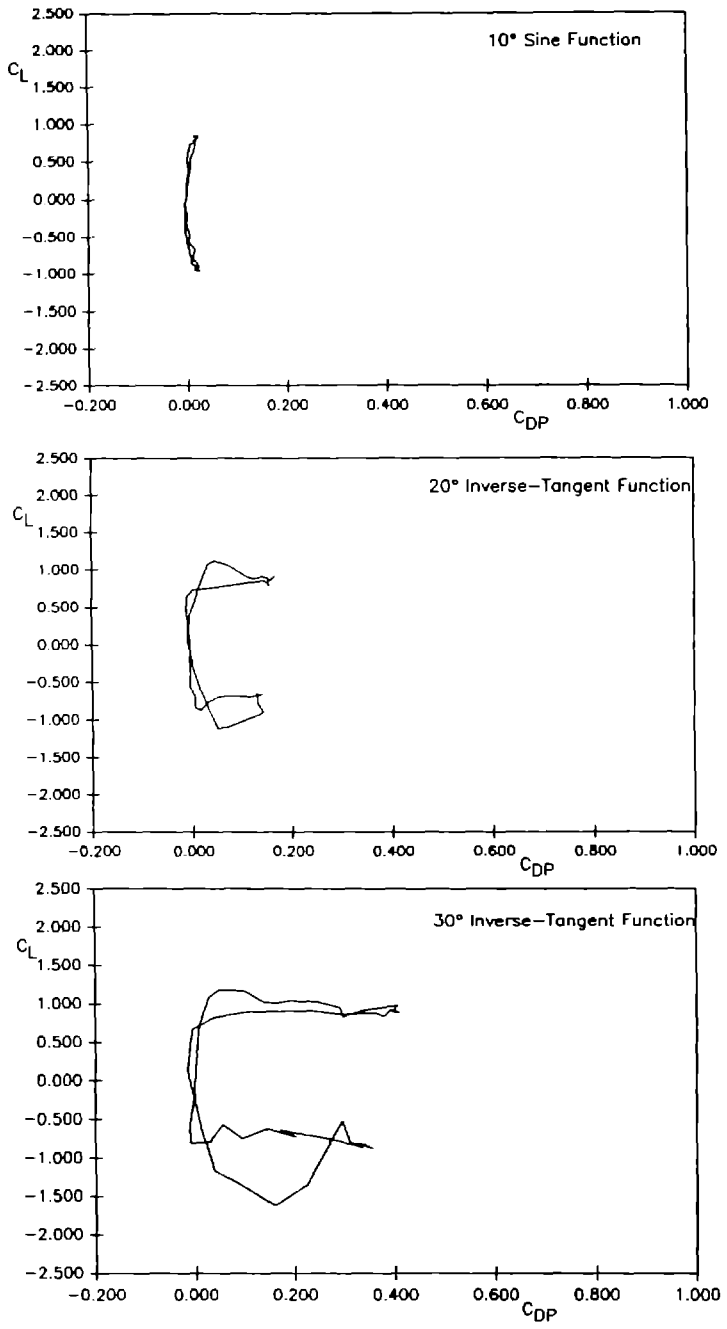

Figure 57. Lift Coefficient versus Pressure Drag Coefficient for NACA 0021 with No Vortex Generators Reduced Frequency = .009

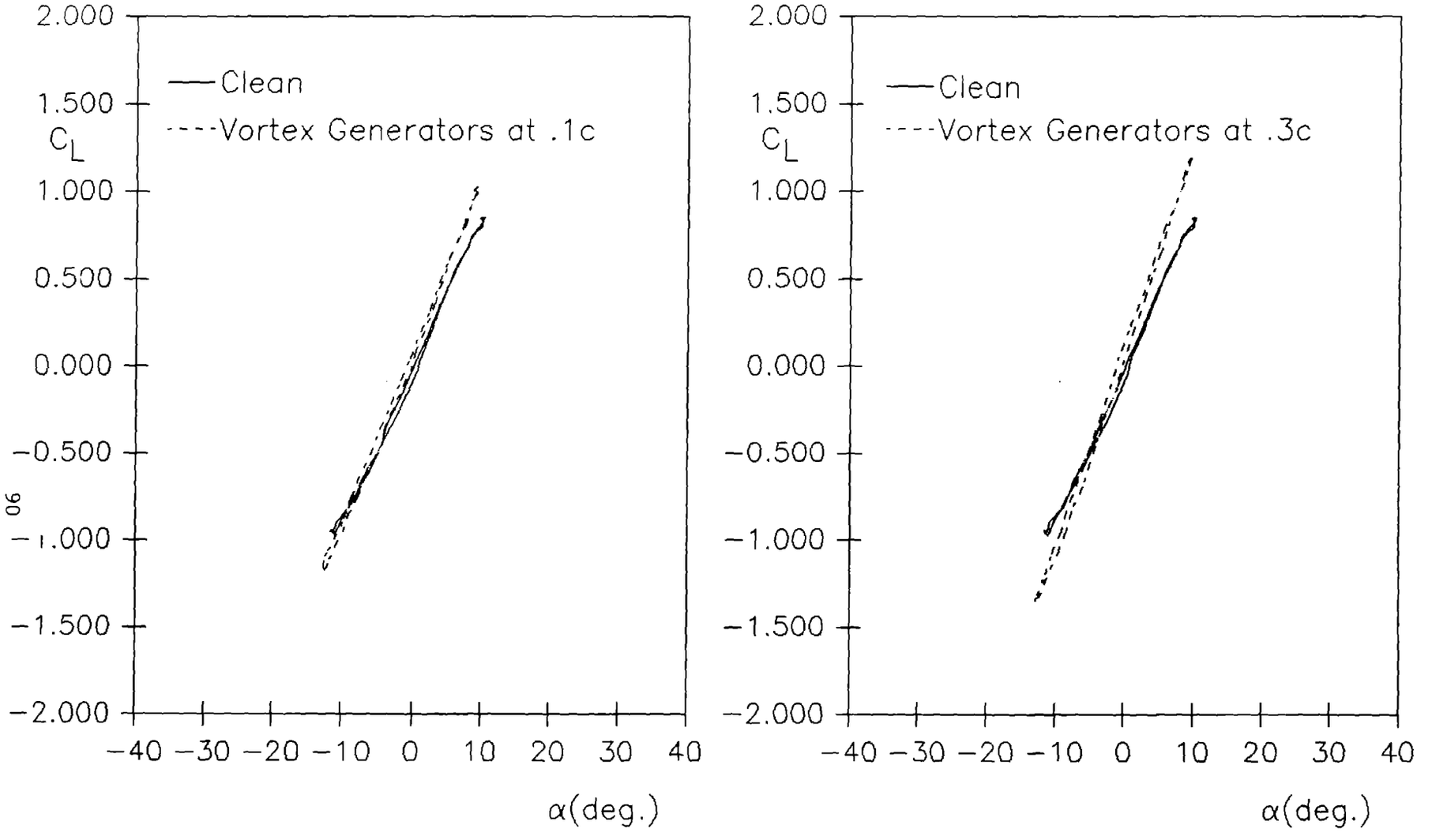

Figure 58. Oscillatory Lift Coefficient versus Angle of Attack for

NACA 0021 – 10° Sine Function, Reduced Frequency = .009

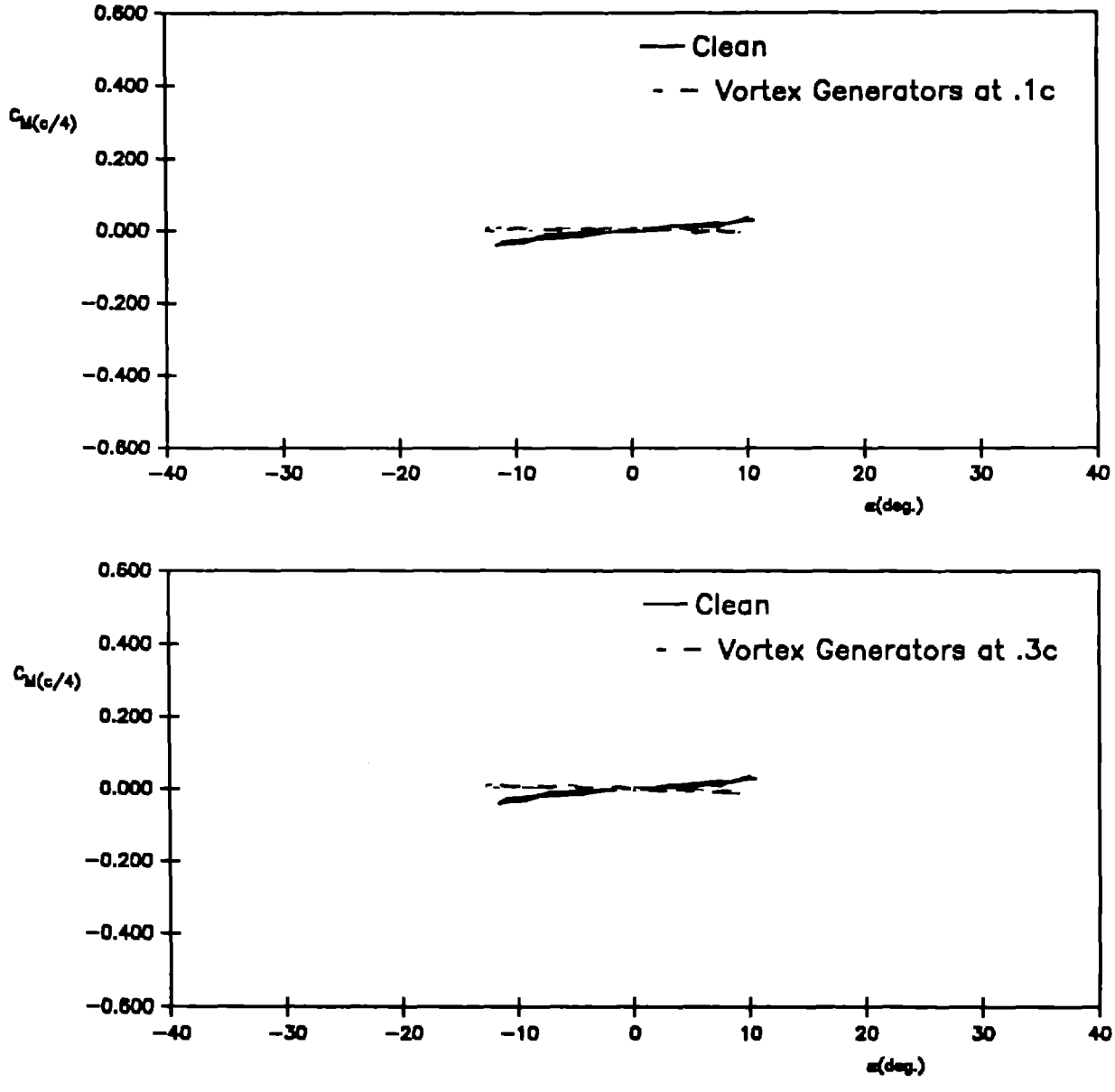

Figure 59. Oscillatory Pitching Moment Coefficient versus Angle of Attack for NACA 0021 – 10° Sine Function, Reduced Frequency = .009

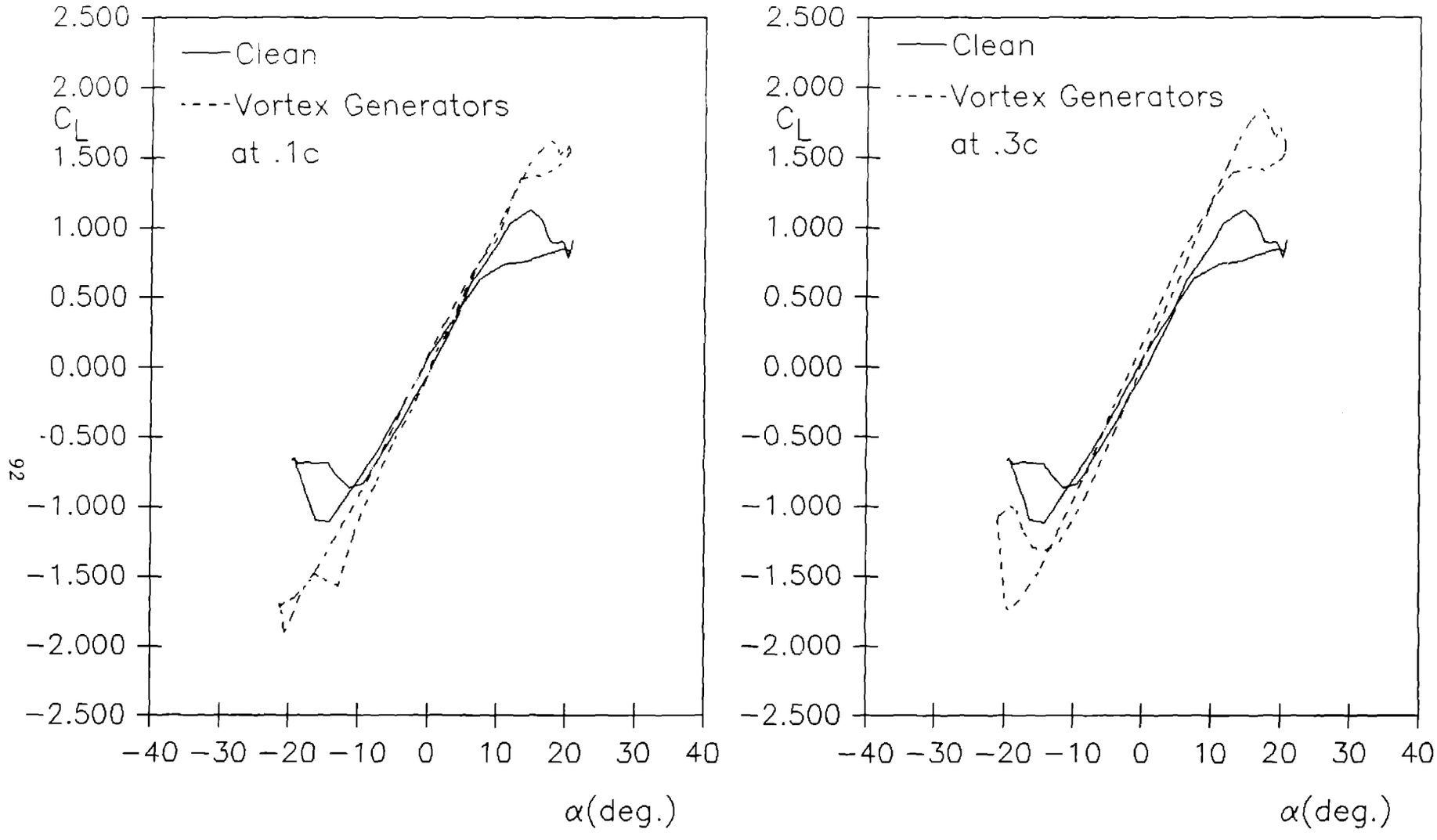

Figure 60. Oscillatory Lift Coefficient versus Angle of Attack for

NACA 0021 – 20° Inverse Tangent Function

Reduced Frequency = .009

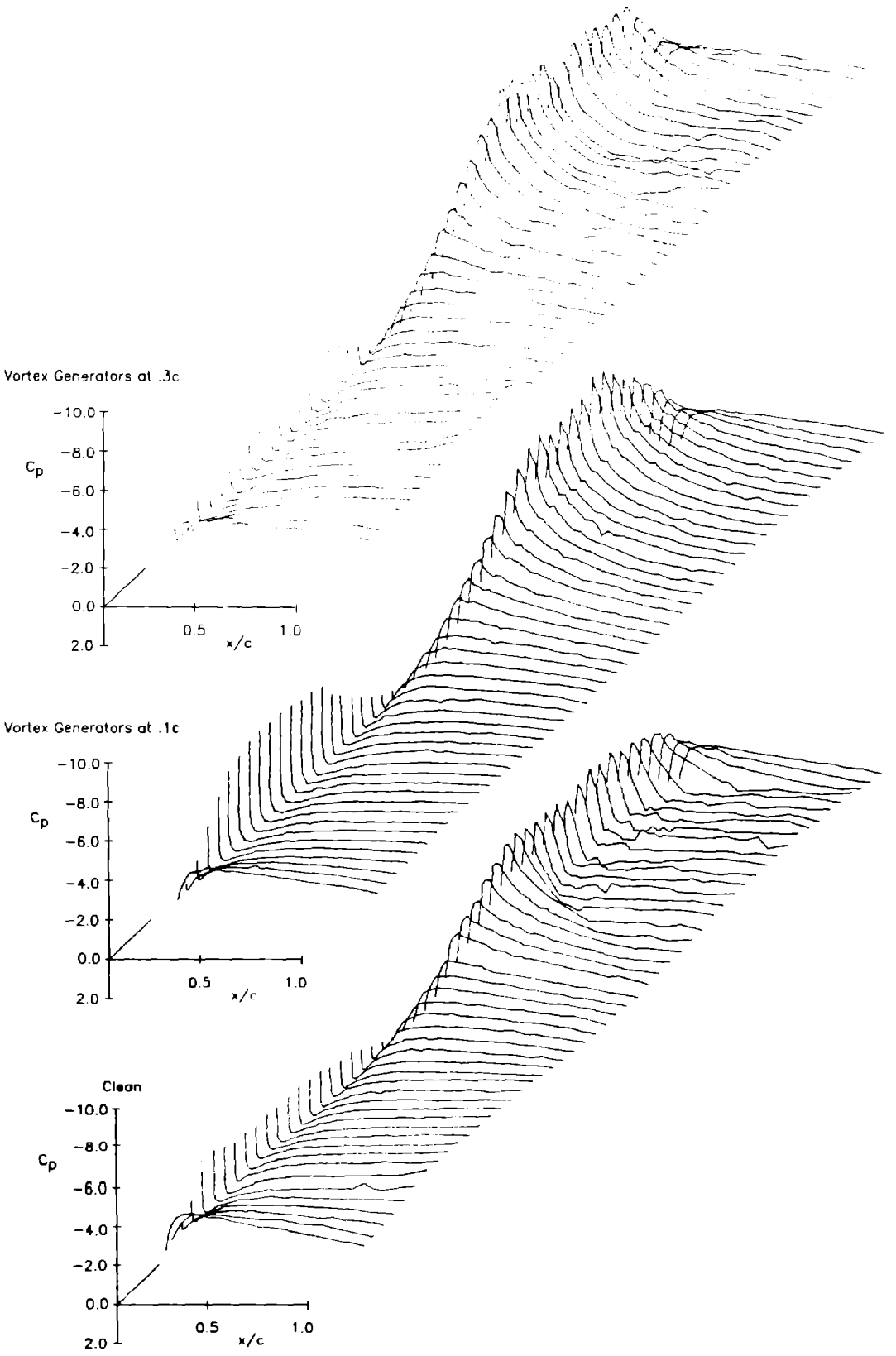

Figure 61. Oscillatory Pressure Distributions for NACA 0021
20° Inverse-Tangent Function, Reduced Frequency=.009

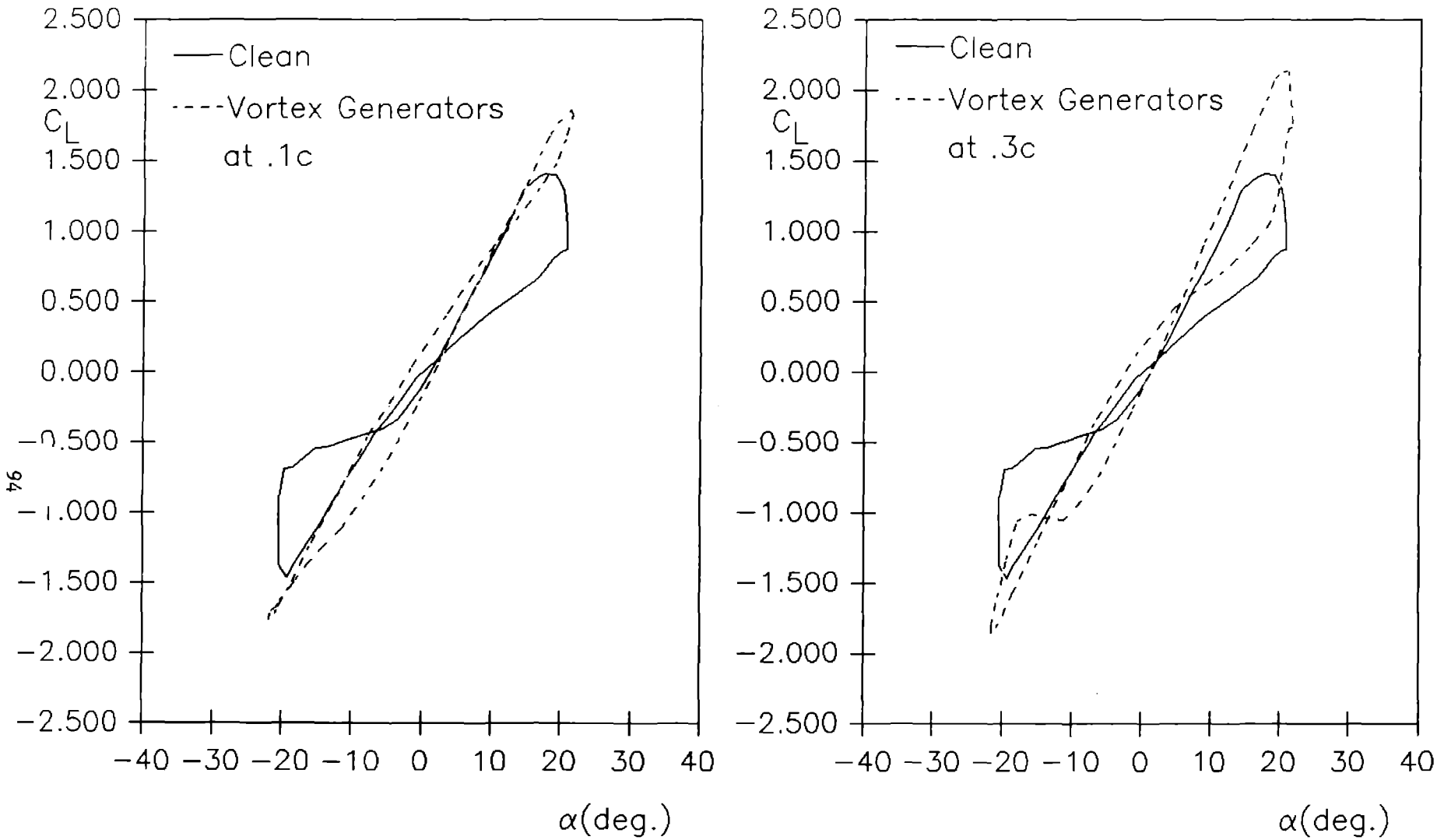

Figure 62. Oscillatory Lift Coefficient versus Angle of Attack for

NACA 0021 — 20° Inverse Tangent Function

Reduced Frequency = .034

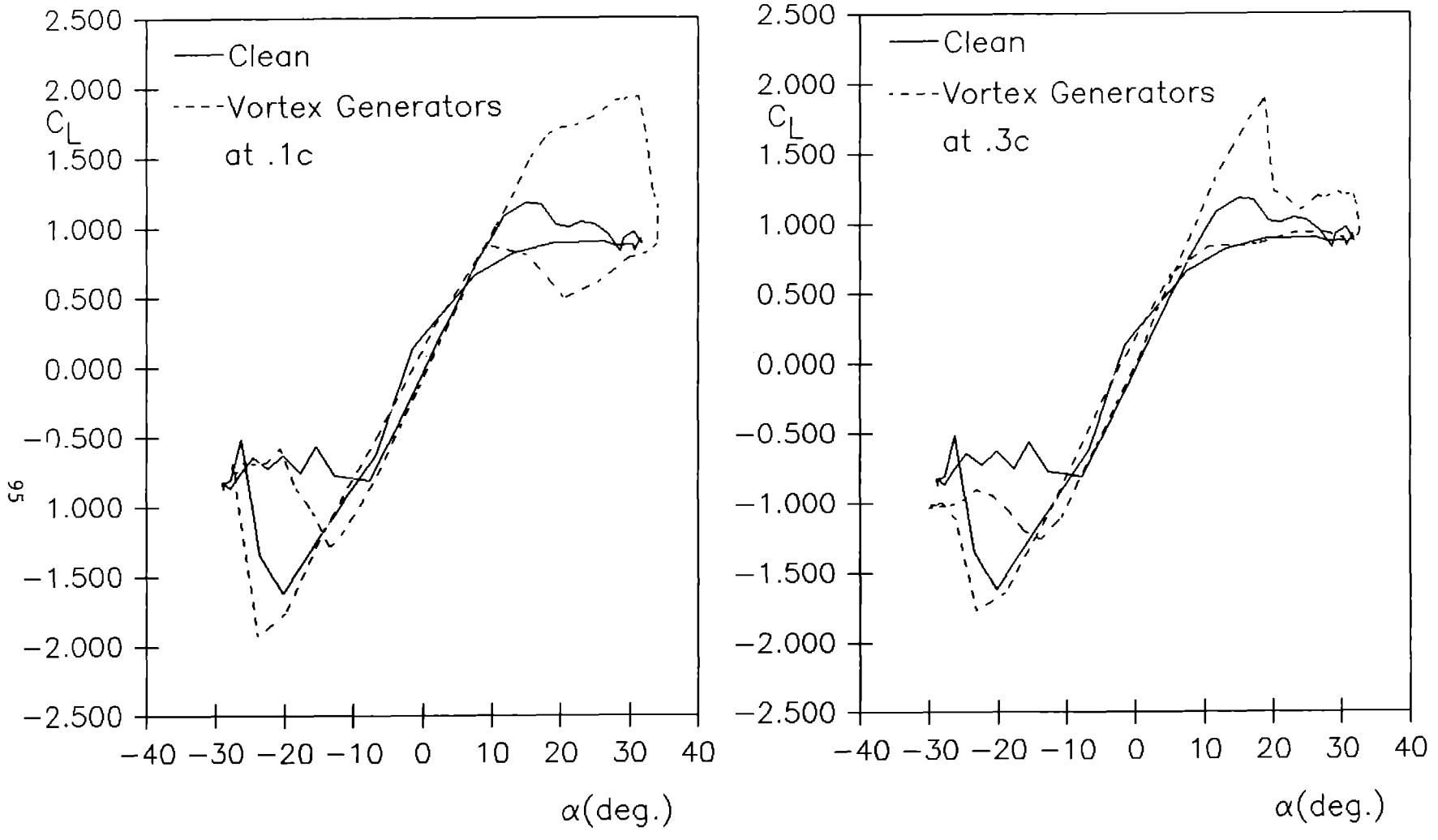

Figure 63. Oscillatory Lift Coefficient versus Angle of Attack for NACA 0021 – 30° Inverse Tangent Function Reduced Frequency = .009

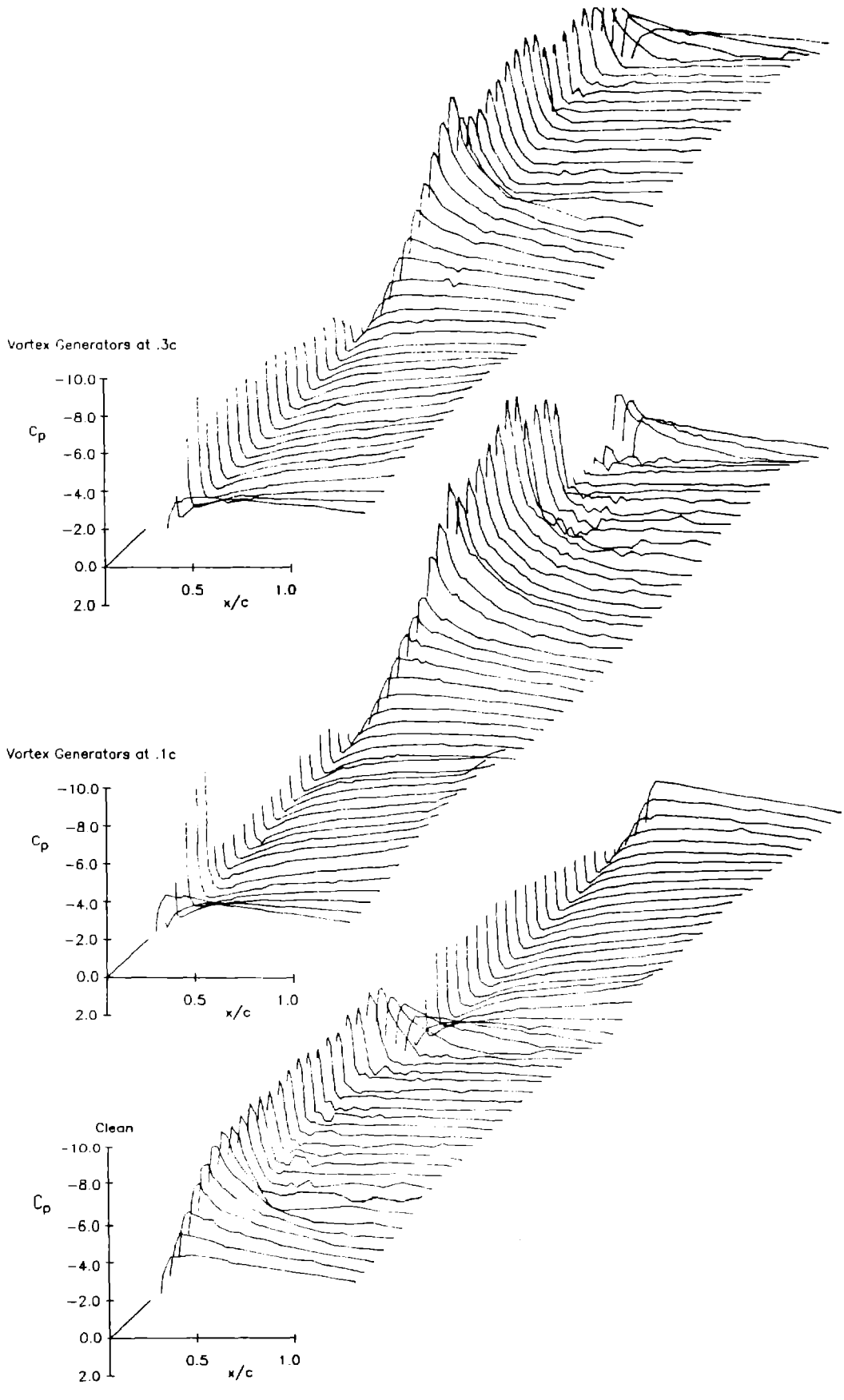

Figure 64. Oscillatory Pressure Distributions for NACA 0021
30° Inverse–Tangent Function, Reduced Frequency=.009

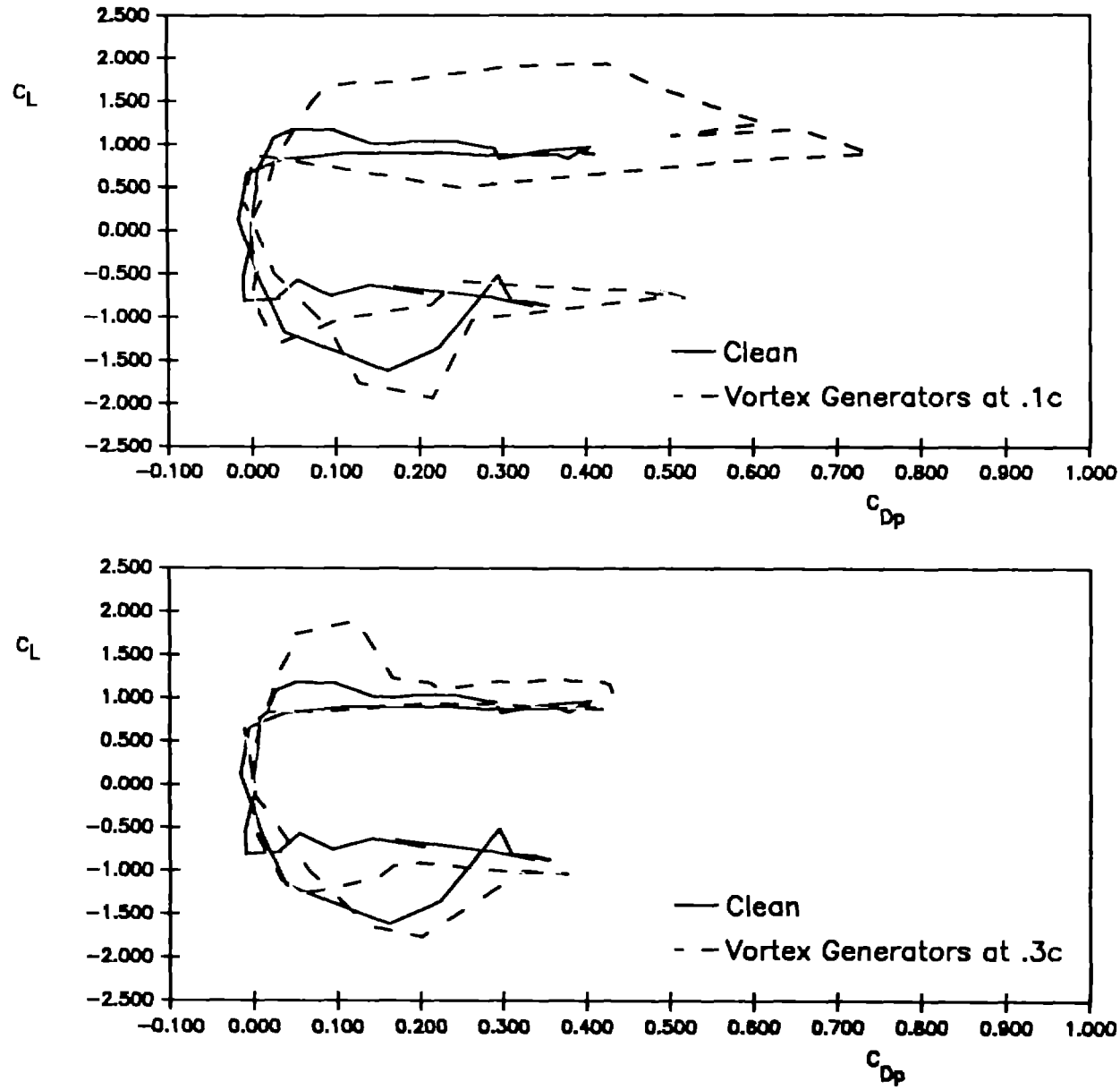

Figure 65. Lift Coefficient versus Pressure Drag Coefficient for NACA 0021 – 30° Inverse Tangent Function

Reduced Frequency = .009

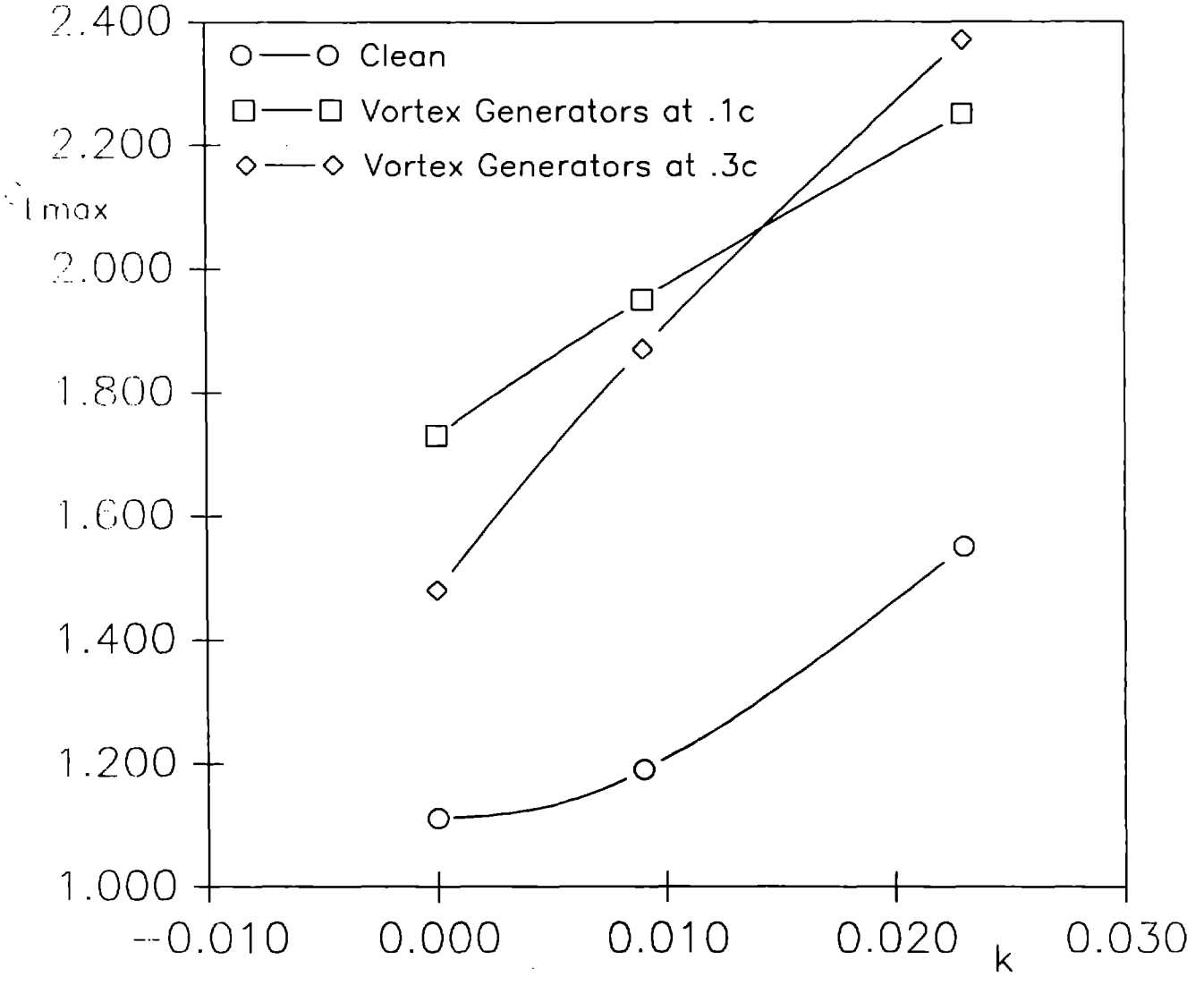

Figure 66. Maximum Lift Coefficient versus Reduced Frequency for NACA 0021 – 30° Inverse Tangent Function

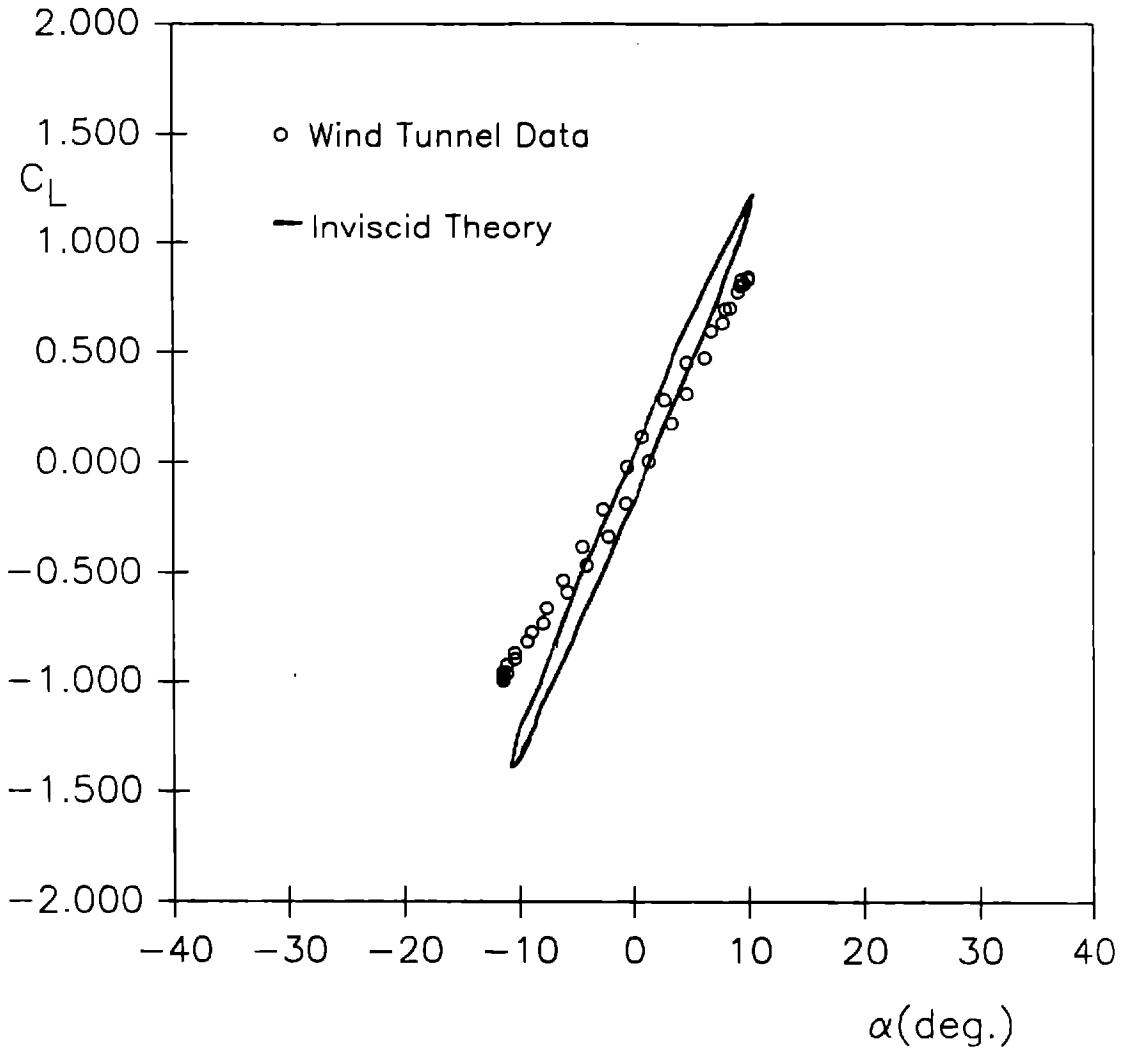

Figure 67. Comparison of Inviscid Theory with Experiment for NACA 0021 with No Vortex Generators– 10° Sine Function, Reduced Frequency=0.034

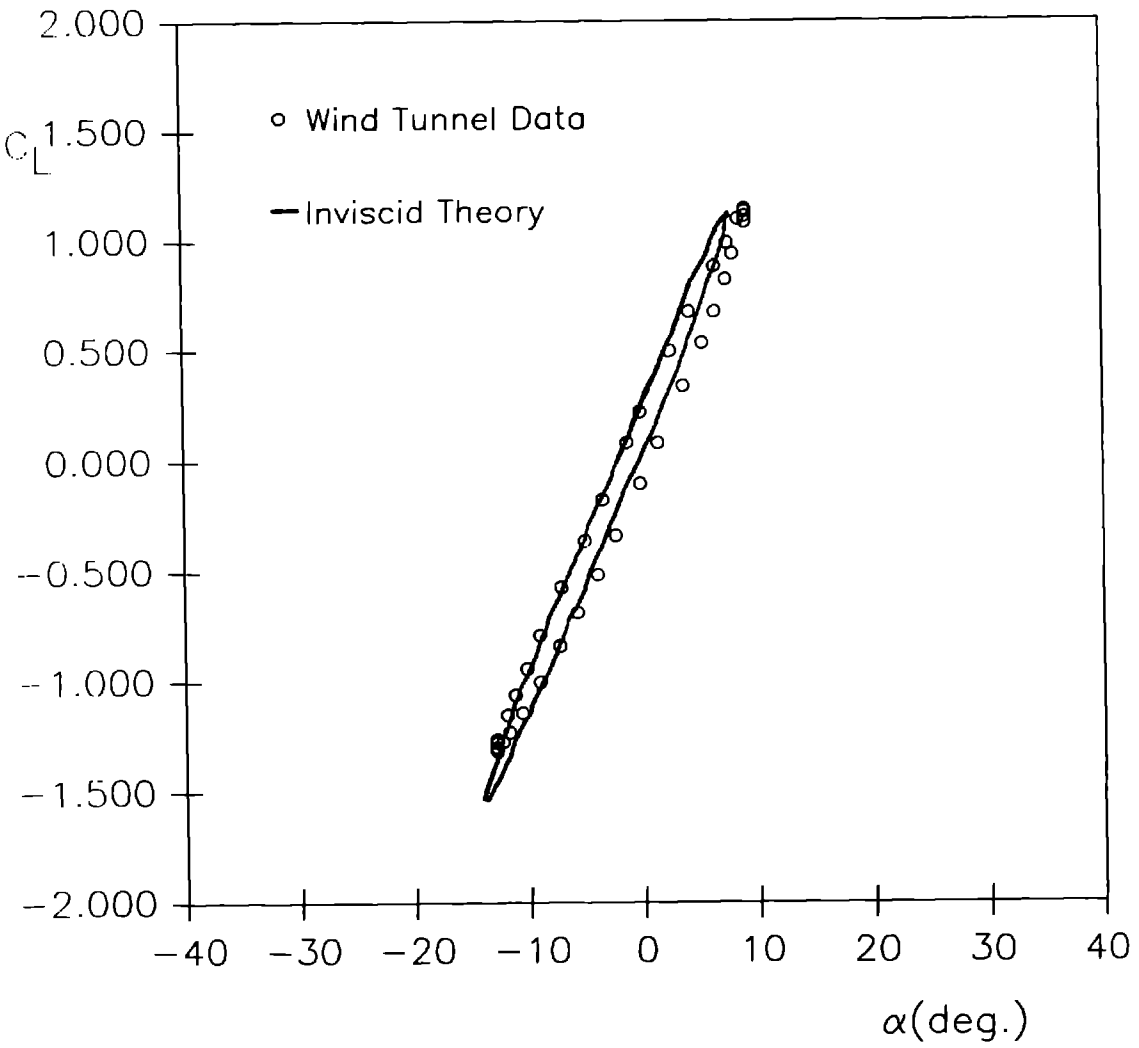

Figure 68. Comparison of Inviscid Theory with Experiment for NACA 0021 with Vortex Generators at .3c Location– 10° Sine Function, Reduced Frequency=0.034

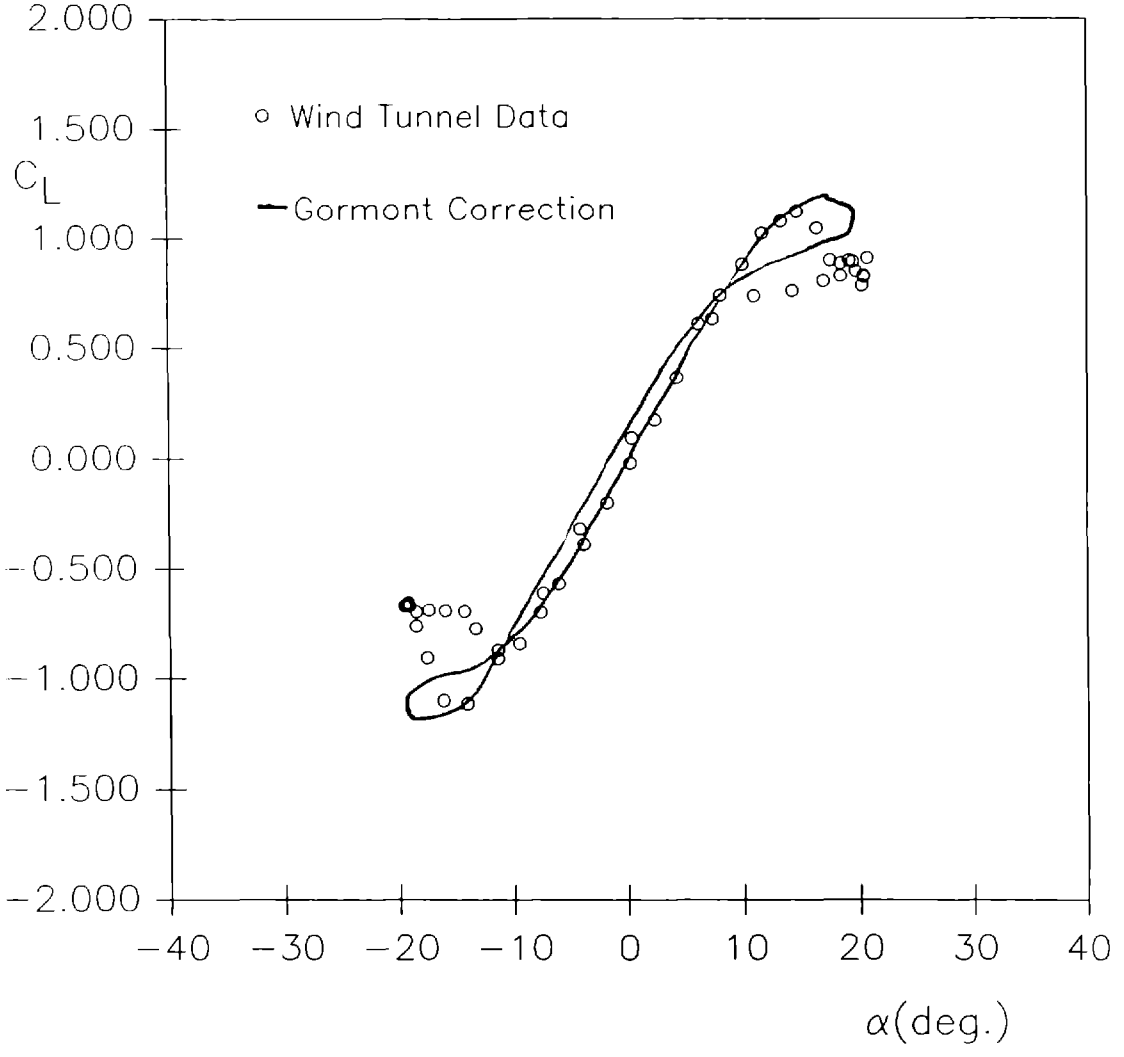

Figure 69. Comparison of Gormont Correction with Experiment for NACA 0021 with No Vortex Generators— 20° Inverse-Tangent, Reduced Frequency=0.009

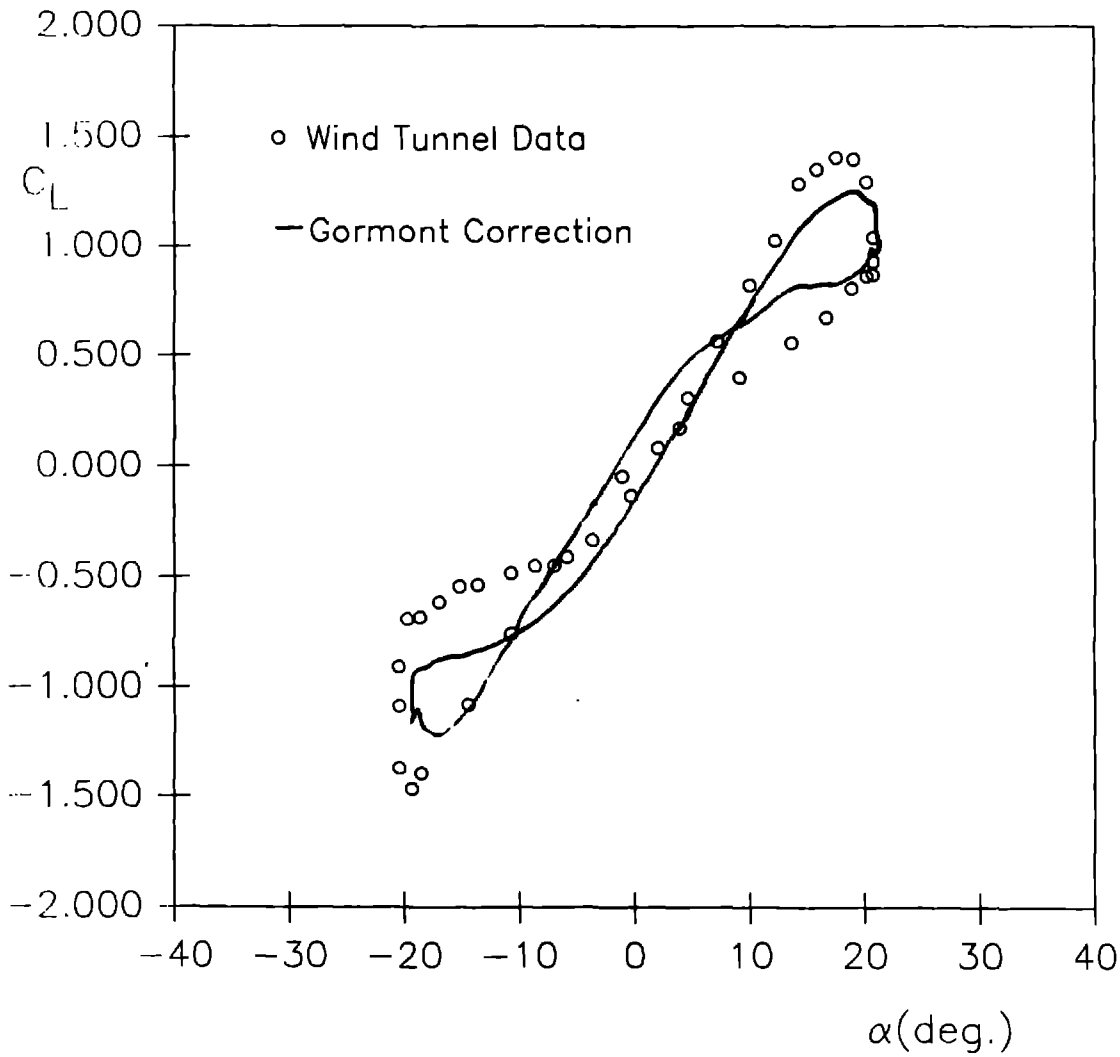

Figure 70. Comparison of Gormont Correction with Experiment for NACA 0021 with No Vortex Generators— 20° Inverse—Tangent, Reduced Frequency=0.034

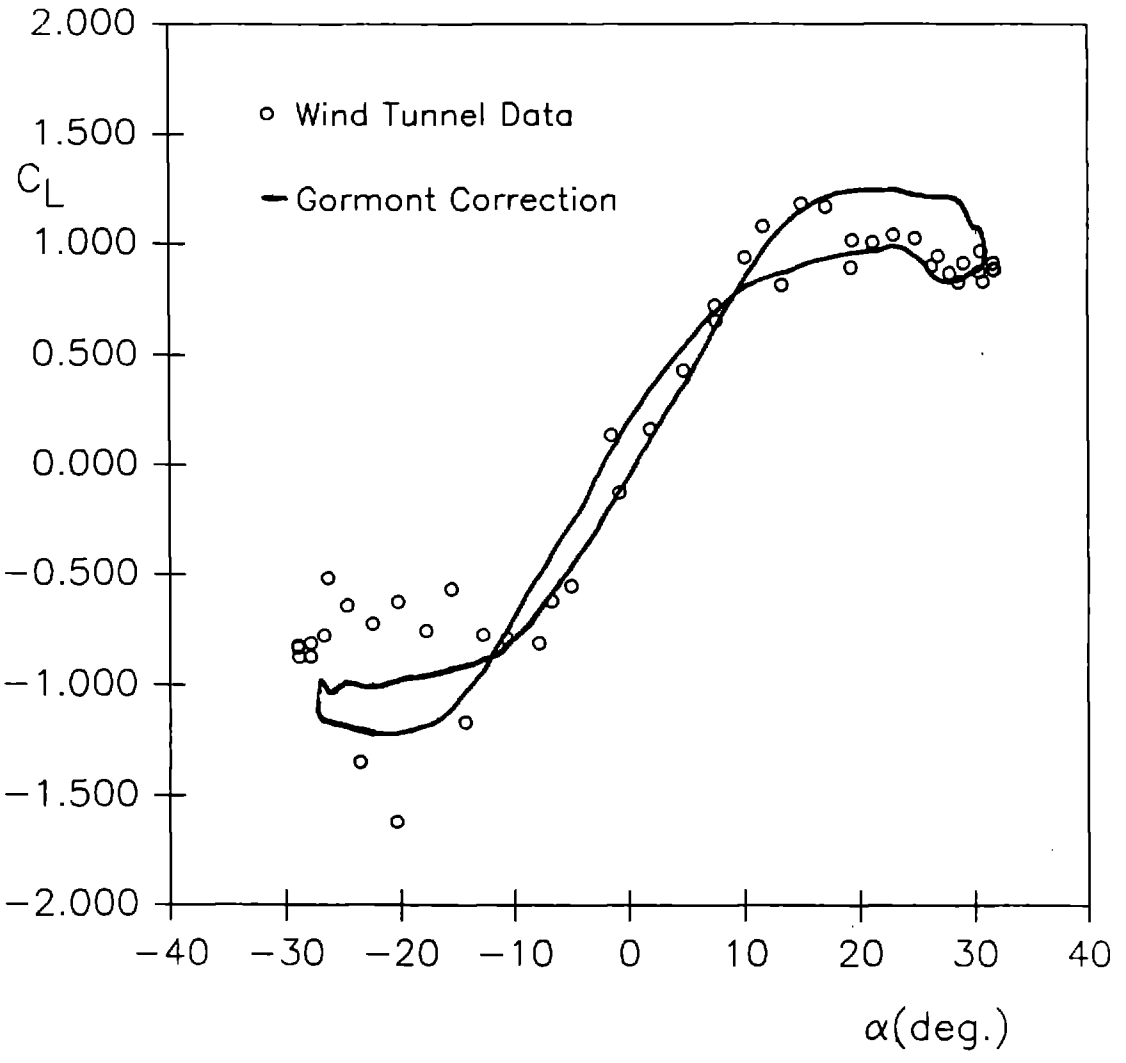

Figure 71. Comparison of Gormont Correction with Experiment for NACA 0021 with No Vortex Generators— 30° Inverse—Tangent, Reduced Frequency=0.009

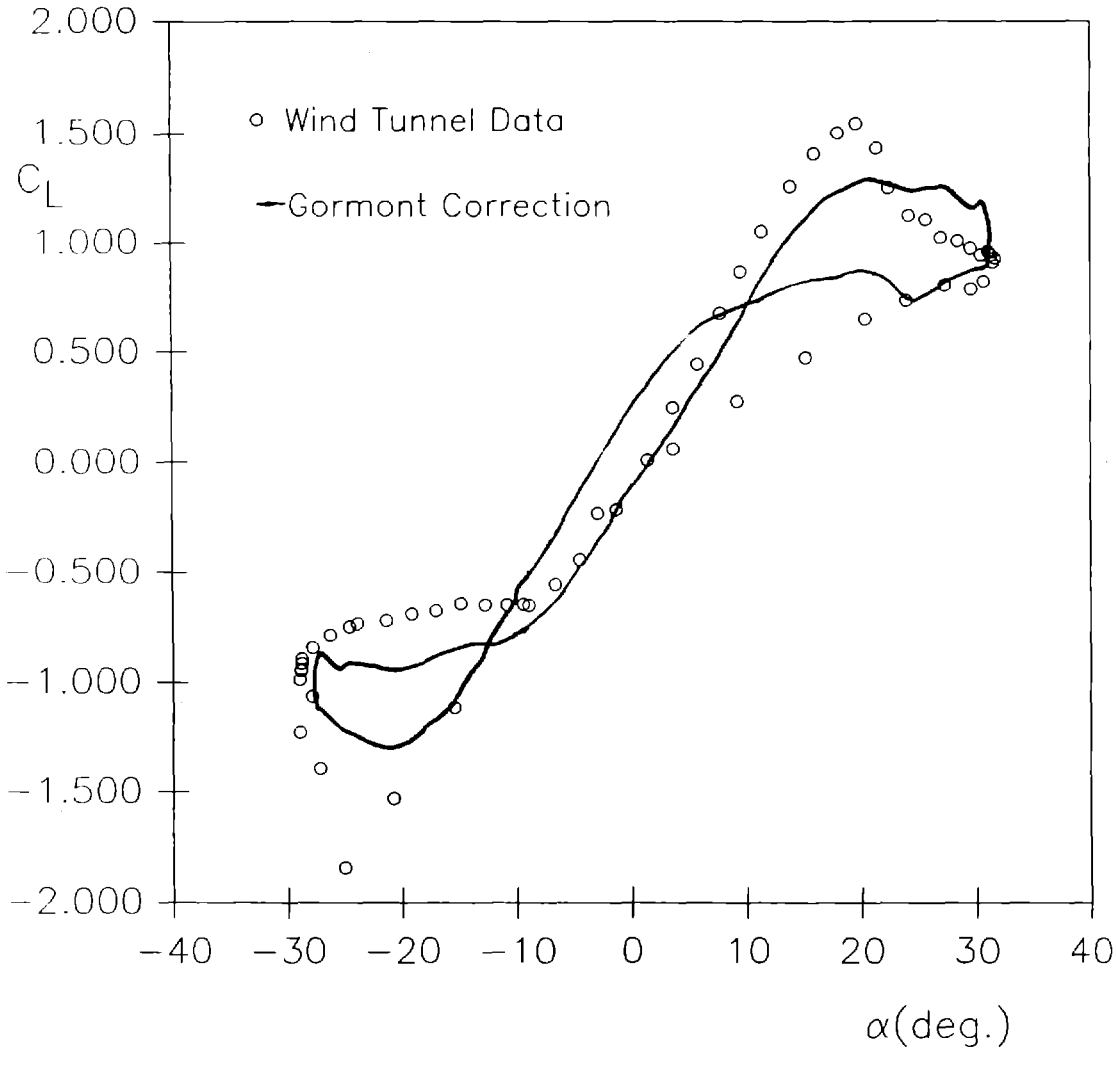

Figure 72. Comparison of Gormont Correction with Experiment for NACA 0021 with No Vortex Generators— 30° Inverse—Tangent, Reduced Frequency=0.023

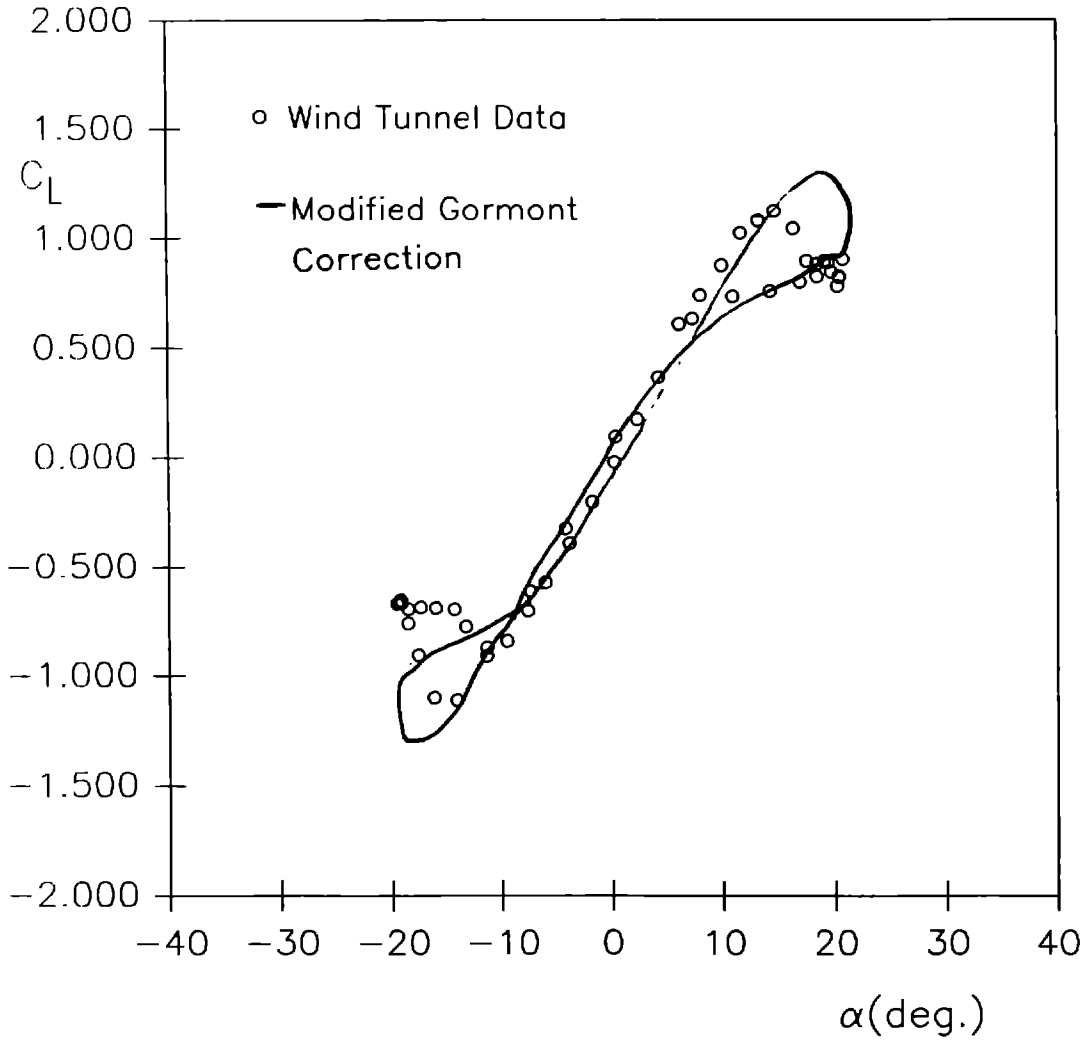

Figure 73. Comparison of Modified Gormont Correction with Experiment for NACA 0021 with No Vortex Generators—
20° Inverse—Tangent, Reduced Frequency=0.009

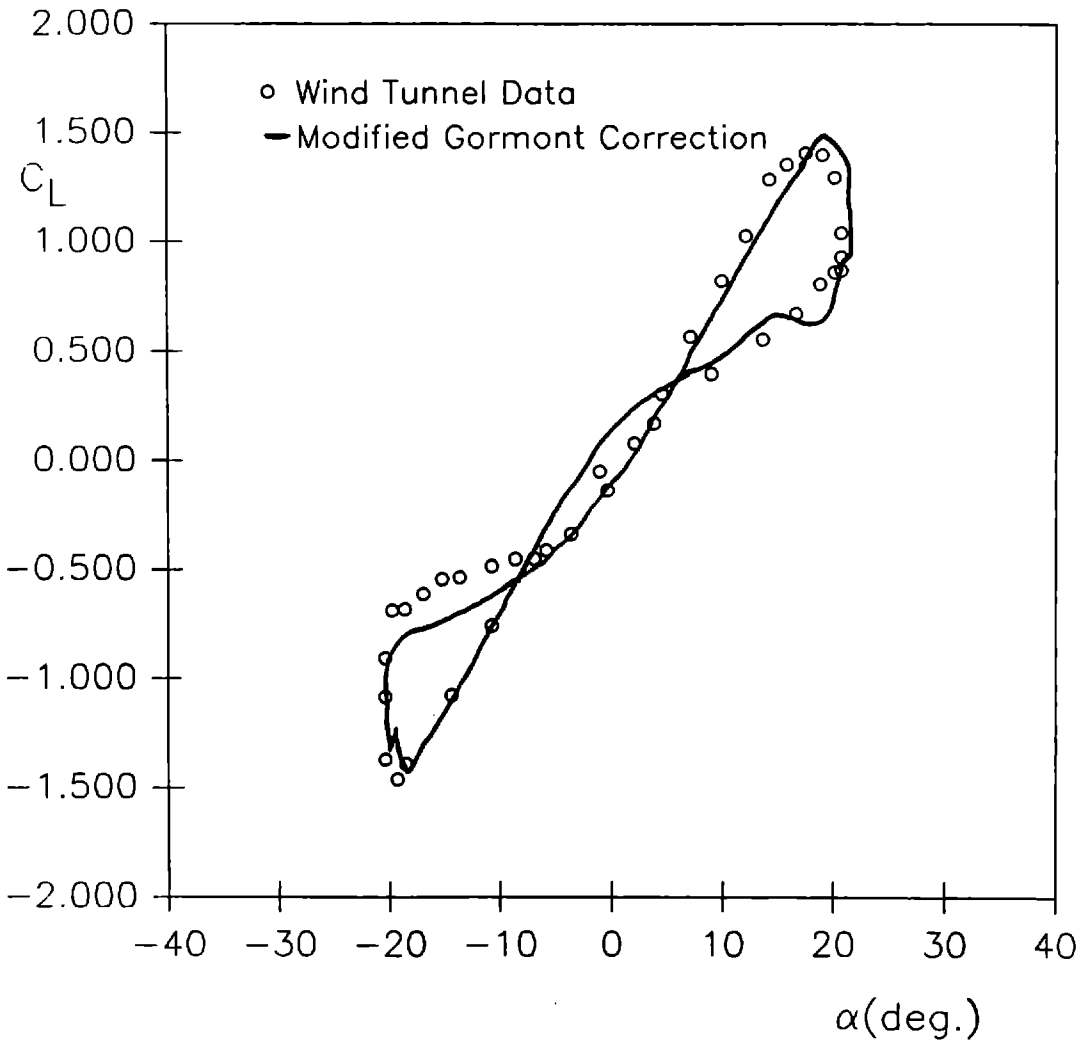

Figure 74. Comparison of Modified Gormont Correction with Experiment for NACA 0021 with No Vortex Generators—
20° Inverse—Tangent, Reduced Frequency=0.034

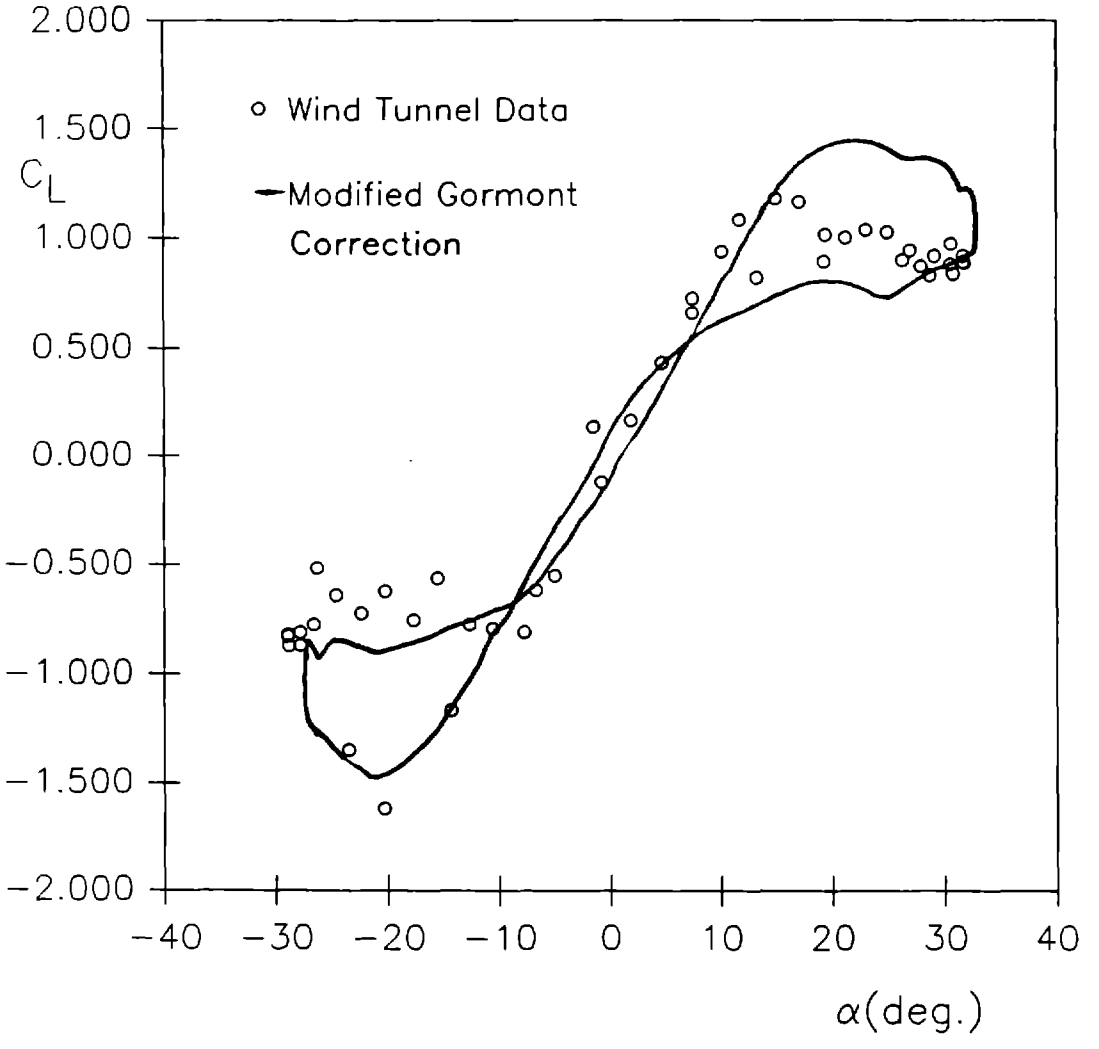

Figure 75. Comparison of Modified Gormont Correction with Experiment for NACA 0021 with No Vortex Generators— 30° Inverse—Tangent, Reduced Frequency=0.009

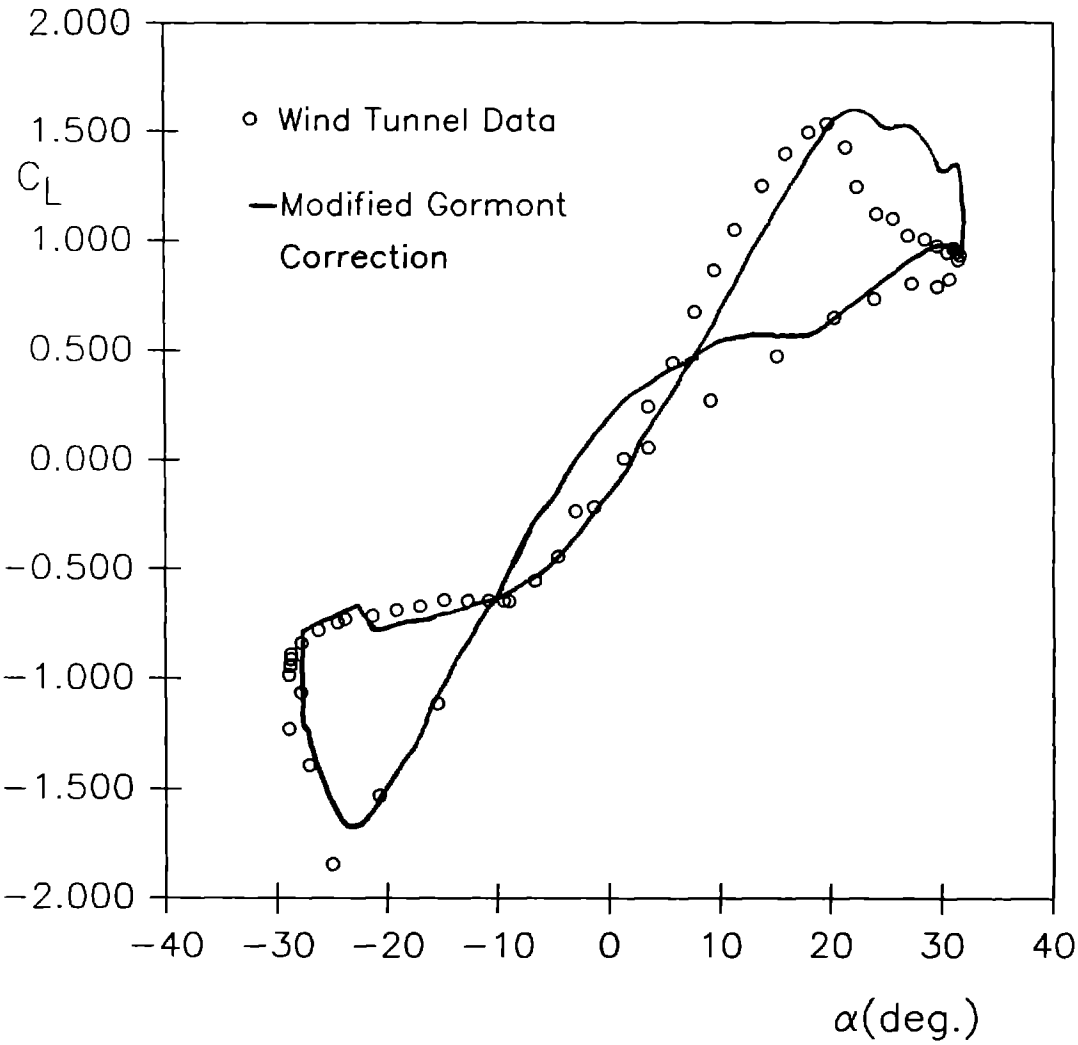

Figure 76. Comparison of Modified Gormont Correction with Experiment for NACA 0021 with No Vortex Generators—
30° Inverse—Tangent, Reduced Frequency=0.023

TABLE 1

Integrated Static Data
with No Vortex Generators

Angle of Attack (deg.)	C_L	$C_{M_{(c/4)}}$	C_D	C_{D_p}	Reynolds Number
-3.4	-0.3450	-0.0065	0.0101	-0.0007	1.26×10^6
-1.6	-0.1447	-0.0015	0.0091	-0.0011	1.25×10^6
0.2	0.0396	0.0039	0.0086	-0.0013	1.25×10^6
2.3	0.2052	0.0051	0.0090	-0.0008	1.25×10^6
4.1	0.3895	0.0095	0.0095	0.0011	1.25×10^6
6.0	0.5606	0.0179	0.0109	0.0033	1.25×10^6
8.1	0.7128	0.0243	0.0124	0.0100	1.25×10^6
9.9	0.8560	0.0318	0.0164	0.0161	1.25×10^6
11.6	0.9307	0.0386	0.0199	0.0257	1.25×10^6
12.5	0.9643	0.0308	0.0385	0.0315	1.25×10^6
13.5	1.0435	0.0313	0.0668	0.0483	1.25×10^6
14.3	1.0761	0.0253	0.0679	0.0661	1.25×10^6
15.3	1.1164	0.0038	***	0.0952	1.23×10^6
16.1	1.1089	0.0002	***	0.1089	1.23×10^6
17.2	1.1380	-0.0035	***	0.1301	1.22×10^6
18.9	1.1219	-0.0066	***	0.1592	1.21×10^6
23.6	1.1488	-0.0441	***	0.2684	1.18×10^6
28.2	1.1463	-0.0630	***	0.3570	1.15×10^6
32.8	0.8713	-0.1526	***	0.6991	1.07×10^6
37.0	1.1606	-0.2392	***	1.0312	1.00×10^6
41.4	1.4623	-0.3675	***	1.4722	0.94×10^6

TABLE 2

Integrated Static Data
with Vortex Generators at 0.1c Chord Location

Angle of Attack (deg.)	C_L	$C_{M_{(c/4)}}$	C_D	C_{D_p}	Reynolds Number
Wake probe 5.88 inches above tunnel centerline					
-3.4	-0.3405	0.0005	0.0239	0.0094	1.25×10^6
-1.6	-0.1546	0.0006	0.0234	0.0070	1.25×10^6
0.2	0.0496	0.0002	0.0227	0.0055	1.25×10^6
2.1	0.2381	-0.0001	0.0232	0.0060	1.25×10^6
3.9	0.4418	0.0007	0.0237	0.0059	1.25×10^6
5.9	0.6382	-0.0011	0.0256	0.0134	1.25×10^6
7.8	0.8423	0.0003	0.0285	0.0143	1.25×10^6
9.6	1.0258	0.0007	0.0328	0.0223	1.25×10^6
10.7	1.0826	0.0023	0.0342	0.0278	1.25×10^6
11.5	1.1893	0.0021	0.0375	0.0304	1.25×10^6
12.5	1.2777	0.0033	0.0384	0.0351	1.24×10^6
13.5	1.3779	0.0020	0.0397	0.0476	1.24×10^6
14.3	1.4150	0.0060	0.0423	0.0507	1.23×10^6
16.1	1.5081	0.0050	***	0.0774	1.22×10^6
17.4	1.5408	0.0090	***	0.1066	1.21×10^6
19.0	1.6493	0.0092	***	0.1343	1.19×10^6
23.9	1.7257	0.0068	***	0.2365	1.16×10^6
28.1	0.7905	-0.1078	***	0.5605	1.11×10^6
32.8	1.1377	-0.2086	***	0.8858	1.06×10^6
37.2	1.1330	-0.2213	***	1.0110	1.02×10^6
42.5	1.5130	-0.3907	***	1.5857	0.97×10^6
Wake probe 6.13 inches above tunnel centerline					
0.0			0.0189		1.11×10^6
3.8			0.0225		1.11×10^6
7.5			0.0310		1.11×10^6
11.2			0.0423		1.10×10^6
Wake probe 5.63 inches above tunnel centerline					
0.0			0.0247		1.11×10^6
3.7			0.0277		1.11×10^6
7.5			0.0328		1.11×10^6
11.2			0.0410		1.11×10^6
15.1			0.0469		1.10×10^6

TABLE 3

Integrated Static Data
with Vortex Generators at 0.3c Chord Location

Angle of Attack (deg.)	C_L	$C_{M_{(c/4)}}$	C_D	C_{D_p}	Reynolds Number
Wake probe 5.88 inches above tunnel centerline					
-4.5	-0.4705	0.0015	0.0197	0.0065	1.10 x 10^6
-2.5	-0.2082	0.0009	0.0218	0.0034	1.10 x 10^6
-0.3	-0.0018	0.0007	0.0221	0.0023	1.10 x 10^6
1.3	0.2076	-0.0015	0.0209	-0.0018	1.10 x 10^6
3.3	0.4278	-0.0006	0.0207	-0.0027	1.10 x 10^6
5.4	0.6391	-0.0047	0.0220	0.0013	1.10 x 10^6
7.0	0.8381	-0.0046	0.0227	-0.0005	1.10 x 10^6
8.8	1.0102	-0.0048	0.0261	0.0078	1.10 x 10^6
9.8	1.1113	-0.0028	0.0276	0.0109	1.10 x 10^6
10.9	1.2190	-0.0020	0.0297	0.0127	1.10 x 10^6
11.7	1.2899	-0.0013	0.0310	0.0137	1.10 x 10^6
12.7	1.3692	-0.0008	0.0320	0.0184	1.10 x 10^6
13.8	1.4365	-0.0002	0.0321	0.0275	1.10 x 10^6
14.6	1.4819	0.0029	***	0.0275	1.10 x 10^6
16.3	1.0300	-0.0048	***	0.0374	1.10 x 10^6
18.1	0.8717	-0.0030	***	0.1072	1.10 x 10^6
22.7	1.0676	-0.0207	***	0.2178	1.10 x 10^6
28.1	0.8223	-0.1195	***	0.5719	1.00 x 10^6
32.1	0.9032	-0.1461	***	0.7010	0.97 x 10^6
36.4	1.194	-0.2399	***	1.0316	0.91 x 10^6
41.4	1.4373	-0.3542	***	1.4305	0.87 x 10^6
Wake probe 6.13 inches above tunnel centerline					
0.4			0.0173		1.23 x 10^6
3.9			0.0184		1.24 x 10^6
7.8			0.0211		1.24 x 10^6
9.7			0.0232		1.25 x 10^6
11.6			0.0267		1.25 x 10^6
13.6			0.0311		1.25 x 10^6
Wake probe 5.69 inches above tunnel centerline					
0.2			0.0203		1.25 x 10^6
3.9			0.0218		1.25 x 10^6
7.8			0.0255		1.25 x 10^6
9.6			0.0268		1.24 x 10^6
11.5			0.0263		1.25 x 10^6
13.6			0.0299		1.25 x 10^6

TABLE 3

Integrated Static Data
with Vortex Generators at 0.3c Chord Location
(Concluded)

Angle of Attack (deg.)	C_L	$C_{M_{(c/4)}}$	C_D	C_{D_p}	Reynolds Number
Wake probe 5.38 inches above tunnel centerline					
0.2			0.0174		1.24×10^6
4.1			0.0188		1.24×10^6
7.8			0.0207		1.24×10^6
9.7			0.0252		1.25×10^6
11.5			0.0294		1.25×10^6
13.3			0.0308		1.25×10^6

TABLE 4

Cycle Averaged Pressure Data with No Vortex Generators
10° Sine Function, k=0.009

FREESTREAM VELOCITY = 142.9 FT/SEC
REYNOLDS NUMBER = 1.221 MILLION

TIME (sec.)	AOA (deg.)	C_L	$C_{M_{(c/4)}}$	C_{D_p}	C_N	C_A
0.0000	0.7	0.046	0.0020	0.0002	0.046	-.0008
0.0619	-0.8	-0.096	0.0028	-.0067	-0.096	-.0080
0.1237	-1.9	-0.207	0.0024	0.0001	-0.207	-.0073
0.1856	-3.3	-0.316	-.0042	-.0035	-0.315	-.0224
0.2474	-4.7	-0.466	-.0060	0.0041	-0.464	-.0342
0.3093	-6.3	-0.588	-.0104	0.0033	-0.585	-.0613
0.3712	-7.4	-0.674	-.0111	0.0126	-0.670	-.0742
0.4330	-8.8	-0.798	-.0212	0.0123	-0.790	-.1100
0.4949	-9.6	-0.851	-.0251	0.0171	-0.842	-.1249
0.5568	-10.1	-0.888	-.0248	0.0207	-0.878	-.1354
0.6186	-10.7	-0.944	-.0277	0.0201	-0.931	-.1549
0.6805	-11.0	-0.969	-.0280	0.0243	-0.956	-.1619
0.7423	-11.5	-0.950	-.0388	0.0164	-0.934	-.1729
0.8042	-11.1	-0.955	-.0365	0.0158	-0.939	-.1739
0.8661	-11.5	-0.944	-.0402	0.0201	-0.929	-.1708
0.9279	-11.5	-0.944	-.0356	0.0156	-0.929	-.1685
0.9898	-11.2	-0.949	-.0368	0.0127	-0.934	-.1716
1.0517	-10.8	-0.894	-.0350	0.0155	-0.882	-.1522
1.1135	-10.1	-0.866	-.0340	0.0074	-0.854	-.1439
1.1754	-9.3	-0.827	-.0314	0.0090	-0.818	-.1245
1.2372	-8.2	-0.746	-.0212	0.0045	-0.739	-.1021
1.2991	-6.8	-0.646	-.0206	0.0014	-0.642	-.0759
1.3610	-5.5	-0.546	-.0160	0.0001	-0.544	-.0527
1.4228	-4.3	-0.446	-.0140	-.0041	-0.445	-.0380
1.4847	-2.5	-0.319	-.0038	-.0063	-0.319	-.0204
1.5466	-1.5	-0.222	-.0021	-.0060	-0.222	-.0120
1.6084	0.4	-0.056	0.0000	-.0041	-0.056	-.0040
1.6703	1.3	0.068	0.0009	-.0016	0.068	-.0035
1.7321	2.9	0.214	0.0044	0.0008	0.214	-.0105
1.7940	3.9	0.331	0.0070	0.0031	0.330	-.0196
1.8559	5.3	0.464	0.0090	0.0074	0.462	-.0357
1.9177	6.3	0.557	0.0117	0.0090	0.555	-.0525
1.9796	7.4	0.647	0.0098	0.0131	0.643	-.0707
2.0415	8.1	0.688	0.0204	0.0146	0.683	-.0821
2.1033	8.4	0.744	0.0206	0.0165	0.739	-.0926
2.1652	9.4	0.791	0.0277	0.0143	0.783	-.1157
2.2270	10.0	0.822	0.0286	0.0206	0.813	-.1220
2.2889	10.5	0.847	0.0282	0.0213	0.837	-.1289
2.3508	9.8	0.840	0.0296	0.0107	0.830	-.1327

TABLE 4

Cycle Averaged Pressure Data with No Vortex Generators
10° Sine Function, k=0.009
(Concluded)

TIME (sec.)	AOA (deg.)	C_L	$C_{M_{(c/4)}}$	C_{D_p}	C_N	C_A
2.4126	10.0	0.851	0.0297	0.0184	0.842	-.1293
2.4745	10.0	0.821	0.0336	0.0196	0.812	-.1228
2.5364	10.0	0.796	0.0336	0.0176	0.787	-.1205
2.5982	9.2	0.762	0.0274	0.0150	0.755	-.1075
2.6601	8.4	0.726	0.0205	0.0051	0.719	-.1007
2.7219	7.5	0.648	0.0219	0.0033	0.643	-.0819
2.7838	6.2	0.539	0.0173	0.0002	0.535	-.0578
2.8457	4.7	0.417	0.0127	0.0024	0.416	-.0320
2.9075	3.3	0.288	0.0115	-.0003	0.288	-.0172
2.9694	1.8	0.143	0.0035	-.0018	0.143	-.0069
3.0312	0.7	0.046	0.0020	0.0002	0.046	-.0008

TABLE 5

Cycle Averaged Pressure Data with No Vortex Generators
10° Sine Function, k=0.034

FREESTREAM VELOCITY = 143.3 FT/SEC
REYNOLDS NUMBER = 1.225 MILLION

TIME (sec.)	AOA (deg.)	C_L	$C_{M_{(c/4)}}$	C_{D_p}	C_N	C_A
0.0000	-0.3	-0.158	-.0117	-.0070	-0.158	-.0084
0.0200	1.3	0.006	-.0077	-.0072	0.006	-.0079
0.0400	3.3	0.177	-.0033	0.0039	0.177	-.0071
0.0600	4.6	0.312	-.0005	0.0118	0.312	-.0134
0.0800	6.2	0.475	0.0055	0.0171	0.474	-.0350
0.1000	7.8	0.633	0.0081	0.0242	0.631	-.0624
0.1200	8.4	0.699	0.0156	0.0217	0.695	-.0802
0.1400	9.3	0.804	0.0135	0.0254	0.797	-.1044
0.1600	9.4	0.827	0.0192	0.0214	0.819	-.1146
0.1800	10.0	0.831	0.0288	0.0214	0.823	-.1223
0.2000	10.0	0.837	0.0311	0.0218	0.828	-.1245
0.2200	10.0	0.832	0.0320	0.0260	0.824	-.1202
0.2400	9.6	0.808	0.0347	0.0169	0.799	-.1184
0.2600	9.1	0.772	0.0335	0.0097	0.764	-.1121
0.2800	8.0	0.694	0.0322	0.0028	0.688	-.0942
0.3000	6.8	0.597	0.0336	-.0022	0.592	-.0735
0.3200	4.6	0.451	0.0271	-.0059	0.449	-.0423
0.3400	2.7	0.285	0.0227	-.0071	0.284	-.0217
0.3600	0.7	0.119	0.0130	-.0048	0.119	-.0066
0.3800	-0.6	-0.012	0.0087	-.0026	-0.012	-.0034
0.4000	-2.7	-0.269	0.0064	-.0001	-0.268	-.0143
0.4200	-4.5	-0.381	0.0058	0.0083	-0.381	-.0222
0.4400	-6.2	-0.535	0.0005	0.0158	-0.533	-.0424
0.4600	-7.6	-0.663	-.0035	0.0205	-0.660	-.0674
0.4800	-8.9	-0.772	-.0107	0.0218	-0.766	-.0984
0.5000	-10.4	-0.896	-.0160	0.0273	-0.886	-.1343
0.5200	-11.1	-0.961	-.0221	0.0213	-0.947	-.1647
0.5400	-11.4	-0.994	-.0233	0.0233	-0.979	-.1744
0.5600	-11.4	-0.980	-.0295	0.0171	-0.964	-.1793
0.5800	-11.4	-0.966	-.0310	0.0166	-0.950	-.1758
0.6000	-11.4	-0.958	-.0330	0.0164	-0.942	-.1724
0.6200	-11.1	-0.924	-.0358	0.0113	-0.909	-.1674
0.6400	-10.4	-0.869	-.0379	0.0052	-0.856	-.1511
0.6600	-9.3	-0.815	-.0359	0.0028	-0.805	-.1293
0.6800	-7.9	-0.729	-.0327	-.0050	-0.722	-.1058
0.7000	-5.8	-0.590	-.0310	-.0106	-0.586	-.0705
0.7200	-4.1	-0.467	-.0237	-.0103	-0.465	-.0436
0.7400	-2.2	-0.336	-.0106	-.0101	-0.335	-.0232
0.7600	-0.3	-0.158	-.0117	-.0070	-0.158	-.0084

TABLE 6

Cycle Averaged Pressure Data with No Vortex Generators
20° Inverse-Tangent Function, k=0.009

FREESTREAM VELOCITY = 141.7 FT/SEC
REYNOLDS NUMBER = 1.211 MILLION

TIME (sec.)	AOA (deg.)	C_L	$C_{M_{(c/4)}}$	C_{D_p}	C_N	C_A
0.0000	0.4	0.120	0.0166	.0107	0.120	-.0160
0.0632	-4.1	-0.309	0.0036	0.0015	-0.308	-.0223
0.1263	-7.4	-0.610	-.0077	0.0167	-0.607	-.0626
0.1895	-10.3	-0.863	-.0215	0.0259	-0.853	-.1309
0.2526	-14.1	-1.110	-.0277	0.0514	-1.089	-.2224
0.3158	-16.2	-1.098	-.0171	0.0700	-1.074	-.2390
0.3789	-17.6	-0.905	0.0460	0.1430	-0.906	-.1375
0.4421	-18.5	-0.759	0.0139	0.1302	-0.761	-.1165
0.5052	-19.1	-0.667	0.0075	0.1305	-0.673	-.0943
0.5684	-19.3	-0.665	0.0170	0.1414	-0.674	-.0869
0.6315	-19.5	-0.669	0.0083	0.1364	-0.676	-.0940
0.6947	-19.2	-0.653	0.0026	0.1276	-0.659	-.0947
0.7578	-19.3	-0.663	0.0019	0.1323	-0.670	-.0942
0.8210	-18.5	-0.694	0.0037	0.1170	-0.695	-.1093
0.8841	-17.4	-0.686	-.0063	0.0988	-0.685	-.1113
0.9473	-16.0	-0.688	-.0134	0.0810	-0.684	-.1124
1.0104	-14.8	-0.666	-.0284	0.0554	-0.658	-.1158
1.0736	-13.3	-0.772	-.0333	0.0301	-0.759	-.1489
1.1367	-11.4	-0.870	-.0369	0.0173	-0.857	-.1544
1.1999	-9.5	-0.819	-.0346	0.0137	-0.810	-.1215
1.2630	-7.6	-0.718	-.0188	0.0029	-0.712	-.0917
1.3262	-6.0	-0.569	-.0135	-.0038	-0.565	-.0633
1.3893	-3.6	-0.378	-.0072	-.0044	-0.377	-.0282
1.4525	-1.7	-0.198	-.0043	-.0055	-0.198	-.0118
1.5156	0.3	-0.018	0.0017	-.0034	-0.018	-.0040
1.5788	2.4	0.177	0.0094	-.0064	0.177	-.0140
1.6419	4.3	0.375	0.0127	-.0048	0.373	-.0335
1.7051	6.2	0.610	0.0100	0.0067	0.608	-.0597
1.7682	8.1	0.739	0.0203	0.0118	0.733	-.0925
1.8314	10.0	0.878	0.0255	0.0189	0.867	-.1341
1.8945	11.7	1.033	0.0257	0.0262	1.016	-.1841
1.9577	13.3	1.083	0.0351	0.0300	1.061	-.2194
2.0208	14.7	1.125	0.0226	0.0461	1.100	-.2408
2.0840	16.4	1.047	-.0109	0.0763	1.026	-.2222
2.1471	17.6	0.899	-.0104	0.1113	0.890	-.1656
2.2103	18.5	0.885	-.0098	0.1234	0.878	-.1645
2.2734	19.2	0.899	-.0279	0.1391	0.895	-.1638
2.3366	19.5	0.892	-.0299	0.1505	0.891	-.1559
2.3997	20.3	0.785	-.0242	0.1541	0.790	-.1275

TABLE 6

Cycle Averaged Pressure Data with No Vortex Generators
20° Inverse-Tangent Function, k=0.009
(Concluded)

TIME (sec.)	AOA (deg.)	C_L	$C_{M_{(c/4)}}$	C_{D_p}	C_N	C_A
2.4629	20.5	0.829	-.0149	0.1511	0.829	-.1493
2.5260	20.8	0.908	-.0336	0.1647	0.910	-.1622
2.5892	20.5	0.824	-.0162	0.1503	0.824	-.1483
2.6523	19.8	0.849	-.0250	0.1444	0.848	-.1512
2.7155	18.5	0.828	-.0020	0.1073	0.820	-.1605
2.7786	17.0	0.803	0.0058	0.0870	0.793	-.1521
2.8418	14.3	0.760	0.0338	0.0398	0.747	-.1493
2.9049	11.0	0.735	0.0515	0.0015	0.722	-.1389
2.9681	7.4	0.632	0.0461	-.0112	0.625	-.0923
3.0312	0.4	0.120	0.0166	-.0107	0.120	-.0160

TABLE 7

Cycle Averaged Pressure Data with No Vortex Generators
20° Inverse-Tangent Function, k=0.034

FREESTREAM VELOCITY = 141.4 FT/SEC
REYNOLDS NUMBER = 1.208 MILLION

TIME (sec.)	AOA (deg.)	C_L	$C_{M_{(c/4)}}$	C_{D_p}	C_N	C_A
0.0000	-0.3	-0.118	-.0164	-.0026	-0.118	-.0046
0.0202	2.1	0.082	-.0084	0.0014	0.082	-.0029
0.0404	4.6	0.308	-.0038	0.0116	0.308	-.0146
0.0605	7.2	0.568	-.0016	0.0246	0.566	-.0486
0.0807	10.0	0.822	0.0047	0.0350	0.815	-.1092
0.1009	12.2	1.026	0.0087	0.0533	1.014	-.1658
0.1211	14.3	1.288	0.0143	0.0504	1.261	-.2683
0.1412	15.9	1.356	0.0152	0.0694	1.323	-.3052
0.1614	17.6	1.407	0.0099	0.0850	1.367	-.3432
0.1816	18.7	1.401	-.0037	0.1029	1.360	-.3521
0.2018	20.2	1.294	-.0357	0.1552	1.268	-.3017
0.2219	20.8	1.040	-.0414	0.1777	1.035	-.2032
0.2421	20.8	0.931	-.0342	0.1740	0.932	-.1687
0.2623	20.8	0.895	-.0316	0.1701	0.897	-.1580
0.2825	20.2	0.863	-.0086	0.1372	0.857	-.1700
0.3026	18.9	0.808	0.0042	0.1170	0.802	-.1518
0.3228	16.7	0.674	0.0374	0.0619	0.663	-.1353
0.3430	13.7	0.557	0.0607	0.0205	0.545	-.1141
0.3632	9.1	0.397	0.0780	-.0087	0.391	-.0735
0.3833	3.9	0.172	0.0861	-.0197	0.170	-.0348
0.4035	-1.0	-0.046	0.0477	-.0051	-0.046	-.0103
0.4237	-6.9	-0.447	0.0199	0.0304	-0.446	-.0286
0.4439	-10.7	-0.756	0.0018	0.0553	-0.753	-.0878
0.4640	-14.4	-1.077	0.0029	0.0970	-1.067	-.1781
0.4842	-18.5	-1.392	-.0059	0.1240	-1.359	-.3240
0.5044	-19.3	-1.463	0.0062	0.1235	-1.421	-.3678
0.5246	-20.4	-1.373	0.0657	0.1763	-1.348	-.3137
0.5447	-20.4	-1.085	0.0650	0.1848	-1.083	-.2031
0.5649	-20.4	-0.908	0.0501	0.1981	-0.918	-.1352
0.5851	-19.7	-0.689	0.0099	0.1480	-0.699	-.0927
0.6053	-18.6	-0.682	-.0062	0.1248	-0.686	-.0992
0.6254	-16.9	-0.612	-.0302	0.0896	-0.611	-.0923
0.6456	-15.2	-0.543	-.0390	0.0578	-0.539	-.0870
0.6658	-13.6	-0.534	-.0458	0.0387	-0.528	-.0877
0.6860	-10.7	-0.484	-.0636	0.0057	-0.477	-.0843
0.7061	-8.6	-0.451	-.0706	-.0070	-0.445	-.0742
0.7263	-5.8	-0.410	-.0501	-.0077	-0.407	-.0497

TABLE 7

Cycle Averaged Pressure Data with No Vortex Generators
20° Inverse-Tangent Function, k=0.034
(Concluded)

TIME (sec.)	AOA (deg.)	C_L	$C_{M_{(c/4)}}$	C_{D_p}	C_N	C_A
0.7465	-3.6	-0.334	-.0309	-.0096	-0.333	-.0313
0.7667	-0.3	-0.118	-.0164	-.0026	-0.118	-.0046
1.1500	0.8	0.137	0.0355	-.0122	0.137	-.0158

TABLE 8

Cycle Averaged Pressure Data with No Vortex Generators
30° Inverse-Tangent Function, k=0.009

FREESTREAM VELOCITY = 137.0 FT/SEC
REYNOLDS NUMBER = 1.029 MILLION

TIME (sec.)	AOA (deg.)	C_L	$C_{M_{(c/4)}}$	C_{D_P}	C_N	C_A
0.0000	-0.8	-0.124	-.0032	-.0006	-0.124	-.0041
0.0645	1.9	0.172	0.0011	0.0002	0.172	-.0074
0.1289	4.7	0.451	0.0086	0.0031	0.449	-.0348
0.1934	7.5	0.723	0.0137	0.0084	0.718	-.0868
0.2578	10.1	0.938	0.0245	0.0207	0.927	-.1445
0.3223	11.7	1.081	0.0275	0.0270	1.064	-.1938
0.3867	15.0	1.181	0.0296	0.0491	1.153	-.2580
0.4512	17.1	1.171	-.0026	0.0977	1.149	-.2509
0.5156	19.4	1.022	-.0173	0.1427	1.012	-.2043
0.5801	21.2	1.004	-.0281	0.1650	0.996	-.2089
0.6445	23.0	1.039	-.0227	0.1905	1.030	-.2310
0.7090	24.9	1.026	-.0450	0.2474	1.035	-.2075
0.7734	26.9	0.943	-.0566	0.2913	0.973	-.1658
0.8379	28.7	0.831	-.0499	0.2967	0.871	-.1399
0.9023	29.1	0.918	-.0718	0.3435	0.970	-.1467
0.9668	30.6	0.972	-.0930	0.4050	1.043	-.1473
1.0313	31.7	0.891	-.0871	0.3968	0.967	-.1311
1.0957	31.8	0.886	-.0883	0.4095	0.969	-.1183
1.1602	31.7	0.917	-.0854	0.3935	0.993	-.1369
1.2246	30.8	0.835	-.0846	0.3787	0.911	-.1024
1.2891	30.5	0.879	-.0738	0.3669	0.944	-.1296
1.3535	27.9	0.871	-.0456	0.2883	0.905	-.1533
1.4180	25.1	0.911	-.0148	0.2177	0.918	-.1896
1.4824	19.3	0.892	0.0276	0.1069	0.877	-.1961
1.5469	13.3	0.818	0.0422	0.0359	0.804	-.1541
1.6113	7.5	0.657	0.0432	-.0053	0.651	-.0911
1.6758	-1.5	0.136	-.0116	-.0156	0.140	0.0225
1.7402	-6.7	-0.618	0.0122	0.0125	-0.615	0.0266
1.8047	-14.3	-1.167	-.0172	0.0392	-1.157	-.1263
1.8691	-20.3	-1.618	0.0124	0.1615	-1.599	-.2904
1.9336	-23.5	-1.348	0.0248	0.2238	-1.338	-.2979
1.9980	-26.3	-0.516	0.0676	0.2948	-0.572	-.0030
2.0625	-27.8	-0.810	0.0536	0.3109	-0.860	-.1043
2.1270	-28.9	-0.828	0.0755	0.3387	-0.888	-.1024
2.1914	-28.9	-0.822	0.0564	0.3371	-0.883	-.1024
2.2559	-28.8	-0.872	0.0678	0.3553	-0.935	-.1094
2.3203	-28.9	-0.821	0.0557	0.3239	-0.877	-.1087
2.3848	-27.8	-0.868	0.0686	0.3352	-0.925	-.1132
2.4492	-26.6	-0.714	0.0300	0.2572	-0.754	-.0869

TABLE 8

Cycle Averaged Pressure Data with No Vortex Generators
30° Inverse-Tangent Function, k=0.009
(Concluded)

TIME (sec.)	AOA (deg.)	C_L	$C_{M_{(c/4)}}$	C_{D_p}	C_N	C_A
2.5137	-24.6	-0.530	-.0548	0.0966	-0.520	-.1180
2.5781	-22.4	-0.723	0.0267	0.2035	-0.746	-.0865
2.6426	-20.2	-0.624	-.0089	0.1434	-0.636	-.0763
2.7070	-17.7	-0.755	-.0122	0.0948	-0.744	-.1437
2.7715	-15.5	-0.566	-.0383	0.0552	-0.560	-.0895
2.8359	-12.7	-0.784	-.0385	0.0299	-0.768	-.1475
2.9004	-10.6	-0.789	-.0334	0.0309	-0.781	-.1164
2.9648	-7.8	-0.808	-.0523	-.0095	-0.797	-.1248
3.0293	-5.0	-0.552	-.0286	-.0107	-0.549	-.0553
3.0938	-0.8	-0.124	-.0032	-.0006	-0.124	-.0041

TABLE 9

Cycle Averaged Pressure Data with No Vortex Generators
30° Inverse-Tangent Function, k=0.023

FREESTREAM VELOCITY = 136.6 FT/SEC
REYNOLDS NUMBER = 1.026 MILLION

TIME (sec.)	AOA (deg.)	C_L	$C_{M_{(c/4)}}$	C_{D_p}	C_N	C_A
0.0000	-1.3	-0.209	-.0158	-.0082	-0.209	-.0136
0.0202	1.4	0.031	-.0122	-.0048	0.031	-.0069
0.0403	3.6	0.248	-.0088	0.0053	0.248	-.0113
0.0605	5.8	0.445	0.0033	0.0160	0.445	-.0294
0.0807	7.8	0.675	0.0044	0.0265	0.672	-.0669
0.1009	9.5	0.866	0.0068	0.0375	0.860	-.1074
0.1210	11.4	1.048	0.0088	0.0536	1.038	-.1546
0.1412	13.9	1.251	0.0104	0.0744	1.232	-.2300
0.1614	16.0	1.399	0.0112	0.0863	1.368	-.3035
0.1816	17.8	1.486	0.0038	0.1054	1.447	-.3534
0.2017	19.7	1.540	-.0308	0.1505	1.501	-.3767
0.2219	21.4	1.426	-.0513	0.1864	1.395	-.3466
0.2421	22.4	1.245	-.0589	0.2087	1.231	-.2817
0.2622	24.2	1.122	-.0585	0.2484	1.125	-.2335
0.2824	25.7	1.101	-.0738	0.2840	1.116	-.2212
0.3026	27.0	1.022	-.0807	0.3224	1.057	-.1770
0.3228	28.5	1.006	-.0828	0.3629	1.057	-.1616
0.3429	29.6	0.975	-.0987	0.3914	1.041	-.1403
0.3631	30.5	0.944	-.0852	0.3905	1.012	-.1430
0.3833	31.2	0.955	-.0982	0.4276	1.038	-.1284
0.4034	31.1	0.961	-.1046	0.4350	1.048	-.1245
0.4236	31.4	0.944	-.1085	0.4426	1.036	-.1132
0.4438	31.7	0.932	-.1019	0.4321	1.020	-.1229
0.4640	31.5	0.911	-.0929	0.4197	0.996	-.1178
0.4841	30.6	0.819	-.0766	0.3706	0.894	-.0976
0.5043	29.6	0.788	-.0501	0.3172	0.842	-.1126
0.5245	27.3	0.802	-.0475	0.2762	0.839	-.1235
0.5447	24.3	0.737	-.0180	0.1962	0.753	-.1257
0.5648	20.4	0.650	0.0352	0.0903	0.641	-.1431
0.5850	15.2	0.475	0.0731	0.0215	0.464	-.1061
0.6052	9.2	0.276	0.0977	-.0220	0.269	-.0680
0.6253	3.6	0.060	0.1085	-.0246	0.057	-.0314
0.6455	-2.9	-0.233	0.0565	0.0111	-0.233	-.0050
0.6657	-9.4	-0.644	0.0291	0.0657	-0.645	-.0466
0.6859	-15.4	-1.112	0.0106	0.1284	-1.105	-.1762
0.7060	-20.7	-1.530	0.0190	0.2026	-1.501	-.3555
0.7262	-25.0	-1.842	0.1120	0.3448	-1.815	-.4685
0.7464	-27.1	-1.394	0.2043	0.4855	-1.463	-.2017
0.7666	-27.8	-1.063	0.1204	0.4146	-1.133	-.1298

TABLE 9

Cycle Averaged Pressure Data with No Vortex Generators
30° Inverse-Tangent Function, k=0.023
(Concluded)

TIME (sec.)	AOA (deg.)	C_L	$C_{M_{(c/4)}}$	C_{D_p}	C_N	C_A
0.7867	-28.9	-1.227	0.1252	0.4372	-1.285	-.2093
0.8069	-28.9	-0.985	0.1020	0.4033	-1.057	-.1226
0.8271	-28.8	-0.941	0.0710	0.3539	-0.996	-.1422
0.8472	-28.8	-0.946	0.0758	0.3579	-1.002	-.1411
0.8674	-28.7	-0.912	0.0657	0.3507	-0.968	-.1330
0.8876	-28.7	-0.891	0.0703	0.3509	-0.950	-.1200
0.9078	-27.8	-0.840	0.0581	0.3213	-0.893	-.1081
0.9279	-26.2	-0.781	0.0433	0.2768	-0.823	-.0963
0.9481	-24.5	-0.745	0.0192	0.2323	-0.774	-.0978
0.9683	-23.8	-0.730	0.0125	0.2130	-0.754	-.1000
0.9884	-21.3	-0.717	-.0166	0.1504	-0.723	-.1204
1.0086	-19.1	-0.687	-.0299	0.1041	-0.684	-.1263
1.0288	-17.0	-0.672	-.0419	0.0781	-0.666	-.1214
1.0490	-14.8	-0.641	-.0530	0.0472	-0.632	-.1179
1.0691	-12.7	-0.646	-.0571	0.0256	-0.635	-.1168
1.0893	-10.8	-0.646	-.0613	0.0107	-0.636	-.1104
1.1095	-8.9	-0.646	-.0545	0.0016	-0.639	-.0982
1.1297	-6.6	-0.550	-.0431	-.0087	-0.545	-.0724
1.1498	-4.5	-0.443	-.0261	-.0069	-0.441	-.0423
1.1700	-1.3	-0.209	-.0158	-.0082	-0.209	-.0136

TABLE 10

Cycle Averaged Pressure Data with Vortex Generators
at 0.1c Chord Location
10° Sine Function, k=0.009

FREESTREAM VELOCITY = 142.4 FT/SEC
REYNOLDS NUMBER = 1.207 MILLION

TIME (sec.)	AOA (deg.)	C_L	$C_{M_{(c/4)}}$	C_{D_p}	C_N	C_A
0.0000	0.6	0.153	0.0048	0.0006	0.153	-.0013
0.0618	-0.5	0.030	0.0070	0.0008	0.030	0.0006
0.1237	-1.8	-0.104	0.0052	0.0024	-0.104	-.0010
0.1855	-3.3	-0.251	0.0035	0.0051	-0.251	-.0098
0.2474	-5.0	-0.399	0.0034	0.0116	-0.399	-.0233
0.3092	-6.6	-0.561	0.0060	0.0204	-0.560	-.0440
0.3711	-7.7	-0.650	0.0013	0.0229	-0.647	-.0644
0.4329	-8.8	-0.768	0.0035	0.0291	-0.764	-.0892
0.4948	-9.8	-0.896	0.0074	0.0364	-0.889	-.1171
0.5566	-10.9	-0.973	0.0013	0.0338	-0.962	-.1511
0.6185	-11.4	-1.040	0.0073	0.0415	-1.027	-.1656
0.6803	-12.0	-1.073	-.0002	0.0409	-1.058	-.1833
0.7422	-12.4	-1.115	0.0061	0.0496	-1.100	-.1913
0.8040	-12.6	-1.125	0.0038	0.0546	-1.110	-.1905
0.8659	-12.5	-1.155	0.0005	0.0489	-1.138	-.2020
0.9277	-12.3	-1.175	0.0074	0.0462	-1.158	-.2056
0.9896	-12.0	-1.162	0.0051	0.0469	-1.147	-.1959
1.0514	-11.8	-1.116	0.0041	0.0446	-1.101	-.1844
1.1133	-10.9	-1.025	0.0027	0.0310	-1.012	-.1637
1.1751	-9.8	-0.955	0.0095	0.0367	-0.947	-.1266
1.2370	-9.1	-0.854	0.0066	0.0316	-0.849	-.1035
1.2988	-7.8	-0.744	0.0024	0.0176	-0.740	-.0835
1.3607	-6.6	-0.620	0.0020	0.0157	-0.617	-.0564
1.4225	-4.7	-0.472	0.0019	0.0058	-0.471	-.0335
1.4844	-3.9	-0.354	0.0062	0.0096	-0.354	-.0149
1.5462	-2.1	-0.189	0.0027	0.0057	-0.189	-.0018
1.6081	-0.4	-0.027	0.0006	-.0003	-0.027	-.0007
1.6699	0.3	0.081	0.0059	0.0043	0.081	0.0034
1.7318	2.2	0.248	0.0025	0.0046	0.248	-.0057
1.7936	3.3	0.366	0.0053	-.0003	0.366	-.0217
1.8555	4.7	0.531	0.0014	-.0055	0.529	-.0492
1.9173	5.5	0.633	-.0047	0.0004	0.630	-.0607
1.9792	6.6	0.721	0.0000	0.0062	0.717	-.0766
2.0410	7.7	0.821	0.0002	0.0090	0.815	-.1007
2.1029	8.4	0.927	-.0042	0.0087	0.918	-.1271
2.1647	8.7	0.963	-.0015	0.0031	0.952	-.1430
2.2266	9.4	1.017	0.0032	0.0040	1.004	-.1604
2.2884	9.2	1.025	0.0027	0.0039	1.012	-.1606
2.3503	9.3	1.024	-.0015	0.0144	1.012	-.1529

TABLE 10

Cycle Averaged Pressure Data with Vortex Generators
at 0.1c Chord Location
10° Sine Function, k=0.009
(Concluded)

TIME (sec.)	AOA (deg.)	C_L	$C_{M_{(c/4)}}$	C_{D_p}	C_N	C_A
2.4121	9.4	1.008	0.0018	0.0115	0.996	-.1533
2.4740	9.4	0.989	0.0026	0.0088	0.977	-.1493
2.5358	9.1	0.971	0.0000	0.0073	0.960	-.1459
2.5977	8.3	0.915	-.0042	0.0007	0.905	-.1313
2.6595	7.3	0.804	0.0029	-.0022	0.797	-.1048
2.7214	6.6	0.731	0.0059	-.0065	0.725	-.0910
2.7832	5.1	0.615	0.0036	-.0065	0.612	-.0611
2.8451	4.2	0.461	0.0066	0.0001	0.460	-.0335
2.9069	2.4	0.309	0.0067	-.0057	0.308	-.0190
2.9687	0.6	0.153	0.0048	0.0006	0.153	-.0013

TABLE 11

Cycle Averaged Pressure Data with Vortex Generators
at 0.1c Chord Location
10° Sine Function, k=0.034

FREESTREAM VELOCITY = 142.6 FT/SEC
REYNOLDS NUMBER = 1.209 MILLION

TIME (sec.)	AOA (deg.)	C_L	$C_{M_{(c/4)}}$	C_{D_p}	C_N	C_A
0.0000	0.5	0.254	0.0098	-.0076	0.254	-.0106
0.0200	-0.5	0.129	0.0017	-.0032	0.129	-.0020
0.0400	-2.7	-0.094	0.0083	0.0055	-0.094	0.0004
0.0600	-4.3	-0.244	0.0054	0.0142	-0.245	-.0047
0.0800	-6.4	-0.450	0.0080	0.0262	-0.450	-.0250
0.1000	-7.8	-0.579	0.0074	0.0369	-0.579	-.0420
0.1200	-9.3	-0.723	0.0078	0.0460	-0.721	-.0716
0.1400	-10.5	-0.855	0.0071	0.0530	-0.850	-.1035
0.1600	-11.5	-0.970	0.0084	0.0544	-0.962	-.1407
0.1800	-12.1	-1.048	0.0040	0.0479	-1.035	-.1711
0.2000	-12.1	-1.066	0.0057	0.0459	-1.052	-.1767
0.2200	-12.1	-1.079	0.0023	0.0415	-1.064	-.1839
0.2400	-12.0	-1.093	0.0039	0.0407	-1.077	-.1885
0.2600	-12.0	-1.101	0.0054	0.0389	-1.085	-.1889
0.2800	-11.5	-1.057	0.0006	0.0320	-1.042	-.1790
0.3000	-10.4	-0.986	-.0007	0.0189	-0.973	-.1593
0.3200	-9.1	-0.871	-.0056	0.0110	-0.862	-.1269
0.3400	-7.1	-0.720	-.0053	0.0012	-0.714	-.0880
0.3600	-5.5	-0.584	-.0031	0.0016	-0.582	-.0546
0.3800	-3.3	-0.391	-.0028	0.0003	-0.390	-.0231
0.4000	-1.9	-0.253	-.0012	0.0046	-0.253	-.0044
0.4200	-0.3	-0.084	-.0027	0.0067	-0.084	0.0058
0.4400	1.4	0.090	-.0040	0.0077	0.091	0.0048
0.4600	3.3	0.272	-.0094	0.0114	0.272	-.0049
0.4800	4.8	0.418	-.0037	0.0156	0.418	-.0200
0.5000	6.1	0.579	-.0092	0.0202	0.578	-.0414
0.5200	7.7	0.732	0.0012	0.0215	0.728	-.0765
0.5400	8.2	0.814	-.0028	0.0222	0.808	-.0942
0.5600	8.8	0.891	-.0003	0.0177	0.883	-.1184
0.5800	9.2	0.968	-.0010	0.0164	0.958	-.1373
0.6000	9.5	0.986	0.0073	0.0120	0.974	-.1491
0.6200	9.4	1.000	0.0013	0.0156	0.989	-.1487
0.6400	9.4	1.008	0.0007	0.0135	0.996	-.1520
0.6600	8.7	0.967	0.0019	0.0042	0.956	-.1426
0.6800	8.3	0.927	0.0038	-.0005	0.917	-.1341
0.7000	7.2	0.842	0.0049	-.0074	0.834	-.1134
0.7200	4.9	0.662	0.0109	-.0168	0.658	-.0740
0.7400	3.3	0.539	-.0006	-.0108	0.538	-.0423
0.7600	0.5	0.254	0.0098	-.0076	0.254	-.0106

TABLE 12

Cycle Averaged Pressure Data with Vortex Generators
at 0.1c Chord Location
20° Inverse-Tangent Function, k=0.009

FREESTREAM VELOCITY = 140.2 FT/SEC
REYNOLDS NUMBER = 1.189 MILLION

TIME (sec.)	AOA (deg.)	C_L	$C_{M_{(c/4)}}$	C_{D_p}	C_N	C_A
0.0000	2.3	0.306	0.0044	-.0049	0.305	-.0184
0.0625	-2.1	-0.126	0.0055	0.0048	-0.126	-.0022
0.1250	-6.4	-0.573	0.0087	0.0216	-0.572	-.0441
0.1875	-9.8	-0.898	0.0091	0.0343	-0.891	-.1206
0.2500	-14.4	-1.322	0.0135	0.0726	-1.298	-.2599
0.3125	-16.9	-1.527	0.0059	0.0897	-1.488	-.3579
0.3750	-19.1	-1.656	-.0011	0.1045	-1.599	-.4433
0.4375	-20.4	-1.682	-.0068	0.1256	-1.620	-.4692
0.5000	-21.0	-1.714	-.0053	0.1313	-1.648	-.4916
0.5625	-21.2	-1.707	-.0086	0.1332	-1.640	-.4935
0.6250	-21.2	-1.713	-.0060	0.1399	-1.647	-.4903
0.6875	-21.2	-1.700	-.0066	0.1382	-1.634	-.4865
0.7500	-21.0	-1.739	-.0072	0.1335	-1.671	-.4981
0.8125	-20.5	-1.913	-.0117	0.1346	-1.839	-.5443
0.8750	-19.4	-1.787	-.0027	0.1321	-1.729	-.4689
0.9375	-18.0	-1.601	-.0050	0.0939	-1.552	-.4046
1.0000	-16.3	-1.479	-.0051	0.0767	-1.441	-.3425
1.0625	-15.1	-1.518	-.0036	0.0724	-1.485	-.3255
1.1250	-12.8	-1.570	-.0004	0.0500	-1.541	-.3004
1.1875	-10.8	-1.211	0.0051	0.0278	-1.195	-.2005
1.2500	-9.2	-0.984	-.0006	0.0173	-0.974	-.1403
1.3125	-7.7	-0.832	0.0020	0.0121	-0.826	-.1003
1.3750	-5.8	-0.595	0.0037	0.0102	-0.593	-.0509
1.4375	-2.6	-0.333	0.0064	0.0020	-0.333	-.0137
1.5000	-0.4	-0.089	0.0013	0.0031	-0.089	0.0015
1.5625	1.2	0.109	-.0017	0.0015	0.109	-.0012
1.6250	3.3	0.309	-.0024	0.0054	0.309	-.0126
1.6875	5.4	0.539	-.0004	0.0092	0.537	-.0420
1.7500	7.2	0.731	-.0003	0.0159	0.727	-.0760
1.8125	9.4	0.925	-.0002	0.0282	0.917	-.1234
1.8750	11.0	1.106	-.0044	0.0381	1.092	-.1738
1.9375	13.3	1.305	0.0026	0.0460	1.281	-.2563
2.0000	14.9	1.464	0.0036	0.0578	1.430	-.3205
2.0625	16.0	1.540	0.0084	0.0573	1.496	-.3684
2.1250	17.5	1.628	0.0071	0.0692	1.573	-.4234
2.1875	18.7	1.564	0.0204	0.0868	1.510	-.4183
2.2500	18.7	1.514	0.0241	0.0874	1.462	-.4028
2.3125	19.9	1.547	0.0135	0.1191	1.495	-.4160
2.3750	20.3	1.587	0.0156	0.1231	1.530	-.4391

TABLE 12

Cycle Averaged Pressure Data with Vortex Generators
at 0.1c Chord Location
20° Inverse-Tangent Function, k=0.009
(Concluded)

TIME (sec.)	AOA (deg.)	C_L	$C_{M_{(c/4)}}$	C_{D_p}	C_N	C_A
2.4375	20.3	1.576	0.0133	0.1244	1.521	-.4289
2.5000	20.6	1.545	0.0154	0.1115	1.488	-.4289
2.5625	20.3	1.537	0.0148	0.1137	1.483	-.4215
2.6250	19.3	1.456	0.0143	0.1060	1.410	-.3810
2.6875	17.8	1.405	0.0150	0.0856	1.363	-.3490
2.7500	16.0	1.366	0.0105	0.0687	1.332	-.3094
2.8125	13.2	1.373	0.0104	0.0365	1.345	-.2793
2.8750	9.9	0.915	0.0042	0.0158	0.904	-.1427
2.9375	6.3	0.671	-.0001	0.0001	0.667	-.0751

TABLE 13

Cycle Averaged Pressure Data with Vortex Generators
at 0.1c Chord Location
20° Inverse-Tangent Function, k=0.034

FREESTREAM VELOCITY = 142.5 FT/SEC
REYNOLDS NUMBER = 1.208 MILLION

TIME (sec.)	AOA (deg.)	C_L	$C_{M_{(c/4)}}$	C_{D_p}	C_N	C_A
0.0000	-0.4	-0.212	-.0040	0.0003	-0.212	-.0021
0.0204	2.4	0.064	-.0069	0.0094	0.065	0.0051
0.0407	5.1	0.346	-.0100	0.0215	0.346	-.0101
0.0611	7.8	0.617	-.0074	0.0405	0.617	-.0452
0.0814	9.9	0.843	-.0096	0.0528	0.839	-.0936
0.1018	12.8	1.125	-.0085	0.0744	1.113	-.1778
0.1222	15.0	1.337	0.0002	0.0804	1.312	-.2689
0.1425	16.3	1.505	-.0017	0.0858	1.469	-.3414
0.1629	18.3	1.685	0.0000	0.0988	1.630	-.4363
0.1832	19.2	1.763	-.0009	0.1049	1.699	-.4822
0.2036	21.0	1.835	0.0061	0.1136	1.755	-.5502
0.2240	21.2	1.857	0.0078	0.1121	1.772	-.5674
0.2443	21.6	1.846	0.0046	0.1172	1.760	-.5696
0.2647	20.5	1.655	0.0119	0.1234	1.594	-.4638
0.2850	19.2	1.482	0.0248	0.1070	1.434	-.3879
0.3054	16.9	1.305	0.0330	0.0648	1.267	-.3194
0.3258	13.9	1.111	0.0367	0.0251	1.084	-.2444
0.3461	8.5	0.788	0.0282	-.0054	0.778	-.1257
0.3665	3.5	0.402	0.0278	-.0110	0.400	-.0399
0.3868	-1.6	0.027	0.0229	0.0009	0.026	-.0057
0.4072	-7.8	-0.455	0.0170	0.0459	-0.457	-.0224
0.4276	-11.8	-0.849	0.0160	0.0808	-0.847	-.0988
0.4479	-16.0	-1.239	0.0216	0.1288	-1.226	-.2221
0.4683	-19.0	-1.532	0.0116	0.1393	-1.493	-.3678
0.4886	-20.6	-1.694	0.0100	0.1415	-1.635	-.4654
0.5090	-21.8	-1.768	-.0034	0.1293	-1.690	-.5360
0.5294	-21.8	-1.747	-.0104	0.1235	-1.668	-.5337
0.5497	-21.5	-1.702	-.0041	0.1257	-1.630	-.5062
0.5701	-20.9	-1.686	-.0089	0.1134	-1.616	-.4971
0.5905	-20.3	-1.633	-.0170	0.0980	-1.565	-.4760
0.6108	-18.1	-1.488	-.0167	0.0654	-1.435	-.3994
0.6312	-16.3	-1.370	-.0171	0.0500	-1.329	-.3370
0.6515	-14.1	-1.250	-.0130	0.0324	-1.220	-.2738
0.6719	-11.3	-1.108	-.0036	0.0165	-1.089	-.2018
0.6923	-8.6	-0.911	-.0093	-.0022	-0.900	-.1389
0.7126	-6.1	-0.709	-.0059	-.0050	-0.705	-.0817
0.7330	-3.6	-0.498	-.0036	-.0058	-0.496	-.0378
0.7533	-0.4	-0.212	-.0040	0.0003	-0.212	-.0021

TABLE 14

Cycle Averaged Pressure Data with Vortex Generators
at 0.1c Chord Location
30° Inverse-Tangent Function, k=0.009

FREESTREAM VELOCITY = 135.3 FT/SEC
REYNOLDS NUMBER = 1.147 MILLION

TIME (sec.)	AOA (deg.)	C_L	$C_{M_{(c/4)}}$	C_{D_p}	C_N	C_A
0.0000	2.1	0.319	0.0141	-.0079	0.318	-.0217
0.0625	-6.6	-0.492	0.0075	0.0267	-0.491	-.0351
0.1250	-14.0	-1.176	0.0124	0.0887	-1.162	-.2021
0.1875	-19.9	-1.755	0.0080	0.1280	-1.694	-.4762
0.2500	-23.8	-1.932	0.0140	0.2155	-1.855	-.5840
0.3125	-26.9	-0.427	-.1205	0.0203	-0.389	-.1885
0.3750	-27.2	-0.751	0.1039	0.5081	-0.900	0.1075
0.4375	-27.5	-0.729	0.0972	0.5042	-0.880	0.1108
0.5000	-27.5	-0.685	0.0841	0.4823	-0.830	0.1119
0.5625	-27.5	-0.710	0.0916	0.4924	-0.857	0.1093
0.6250	-27.2	-0.776	0.1022	0.5171	-0.926	0.1057
0.6875	-26.0	-0.683	0.0889	0.4487	-0.811	0.1031
0.7500	-24.8	-0.688	0.0844	0.4332	-0.806	0.1052
0.8125	-22.7	-0.682	0.0815	0.4019	-0.785	0.1077
0.8750	-20.7	-0.580	0.0208	0.2479	-0.630	0.0266
0.9375	-18.4	-0.856	0.0369	0.2137	-0.881	-.0665
1.0000	-16.0	-1.028	-.0042	0.1031	-1.017	-.1835
1.0625	-13.1	-1.284	-.0054	0.0300	-1.257	-.2625
1.1250	-11.7	-1.196	0.0024	0.0220	-1.176	-.2207
1.1875	-8.9	-0.971	0.0059	0.0097	-0.961	-.1407
1.2500	-6.4	-0.744	0.0012	0.0017	-0.740	-.0808
1.3125	-3.5	-0.438	0.0018	0.0054	-0.438	-.0228
1.3750	-0.6	-0.151	-.0022	-.0003	-0.151	-.0030
1.4375	2.3	0.169	-.0032	0.0020	0.169	-.0060
1.5000	5.6	0.499	-.0030	0.0193	0.499	-.0312
1.5625	7.8	0.752	-.0010	0.0268	0.749	-.0767
1.6250	10.6	1.013	-.0063	0.0414	1.003	-.1465
1.6875	13.0	1.225	0.0031	0.0535	1.205	-.2227
1.7500	15.6	1.500	0.0012	0.0725	1.464	-.3329
1.8125	18.2	1.669	0.0128	0.0881	1.613	-.4376
1.8750	20.3	1.714	0.0090	0.1272	1.652	-.4738
1.9375	22.0	1.722	0.0067	0.1727	1.661	-.4865
2.0000	24.2	1.778	0.0085	0.2085	1.708	-.5374
2.0625	26.1	1.835	0.0018	0.2590	1.762	-.5756
2.1250	28.0	1.910	-.0067	0.3175	1.836	-.6152
2.1875	29.9	1.892	-.0063	0.3556	1.817	-.6350
2.2500	31.7	1.925	-.0502	0.4408	1.870	-.6359
2.3125	32.5	1.630	-.0830	0.4953	1.641	-.4578
2.3750	33.4	1.245	-.1591	0.6146	1.378	-.1721

TABLE 14

Cycle Averaged Pressure Data with Vortex Generators
at 0.1c Chord Location
30° Inverse-Tangent Function, k=0.009
(Concluded)

TIME (sec.)	AOA (deg.)	C_L	$C_{M_{(c/4)}}$	C_{D_p}	C_N	C_A
2.4375	34.0	1.173	-.1129	0.5538	1.283	-.1964
2.5000	34.1	1.102	-.0790	0.5030	1.195	-.2031
2.5625	34.1	1.169	-.1551	0.6576	1.328	-.1204
2.6250	34.1	0.882	-.1797	0.7425	1.146	0.1196
2.6875	32.6	0.822	-.1171	0.6070	1.019	0.0681
2.7500	29.8	0.778	-.1218	0.5570	0.952	0.0964
2.8125	25.9	0.622	-.0710	0.3861	0.729	0.0752
2.8750	20.5	0.499	-.0321	0.2467	0.555	0.0546
2.9375	15.1	0.803	0.0396	0.0553	0.790	-.1551
3.0000	9.2	0.879	0.0135	0.0028	0.868	-.1369
3.0625	2.1	0.319	0.0141	-.0079	0.318	-.0217

TABLE 15

Cycle Averaged Pressure Data with Vortex Generators
at 0.1c Chord Location
30° Inverse-Tangent Function, k=0.023

FREESTREAM VELOCITY = 136.3 FT/SEC
REYNOLDS NUMBER = 1.156 MILLION

TIME (sec.)	AOA (deg.)	C_L	$C_{M_{(c/4)}}$	C_{D_p}	C_N	C_A
0.0000	-2.1	-0.406	-.0046	-.0084	-0.405	-.0238
0.0200	0.3	-0.185	-.0025	-.0006	-0.185	0.0002
0.0400	2.4	0.036	-.0053	0.0080	0.037	0.0065
0.0600	4.6	0.290	-.0078	0.0133	0.290	-.0105
0.0800	7.0	0.515	-.0038	0.0252	0.514	-.0382
0.1000	9.6	0.797	-.0117	0.0514	0.794	-.0815
0.1200	11.7	0.964	-.0079	0.0627	0.957	-.1343
0.1400	13.9	1.209	-.0064	0.0897	1.195	-.2041
0.1600	15.7	1.405	-.0078	0.1011	1.380	-.2844
0.1800	17.8	1.598	-.0056	0.1120	1.556	-.3806
0.2000	19.9	1.804	-.0055	0.1407	1.744	-.4822
0.2200	22.7	1.964	-.0046	0.1817	1.882	-.5906
0.2400	23.8	2.026	-.0039	0.1671	1.921	-.6664
0.2600	25.4	2.273	-.0405	0.2709	2.169	-.7293
0.2800	26.6	2.027	-.0691	0.3312	1.961	-.6102
0.3000	27.6	1.895	-.0642	0.3695	1.851	-.5505
0.3200	29.2	1.852	-.0727	0.3964	1.810	-.5587
0.3400	30.3	1.767	-.0529	0.3793	1.717	-.5649
0.3600	31.7	1.856	-.0986	0.4910	1.837	-.5590
0.3800	33.1	1.805	-.1198	0.5391	1.806	-.5350
0.4000	33.6	1.604	-.1161	0.5574	1.644	-.4234
0.4200	34.2	1.290	-.2054	0.7571	1.493	-.0987
0.4400	34.2	1.296	-.2239	0.8980	1.577	0.0144
0.4600	34.6	0.943	-.1858	0.7148	1.190	0.0687
0.4800	34.2	0.958	-.1876	0.7242	1.207	0.0722
0.5000	33.7	0.878	-.1635	0.6831	1.110	0.0817
0.5200	32.5	0.794	-.1370	0.6181	1.002	0.0941
0.5400	30.1	0.715	-.0905	0.5168	0.877	0.0889
0.5600	26.8	0.595	-.0603	0.4046	0.714	0.0922
0.5800	21.8	0.429	-.0308	0.2811	0.503	0.1003
0.6000	17.0	0.292	0.0086	0.1622	0.327	0.0686
0.6200	11.2	0.098	0.0916	0.0142	0.099	-.0058
0.6400	5.7	0.227	0.0649	-.0067	0.225	-.0288
0.6600	-0.9	-0.025	0.0389	0.0074	-0.025	0.0043
0.6800	-7.4	-0.478	0.0350	0.0508	-0.481	-.0135
0.7000	-14.0	-0.994	0.0297	0.1290	-0.995	-.1193
0.7200	-19.7	-1.467	0.0280	0.1925	-1.445	-.3150
0.7400	-24.2	-1.847	0.0241	0.2401	-1.783	-.5395
0.7600	-26.9	-2.083	0.0173	0.2379	-1.965	-.7306

TABLE 15

Cycle Averaged Pressure Data with Vortex Generators
at 0.1c Chord Location
30° Inverse-Tangent Function, k=0.023
(Concluded)

TIME (sec.)	AOA (deg.)	C_L	$C_{M_{(c/4)}}$	C_{D_p}	C_N	C_A
0.7800	-27.9	-2.101	0.0391	0.4056	-2.015	-.6871
0.8000	-28.3	-2.012	0.0618	0.4526	-1.956	-.6109
0.8200	-28.3	-1.437	0.1966	0.7473	-1.652	0.0378
0.8400	-28.3	-1.118	0.1929	0.6783	-1.315	0.0838
0.8600	-28.3	-0.911	0.1499	0.5711	-1.087	0.0977
0.8800	-28.2	-0.749	0.1139	0.5342	-0.912	0.1166
0.9000	-27.7	-0.730	0.1014	0.5109	-0.883	0.1119
0.9200	-26.3	-0.646	0.0805	0.4490	-0.778	0.1167
0.9400	-24.9	-0.595	0.0659	0.4076	-0.712	0.1180
0.9600	-22.4	-0.471	0.0337	0.3160	-0.556	0.1120
0.9800	-20.7	-0.350	-.0082	0.2117	-0.403	0.0740
1.0000	-19.0	-0.553	-.0395	0.1131	-0.560	-.0718
1.0200	-17.2	-0.843	-.0435	0.0846	-0.830	-.1674
1.0400	-15.7	-1.090	-.0201	0.0687	-1.068	-.2282
1.0600	-14.1	-1.166	-.0109	0.0496	-1.143	-.2351
1.0800	-11.9	-1.070	-.0100	0.0172	-1.051	-.2036
1.1000	-9.1	-0.933	-.0115	-.0096	-0.920	-.1574
1.1200	-6.9	-0.795	-.0042	-.0107	-0.787	-.1070
1.1400	-4.1	-0.582	-.0011	-.0104	-0.579	-.0522
1.1600	-2.1	-0.406	-.0046	-.0084	-0.405	-.0238

TABLE 16

Cycle Averaged Pressure Data with Vortex Generators
at 0.3c Chord Location
10° Sine Function, k=0.009

FREESTREAM VELOCITY = 137.6 FT/SEC
REYNOLDS NUMBER = 1.161 MILLION

TIME (sec.)	AOA (deg.)	C_L	$C_{M_{(c/4)}}$	C_{D_p}	C_N	C_A
0.0000	0.8	0.215	0.0009	-.0012	0.215	-.0046
0.0625	-0.8	0.060	-.0070	-.0014	0.060	-.0006
0.1250	-1.9	-0.108	0.0050	0.0025	-0.108	-.0013
0.1875	-3.5	-0.299	0.0049	0.0048	-0.298	-.0138
0.2500	-5.2	-0.491	0.0077	0.0120	-0.490	-.0335
0.3125	-6.8	-0.667	0.0083	0.0187	-0.665	-.0607
0.3750	-8.5	-0.850	0.0066	0.0238	-0.844	-.1022
0.4375	-9.3	-0.964	0.0064	0.0248	-0.955	-.1316
0.5000	-10.6	-1.091	0.0085	0.0363	-1.079	-.1654
0.5625	-11.2	-1.169	0.0118	0.0418	-1.155	-.1855
0.6250	-11.7	-1.218	0.0045	0.0390	-1.200	-.2096
0.6875	-12.3	-1.289	0.0101	0.0455	-1.269	-.2298
0.7500	-12.8	-1.330	0.0080	0.0470	-1.308	-.2474
0.8125	-12.8	-1.330	0.0086	0.0509	-1.308	-.2459
0.8750	-12.8	-1.348	0.0064	0.0508	-1.326	-.2496
0.9375	-12.8	-1.336	0.0032	0.0440	-1.313	-.2531
1.0000	-12.8	-1.336	0.0048	0.0463	-1.313	-.2506
1.0625	-12.3	-1.328	0.0069	0.0412	-1.306	-.2416
1.1250	-11.4	-1.234	0.0082	0.0370	-1.217	-.2074
1.1875	-10.6	-1.160	0.0070	0.0328	-1.146	-.1819
1.2500	-9.5	-1.058	0.0101	0.0242	-1.047	-.1513
1.3125	-8.4	-0.946	0.0084	0.0227	-0.939	-.1166
1.3750	-7.3	-0.804	0.0046	0.0188	-0.800	-.0834
1.4375	-5.8	-0.663	0.0081	0.0088	-0.660	-.0588
1.5000	-4.0	-0.439	0.0021	0.0034	-0.438	-.0283
1.5625	-3.0	-0.308	0.0041	0.0034	-0.307	-.0127
1.6250	-1.3	-0.150	0.0051	0.0026	-0.150	-.0014
1.6875	-0.2	0.012	0.0024	-.0022	0.012	-.0023
1.7500	1.4	0.206	-.0039	0.0038	0.206	-.0017
1.8125	3.1	0.399	-.0055	0.0034	0.399	-.0185
1.8750	4.2	0.540	-.0091	0.0033	0.539	-.0359
1.9375	5.3	0.659	-.0034	0.0040	0.656	-.0565
2.0000	6.3	0.801	-.0073	0.0097	0.797	-.0792
2.0625	7.5	0.947	-.0111	0.0111	0.941	-.1120
2.1250	8.0	0.992	-.0113	0.0129	0.984	-.1253
2.1875	8.6	1.098	-.0101	0.0149	1.087	-.1498
2.2500	9.1	1.160	-.0111	0.0097	1.147	-.1726
2.3125	9.4	1.191	-.0143	0.0148	1.178	-.1793
2.3750	9.6	1.191	-.0088	0.0187	1.178	-.1798

TABLE 16

Cycle Averaged Pressure Data with Vortex Generators
at 0.3c Chord Location
10° Sine Function, k=0.009
(Concluded)

TIME (sec.)	AOA (deg.)	C_L	$C_{M_{(c/4)}}$	C_{D_p}	C_N	C_A
2.4375	9.6	1.181	-.0089	0.0164	1.167	-.1803
2.5000	9.5	1.172	-.0097	0.0141	1.158	-.1793
2.5625	9.1	1.117	-.0082	0.0024	1.103	-.1745
2.6250	8.5	1.033	-.0068	0.0044	1.023	-.1490
2.6875	7.8	0.963	-.0056	0.0008	0.954	-.1302
2.7500	6.9	0.891	-.0096	-.0001	0.885	-.1072
2.8125	5.8	0.785	-.0081	-.0066	0.781	-.0862
2.8750	4.2	0.602	-.0021	-.0061	0.599	-.0498
2.9375	2.9	0.430	-.0013	-.0054	0.430	-.0271

TABLE 17

Cycle Averaged Pressure Data with Vortex Generators
at 0.3c Chord Location
10° Sine Function, k=0.035

FREESTREAM VELOCITY = 138.3 FT/SEC
REYNOLDS NUMBER = 1.167 MILLION

TIME (sec.)	AOA (deg.)	C_L	$C_{M_{(c/4)}}$	C_{D_p}	C_N	C_A
0.0000	-0.2	-0.101	-.0035	0.0014	-0.101	0.0005
0.0200	1.4	0.083	-.0071	0.0029	0.083	0.0005
0.0400	3.6	0.338	-.0140	0.0086	0.338	-.0138
0.0600	5.3	0.535	-.0098	0.0166	0.535	-.0332
0.0800	6.4	0.675	-.0078	0.0181	0.673	-.0571
0.1000	7.4	0.823	-.0094	0.0219	0.819	-.0850
0.1200	8.0	0.940	-.0139	0.0231	0.934	-.1080
0.1400	9.1	1.083	-.0090	0.0163	1.073	-.1530
0.1600	9.1	1.109	-.0080	0.0123	1.097	-.1606
0.1800	9.1	1.132	-.0081	0.0073	1.120	-.1693
0.2000	9.1	1.136	-.0040	0.0072	1.122	-.1738
0.2200	9.1	1.144	-.0073	0.0031	1.130	-.1774
0.2400	8.5	1.096	-.0035	-.0054	1.083	-.1681
0.2600	7.5	0.987	0.0026	-.0136	0.977	-.1426
0.2800	6.4	0.881	0.0018	-.0127	0.874	-.1104
0.3000	4.2	0.675	0.0026	-.0189	0.672	-.0690
0.3200	2.5	0.497	0.0043	-.0143	0.495	-.0370
0.3400	-0.2	0.222	0.0059	-.0085	0.222	-.0088
0.3600	-1.3	0.083	0.0056	-.0027	0.083	-.0013
0.3800	-3.5	-0.177	0.0066	0.0080	-0.177	-.0038
0.4000	-5.1	-0.359	0.0112	0.0178	-0.359	-.0156
0.4200	-7.1	-0.572	0.0151	0.0335	-0.572	-.0385
0.4400	-9.0	-0.789	0.0171	0.0451	-0.786	-.0792
0.4600	-10.2	-0.943	0.0136	0.0520	-0.937	-.1168
0.4800	-11.2	-1.062	0.0101	0.0527	-1.052	-.1543
0.5000	-11.9	-1.155	0.0106	0.0528	-1.141	-.1861
0.5200	-12.8	-1.264	0.0091	0.0560	-1.245	-.2260
0.5400	-12.8	-1.277	0.0077	0.0520	-1.257	-.2329
0.5600	-12.8	-1.302	0.0097	0.0516	-1.282	-.2380
0.5800	-12.8	-1.314	0.0141	0.0511	-1.293	-.2408
0.6000	-12.3	-1.276	0.0049	0.0386	-1.255	-.2336
0.6200	-11.7	-1.234	0.0037	0.0304	-1.214	-.2211
0.6400	-10.6	-1.144	0.0009	0.0180	-1.128	-.1938
0.6600	-9.0	-1.002	0.0040	0.0072	-0.990	-.1498
0.6800	-7.3	-0.840	-.0010	0.0013	-0.833	-.1069
0.7000	-5.7	-0.686	0.0014	-.0026	-0.682	-.0716
0.7200	-3.9	-0.516	-.0002	-.0058	-0.514	-.0414
0.7400	-2.4	-0.337	-.0007	-.0016	-0.336	-.0162
0.7600	-0.2	-0.101	-.0035	0.0014	-0.101	0.0005

TABLE 18

Cycle Averaged Pressure Data with Vortex Generators
at 0.3c Chord Location
20° Inverse-Tangent Function, k=0.009

FREESTREAM VELOCITY = 136.9 FT/SEC
REYNOLDS NUMBER = 1.154 MILLION

TIME (sec.)	AOA (deg.)	C_L	$C_{M_{(c/4)}}$	C_{D_p}	C_N	C_A
0.0000	0.9	0.269	-.0014	-.0126	0.268	-.0205
0.0625	-4.1	-0.261	0.0043	0.0088	-0.261	-.0128
0.1250	-7.9	-0.722	0.0090	0.0313	-0.719	-.0717
0.1875	-12.3	-1.181	0.0134	0.0639	-1.167	-.1908
0.2500	-15.0	-1.464	0.0088	0.0785	-1.434	-.3042
0.3125	-17.9	-1.679	0.0088	0.1120	-1.632	-.4110
0.3750	-19.4	-1.750	0.0041	0.1343	-1.695	-.4546
0.4375	-20.0	-1.657	0.0054	0.1688	-1.615	-.4070
0.5000	-20.5	-1.332	0.0088	0.1945	-1.316	-.2845
0.5625	-21.0	-1.123	0.0408	0.2360	-1.133	-.1830
0.6250	-20.9	-1.101	0.0160	0.2066	-1.102	-.2007
0.6875	-20.8	-1.073	0.0046	0.1823	-1.067	-.2101
0.7500	-20.5	-1.063	-.0085	0.1749	-1.057	-.2087
0.8125	-19.3	-1.003	-.0117	0.1436	-0.994	-.1951
0.8750	-18.3	-1.025	-.0192	0.1234	-1.012	-.2046
0.9375	-17.2	-1.185	0.0178	0.1417	-1.173	-.2150
1.0000	-15.8	-1.297	-.0042	0.1014	-1.275	-.2569
1.0625	-13.9	-1.310	-.0041	0.0583	-1.286	-.2580
1.1250	-12.0	-1.256	-.0002	0.0365	-1.236	-.2271
1.1875	-9.6	-1.051	0.0094	0.0255	-1.041	-.1497
1.2500	-8.2	-0.915	0.0096	0.0212	-0.908	-.1097
1.3125	-6.2	-0.696	0.0047	0.0116	-0.693	-.0649
1.3750	-4.1	-0.457	0.0010	0.0027	-0.456	-.0311
1.4375	-1.9	-0.217	-.0006	0.0016	-0.217	-.0063
1.5000	0.0	0.043	-.0058	-.0003	0.043	-.0014
1.5625	2.2	0.297	-.0059	0.0018	0.297	-.0107
1.6250	4.2	0.513	-.0077	0.0043	0.512	-.0342
1.6875	6.3	0.760	-.0062	0.0125	0.756	-.0721
1.7500	8.3	0.987	-.0062	0.0176	0.979	-.1266
1.8125	10.2	1.203	-.0107	0.0233	1.188	-.1904
1.8750	12.4	1.453	-.0120	0.0325	1.426	-.2803
1.9375	13.9	1.618	-.0042	0.0327	1.578	-.3582
2.0000	15.7	1.770	-.0040	0.0479	1.717	-.4321
2.0625	17.1	1.849	0.0064	0.0581	1.784	-.4879
2.1250	17.9	1.801	0.0033	0.0802	1.739	-.4758
2.1875	19.0	1.640	0.0052	0.1324	1.594	-.4080
2.2500	19.8	1.714	-.0289	0.1878	1.676	-.4032
2.3125	20.6	1.606	-.0223	0.2061	1.576	-.3721
2.3750	20.6	1.553	-.0220	0.2049	1.525	-.3544

TABLE 18

Cycle Averaged Pressure Data with Vortex Generators
at 0.3c Chord Location
20° Inverse-Tangent Function, k=0.009
(Concluded)

TIME (sec.)	AOA (deg.)	C_L	$C_{M_{(c/4)}}$	C_{D_p}	C_N	C_A
2.4375	20.6	1.567	-.0187	0.1995	1.538	-.3618
2.5000	20.6	1.526	-.0069	0.1860	1.494	-.3610
2.5625	20.1	1.500	-.0014	0.1708	1.467	-.3551
2.6250	19.0	1.456	0.0068	0.1449	1.424	-.3357
2.6875	17.6	1.405	0.0144	0.1135	1.374	-.3169
2.7500	15.9	1.430	0.0098	0.0774	1.397	-.3176
2.8125	12.9	1.389	0.0056	0.0238	1.359	-.2889
2.8750	9.6	1.143	0.0009	-.0010	1.127	-.1933
2.9375	5.8	0.818	-.0023	-.0089	0.812	-.0949
3.0000	0.9	0.269	-.0014	-.0126	0.268	-.0205

TABLE 19

Cycle Averaged Pressure Data with Vortex Generators
at 0.3c Chord Location
20° Inverse-Tangent Function, k=0.036

FREESTREAM VELOCITY = 136.7 FT/SEC
REYNOLDS NUMBER = 1.152 MILLION

TIME (sec.)	AOA (deg.)	C_L	$C_{M_{(c/4)}}$	C_{D_p}	C_N	C_A
0.0000	4.7	0.453	0.0567	-.0253	0.449	-.0650
0.0198	-0.6	0.152	0.0243	-.0117	0.152	-.0140
0.0396	-6.8	-0.358	0.0244	0.0363	-0.360	-.0117
0.0595	-11.2	-0.815	0.0226	0.0823	-0.815	-.0806
0.0793	-15.0	-1.214	0.0257	0.1288	-1.205	-.1938
0.0991	-18.6	-1.587	0.0193	0.1623	-1.555	-.3547
0.1189	-20.4	-1.782	0.0211	0.1703	-1.730	-.4608
0.1388	-21.5	-1.853	0.0037	0.1448	-1.777	-.5451
0.1586	-21.6	-1.821	-.0073	0.1386	-1.744	-.5409
0.1784	-21.5	-1.784	-.0011	0.1532	-1.716	-.5104
0.1982	-20.5	-1.603	0.0039	0.1609	-1.558	-.4104
0.2181	-19.4	-1.332	0.0187	0.1631	-1.310	-.2889
0.2379	-17.8	-1.059	-.0191	0.1118	-1.043	-.2176
0.2577	-15.6	-1.007	-.0316	0.0762	-0.991	-.1966
0.2775	-13.7	-1.039	-.0338	0.0391	-1.019	-.2079
0.2974	-11.2	-1.049	-.0126	0.0204	-1.032	-.1840
0.3172	-9.0	-0.944	-.0053	0.0085	-0.934	-.1396
0.3370	-6.2	-0.742	-.0068	-.0043	-0.737	-.0862
0.3568	-4.1	-0.534	-.0083	-.0058	-0.532	-.0446
0.3767	-1.3	-0.257	-.0101	-.0063	-0.257	-.0133
0.3965	1.4	0.022	-.0114	0.0023	0.022	0.0006
0.4163	4.2	0.331	-.0177	0.0153	0.331	-.0103
0.4361	6.9	0.644	-.0160	0.0336	0.643	-.0451
0.4560	9.1	0.920	-.0198	0.0513	0.917	-.0961
0.4758	11.8	1.213	-.0204	0.0752	1.203	-.1761
0.4956	14.0	1.477	-.0204	0.0854	1.453	-.2760
0.5154	16.2	1.730	-.0158	0.0949	1.687	-.3929
0.5353	17.9	1.922	-.0108	0.0937	1.858	-.5004
0.5551	19.2	2.080	-.0145	0.1069	2.000	-.5844
0.5749	20.3	2.128	-.0027	0.1026	2.032	-.6404
0.5947	21.2	2.137	-.0095	0.1320	2.039	-.6526
0.6146	21.7	1.737	-.1273	0.2990	1.723	-.3669
0.6344	21.2	1.731	-.1297	0.2872	1.717	-.3586
0.6542	19.7	1.282	-.0474	0.1927	1.271	-.2525
0.6740	18.4	1.052	-.0001	0.1373	1.042	-.2022
0.6939	15.7	0.892	0.0300	0.0726	0.879	-.1717
0.7137	11.9	0.719	0.0627	0.0106	0.705	-.1387
0.7335	7.4	0.557	0.0676	-.0131	0.551	-.0860
0.7533	4.7	0.453	0.0567	-.0253	0.449	-.0650

TABLE 20

Cycle Averaged Pressure Data with Vortex Generators
at 0.3c Chord Location
30° Inverse-Tangent Function, k=0.009

FREESTREAM VELOCITY = 137.0 FT/SEC
REYNOLDS NUMBER = 1.153 MILLION

TIME (sec.)	AOA (deg.)	C_L	$C_{M_{(c/4)}}$	C_{D_p}	C_N	C_A
0.0000	5.2	0.644	0.0146	-.0112	0.640	-.0716
0.0625	-3.5	-0.133	0.0092	0.0024	-0.133	-.0125
0.1250	-12.0	-1.012	0.0204	0.0671	-1.003	-.1508
0.1875	-18.9	-1.641	0.0166	0.1382	-1.596	-.4036
0.2500	-23.2	-1.770	0.0070	0.2006	-1.706	-.5133
0.3125	-26.2	-1.113	0.0462	0.3049	-1.134	-.2176
0.3750	-28.2	-0.999	0.0592	0.3245	-1.034	-.1847
0.4375	-29.3	-1.006	0.0621	0.3473	-1.047	-.1890
0.5000	-29.8	-1.039	0.0705	0.3763	-1.087	-.1931
0.5625	-30.0	-1.038	0.0651	0.3727	-1.084	-.1971
0.6250	-29.6	-1.009	0.0631	0.3632	-1.057	-.1831
0.6875	-28.7	-1.020	0.0606	0.3466	-1.061	-.1858
0.7500	-27.1	-1.015	0.0451	0.3166	-1.048	-.1804
0.8125	-25.4	-0.984	0.0319	0.2781	-1.008	-.1713
0.8750	-23.2	-0.905	0.0018	0.2008	-0.910	-.1726
0.9375	-21.0	-0.946	-.0070	0.1666	-0.943	-.1840
1.0000	-18.6	-1.060	0.0039	0.1522	-1.053	-.1942
1.0625	-16.2	-1.198	-.0077	0.0976	-1.178	-.2411
1.1250	-13.9	-1.260	-.0014	0.0536	-1.236	-.2513
1.1875	-10.9	-1.103	0.0046	0.0318	-1.089	-.1779
1.2500	-8.4	-0.868	0.0018	0.0211	-0.861	-.1075
1.3125	-5.7	-0.592	0.0014	0.0043	-0.589	-.0552
1.3750	-2.7	-0.297	0.0006	-.0005	-0.297	-.0159
1.4375	0.6	0.055	-.0050	-.0025	0.055	-.0038
1.5000	3.1	0.368	-.0043	0.0014	0.367	-.0195
1.5625	5.8	0.664	-.0081	0.0072	0.661	-.0611
1.6250	8.7	0.988	-.0130	0.0196	0.979	-.1307
1.6875	11.3	1.295	-.0104	0.0300	1.276	-.2234
1.7500	14.0	1.532	-.0076	0.0440	1.496	-.3295
1.8125	16.4	1.740	-.0013	0.0505	1.683	-.4444
1.8750	18.9	1.892	-.0369	0.1237	1.830	-.4981
1.9375	20.1	1.230	-.0295	0.1671	1.213	-.2652
2.0000	22.2	1.173	-.0373	0.2132	1.166	-.2467
2.0625	23.9	1.087	-.0265	0.2233	1.084	-.2358
2.1250	26.6	1.195	-.0514	0.2924	1.200	-.2743
2.1875	27.7	1.179	-.0621	0.3197	1.192	-.2651
2.2500	29.4	1.225	-.0715	0.3627	1.245	-.2847
2.3125	30.5	1.201	-.0787	0.3811	1.229	-.2806
2.3750	31.6	1.202	-.0973	0.4156	1.241	-.2759
2.4375	32.1	1.157	-.0888	0.4281	1.207	-.2521

TABLE 20

Cycle Averaged Pressure Data with Vortex Generators
at 0.3c Chord Location
30° Inverse-Tangent Function, k=0.009
(Concluded)

TIME (sec.)	AOA (deg.)	C_L	$C_{M_{(c/4)}}$	C_{D_p}	C_N	C_A
2.5000	32.6	0.968	-.1030	0.4323	1.050	-.1529
2.5625	32.6	0.932	-.0993	0.4253	1.017	-.1388
2.6250	32.1	0.872	-.1007	0.4165	0.960	-.1108
2.6875	30.5	0.888	-.0808	0.3653	0.951	-.1356
2.7500	27.7	0.931	-.0490	0.2890	0.959	-.1772
2.8125	23.3	0.935	-.0124	0.1966	0.937	-.1899
2.8750	17.7	0.851	0.0254	0.0951	0.839	-.1696
2.9375	10.8	0.833	0.0352	0.0169	0.822	-.1394
3.0000	5.2	0.644	0.0146	-.0112	0.640	-.0716

TABLE 21

Cycle Averaged Pressure Data with Vortex Generators
at 0.3c Chord Location
30° Inverse-Tangent Function, k=0.024

FREESTREAM VELOCITY = 135.1 FT/SEC
REYNOLDS NUMBER = 1.138 MILLION

TIME (sec.)	AOA (deg.)	C_L	$C_{M_{(c/4)}}$	C_{D_p}	C_N	C_A
0.0000	0.6	0.157	0.0479	-.0194	0.156	-.0257
0.0200	-6.3	-0.294	0.0299	0.0287	-0.295	-.0109
0.0400	-12.8	-0.904	0.0408	0.1196	-0.907	-.0945
0.0600	-19.4	-1.494	0.0344	0.2167	-1.479	-.2979
0.0800	-24.1	-1.936	0.0371	0.2826	-1.881	-.5364
0.1000	-27.7	-2.212	0.0793	0.3460	-2.120	-.7219
0.1200	-28.7	-2.065	0.3423	0.7810	-2.187	-.3079
0.1400	-28.7	-1.798	0.2434	0.7157	-1.920	-.2365
0.1600	-28.7	-1.501	0.2744	0.8169	-1.708	-.0050
0.1800	-28.7	-1.089	0.1383	0.5254	-1.213	-.0555
0.2000	-28.7	-0.976	0.1226	0.5170	-1.107	-.0155
0.2200	-28.7	-0.883	0.0886	0.4538	-0.992	-.0304
0.2400	-28.7	-0.888	0.1025	0.4703	-1.005	-.0184
0.2600	-27.9	-0.811	0.0812	0.4174	-0.912	-.0114
0.2800	-26.5	-0.810	0.0572	0.3970	-0.902	-.0057
0.3000	-24.7	-0.733	0.0350	0.3530	-0.813	0.0143
0.3200	-23.2	-0.628	0.0363	0.3414	-0.711	0.0656
0.3400	-21.4	-0.487	0.0058	0.2341	-0.540	0.0400
0.3600	-20.0	-0.694	-.0038	0.1763	-0.713	-.0696
0.3800	-17.8	-0.968	0.0255	0.1702	-0.974	-.1330
0.4000	-15.6	-0.977	-.0227	0.0666	-0.959	-.1984
0.4200	-13.1	-1.035	-.0192	0.0396	-1.017	-.1970
0.4400	-11.2	-1.026	-.0098	0.0257	-1.011	-.1744
0.4600	-9.0	-0.936	0.0013	0.0107	-0.926	-.1367
0.4800	-6.8	-0.774	-.0067	-.0046	-0.768	-.0972
0.5000	-4.6	-0.586	-.0008	0.0003	-0.584	-.0482
0.5200	-2.4	-0.349	-.0054	0.0025	-0.348	-.0131
0.5400	-0.1	-0.099	-.0056	0.0052	-0.099	0.0039
0.5600	3.1	0.210	-.0134	0.0124	0.211	-.0002
0.5800	5.2	0.477	-.0122	0.0212	0.477	-.0236
0.6000	7.4	0.745	-.0168	0.0316	0.742	-.0661
0.6200	9.1	0.952	-.0196	0.0423	0.947	-.1094
0.6400	11.1	1.193	-.0169	0.0574	1.182	-.1755
0.6600	13.5	1.461	-.0255	0.0782	1.439	-.2649
0.6800	15.9	1.720	-.0197	0.0904	1.678	-.3855
0.7000	18.4	1.976	-.0171	0.1181	1.912	-.5130
0.7200	20.6	2.153	-.0079	0.1244	2.059	-.6413
0.7400	22.3	2.241	-.0033	0.1314	2.124	-.7270
0.7600	23.3	2.346	-.0956	0.2718	2.262	-.6802
0.7800	24.4	2.370	-.2784	0.5636	2.391	-.4673

TABLE 21

Cycle Averaged Pressure Data with Vortex Generators
at 0.3c Chord Location
30° Inverse-Tangent Function, k=0.024
(Concluded)

TIME (sec.)	AOA (deg.)	C_L	$C_{M_{(c/4)}}$	C_{D_p}	C_N	C_A
0.8000	25.0	1.559	-.1809	0.4625	1.609	-.2390
0.8200	27.2	1.587	-.1173	0.3979	1.594	-.3710
0.8400	28.6	1.445	-.1117	0.3931	1.457	-.3454
0.8600	29.9	1.327	-.1211	0.4527	1.376	-.2700
0.8800	31.4	1.235	-.1147	0.4714	1.300	-.2401
0.9000	31.6	1.161	-.1136	0.4634	1.232	-.2128
0.9200	32.1	1.128	-.1357	0.5180	1.231	-.1609
0.9400	32.3	1.054	-.1438	0.5307	1.174	-.1147
0.9600	32.2	1.032	-.1326	0.4975	1.144	-.1199
0.9800	32.3	0.960	-.1116	0.4716	1.063	-.1134
1.0000	32.1	0.922	-.1117	0.4607	1.026	-.0998
1.0200	31.0	0.830	-.0865	0.3930	0.914	-.0907
1.0400	28.6	0.804	-.0472	0.2901	0.845	-.1306
1.0600	25.1	0.772	-.0132	0.2073	0.787	-.1408
1.0800	20.6	0.643	0.0238	0.1105	0.641	-.1244
1.1000	15.7	0.399	0.0625	0.0224	0.390	-.0890
1.1200	9.6	0.312	0.0829	-.0158	0.304	-.0683
1.1400	0.6	0.157	0.0479	-.0194	0.156	-.0257

TABLE 21

Cycle Averaged Pressure Data with Vortex Generators
at 0.3c Chord Location
30° Inverse-Tangent Function, k=0.024
(Concluded)

TIME (sec.)	AOA (deg.)	C_L	$C_{M_{(c/4)}}$	C_{D_p}	C_N	C_A
0.8000	25.0	1.559	-.1809	0.4625	1.609	-.2390
0.8200	27.2	1.587	-.1173	0.3979	1.594	-.3710
0.8400	28.6	1.445	-.1117	0.3931	1.457	-.3454
0.8600	29.9	1.327	-.1211	0.4527	1.376	-.2700
0.8800	31.4	1.235	-.1147	0.4714	1.300	-.2401
0.9000	31.6	1.161	-.1136	0.4634	1.232	-.2128
0.9200	32.1	1.128	-.1357	0.5180	1.231	-.1609
0.9400	32.3	1.054	-.1438	0.5307	1.174	-.1147
0.9600	32.2	1.032	-.1326	0.4975	1.144	-.1199
0.9800	32.3	0.960	-.1116	0.4716	1.063	-.1134
1.0000	32.1	0.922	-.1117	0.4607	1.026	-.0998
1.0200	31.0	0.830	-.0865	0.3930	0.914	-.0907
1.0400	28.6	0.804	-.0472	0.2901	0.845	-.1306
1.0600	25.1	0.772	-.0132	0.2073	0.787	-.1408
1.0800	20.6	0.643	0.0238	0.1105	0.641	-.1244
1.1000	15.7	0.399	0.0625	0.0224	0.390	-.0890
1.1200	9.6	0.312	0.0829	-.0158	0.304	-.0683
1.1400	0.6	0.157	0.0479	-.0194	0.156	-.0257

DISTRIBUTION:

D. K. Ai
Alcoa Technical Center
Aluminum Company of America
Alcoa Center, PA 15069

Dr. R. E. Akins
Washington & Lee University
P.O. Box 735
Lexington, VA 24450

The American Wind Energy Association
777 N. Capitol Street, NE
Suite 805
Washington, DC 20002

Dr. Mike Anderson
VAWT, Ltd.
1 St. Albans
Hemel Hempstead
Herts HP2 4TA
UNITED KINGDOM

Dr. M. P. Ansell
School of Material Science
University of Bath
Claverton Down
Bath BA2 7AY
Avon
UNITED KINGDOM

Holt Ashley
Dept. of Aeronautics and
Astronautics Mechanical Engr.
Stanford University
Stanford, CA 94305

K. Bergey
University of Oklahoma
Aero Engineering Department
Norman, OK 73069

Ir. Jos Beurskens
Programme Manager for
Renewable Energies
Netherlands Energy Research
Foundation ECN
Westerduinweg 3
P.O. Box 1
1755 ZG Petten (NH)
THE NETHERLANDS

J. R. Birk
Electric Power Research Institute
3412 Hillview Avenue
Palo Alto, CA 94304

N. Butler
Bonneville Power Administration
P.O. Box 3621
Portland, OR 97208

Monique Carpentier
Energy, Mines and Resources
Renewable Energy Branch
460 O'Connor Street
Ottawa, Ontario K1A OE4
CANADA

Dr. R. N. Clark
USDA
Agricultural Research Service
Southwest Great Plains Research
Center
Bushland, TX 79012

Otto de Vries
National Aerospace Laboratory
Anthony Fokkerweg 2
Amsterdam 1017
THE NETHERLANDS

E. A. DeMeo
Electric Power Research Institute
3412 Hillview Avenue
Palo Alto, CA 94304

C. W. Dodd
Universal Data Systems
5000 Bradford Drive
Huntsville, AL 35805

J. B. Dragt
Physics Department
Nederlands Energy Research
Foundation
(E.C.N.)
Westerduinweg 3 Petten (NH)
THE NETHERLANDS

A. J. Eggers, Jr.
RANN, Inc.
260 Sheridan Ave., Suite 414
Palo Alto, CA 94306

John Ereaux
RR No. 2
Woodbridge, Ontario L4L 1A6
CANADA

Dr. R. A. Galbraith
Dept. of Aerospace Engineering
James Watt Building
University of Glasgow
Glasgow G12 8QG
Scotland

A. D. Garrad
Garrad Hasson
10 Northampton Square
London EC1M 5PA
UNITED KINGDOM

P. R. Goldman
Wind/Hydro/Ocean Division
U.S. Department of Energy
1000 Independence Avenue
Washington, DC 20585

Dr. I. J. Graham
Dept. of Mechanical Engineering
Southern University
P.O. Box 9445
Baton Rouge, LA 70813-9445

Professor G. Gregorek
Aeronautical & Astronautical Dept.
Ohio State University
2300 West Case Road
Columbus, OH 43220

Professor N. D. Ham
Aero/Astro Dept.
Massachusetts Institute of Technology
77 Massachusetts Avenue
Cambridge, MA 02139

T. Hillesland
Pacific Gas and Electric Co.
3400 Crow Canyon Road
San Ramon, CA 94583

Eric N. Hinrichsen
Power Technologies, Inc.
P.O. Box 1058
Schenectady, NY 12301-1058

W. E. Holley
U.S. WindPower
6952 Preston Avenue
Livermore, CA 94550

M. A. Ilyan
Pacific Gas and Electric Co.
3400 Crow Canyon Road
San Ramon, CA 94583

K. Jackson
Dynamic Design
123 C Street
Davis, CA 95616

O. Krauss
Division of Engineering Research
Michigan State University
East Lansing, MI 48825

V. Lacey
Indal Technologies, Inc.
3570 Hawkestone Road
Mississauga, Ontario L5C 2V8
CANADA

A. Laneville
Faculty of Applied Science
University of Sherbrooke
Sherbrooke, Quebec J1K 2R1
CANADA

G. G. Leigh
New Mexico Engineering Research Institute
Campus P.O. Box 25
Albuquerque, NM 87131

L. K. Liljegren
120 East Penn Street
San Dimas, CA 71773

R. R. Loose, Director
Wind/Hydro/Ocean Division
U.S. Department of Energy
1000 Independence Ave., SW
Washington, DC 20585

Robert Lynette
R. Lynette & Assoc., Inc.
15042 NE 40th Street
Suite 206
Redmond, WA 98052

Peter Hauge Madsen
Riso National Laboratory
Postbox 49
DK-4000 Roskilde
DENMARK

David Malcolm
Lavalin Engineers, Inc.
Atria North - Phase 2
2235 Sheppard Avenue East
Willowdale, Ontario M2J 5A6
CANADA

Bernard Masse
Institut de Recherche d'Hydro-Quebec
1800, Montee Ste-Julie
Varennes, Quebec J3X 1S1
CANADA

Gerald McNerney
U.S. Windpower, Inc.
6952 Preston Avenue
Livermore, CA 94550

R. N. Meroney
Dept. of Civil Engineering
Colorado State University
Fort Collins, CO 80521

Alan H. Miller
10013 Tepopa Drive
Oakdale, CA 95361

D. Morrison
New Mexico Engineering
Research Institute
Campus P.O. Box 25
Albuquerque, NM 87131

V. Nelson
Department of Physics
West Texas State University
P.O. Box 248
Canyon, TX 79016

J. W. Oler
Mechanical Engineering Dept.
Texas Tech University
P.O. Box 4289
Lubbock, TX 79409

Dr. D. I. Page
Energy Technology Support Unit
B 156.7 Harwell Laboratory
Oxfordshire, OX11 ORA
UNITED KINGDOM

Ion Paraschivoiu
Dept. of Mechanical Engineering
Ecole Polytecnique
CP 6079
Succursale A
Montreal, Quebec H3C 3A7
CANADA

Troels Friis Pedersen
Riso National Laboratory
Postbox 49
DK-4000 Roskilde
DENMARK

Helge Petersen
Riso National Laboratory
Postbox 49
DK-4000 Roskilde
DENMARK

Dr. R. Ganesh Rajagopalan
Assistant Professor
Aerospace Engineering Department
Iowa State University
404 Town Engineering Bldg.
Ames, IA 50011

R. Rangi
Low Speed Aerodynamics Laboratory
NRC-National Aeronautical
Establishment
Montreal Road
Ottawa, Ontario K1A OR6
CANADA

Markus G. Real, President
Alpha Real Ag
Feldeggstrasse 89
CH 8008 Zurich
Switzerland

R. L. Scheffler
Research and Development Dept.
Room 497
Southern California Edison
P.O. Box 800
Rosemead, CA 91770

L. Schienbein
FloWind Corporation
1183 Quarry Lane
Pleasanton, CA 94566

Loretta Helling
Librarian
National Atomic Museum
Albuquerque, NM 87185

Thomas Schweizer
Science Applications International
Corp.
4300 King Street, Suite 310
Alexandria, VA 22302

David Sharpe
Dept. of Aeronautical Engineering
Queen Mary College
Mile End Road
London, E1 4NS
UNITED KINGDOM

J. Sladky, Jr.
Kinetics Group, Inc.
P.O. Box 1071
Mercer Island, WA 98040

M. Snyder
Aero Engineering Department
Wichita State University
Wichita, KS 67208

L. H. Soderholm
Agricultural Engineering
Room 213
Iowa State University
Ames, IA 50010

Peter South
ADECON
6535 Millcreek Dr., Unit 67
Mississauga, Ontario L5N 2M2
CANADA

W. J. Steeley
Pacific Gas and Electric Co.
3400 Crow Canyon Road
San Ramon, CA 94583

Forrest S. Stoddard
West Texas State University
Alternative Energy Institute
WT Box 248
Canyon, Texas 79016

Derek Taylor
Alternative Energy Group
Walton Hall
Open University
Milton Keynes MK7 6AA
UNITED KINGDOM

G. P. Tennyson
DOE/AL/ETWMD
Albuquerque, NM 87115

Walter V. Thompson
410 Ericwood Court
Manteca, CA 95336

R. W. Thresher
Solar Energy Research Institute
1617 Cole Boulevard
Golden, CO 80401

K. J. Touryan
3701 Hawkins Street, NE
Albuquerque, NM 87109-4512

W. A. Vachon
W. A. Vachon & Associates
P.O. Box 149
Manchester, MA 01944

P. Vittecoq
Faculty of Applied Science
University of Sherbrooke
Sherbrooke, Quebec J1K 2R1
CANADA

T. Watson
Canadian Standards Association
178 Rexdale Boulevard
Rexdale, Ontario M9W 1R3
CANADA

L. Wendell
Battelle-Pacific Northwest
Laboratory
P.O. Box 999
Richland, WA 99352

W. Wentz
Aero Engineering Department
Wichita State University
Wichita, KS 67208

R. E. Wilson
Mechanical Engineering Dept.
Oregon State University
Corvallis, OR 97331

400	R. C. Maydew
1514	J. G. Arguello
1514	H. S. Morgan
1540	J. R. Asay
1544	K. E. Metzinger
1544	E. D. Reedy
1544	R. C. Reuter, Jr.
1545	C. R. Dohrmann
1545	D. W. Lobitz
1545	D. R. Martinez
1552	J. H. Strickland
1556	G. F. Homicz
3141	S. A. Landenberger (5)
3151	G. L. Esch, Acting (3)
3145	Document Processing (8) For DOE/OSTI
3161	P. S. Wilson
6000	V. L. Dugan, Acting
6200	B. W. Marshall, Acting
6220	D. G. Schueler
6225	H. M. Dodd (50)
6225	T. D. Ashwill
6225	D. E. Berg
6225	M. A. Rumsey
6225	L. L. Schluter
6225	W. A. Stephenson
6225	H. J. Sutherland
6225	P. S. Veers
7543	G. H. James III
7543	R. Rodeman
7543	T. G. Carne
7543	J. P. Lauffer
8524	J. A. Wackerly